August 25, 2005

Ms. Michelle Swanson
Manager, Policy Analysis
Xcel Energy
414 Nicollet Mall RS-5
Minneapolis, MN 55401

Dear Michelle:

Subject: Final Report for JV Task 64 – Impacts of Biomass Cofiring on the Operation of a Next-Generation Power System; Contract No. RDF 2001 BB09; EERC Fund 5137

Enclosed is the final report for the subject project, which was funded by the Xcel Energy Renewable Development Fund and the U.S. Department of Energy. I would like to thank Xcel Energy for funding this project which has taken an important step to show that biomass can successfully be cofired with coal in a next generation power plant of a type which could be configured to create near zero emissions, and yet have operations essentially the same as modern plants. Will you please also thank Bob Kermes for his helpful comments about the report, I've incorporated most of them in this final version. Finally, I want to thank you personally for your support throughout this project. I think that we have accomplished some important work, and it always is much easier to do so with a champion such as you at the funding organization.

If you have any questions, please call me at (701) 777-5159, fax at (701) 777-5181, or e-mail jhurley@undeerc.org.

Sincerely,

John P. Hurley
Senior Research Advisor

JPH/krg

Enclosure

IMPACTS OF BIOMASS COFIRING ON THE OPERATION OF A NEXT-GENERATION POWER SYSTEM

Final Report

(For the period of June 1, 2002–March 31, 2005)

Prepared for:

Ms. Michelle Swanson

Manager, Policy Analysis
Xcel Energy
414 Nicollet Mall RS-5
Minneapolis, MN 55401

Prepared by:

John P. Hurley
Michael E. Collings
Douglas R. Hajicek
Ann K. Henderson
Nathan J. Kadrmas
Greg F. Weber
Bruce C. Folkedahl

Energy & Environmental Research Center
University of North Dakota
Box 9018
Grand Forks, ND 58202-9018

Stelios Arvelakis

Material Science and Technology Department
University of Limerick
Limerick, Ireland

Fred Robson

kraftWork Systems, Inc.
PO Box 115
Amston, CT 06231

2005-EERC-08-09

August 2005

DOE DISCLAIMER

This report was prepared as an account of work sponsored by an agency of the United States Government. Neither the United States Government, nor any agency thereof, nor any of their employees makes any warranty, express or implied, or assumes any legal liability or responsibility for the accuracy, completeness, or usefulness of any information, apparatus, product, or process disclosed or represents that its use would not infringe privately owned rights. Reference herein to any specific commercial product, process, or service by trade name, trademark, manufacturer, or otherwise does not necessarily constitute or imply its endorsement, recommendation, or favoring by the United States Government or any agency thereof. The views and opinions of authors expressed herein do not necessarily state or reflect those of the United States Government or any agency thereof.

This report is available to the public from the National Technical Information Service, U.S. Department of Commerce, 5285 Port Royal Road, Springfield, VA 22161; phone orders accepted at (703) 487-4650.

ACKNOWLEDGMENT

This report was prepared with the support of the U.S. Department of Energy (DOE) National Energy Technology Laboratory Cooperative Agreement No. DE-FC26-98FT40321. However, any opinions, findings, conclusions, or recommendations expressed herein are those of the authors(s) and do not necessarily reflect the views of DOE.

EERC DISCLAIMER

LEGAL NOTICE. This research report was prepared by the Energy & Environmental Research Center (EERC), an agency of the University of North Dakota, as an account of work sponsored by DOE and Xcel Energy. Because of the research nature of the work performed, neither the EERC nor any of its employees makes any warranty, express or implied, or assumes any legal liability or responsibility for the accuracy, completeness, or usefulness of any information, apparatus, product, or process disclosed, or represents that its use would not infringe privately owned rights. Reference herein to any specific commercial product, process, or service by trade name, trademark, manufacturer, or otherwise does not necessarily constitute or imply its endorsement or recommendation by the EERC.

TABLE OF CONTENTS

Continued…

TABLE OF CONTENTS (continued)

Continued…

TABLE OF CONTENTS (continued)

LIST OF FIGURES

Continued…

LIST OF FIGURES (continued)

Continued…

LIST OF FIGURES (continued)

Continued…

LIST OF FIGURES (continued)

Continued…

LIST OF FIGURES (continued)

LIST OF TABLES

Continued…

LIST OF TABLES (continued)

NOMENCLATURE

acfm	actual cubic feet per minute
Al_2O_3	alumina (aluminum oxide)
ASU	air separation unit
Btu	British thermal unit
°C	degrees Celsius
CAH	convective air heater
CaO	calcium oxide
cm	centimeters
CO	carbon monoxide
CO_2	carbon dioxide
COE	cost of electricity
DOE	U.S. Department of Energy
DSAF	dynamic slag application furnace
EERC	Energy & Environmental Research Center
ESP	electrostatic precipitator
EU	the European Union
°F	degrees Fahrenheit
FD	forced draft
Fe_2O_3	iron(III) oxide
FGR	flue gas recirculation
ft	feet
ft^2	square feet
ft^3	cubic feet
ft/s	feet per second
g	gram
GT	gas turbine
HAT	humid air turbine
HHV	higher heating value
HiPPS	High-Performance Power System
HTHX	high-temperature heat exchanger
hr	hour
HRSG	heat recovery steam generator
HX	heat exchanger
IFCC	indirectly fired combined cycle
IGCC	integrated gasification combined cycle
in.	inch
ITM	ion transport membrane
K_2O	potassium oxide
kg	kilogram
kJ	kilojoule
lb	pound
LCOE	levelized cost of electricity

m	meter
M	mole
m^2	square meter
m^3	cubic meter
MA754	oxide dispersion strengthened high-temperature nickel alloy
MA956	oxide dispersion strengthened high-temperature nickel alloy
MgO	magnesium oxide
min	minute
MMBtu	million (10^6) British thermal units
mm	millimeter
mmHg	millimeter mercury
MOR	modulus of rupture
MSW	municipal solid waste
NGCC	natural gas-fired combined-cycle
Na_2O	sodium oxide
NG	natural gas
NO_x	nitrogen oxides (nitric oxide and nitrogen dioxide)
O_2	oxygen
o.d.	outside diameter
ODS	oxide dispersion strengthened
ORNL	Oak Ridge National Laboratory
OTM	oxygen transport membrane
pc	pulverized coal
PCA	primary combustion air
P_2O_5	phosphorus pentoxide
PSD	particle-size distribution
psi	pounds per square inch
psig	pounds per square inch gauge
PTFE	polytetrafluoroethylene
RAH	radiant air heater
RDF	refuse-derived fuel
s	second
scfm	standard cubic feet per minute
SEM	scanning electron microscopy
SFS	slagging furnace system
SiO_2	silica (silicon dioxide)
SO_2	sulfur dioxide
SO_3	sulfur trioxide
std. dev.	standard deviation
TiO_2	titanium dioxide
TLP	transient liquid phase
UTRC	United Technologies Research Center
vol%	volume percent
W	watt
wt%	weight percent
W.C.	water column

XRD	x-ray diffraction
XRF	x-ray fluorescence
µm	micrometer

IMPACTS OF BIOMASS COFIRING ON THE OPERATION OF A NEXT-GENERATION POWER SYSTEM
Contract No. RDF 2001 BB09
Draft Project Report
June 2002 – March 2005

EXECUTIVE SUMMARY

Introduction and Objectives

Modern solid fuel power plants generate steam at 180 bar and 540°C (2600 psi and 1000°F) to turn a steam turbine which turns a generator to make electricity. They are typically 35% efficient at converting the chemical energy in coal to electrical energy, but many old units struggle to maintain cycle efficiencies above 30%. The steam cycle that they use is limited in efficiency by the low temperatures achievable by standard steel piping, and by the high thermal penalty incurred during boiling the water to make steam. Much higher efficiencies can be reached in an indirectly fired combined cycle (IFCC) using a slagging high-temperature pulverized coal (pc)-fired combustor and heat exchangers (HXs) to produce clean air at up to 1100°C and 17 bar (2000°F and 250 psi) to turn an aeroderivative turbine, followed by a standard boiler and steam turbine to take advantage of the waste heat. Approximately one-half of the power is produced using the more efficient aeroderivative turbine cycle as compared to a steam cycle, resulting in **a reduction of 50% in the cooling water required by the plant** and a more efficient overall method of producing electricity. To achieve the highest temperatures and **efficiencies of up to 55%**, a gas-fired duct burner can be used to additionally heat the gas entering the turbine. The overall system design is like that of a natural gas-fired combined-cycle (NGCC) system except that a pc-fired furnace is used to preheat the air entering the gas turbine (GT). Because of the very high temperatures, advanced oxide dispersion-strengthened (ODS) alloys must be used to construct the high temperature heat exchanger (HTHX) built into the walls of the furnace used to heat the process air going to the GT. The similarity of designs makes it especially suitable as a pc-fired boiler retrofit technology **and assures that operations are essentially the same as for existing plants**. The HTHX and a GT could conceivably be retrofitted to smaller industrial boiler systems to produce electricity and heat for industrial or domestic use. The retrofit is equally applicable to district heating boilers, including those cofiring opportunity sources of biomass such as might be used in smaller towns or tribal communities to produce both heat and power.

In previous pilot-scale testing of key IFCC subsystems at the University of North Dakota Energy & Environmental Research Center (EERC) funded by the U.S. Department of Energy (DOE) and the North Dakota Industrial Commission, no biomass testing was performed. Therefore, the EERC requested funding from the Renewable Development Fund with the objective of determining the feasibility of using coal–biomass cofiring in the operation of an advanced IFCC power plant. That work is summarized in this report. It involved two main efforts. In the first activity, the pilot-scale slagging furnace system (SFS) was fired with three coal–biomass blends to evaluate the impact of biomass cofiring on the performance of the system and the HTHX. Specific pilot-scale combustion test objectives included 1) coal–biomass cofiring for a period of 85 hr to establish an ash–slag layer on the HTHX tubes and obtain steady-state heat transfer data, 2) evaluating the impact of biomass cofiring on convective air heater (CAH) performance as well as other SFS

components, 3) determining flue gas particulate mass loading and particle size at the baghouse inlet and baghouse particulate collection efficiency, 4) evaluating baghouse differential pressure control, and 5) documenting flue gas composition for SO_2, NO_x, CO_2, CO, and O_2. The operational data from the tests were then used in performing efficiency and economic analyses of IFCC systems fired with several fuels and oxidizers for comparison to existing and other developing power system concepts. In the second activity, several laboratory-scale series of tests were performed. The objective of one series was to further test methods of joining the ODS alloy, initially developed under separate DOE funding, since it can not be welded in the typical manner of other HX alloys. The objective of another series was to determine the physical and chemical behaviors of the slags formed during firing of the coal–biomass blends in order to better understand the best possible operating conditions of the HTHX for each fuel blend. The objective of the final series of tests was to determine the mechanisms and rates of flowing slag corrosion of the HTHX alloy.

Testing Results and Conclusions

Task 1 – Pilot-Scale Testing

Three pilot-scale SFS coal–biomass cofiring tests were completed in support of this project. Each test involved cofiring biomass with North Antelope subbituminous coal on a nominal-firing-rate (kJ/hr [MMBtu/hr]) basis of 80% coal and 20% biomass. The three biomass fuel types selected through discussions with Mr. Joseph Brobjorg, the Xcel Energy technical representative for this project. They were hog fuel (a forest industry by-product) fired during Test XCEL1, and two agriculture-based fuel sources, corn stover fired during Test XCEL2 and switchgrass fired during Test XCEL3. Coal and biomass fuels were blended on a mass basis using two loss-in-weight gravimetric feeders into the primary air line supporting the operation of a single burner. Each coal–biomass cofired test involved preheating the SFS while natural gas (NG) was fired prior to initiating coal–biomass cofiring. Each cofiring test nominally ran 85 hr of continuous solid fuel firing.

The SFS operation was evaluated based on furnace temperature (flue gas and refractory) and pressure measurements and online flue gas instrumentation readings (O_2, CO, CO_2, NO_x, and SO_2). A nominal cofiring rate of 2.3×10^6 kJ/hr (2.2 MMBtu/hr) at an air-to-fuel ratio of about 1.2:1 was anticipated to achieve nominal furnace gas temperatures of 1483°C (2700°F) near the HTHX and furnace exit. The North Antelope subbituminous coal used for these tests is similar to other subbituminous coals fired in the SFS. Therefore, where appropriate, comparative data are presented for 100% coal-fired SFS tests for discussion purposes and development of conclusions concerning the impacts of biomass cofiring.

Description of the Pilot-Scale SFS

The EERC pilot-scale SFS was designed to simulate the conditions in a commercial-scale IFCC employing a slagging furnace, and can be operated in an air-blown or oxygen (O_2)-blown configuration. The air-blown system configuration used in support of this project is shown in Figure ES-1. Switching between 100% coal firing and coal–biomass cofiring is accomplished by changing a few piping connections associated with primary combustion air flow and setting up a

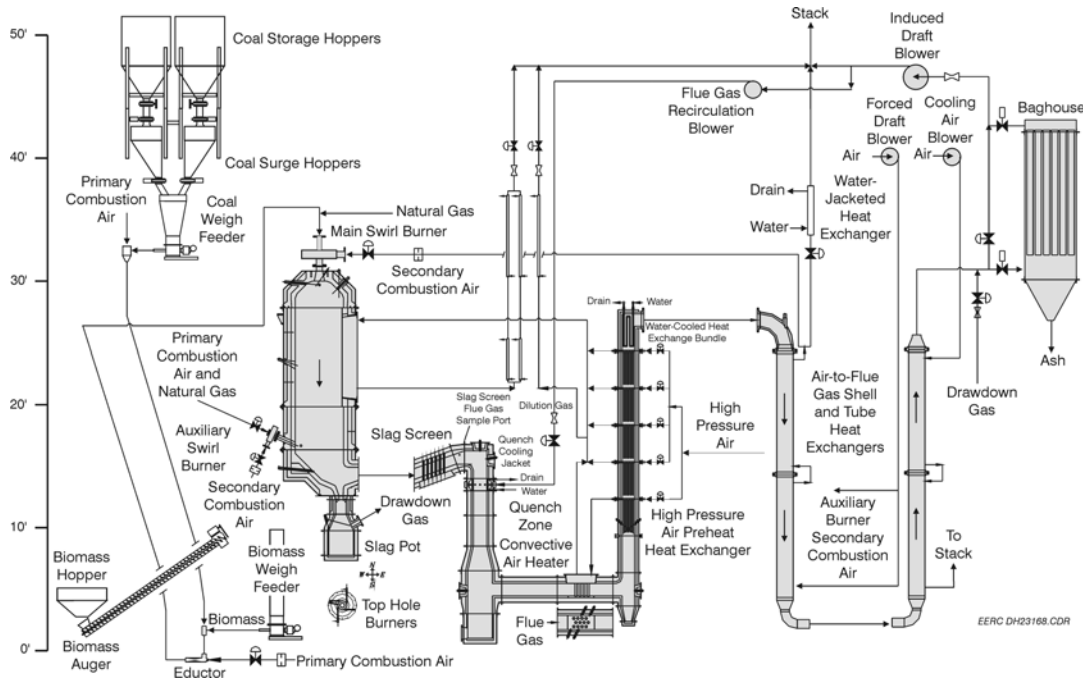

Figure ES-1. Illustration of the air-blown SFS configuration modified for biomass cofiring.

portable biomass refill system to support the loss-in-weight feeder metering biomass to the primary air line conveying fuel to the main burner.

The pilot-scale slagging furnace is intended to be as fuel-flexible as possible, with maximum furnace exit temperatures of 1483°–1593°C (2700°–2900°F) to maintain the desired heat transfer to the HTHX and slag flow. The furnace has a nominal firing rate of 2.6×10^6 kJ/hr (2.5 MMBtu/hr) and a range of $2.1–3.2 \times 10^6$ kJ/hr (2.0–3.0 MMBtu/hr) using a single burner. The design is based on Illinois No. 6 bituminous coal (25,800 kJ/kg [11,100 Btu/lb]) and a nominal furnace residence time of 3.5 s. Flue gas flow rates range from 12.0 to 18.6 m^3/min (425 to 645 scfm), with a nominal value of 15 m^3/min (530 scfm), based on 20% excess air. Firing a subbituminous coal or lignite increases the flue gas volume, decreasing residence time to roughly 2.6 s, and decreases flame temperature because of the higher moisture content of these fuels. However, the high volatility of the low-rank fuels results in high combustion efficiency (>99%). The EERC oriented the furnace vertically (downfired) and based the burner design on that of a swirl burner used on two smaller EERC pilot-scale pc-fired units (633,000 kJ/hr [600,000 Btu/hr]). Slagging furnace internal dimensions are 119 cm (47 in.) in diameter by 4.9 m (16 ft) in total length.

High-Temperature Heat Exchanger

A key feature of the furnace is accessibility for installation and testing of the HTHX. The HTHX panel was designed for testing alloy tube material lifetimes and heat exchange coefficients and is 0.46 × 1.96 m (1.5 × 6.4 ft). The HTHX contains three vertically oriented tubes originally made of MA754, a nickel-based ODS alloy. Process air for the HTHX is provided by an EERC air

compressor system and preheater tube bundles located in the flue gas stream and the CAH tube bank. Maximum air capacity available to support the HTHX is 11.3 m^3/min (400 scfm) at a delivery pressure of 10.3 bar (150 psig). As it passes through the HTHX, the process air is heated from nominally 538° to 705°C (1000° to 1300°F) to as high as 1094°C (2000°F). Concurrent to SFS modifications to permit coal–biomass cofiring, one of the MA754 alloy tubes in the HTHX was replaced with a tube manufactured using a new MA956 alloy. As was the case for previous air-blown tests without tile protection, the lower half of the HTHX was encased in insulation and refractory to limit furnace exposure to the top half of the HTHX because of process air limitations. In addition, it was necessary to encase the top 15 cm (6 in.) of the HTHX in low- and high-density insulating materials to protect bolting materials and connections used to install the MA956 alloy tube from furnace conditions. Therefore, only 39% of the HX surface was exposed to furnace conditions during the coal–biomass cofiring tests. Based on ash characterization, alloy tube surface temperature was limited to <1052°C (<1925°F) to minimize the potential for slag corrosion of the alloy tube surfaces. Figure ES-2 is a photograph of the HTHX after the MA956 alloy tube was added and the HTHX was installed in the slagging furnace.

Fuel Characteristics

As a result of discussions with Xcel Energy personnel, North Antelope subbituminous coal was selected for use in this project because it is fired at the Xcel Energy King Station. Biomass fuel selections included hog fuel, corn stover, and a switchgrass. Hog fuel was selected because wood residues are the most widely available biomass fuels; hog fuel is fired at Xcel's Ashland, Wisconsin, plant. Hog fuel consists of bark and wood remnants from the processing of trees.

Figure ES-2. Photograph of the HTHX, modified to include a center tube of MA956 alloy, prior to Test SFS-XCEL1-0303.

While sawdust is much more desirable because of its handling characteristics and typically small inorganic content, hog fuel is more abundant and cheaper because it has a higher inorganic content. Corn stover, an agricultural by-product, was selected because of its availability in the upper Midwest, and switchgrass was selected because a number of technical and economic biomass energy studies identified it as a potential energy crop.

Slagging Furnace Operation

Coal and biomass feed rates were adjusted and controlled to achieve a nominal 80%–20% coal–biomass cofiring contribution on a firing-rate basis and to avoid exceeding a 1052°C (1925°F) temperature limit imposed for the HTHX alloy tube surfaces. North Antelope coal feed rates ranged from 75 to 84 kg/hr (166 to 186 lb/hr). Biomass feed rates typically ranged from 27 to 32 kg/hr (60 to 70 lb/hr). Generally, both the coal and biomass feed rates were stable. Momentary spikes in the coal and biomass feed rates were observed during feed hopper refill cycles. The switchgrass feed rate was less stable than the hog fuel or corn stover, possibly related to the cylindrical geometry of the material and the impact of that geometry on mass flow through the feed hopper. It likely bridges more than the other two biomass materials. Inspection of the biomass feeder indicated switchgrass packing around the screw within the housing, which was not evident with the hog fuel or corn stover.

Furnace exit temperatures during the cofiring test periods ranged from 1410° to 1494°C (2570° to 2720°F) as a result of main burner firing rates of $2.1–2.4 \times 10^6$ kJ/hr (2.0–2.3 MMBtu/hr). The hog fuel had the highest moisture level of the three biomass fuels and resulted in the lowest average furnace exit temperature, even though in combination with the coal, it represented the highest average firing rate. Based on the temperature and firing rate data and fuel characteristics, the differences in the furnace exit temperatures for the corn stover and switchgrass tests were likely a function of firing rate alone.

Although the particle size of the biomass fuels was significantly larger than the coal, overall carbon burnout during the coal–biomass-cofiring tests was high, as indicated by baghouse ash analysis that reported carbon values of 0.18–0.33 wt%. The high degree of carbon burnout, >99.6%, observed in the SFS system for these tests is a direct result of adequate furnace temperature and residence time.

During future cofiring tests with the SFS, the biomass fuel should be prepared through a 1.59-mm (0.0625-in.) screen. A smaller screen should result in a more uniform hammer mill product, potentially improving biomass feed stability for the pilot-scale system.

Baghouse Performance

The fly ash generated in the high-temperature SFS is different than observed for a given fuel fired in a conventional pc-fired system. Specific differences include a reduction in mass loading and particle size and a higher concentration of alkaline-earth components. This shift in ash properties was anticipated based on the use of a slag screen at the furnace exit to promote ash collection as slag. Ash passing through the slag screen is expected to represent smaller ash particles as well as

ash components volatilized in the furnace and subsequently condensed at lower temperatures. Therefore, the SFS produces a fly ash more representative of a cyclone-fired system.

Baghouse temperatures ranged from 163° to 174°C (325° to 345°F) for Tests XCEL1 and XCEL2 and from 152° to 166°C (305° to 330°F) for Test XCEL3. The filter face velocities for the three coal–biomass-cofiring tests were 0.70–0.85 m/min (2.0–2.9 ft/min). These filter face velocities are low compared to conventional pulse-jet filtration systems typically operating at or near 1.2 m/min (4 ft/min). The bags used in this project were a 747 g/m^2 (22-oz/yd^2)-woven glass–polytetrafluoroethylene (PTFE) membrane-fabric combination representing a total filtration area of 52.5 m^2 (565 ft^2). Online pulse cleaning of the PTFE membrane bags was attempted using reservoir pulse-air pressures of nominally 2.8–4.1 bar (40–60 psig). The baghouse differential pressure cleaning set points ranged from 11.2 to 16.8 mmHg (6 to 9 in. W.C.). However, online cleaning was unsuccessful, forcing off-line cleaning for all three biomass cofiring tests. Off-line cleaning frequency was 2–6 hr, depending on the biomass fuel cofired and the off-line cleaning trigger point.

Online baghouse cleaning had not been a problem previously when firing a subbituminous coal. Fly ash chemical composition resulting from biomass cofiring was determined to be the primary contributing factor to online cleaning difficulties. Specifically, concentrations of alkali components increased while silica and alumina concentrations decreased. The primary difference in composition data was an order-of-magnitude or near-order-of-magnitude increase in the potassium content for the baghouse ash resulting from biomass cofiring.

Scanning electron microscopy (SEM) data support the hypothesis that potassium sulfate formation and condensation were responsible for altering the cohesive properties of the baghouse ash, resulting in an inability to control baghouse differential pressure using online cleaning when cofiring coal and biomass. Some sodium enrichment was also observed in the case of hog fuel cofiring. The highest degree of potassium enrichment was observed for corn stover cofiring, consistent with the bulk fuel data showing the corn stover to have the highest ash content and the highest potassium content in the ash. Calculated mole ratios based on the elemental analysis data indicate that the potassium and sodium were present as sulfates. The composition implies that the online cleaning difficulties appear to be related to ash chemistry and a resulting inability to dislodge the dust cake from the bag surface. The slagging system magnifies the problem because of the reduced total mass loading to the baghouse and enrichment of alkali sulfates in the baghouse ash. In order to successfully control baghouse differential pressure with online cleaning, substantially more energy would have to be employed during online cleaning (pulse pressures of >5.9 bar [>85 psig]) or biomass cofiring would have to be reduced from the 20% cofiring rate used during these tests.

Assuming baghouse differential pressure can be controlled using online pulse cleaning as a result of operating parameter changes or a reduced biomass cofiring rate in the SFS, the cohesive character of the ash may be beneficial. Specifically, it may reduce emission spikes as a function of cleaning cycle. This benefit would also be likely in a conventional dry-ash pc-fired system.

CAH Performance

CAH tube bank performance has met all objectives relative to heat transfer and its support of the HTHX panel during this, as well as previous, projects. Performance differences relative to fuel ash properties were expected. The potential effectiveness of sootblowing was not addressed during this project because the EERC elected to permit the formation of ash deposits on CAH tube bank surfaces in order to develop deposits for subsequent recovery and characterization.

The CAH deposits that formed during the coal–biomass-cofiring tests were limited to the leading and trailing edges of the tubes. However, these deposits were found to be friable. CAH tube bank plugging was not a problem when cofiring the North Antelope coal nor any of the three biomass fuels. No deposits were observed bridging the flue gas path between the tubes.

Deposit strength is a function of ash chemistry, particle size, and temperature history. The relatively low strength of the deposits formed when cofiring the North Antelope coal and the three biomass fuels indicates that the deposits could be easily removed by sootblowing.

CAH heat-transfer data when cofiring hog fuel and switchgrass were similar. However, the CAH heat recovery rate when cofiring corn stover did not degrade to <21,100 kJ/hr (<20,000 Btu/hr), as was observed for the hog fuel and switchgrass. One possible explanation may be related to the higher density of the ash deposits formed.

One of the CAH standards of success identified for this project in the original proposal was the production of clean pressurized air at 705°C (1300°F) while limiting convective pass flue gas temperature to 1010°C (1850°F). Based on temperature measurements, clean pressurized-air temperatures generally stabilized at 510°–538°C (950°–1000°F), indicating that the proposed standard of success was not achieved. However, based on previous HTHX tests and the data generated during the coal–biomass-cofiring tests, reducing the process air flow rate to design volumes or adding sufficient CAH surface and surface to adequately preheat process air upstream of the CAH, and employing sootblowing would easily result in CAH outlet process air temperatures of 927°C (1300°F).

HTHX Performance

Alloy tube surface temperature was to be limited to <1052°C (<1925°F) when cofiring coal and biomass to minimize the potential for slag corrosion–erosion of the alloy tube surfaces. However, the control thermocouple failed during each test period, and two compressor trips resulted in minor temperature spikes. As a result, indicated maximum HTHX tube surface temperatures were controlled at <1055°C (<1930°F) and typically ranged from 1033° to 1049°C (1890° to 1920°F).

Tube surface temperatures during the coal–biomass-cofiring tests were lower than values observed for previous HTHX tests (110°–205°C [230°–400°F]) because of the lower alloy surface temperature limit selected for the coal–biomass-cofiring tests. The range of process air temperatures at the exit of the HTHX decreased from nominally 721° to 749°C (1330° to 1380°F) to 635° to 666°C (1175° to 1230°F). This decrease is a direct result of decreasing heat transfer caused by ash–slag deposition on HTHX alloy tube surfaces as well as ash deposition on downstream heat-transfer

surfaces (CAH and air preheat surfaces) preheating HTHX process air. Differences in HTHX outlet process air temperatures between individual coal–biomass-cofiring tests were consistent with a combination of furnace temperature and process air flow rates.

Deposition on the HTHX alloy tube surfaces began with a low-density sintered layer, followed by a higher-density intermediate layer, and finally a high-density molten slag layer. During cooldown, the slag layer consistently fractured on the surface of the alloy tubes and either partially or completely fell off of the tubes. Also, there was no evidence of slag flow down the surface of the alloy tubes. The inner layer was enriched in alkali metal and alkaline earth sulfates relative to the fuel slag. This phenomenon is often observed on steam HX surfaces in typical pc or cyclone fired power plants, but is usually not seen on the HTHX when firing coal. The presence of the sulfates in the inner layers during the cofiring tests is due to the relatively low metal temperatures maintained during these tests. Such enrichment is not seen when firing only coal because the tube surfaces are kept near 1090°C (2000°F) which is above the temperature of thermodynamic stability for sulfates. In addition, the outer slag layers on the HTHF were enriched in silica relative to the slag, most likely because this layer was enriched in larger ash particles which tend to have higher silica contents for these fuels. These differences in deposit composition relative to the slag indicate that using the fuel slag for longer-term laboratory corrosion testing is not sufficient to understanding the alloy corrosion mechanisms or rates. Instead, some computer modeling of ash formation and deposition should be performed in order to better understand the properties of the inner deposit layers so that more realistic laboratory corrosion tests can be designed.

The corrected HTHX heat recovery rates for coal–biomass-cofiring tests were 66%–84% of those observed for firing an Illinois No. 6 bituminous coal. The primary reason for this difference was furnace temperature—1433°–1488°C (2610°–2710°F) for the biomass-cofiring tests versus 1571°C (2860°F) when firing the bituminous coal. At an equivalent furnace temperature, HTHX heat recovery during the coal–biomass-cofiring tests was comparable to previous HTHX tests firing just coal indicating that there are no inherent problems with radiant heat transfer from the cofired flame.

Comparisons of heat recovery data for the coal–biomass-cofiring test periods showed that heat recovery was 27% and 24% greater for the switchgrass and corn stover tests, respectively, when compared to the hog fuel test. The reason for the difference in heat recovery rates was furnace temperature—1488°C (2710°F), 1477°C (2690°F), and 1433°C (2610°F) for the switchgrass, corn stover, and hog fuel, respectively. Overall, cofiring resulted in HTHX heat recovery rates consistent with previous tests firing NG and bituminous coal. Therefore, at comparable furnace temperatures, coal–biomass cofiring does not present any unique impediments to HTHX heat recovery. However, a better understanding must be developed of the mechanisms and rates of corrosion of the alloy tubes when firing different fuel blends before deciding on the appropriate surface temperatures at which to operate. At any rate, because of the lower temperatures at which the cofired slag freezes, it is not likely that HTHX heat recovery rates observed for bituminous coal can be practically achieved when cofiring biomass.

One of the standards of success identified for this project in the original proposal was the production of clean pressurized air at 927°C (1700°F) while the slagging furnace was operated at a temperature of no more than 1566°C (2850°F). Clean pressurized-air temperatures generally

stabilized at 635°–666°C (1175°–1230°F) near the end of each test. At face value, these data indicate that the proposed standard of success was not achieved. However, the lower process air exit temperatures were the result of lower inlet temperatures, having only a portion of the original HTHX surface exposed, and that which was exposed was maintained at a lower temperature than previous tests as a precaution against corrosion. Therefore, the EERC is confident that process air temperatures of >927°C (>1700°F) can be achieved and maintained if the entire surface of the HTHX is exposed to the furnace, the alloy tube surface temperature limit is raised to 1094°C (2000°F), and routine sootblowing of CAH and air preheat surfaces is employed to maintain inlet process air temperatures at 705°C (1300°F).

Economic Analysis of IFCC Systems

A brief study was performed to identify the performance and the first-order economics of an IFCC employing a bare-tube HTHX. The study was performed by Dr. Fred Robson of kraftWorks Systems, a consultant hired by the EERC. Dr. Robson served as the primary systems analyst for the United Technologies Research Center under the original High-Performance Power System Program. The results were compared to a variety of systems including typical pc-fired plants, integrated gasification combined cycles (IGCCs), and NGCCs. Since the pilot-scale testing of coal–biomass cofiring showed no significant influence of biomass cofiring on the operation of the combustor, and since the cost of biomass is only slightly less than that of coal, it was assumed that costs for cofiring would be essentially the same as for just firing coal so no separated calculations were included for cofiring. Two main IFCC firing scenarios were investigated; coal-fired with air and coal-fired with O_2. Because IFCC systems have a high potential for operation as zero-emission power plants, special focus was placed on firing with O_2, and including CO_2 recovery. Three main IFCC energy cycles were investigated:

- Commercially available GT with coal-fired HTHX with 927°C (1700°F) exit and NG-boost fuel.

- Advanced aeroderivative GT with coal-fired HTHX with 1489°C (2100°F) exit and NG-boost fuel.

- Commercially available aeroderivative GT with using only a coal-fired HTHX with 1489°C (2100°F) exit, i.e. all-coal IFCC.

Even with the limited number of configurations analyzed, it is apparent that the IFCC with CO_2 recovery offers better performance and lower cost of electricity (COE) than pc plants with CO_2 recovery. This is also true with the lower-performing all-coal IFCC. The IFCC also has competitive COE's to IGCC plants. At NG prices above \$4.70/10^6 kJ (\$5.00/MMBtu), the IFCC systems are attractive alternatives NGCC systems with CO_2 recovery while maintaining the standard operations of a pc plant. A near zero-emission IFCC is also cheaper to operate than a modern pc system if a carbon tax of more than \$55/metric ton (\$50/ton) C is imposed. If 20% biomass cofiring is employed, the break-even point would be \$44/metric ton (\$40/ton) of carbon.

A more detailed analysis allowing wider evaluation of alternative IFCC configurations and lower level cost analysis should be performed. For example, the IFCC is uniquely suitable for use

with membrane transfer oxygen units and such a system should have significantly higher performance and lower costs. More detailed design and accompanying cost analysis, especially for alternative firing sequences for the HTHX and also the entire furnace assembly and enclosure, would identify critical issues and supply better cost estimates for this unique enabling technology. The EERC is currently in discussions with the DOE National Energy Technology Laboratory to have it perform these calculations in a manner consistent with its previous analyses of other advanced power system concepts.

Task 2 – Laboratory-Scale Testing

Joining MA956 Alloy

The ODS alloys used to construct the HTHX exhibit extremely high corrosion and creep resistance. These properties are imparted to the alloys because of the dispersion of the yttria particles throughout the alloy structure. However, because they must remain dispersed, the alloys cannot be welded because melting would allow the oxides to segregate in the joint, diminishing the usefulness of the metal. Therefore, the EERC has been working with Oak Ridge National Laboratory (ORNL) to develop a method for joining the MA956 using transient liquid-phase (TLP) bonding. In the TLP method, a thin layer of a proprietary alloy is placed between the pieces to be joined, and the joint is heated, causing interdiffusion of the ODS and joining alloy at temperatures well below the melting point of the ODS metal. If the oxides stay well-dispersed within the joint, then the joint should maintain a high fraction of the maximum usable temperature of the ODS material. This work was begun under an earlier DOE program, but was further advanced under the Xcel biomass cofiring program.

Three main ways of applying the thin joining metal layer to the surfaces of the MA956 were tested. In addition, two joining alloys and a number of process conditions were investigated. Because of the proprietary nature of the results of the method development, full details can not be disclosed in this document. However, a method of joining the MA956 has been developed in which only a few pores remain along the line of the joint, and in which the joining alloy is approximately 95% dispersed within the ODS alloy. Samples of different joints have been sent to ORNL for evaluation and tensile strength testing under its Fossil Energy Materials program, but these initial results indicate that the TLP method is likely to be suitable for joining the alloy for use in construction of a demonstration-sized HTHX.

Coal–Biomass Slag Behavior

The use of biomass alone or in combination with coal for power production in conventional coal-fired units is associated with a number of problems mainly created by the extremely reactive nature of its ash. These include slagging, fouling, corrosion, and erosion which can cause frequent unscheduled shutdowns, decreasing the availability and increasing the cost of the produced power. In particular, the flowing slag may severely corrode the HTHX if liquid slag is in contact with the alloy. To prevent corrosion, the surface of the HTHX must be operated below the solidus temperature of the slag. In order to determine the melting and rheological properties of the biomass and biomass–coal slags so that the solidus temperatures can be inferred, their viscosities were measured with a high-temperature rotational viscometer, and their crystallization behavior upon

cooling was measured by heated-stage x-ray diffraction. These tests were performed by Dr. Stelios Arvelakis, a post-doctoral student from the Denmark Technical University, during the summer and fall of 2003. In addition, the behavior of synthetic slags made from fuel ash was compared to that of the slags made in the SFS. The comparison was made to determine if testing of synthetic slags, which are much more easily produced than combustor slags, can be a valid way of determining probable slag behavior.

The synthetic coal–biomass ash mixtures were prepared by mixing ash from the biomass fuels with coal ash on a basis of 20% thermal input of the correspondent coal–biomass blends. Furthermore, in the case of the hog fuel, one additional mixture was formed on the basis of 10% thermal input. Viscosity measurements indicated that these synthetic mixtures behaved similarly to the slags produced in the SFS, but were not exactly the same. Due to variations in mineral deposition behavior, the combustor slags contain higher amounts of silica and alumina and lower levels of alkali metals, causing the viscosity to be slightly higher and the solidification of the slags to proceed at slightly higher temperatures. The temperature at which the viscosity of the slag reached 250 poise (T_{250}), and therefore may cause flow problems, is similar to that of the coal–hog fuel slag, slightly lower than the T_{250} for the coal–corn stover slag, but higher than that of the coal–switchgrass slag, although only the synthetic coal–switchgrass ash slag was tested (i.e. not the actual SFS slag). It is somewhat surprising that the synthetic coal–switchgrass slag would have a significantly lower T_{250} than the other cofire test slags because of its similar composition, although it does have somewhat higher alkali metal and lower alumina contents.

Generally, the viscosity characteristics of the synthetic coal–biomass ash mixtures behave similarly to the SFS slags, and so their behaviors can be used to provide rough approximations of the flow behavior of the slags within the SFS. In addition, the similarity of the curves made when using different rotational rates for the viscometer bob indicate that the slags are Newtonian in that they are not prone to shear thinning or thickening. However, the compositions of the synthetic and even actual slags do not approximate the compositions of the ash and slag initially depositing on the HTHX, and therefore cannot be used to predict the solidus temperatures of the HX deposits in order to determine the appropriate operating temperature of the HTHX so as to reduce corrosion of the alloy by the slag. This implies that instead of performing simple laboratory experiments to determine the appropriate operating temperature, it will be necessary either to employ computer models of ash formation and deposition, or perform pilot-scale tests of the fuels using air-cooled probes on which to form ash deposits for further analysis.

Flowing Slag Corrosion Testing of MA956 Alloy

The EERC bench-scale dynamic slag application furnace (DSAF) was modified to permit measuring the corrosion rates of sections of cooled alloy pipe to flowing slag. During a test, the furnace is heated to 1500°C (2730°F) while the surface of the alloy tube section is cooled to the desired temperature by an internal air flow. The slag is screw-fed into the furnace system as sandlike grains where it drops into a platinum melting pan. After melting, the slag drips onto the surface of the cooled alloy tube section at approximately the 11 o'clock position. It is administered at a rate equal to the maximum expected in the pilot-scale system. It then flows around the cooled tube and drips off the alloy and out of the furnace through a hole in its bottom. After 100 h of slag exposure, the DSAF is cooled, the alloy tube is removed and photographed, and its diameter is measured with

a caliper. The surface is then sprayed with dilute epoxy to hold the remaining slag in place, and the tube section is cut into pieces, then embedded in epoxy, cross-sectioned, and polished for analysis in a SEM.

The DSAF testing provides a worst-case-scenario type of test for the alloys because the corrosion mechanism is more severe than would be encountered by a HX in a power system. It is more severe because the slag is dripped directly onto the surface of the alloy whereas in a power system the surface would be coated with a thin layer of less reactive fly ash before building to the thickness at which the slag would become molten. Six corrosion tests were performed on MA956, the alloy used in the HTHX. The three SFS cofire slags were used, each at two temperatures. The 100-hr tests were performed in the DSAF by pouring slag at 1500°C (2730°F) onto pipe sections which were air-cooled to surface temperatures of 1050°C (1922°F) for the first three tests and 1150°C (2102°F) for the final three. The lower temperature was chosen because it was substantially below the temperature at which the slag begins to solidify. This means that the slag would essentially freeze to the surface of the alloy, and therefore the rate of reaction between the slag and the alloy or oxide scale on the surface of the alloy would be relatively low. The higher temperature was chosen because it was closer to, but still below, the temperature at which solidification begins, but slightly above the T_{250} for the synthetic switchgrass blend so that the slag would not freeze at the point at which it dropped on to the surface of the alloy for that slag. Because the switchgrass slag is molten at 1150°C (2102°F), we expect that it would be more reactive toward the alloy than the frozen slags.

In all cases, the surface recessions due to slag corrosion were too small to measure with a caliper. During the 1150°C (2102°F) tests, the slag wetted the surface more broadly and flowed farther around the circumference before dripping off than at the lower temperature. In all tests, the ribbon of slag frozen to the surface fell off upon cooling. With the exception of the switchgrass test at 1150°C (2102°F), the frozen slag broke from the alloy surface within the slag itself, leaving behind a thin layer of slag on the surface of the alloy. During temperature cycling, this remaining slag serves as a protective layer that reduces the attack on the alloy by the initial contact with the molten slag. For the switchgrass test at 1150°C (2102°F), the slag broke off near where the slag dripped onto the alloy, taking any remaining alumina scale with it. Since the slag layer did not remain attached for the switchgrass test at 1150°C (2102°F), the protective layer would not remain, and corrosion could be unacceptably high at that temperature for that slag. SEM measurements of aluminum concentration remaining after the tests versus depth within the alloy showed no significant depletion of the protective scale forming element from the alloy at 1150°C (2102°F), even in the case of the switchgrass slag. This indicates that HTHX surface temperatures at least that high may be commercially viable when cofiring with biomass, which would significantly increase the maximum temperature reachable for the process air, in turn increasing system efficiencies. However, although these flowing slag tests represent a worst-case scenario for slag corrosion by dripping the slag directly onto the alloy, the ash deposits that formed on the HTHX during the cofiring tests were not of the same composition as the slag. Therefore, additional corrosion tests should be performed with ashes more representative of the composition of the inner layers of those deposits.

Summary

The pilot-scale cofiring tests showed that although there are some differences in deposit formation and baghouse performance between firing just coal and cofiring with biomass, there are no significant issues that represent barriers to larger scale demonstrations of the HTHX technology. The testing also showed that construction methods for making the ODS-alloy HTHX are available since the laboratory testing showed that the TLP bonding method join pieces of the ODS alloy, and as a backup, mechanical methods involving threading can be used which were successfully demonstrated in the SFS. Also, corrosion of the alloy does not appear to be a problem in a likely worst-case scenario with slag dripping directly on alloy as long as the surface temperature of the alloy is above the solidus temperature of the slag. However, additional tests should be performed with ash compositions richer in sulfur and alkali such as those that formed the inner deposit layer formed on the HTHX during the cofiring tests. Finally, economic analyses indicate that if carbon dioxide taxes are imposed, construction and operation of a near zero-emission oxygen-blown coal-fired IFCC with carbon dioxide sequestration would be less expensive than paying the taxes if they are over approximately $55/metric ton ($50/ton) of carbon emitted. With 20% biomass firing, this breakeven would drop to approximately $44/metric ton ($40/ton) of carbon.

IMPACTS OF BIOMASS COFIRING ON THE OPERATION OF A NEXT-GENERATION POWER SYSTEM
Contract No. RDF 2001 BB09
Final Project Report
June 2002 – December 2004

INTRODUCTION AND OBJECTIVES

The U.S. Department of Energy (DOE) projects that by 2015 worldwide use of electricity will approach 72 trillion mJ (20 trillion kWh), a 100% growth in only 20 years. This growth comes during a time of concern over global warming, thought by many policy makers to be caused primarily by increases in CO_2 emissions through the use of fossil fuels. Future government regulations resulting from negotiated global treaties may force electric utilities to reduce CO_2 emissions or buy CO_2 credits from nations producing less CO_2 per capita. Renewable energy sources can also play a role supplying the electrical demand necessary to sustain a growing economy, but they cannot completely replace our reliance on fossil fuels in the foreseeable future. In thermal systems, biomass fuels can offset the demand for fossil fuels where sufficient biomass resources exist, but they are not abundant enough for 100% firing in a large baseload electrical generation plant. Therefore, in order to conserve valuable fossil fuel resources and reduce the impact of electrical generation on our global environment, more efficient electrical generation cycles employing biomass cofiring are necessary.

Modern solid-fuel power plants generate steam at 180 bar and 540°C (2600 psi and 1000°F) to turn a steam turbine which turns a generator to make electricity. They are typically 35% efficient at converting the chemical energy in coal to electrical energy, but many old units struggle to maintain cycle efficiencies above 30%. They are limited in efficiency by the low temperatures achievable by standard steel piping and by using steam as the process gas because of the high thermal penalty incurred during the boiling of water. In 1991, DOE started the High-Performance Power System, or HiPPS program, which was designed to work with industry in the development of an ambitious high-efficiency coal-fired power plant technology. The goals for the HiPPS system were a one-third increase in system efficiency, emissions of only one-tenth of the particulate SO_x, and NO_x allowed under the New Source Performance Standards, and a reduction in the cost of electricity (COE) by 10% (1, 2). The University of North Dakota Energy & Environmental Research Center (EERC) worked with a team led by the United Technologies Research Center (UTRC) in the development of this system. Two Xcel employees, Dr. Max Delong and Mr. Gerald Goblirsch, served on a utility advisory board for the project.

The heart of the UTRC HiPPS system is an indirectly fired combined cycle (IFCC) using a slagging high-temperature pulverized coal (pc)-fired combustor and heat exchangers (HXs) to produce clean air at up to 1100°C and 17 bar (2000°F and 250 psi) to turn an aeroderivative turbine, followed by a standard boiler and steam turbine to take advantage of the waste heat (3). Approximately one-half of the power is produced using the more efficient aeroderivative turbine cycle as compared to a steam cycle, resulting in **a reduction of 50% in the cooling water required by the plant** and a more efficient overall method of producing electricity. To achieve the highest temperatures and **efficiencies of up to 55%**, a gas-fired duct burner can be used to additionally heat

the gas entering the turbine. A process flow diagram of an IFCC is shown in Figure 1. The overall system design is like that of a natural gas combined-cycle (NGCC)-fired turbine system (along the top of the diagram), except that a pc-fired furnace is used to preheat the air entering the gas turbine (GT). Because of the very high temperatures, advanced oxide dispersion strengthened (ODS) alloys must be used to construct the high temperature heat exchanger (HTHX) built into the walls of the furnace used to heat the process air going to the GT (4). The similarity of designs makes it especially suitable as a pc-fired boiler retrofit technology **and assures that operations are essentially the same as for existing plants**. The HTHX and a GT could conceivably be retrofitted to smaller industrial boiler systems to produce electricity and heat for industrial or domestic use. The retrofit is equally applicable to district heating boilers, including those cofiring opportunity sources of biomass such as might be used in smaller towns or tribal communities to produce both heat and power.

During and after the HiPPS program, the EERC performed lab- and bench-scale determinations of the corrosion resistance of the refractory and structural materials, developed methods to construct and improve corrosion resistance of the HTHX, and constructed and operated a 2.5-million-Btu/hr slagging combustor system for materials and subsystem testing. **In over 2000 h of testing, it was shown that the HTHX could produce pressurized process air routinely at 954°C (1750°F) to turn a turbine and even operate for a short time producing process air at up to 1100°C (2000°F)** (5). The work has demonstrated that the IFCC plant and subsystem designs were sound, and the temperatures reached indicated that the system could be capable of reaching efficiencies of up to 45% while firing coal and 55% when using a gas-topping burner, leading to reductions in CO_2 emissions of 40%, as compared to today's coal-fired systems.

In addition to the successful demonstration of the HX technologies while coal is fired in air, one test was performed with recycled flue gas supplemented with oxygen as the coal oxidizer. The

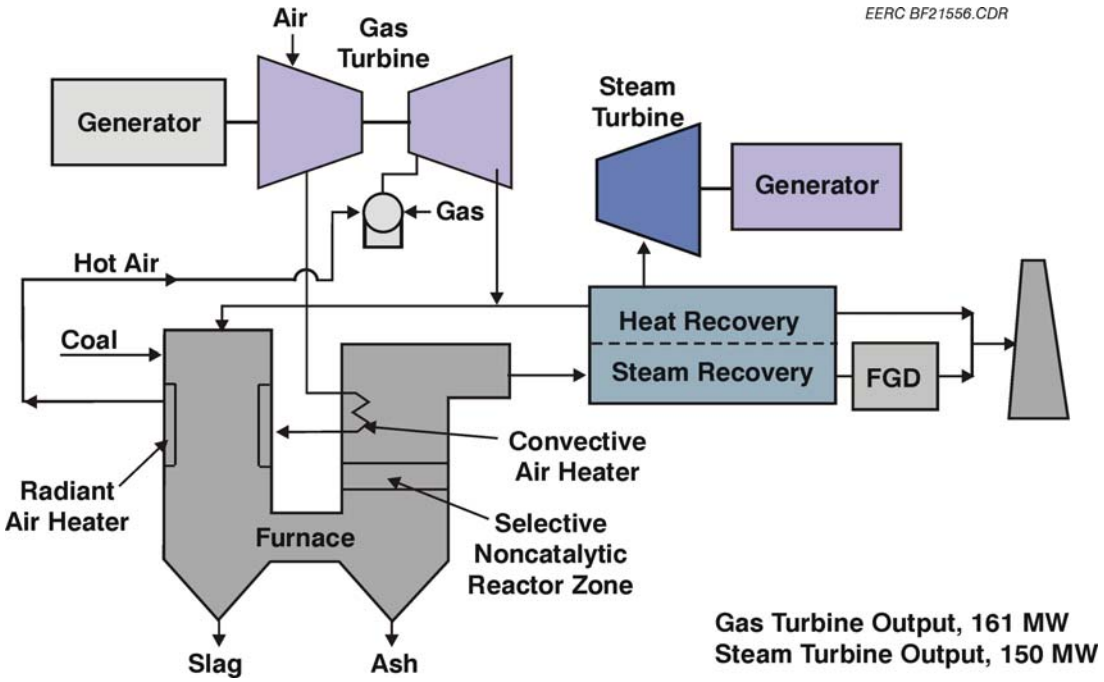

Figure 1. Process flow diagram of an IFCC power system.

recycled flue gas was used to keep the gas flow rate and flame temperature similar to that of the air-blown combustion. The oxygen-enriched test demonstrated much higher heat-transfer rates to the HTHX at similar gas temperatures because the flue gas is composed almost solely of carbon dioxide and water vapor, which are both very strong infrared radiation emitters. Specifically, the O_2-blown heat recovery rate could be 50% greater than the air-blown heat recovery rate at a given furnace temperature (6). Also, by reducing the amount of flue gas recirculation (FGR), the EERC demonstrated that flue gas flow rates could be substantially reduced relative to air-blown operation, conceivably **reducing the size of the furnace and downstream pollution control devices**. Also, after particulate cleanup and SO_2 scrubbing, the final flue gas consists almost completely of carbon dioxide and water vapor. Therefore, it would be possible to **condense most of the water for reuse in the plant** and harvest the remaining carbon dioxide for industrial use or geological sequestration so that the **plant could operate essentially emission-free**.

In this initial successful testing of the IFCC concepts funded by DOE and the North Dakota Industrial Commission, no biomass testing was performed. Therefore, the EERC requested funding from the Renewable Development Fund to test coal–biomass cofiring in the operation of the HTHX which is the heart of an advanced IFCC power plant. That work is summarized in this report. It involved two main efforts. In the first activity, the slagging furnace system (SFS) was fired with three coal–biomass blends to evaluate the impact of biomass cofiring on the performance of the system and the HTHX. The operational data from the tests was then used in performing efficiency and economic analyses of IFCC systems fired with several fuels and oxidizers for comparison to existing and other developing power system concepts. In the second activity, several types of laboratory-scale testing were performed. One was to further test methods of joining the alloy, initially developed under separate DOE funding, since it can not be welded in the typical manner of other HX alloys. Another was to perform detailed analyses of the physical and chemical behaviors of the slags formed during firing of the coal–biomass blends in order to better understand the best possible operating conditions of the HTHX for each fuel blend. The final laboratory activity was to determine the mechanisms and rates of flowing coal–biomass slag corrosion of the HTHX alloy.

BACKGROUND ON BIOMASS COFIRING

Many electric utilities that use coal for power generation are considering the use of renewable fuels such as waste products or energy crop-derived biomass fuels as a potential economic option for reducing greenhouse gas emissions. Calculations by the National Renewable Energy Laboratory (7) show that cofiring 15% and 5% by heat input of urban waste biomass with Illinois No. 6 coal reduces greenhouse gas emissions by 22% and 7%, respectively, on a CO_2-equivalent basis per unit of electricity produced. Therefore, biomass cofiring in coal-fired plants has the potential to significantly reduce greenhouse gas emissions.

Some experts estimate that 14%–15% of total world energy consumption is already accounted for by biomass (8). Energy production from biomass fuel sources such as wood wastes, municipal wastes, agricultural wastes, and landfill or digester gases is currently only about 1% of the total U.S. output (9). However, recent projections show that production capacity could rise to 10% of the total U.S. output by the year 2010 (10) if more companies take on cofiring strategies and dedicated sources of energy crops are produced (11). The European Union (EU), in response to its agreements under the Kyoto Protocol, committed to reduce greenhouse gas emissions between 2008 and 2012 by 8% of 1990 levels. EU statistics show that currently about 2%–8% more CO_2 would be emitted within the EU without the current use of biomass (12). Estimates of remaining available solid biomass fuel potential indicate that further reduction of CO_2 emissions of 7%–28% could be achieved.

Biomass types available for use as a cofiring fuel with coal fall into two major categories: biomass wastes and biomass energy crops. Waste products include wood wastes, such as wooden pallets, telephone poles, sawdust, manufacturing scraps, and municipal solid waste (MSW) or sludge and lignin derived from biomass-to-ethanol processes. Agricultural wastes may include peach pits, rice hulls, and straws of wheat, alfalfa, rapeseed, timothy grass, and barley. Energy crops include fast-growing switchgrass and hybrid trees such as poplar and willow. European research into direct firing and cofiring biomass with coal for power generation has been fairly extensive with various agricultural biomass fuels such as wheat straw and wood waste product fuels (13–18). In the United States, research has focused primarily on cofiring arrangements for wood (19–26); more localized agricultural waste biomass fuels have been studied less intensely (27–31). A recent synopsis of biomass for energy production written by European researchers discussed issues and barriers to using biomass such as wood for energy production (32). Biomass combustion is summarized as having the following impacts: being excellent at reducing greenhouse gases, decreasing NO_x, destroying polychlorinated biphenyls, decreasing smog, increasing volatile organic compounds (greatly dependent upon combustion process), decreasing CO, stimulating landscape and forest conservation, and reducing soil erosion if the wood source is from dedicated resources such as tree farms (32, 33).

Biomass utilization by conventional coal-fired utilities will create some technical challenges. Design limitations of coal-fired boilers may also preclude the use of biomass beyond certain weight fractions of total fuel feed. Such limitations may include physical processing of the biomass for proper injection or feeding into the boiler. Other limitations include fireside performance of the biomass including its impact on flame stability, boiler HX surface fouling or slagging, and corrosion. With respect to processing and feeding biomass, various utilities in Europe and the United States

have either developed size-reducing methods that facilitate feeding the more fibrous and pliable biomass fuel into the boiler or, in many cases, separate injection ports have been installed (13, 14). Ash deposition and boiler tube corrosion can be issues because biomass can contain considerable alkali and alkaline-earth elements and chlorine which, when mixed with other gas components derived from coal such as sulfur compounds, promote a different array of vapor and fine particulate deposition in a coal-fired boiler (13–15, 18, 29). Biomass can also contain organically deposited minerals such as amorphous silica phytoliths (34) which are difficult to characterize with standard coal analysis methods and also behave differently than mineral silica forms such as quartz in coal. Initial assessments have been performed on the behavior of inorganic constituents of biomass during combustion (35) along with issues related to the cofiring of biomass–coal blends (36).

U.S. Biomass Resources

In most U.S. locations, the availability of biomass as a fuel feedstock is not reliable beyond 20% of a normal firing rate for coal, and usually much less. Cofiring biomass up to 20%, therefore, is a practical application for incorporating a renewable energy fuel into a coal-fired plant. Agricultural residuals are primarily available in the Midwest, Southeast, and mid-Atlantic regions, where there is a significant amount of farming. Forest resources and residuals are available in New England, mid-Atlantic, Southeast, upper Midwest, and Pacific Northwest.

Biomass has the potential to supply 24.7 EJ (23.5 quads) of energy for the United States, which represents approximately 28% of the U.S. energy consumption. This potential, as a function of the four major biomass categories, includes the following (37):

- Wood residuals – 3.7 EJ (3.5 quads)
- Agricultural residuals (from crops, food processing, and animals) – 1.7 EJ (1.6 quads)
- Dedicated energy crops – 17 EJ (16.1 quads)
- Urban wastes – 2.1 EJ (2.0 quads)

The alternative fuels under each category that can be considered as a resource for cofiring are listed in Table 1. To some extent, all of these fuels are candidates for use in industrial and institutional stoker-fired combustion units. The availability of each resource, however, may be limited to certain areas. A recent study completed by Schmidt and Pinapati concluded that collectible quantities of biomass (excluding energy crops) totaled 7 EJ (6.65 quads) (38).

Large volumes of wood residuals are generated by the wood products industry, including paper mills, sawmills, and furniture factories. While the wood products industry currently uses much of its own residuals, there is still a substantial amount available, particularly from smaller sawmills that individually have too little waste wood to justify investing in steam or power production. In cases where a number of these smaller mills are in the same vicinity, a centrally located plant can purchase residuals from sawmills within an approximately 120-km (75-mile) radius to secure a supply of wood residuals sufficient to generate a significant amount of steam and/or power. Another significant source of wood residuals culls from forest management (precommercial thinning of commercial forests where dead, dying, or unmerchantable trees are selectively removed to increase the productivity of forests).

Table 1. Biomass Subtypes

Agriculture Based	Forest Products	Urban Wastes	Dedicated Energy Crops
Harvest Residuals	*Logging Residuals*	*Residential*	*Grasses*
Wheat straw	Cull trees	MSW	Switchgrass
Rice straw	Tops	RDF (refuse-derived fuel)	Native grasses
Flax straw	Dead wood	Mixed paper	
Cornstalks	Small-diameter stock	Yard waste	
		Demolition wood waste	
		Scrap tires	
Processing Residuals	*Primary Wood-Processing Residuals*	*Urban and Landscape Residue*	*Trees*
Rice hulls	Sawdust	Leaves and grass clippings	Willow
Sugarcane bagasse	Bark	Chipped and unchipped wood	Cottonwood
Almond shells/hull	Edgings	Construction and demolition waste	Hybrid poplar
Olive pits	Slabs	Pallets/scrap	
Sugar beet pulp		Railroad ties	
Sunflower hulls			
Animal Wastes	*Secondary Wood-Processing Residuals*		*Others*
Poultry litter	Sawdust		Alfalfa stems
Feedlot wastes	Edgings		Specialty crops

Wood residuals obtained from sound forest management do not deplete the net forest resource base. Through sustainable practices, trees are either replanted or the forest resource is managed for regeneration to enhance its health and productivity in the future. In some areas of the country, like the Tahoe Basin, forest management is essential to prevent major forest fires.

Agricultural residuals offer substantial energy resources for various applications. Crop residuals, processing residuals, and food processing wastes are some components of the agricultural residual supply that can be used on-site or in regional facilities. Open-field burning of agricultural residuals was a common practice until recently when it was banned in many locations because of air pollution concerns. Opportunities to use these residuals for fuel have been tempered, however, by a number of concerns related to their transport, handling, and impact on combustion system performance.

Dedicated energy crops, including short-rotation woody and herbaceous crops (primarily tall grasses such as switchgrass) represent the greatest potential source of biomass resources. Hybrid poplar and willow are two common trees being studied for energy production. These trees will regrow vigorous shoots from the tree stumps that remain after harvesting, a form of regrowth that is known as coppicing. The resulting abundant new growth can be harvested again in 5–10 years. The ability to obtain numerous harvests from a single planting significantly reduces average annual costs for establishing and managing energy crops.

Production of energy crops also requires much less intensive management than for most traditional agricultural crops, especially in terms of lower inputs of fertilizers and pesticides. In addition, because the root systems of energy crops remain in the ground between harvests, energy

crops can help reduce soil erosion. The current cost of growing, harvesting, and transporting dedicated energy crops exceeds that of other waste biomass (as well as some fossil fuels), so subsidies of some sort or a mandatory percentage of biomass in the fuel mix will be required to promote near-term use of these materials.

MSW represents another significant source of biomass fuel. In the United States, paper and other organic materials typically represent a large portion of the waste stream—materials that make good combustion feedstock. Typically, 90% of the volume of MSW is combustible material. Other municipal and industrial wastes could also fuel an energy plant. Urban wood waste is another source of wood residuals, including tree trimmings, right-of-way and land clearance, waste wood from construction and demolition, broken wood pallets, fruit boxes, and other wood packaging. Nonbiomass urban wastes, including sewage sludge, also represent potential sources of energy in urban areas.

Technical Issues of Biomass Combustion

The usable energy in biomass typically ranges from about 15,105 to 19,752 kJ/kg (6500 to 8500 Btu/lb) on a dry basis. However, biomass is generally not delivered dry. On a wet (green) basis, biomass typically has a moisture content of 40%–50%, which reduces the energy value of green hardwoods to about 9295–10,457 kJ/kg (4000–4500 Btu/lb). The moisture content of a single source of biomass fuel delivered to a plant can vary significantly because of differences in factors such as harvesting, storage, and drying conditions. Biomass with a heating value of <8133 kJ/kg (<3500 Btu/lb) would be of little value to a suspension-fired or grate-fired plant since it would require a net energy input in order to sustain combustion.

Physical characteristics vary widely with biomass materials. For example, wood and grass have very different bulk densities. Nonwoody biomass spans a much wider range of characteristics than woody biomass. The bulk density of woody material is generally in the range of 160–240 kg/m^3 (10– 15 lb/ft^3). When biomass is densified by processing and compaction, its bulk density can be increased by 2 to 3 times. For example, the bulk volume of RDF, a processed form of MSW, is in the range of 400–433 kg/m^3 (25–27 lb/ft^3). By comparison, the bulk density of coal is approximately 721 kg/m^3 (45 lb/ft^3).

At the other end of the spectrum, agricultural materials such as loose straw can have a bulk density in the range of 16–40 kg/m^3 (1–2.5 lb/ft^3), although chopping or baling this type of material significantly increases its density. The tendency toward low weight per unit of volume translates into higher transportation costs. Thus options such as baling that keep the density higher for transportation purposes are especially important in considering the use of agricultural residuals (or herbaceous crops such as switchgrass). Their lower bulk density also means that special consideration must be given to handling and processing these materials as well as feeding them into combustion systems.

An important consideration for biomass is that the ash from some agricultural residuals and from new tree growth (e.g., the tops of trees or the ends of tree limbs) can have a relatively high alkaline metal content, particularly potassium and sodium. These alkaline metals tend to lower ash-melting temperatures and can increase ash deposition and fouling of boiler equipment. Other ash

constituents, such as chlorine, silica phytoliths, and phosphorus, can play a major role in developing ash deposits and fine particulate emissions. Special precautions such as temperature control can be taken to limit fouling. However, there will be certain biomass materials that will only make an acceptable fuel when blended with other low-alkali biomass or coal in cofiring applications. Biomass materials high in silica, such as rice hulls, can cause erosion problems in the convective pass of the boiler; however, proper selection of gas velocities and selective use of refractory can minimize the erosion.

The inert materials, plastics, and various types of contaminants in municipal waste are of concern when using these materials to produce energy. Experience with separation and processing of municipal waste into RDF and cofiring in boilers has shown that RDF can be an acceptable fuel for some boiler applications, especially fluid beds. Fluid-bed systems are much more forgiving of this "tramp" material than other combustion systems. Chlorine corrosion can be a concern with materials high in plastics.

The primary characteristics of biomass that require special attention when it is used as a fuel are summarized in Table 2. In all except the extreme cases, the stoker, in combination with cofiring, can be designed to deal with these troublesome characteristics.

Table 2. Fuel Characteristics Requiring Special Attention

Fuel Property	Troublesome Characteristics	Potential Problem	Proposed Solution
High Alkali (Na, K)	Formation of low-melting-point compounds	Slagging/fouling of convective surfaces	Low convective pass temperature (<760°C) Sootblowing
		Sintering on the grate	Low firing temperature Fuel mixing (dilution)
Scrap Material (rock, dirt, metals, glass)	Accumulation of rock and metal	Plugging, mechanical breakdown	Tramp removal system
	Glass and aluminum become molten	Sintering convective pass fouling	Presorting Sootblowing
Chlorine	Formation of alkali chlorides and HCl	Corrosion	On-grate chlorine capture Fuel mixing/dilution
	Formation of chlorinated organic compounds	Emissions exceeding local, state, or federal limits	Combustion air and temperature control
Bulk Density	Low bulk density	High transportation costs	Baling (compacting)
		High processing costs	Hydraulic ram feeder Fuel preparation

Direct combustion of biomass for energy production was initially viewed as a suitable replacement for fossil fuels. Ash-related problems, including slagging, agglomeration, corrosion, and erosion, can cause frequent unscheduled shutdowns, decreasing the availability and reliability of this energy source. In addition, fouling of heat exchange surfaces coupled with the high moisture in the fuel reduces system efficiency. The variable nature of the quality of biomass fuel also impacts the reliability and availability of biomass systems.

APPROACH

Task 1 – Pilot-Scale Testing

Description of the Pilot-Scale SFS

The EERC pilot-scale SFS was designed to simulate the conditions in a commercial-scale slagging furnace incorporating a HTHX for preheating the process air going to the GT in an IFCC system. It can be operated in an air-blown or oxygen (O_2)-blown configuration. The overall SFS is pictured in Figure 2, with a schematic of the air-blown system configuration shown in Figure 3. Figure 3 was recently updated to include system modifications made to permit SFS biomass cofiring in an air-blown configuration. The modifications were made such that switching between 100% coal firing and coal–biomass cofiring could be accomplished by changing a few piping connections associated with primary combustion air (PCA) flow and setting up a portable biomass refill system to support the loss-in-weight feeder metering biomass to the primary air line conveying fuel to the main burner.

Slagging Furnace

The pilot-scale slagging furnace is intended to be as fuel-flexible as possible, with maximum furnace exit temperatures of 1483°–1593°C (2700°–2900°F) to maintain the desired heat transfer to the HTHX and slag flow. The furnace has a nominal firing rate of 2.6×10^6 kJ/hr (2.5 MMBtu/hr) and a range of $2.1–3.2 \times 10^6$ kJ/hr (2.0–3.0 MMBtu/hr) using a single burner. The design is based on Illinois No. 6 bituminous coal (25,800 kJ/kg, or 11,100 Btu/lb) and a nominal furnace residence time of 3.5 s. Flue gas flow rates range from 12.0 to 18.6 m^3/min (425 to 645 scfm), with a nominal value of 15 m^3/min (530 scfm), based on 20% excess air. Firing a subbituminous coal or lignite increases the flue gas volume, decreasing residence time to roughly 2.6 s, and decreases flame temperature because of the higher moisture content of these fuels. However, the high volatility of the low-rank fuels results in high combustion efficiency (>99%). The EERC oriented the furnace vertically (downfired) and based the burner design on that of a swirl burner used on two smaller EERC pilot-scale pc-fired units (633,000 kJ/hr [600,000 Btu/hr]). Slagging furnace internal dimensions are 119 cm (47 in.) in diameter by 4.9 m (16 ft) in total length.

The vertically oriented furnace shell was designed to include four distinct furnace sections. The top section of the furnace supports the main burner connection, while the upper-middle furnace section provides a location for installation of the HTHX tubes. A 15-cm (6-in.) sight port is located in this section, directly across from the HTHX tubes, to allow for periodic observation of the tubes at furnace operating temperatures. The lower-middle furnace section supports the auxiliary gas burner; the bottom section includes the furnace exit to the slag screen as well as the slag tap opening. Flue gas temperature measurements are made using two Type S thermocouples protruding 2.5 cm (1 in.) into the furnace through the refractory wall and three optical pyrometers (flame, flue gas along the furnace wall near the HTHX tubes, and flue gas at the furnace exit). Furnace temperature is also measured using thermocouples located at the interface between the high-density and intermediate refractory layers and between the intermediate and insulating refractory layers. A pressure transmitter and gauges are used to monitor static pressures in order to track furnace performance. These data

Figure 2. Photograph of the pilot-scale SFS.

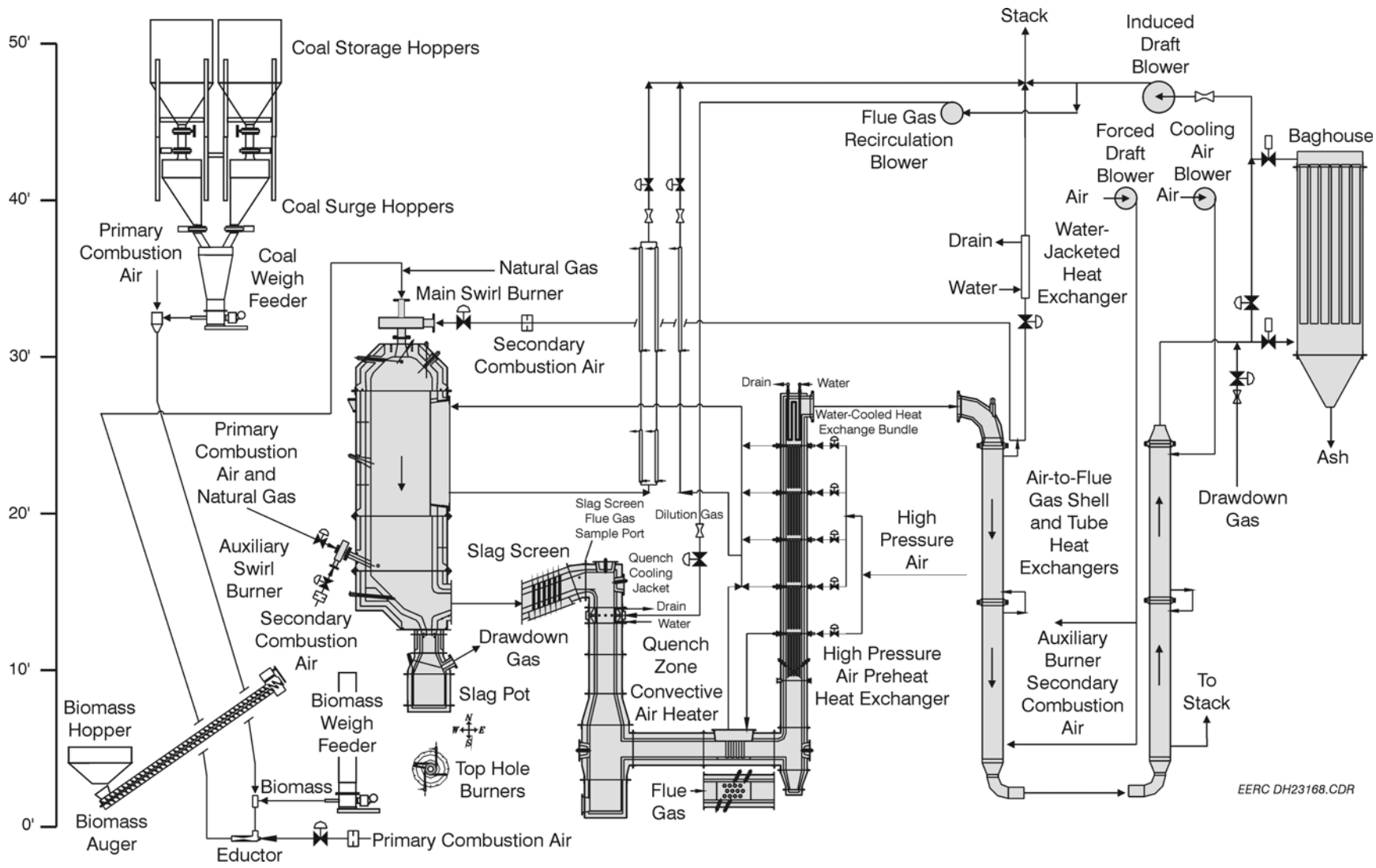

Figure 3. Illustration of the air-blown SFS configuration modified for biomass cofiring.

(temperatures and pressures) are automatically logged into the data acquisition system and periodically are recorded manually on data sheets as a backup. No furnace modifications were necessary to support coal–biomass cofiring in the SFS.

The slag tap is intended to be as functional yet low-maintenance as possible. The tap is lined with highly corrosion-resistant refractory. Its diameter is nominally 10 cm (4 in.), which is small enough to reduce radiant heat losses out of the furnace while minimizing plugging, and it has a well-defined drip edge. A two-port natural gas (NG)-fired burner is used to maintain slag tap temperature for good slag flow. To further minimize heat losses, slag is collected in an uncooled, dry container with refractory walls, rather than in a more typical water bath.

The refractory walls in the slagging furnace are composed of three layers of castable refractory. They consist of an inner 10.2-cm (4-in.) layer of high-density (2.1-W/m-K [14-Btu-in./ft^2 °F-hr]) slag-resistant material, 10.2 cm (4 in.) of an intermediate refractory (0.6 W/m-K [4.0 Btu-in./ft^2 °F-hr]), and a 8.3-cm (3.25-in.) outer layer of a low-density insulating refractory (0.2 W/m-K [1.3 Btu-in./ft^2 °F-hr]). Three refractory layers were selected as a cost-effective approach to keeping the overall size and weight of the furnace to a minimum while reducing slag corrosion and heat loss. The inner layer is composed of an alumina castable, developed by the EERC in cooperation with Plibrico, that was shown in laboratory tests to be extremely resistant to slag corrosion relative to other commercially available castable refractories. Table 3 summarizes properties for refractory material used in the SFS.

Fuel Feed System

The slagging furnace fuel feed system provides a NG- and a solid fuel-firing capability. The NG-firing capability supports preheating the SFS with the main burner as well as the operation of the auxiliary burner and the two-port slag tap burner. Each of the three burners has its own set of controls and flame safety system. The NG feed system is integrated into the overall process control and data acquisition system.

Solid-fuel firing only supports the operation of the main burner. Prior to this project, solid-fuel firing had only included pulverized (70% 75 µm, or <0.0030 in., with a 300-µm top size) bituminous and subbituminous coal, lignite, and limited petcoke cofiring. Two sets of feeder screws were acquired to meet coal–lignite feeder performance requirements for variations in fuel properties; the feeder gear ratio can be adjusted to achieve a fivefold change in feed rate capacity. Coal–lignite feed rates have ranged from 68.1 to 181.6 kg/hr (150 to 400 lb/hr) with the potential for the feeder to deliver fuel at rates of >227 kg/hr (>500 lb/hr). The three primary components of the coal–lignite feed system consist of two storage hoppers (1090 kg [2400 lb] each), two surge hoppers (227 kg [500 lb] each), and a loss-in-weight feeder. Each surge hopper has the capacity to refill the weigh feeder hopper twice, allowing for adequate time to change out the storage hoppers. Each surge hopper has a level indicator integrated with the process control and data acquisition system, which then opens and closes a valve supplying pc–lignite from the storage hopper in auto mode. The surge hoppers also can be manually refilled. A K-Tron solids feeder capable of operating in gravimetric (loss-in-weight) or volumetric feed modes using a twin-screw design to provide a uniform nonpulsing feed is being used.

Table 3. SFS Refractory Properties

Refractory:	Plicast Cement Free 99V KK/99V[1]	Plicast Cement Free 98V KK/98V[1]	Plicast Cement Free 96V KK/96V[1]	Narco Cast 60	Plicast LWI-28	Plicast LWI-20	Harbison-Walker 26
Function	High density	High density	High density	High density	Insulating	Insulating	Insulating
Service Limit, °C	1870	1870	1820	1700	1540	1100	1430
Density, kg/m^3	2960	2960	2960	2320	1300	880	1100
K, W/m-K @ 1100°C	2.18	2.18	2.10	0.98	0.60	NA[2]	0.33
K, W/m-K @ 816°C	2.21	2.21	2.13	0.90	0.45	0.26	0.29
K, W/m-K @ 540°C	2.33	2.33	2.25	0.84	0.41	0.20	0.26
Hot MOR[3] @ 1370°C, bar	44.8	51.7	96.5	NA	NA	NA	NA
Hot MOR @ 816°C, bar	—	—	140	69	17.2	6.9	7.58
Cold Crush Strength @ 816°C, bar	—	—	690	NA	51.7	28	24.1
Typical Chemical Analysis, wt% (calcined)							
Al_2O_3	99.6	98.6	95.5	62.2	54.2	39.6	53.8
SiO_2	0.1	1.0	3.8	28.0	36.3	31.5	36.3
Fe_2O_3	0.1	0.1	0.1	1.0	0.8	5.4	0.5
TiO_2	0.0	0.0	0.0	1.7	0.5	1.5	0.6
CaO	0.1	0.1	0.1	2.8	5.7	19.5	7.2
MgO	0.0	0.0	0.0	0.1	0.2	0.8	0.2
Alkalies	0.2	0.2	0.2	0.2	1.5	1.4	1.4

[1] The "KK" designation indicates the presence of fibers that promote dewatering during curing.
[2] Not applicable.
[3] Modulus of rupture.

Operation of the coal weigh feeder is integrated into the overall process control and data acquisition system with a user-programmable microprocessor and a 20-bit resolution load cell (high-resolution digital) assembly. Solids from the weigh feeder are discharged from the screws into an air eductor. The fuel is then pneumatically conveyed to the main burner through the primary air line. The feed hopper can be manually or automatically refilled. Initial pilot-scale project activities focused on acquisition and installation of a feed system to support biomass cofiring in the SFS and preparation of the fuel for the three pilot-scale coal–biomass cofiring tests planned. Design work for the biomass fuel feed system began in April 2003 and included specifications. Three equipment vendors were contacted based on operational experience with the existing coal feed system and with other projects having a biomass feed requirement. Based on vendor specifications and quotes, the EERC placed an order in June 2003 for a K-Tron K2-MLS100 feeder capable of operating in both gravimetric and volumetric modes. Other feeder specifications included 1) modular single-screw loss-in-weight feeder, 2) 20-bit resolution load cell (high-resolution digital), 3) user-programmable microprocessor control, 4) a feed rate of 0.04–0.57 m^3/hr (1.5–20 ft^3/hr) for low bulk-density materials (<641 kg/m^3 [<20 lb/ft^3]) and a nominal particle size of 3.18-mm (0.125 in.) top size, and 5) a minimum hopper capacity of 0.3 m^3 (10 ft^3).

To support operation of the biomass feeder, the EERC both procured and fabricated components to assemble a system to automatically refill the biomass feed hopper on a periodic basis. These components included an 20-cm × 9.5-m (8-in. × 31-ft) grain auger with a polymer hopper, a 4-kW (5-hp) electric motor and associated switching and wiring to operate the grain auger, and a stand to support a biomass charge hopper at the inlet of the auger. Modifications to existing piping runs and installation of new piping runs were necessary to simultaneously blend and transport the coal and biomass fuels in the PCA stream to the main burner. Software changes were made to the SFS data acquisition–process control system to continuously log biomass feed rate data and automatically refill the biomass feed hopper based on mass set points to start and stop the refill cycle.

Figures 4–6 are photographs of the biomass feed system set up to support this project. Figure 4 is a photograph of the biomass charge hopper and inlet of the grain auger used to deliver biomass to the loss-in-weight feeder as well as a dust control device used during refill cycles. Two charge hoppers, like the one positioned above the grain auger inlet in Figure 4, were used to transport air-dried biomass sized in a hammer mill and stored in steel bins for later use. Figure 5 is a photograph of the discharge end of the grain auger showing the flexible canvas connection to the biomass feed hopper, dust bag, and a cage around the top of the long straight-walled biomass feed hopper. The purpose of the cage was to prevent unintentional contact with, and impact on, weigh cell performance. Figure 6 is a photograph of the loss-in-weight screw feeder purchased to deliver biomass into the PCA stream supporting the main burner.

The main burner is NG- and pulverized fuel-capable. The basic design is an International Flame Research Foundation-type adjustable secondary-air swirl generator which uses primary and

Figure 4. Photograph of the biomass charge hopper and grain auger supporting the biomass feeder.

Figure 5. Photograph of the grain auger discharge and top of the biomass feed hopper.

Figure 6. Photograph of the biomass loss-in-weight screw feeder.

secondary air at approximately 15% and 85% of the total air, respectively, to adjust swirl. Increasing swirl to provide flame stability and increased carbon conversion can also affect the formation of NO_x. Carbon conversion has been >99% when bituminous, subbituminous, and lignite fuels are fired. High carbon efficiencies can be obtained at low swirl settings because of the high furnace operating temperature and adequate residence time. Combustion air flow rates through the main burner range from about 11 to 17 m^3/min (400 to 600 scfm), depending on furnace firing rate and the fuel type (bituminous, subbituminous, or lignite).

An auxiliary gas burner (maximum firing rate of 896,750 kJ/hr [850,000 Btu/hr]) is located near the furnace exit in order to control furnace exit temperature, ensuring desired slag flow from the furnace and the slag screen. This burner is used to compensate for heat losses through the furnace walls, sight ports, and HTHX test panel. Use of the auxiliary gas burner is beneficial during start-up to reduce heating time and to prevent slag from freezing on the slag screen tubes when the switch is initially made to coal firing.

NG-fired slag tap burners support operation of the SFS with respect to maintaining desired slag flow. The drawdown gas line, through which the flue gas generated by these burners is discharged, diverts this flue gas stream to the inlet of the baghouse during air-blown operation of the SFS. A flow measurement device and a control valve are used to control drawdown gas flow rate. The use of these burners is necessary to maintain proper slag flow when firing coal or other solid fuels in the slagging furnace.

Combustion Air System

Combustion air supporting the SFS's primary and auxiliary burners is supplied from compressed air for the primary air stream and a forced draft (FD) fan for the secondary air stream. The primary air stream is unheated and typically represents 15–20 vol% of the total combustion air; it conveys solid fuel to the primary burner from an eductor and screw feeder arrangement. For the purpose of this project, the eductor was relocated in the primary air stream, and modifications were made to the primary air line to allow pickup of the coal followed by the biomass from the two loss-in-weight feeders.

During air-blown operation, the secondary air stream supporting the main burner is preheated in two tube-and-shell HXs that recover heat from the flue gas. Secondary air for the auxiliary burner is unheated. The secondary air stream to the burners represents 80–85 vol% of the total.

Slag Screen

As the hot gases leave the combustion zone, they pass through a slag screen that removes the entrained ash as a nonleachable slag. The slag screen design for the pilot-scale SFS is the result of a cooperative effort between the EERC, UTRC, and Physical Sciences, Inc. The primary objective for the slag screen is to reduce the concentration of ash particles entering the convective air heater (CAH). Criteria specific to the pilot-scale slag screen include 1) a simple design permitting modifications using readily available, inexpensive materials; 2) matching duct dimensions and flue gas flow rates to maintain turbulent flow conditions; 3) minimizing the potential for plugging as the result of slag deposit growth on tube surfaces or the sloped floor; 4) limiting differential pressure

across the slag screen to 4 mmHg (2-in. W.C.); and 5) limiting heat losses to ensure desired slag flow from the slag screen to the furnace slag tap. The slag screen flue-gas approach velocity is 21.4–22.9 m/s (70–75 ft/s), depending on furnace firing rate and fuel type. The flue gas outlet temperature from the slag screen must be >1371°C (>2500°F) for a bituminous coal to minimize the potential for slag freezing in the slag screen. However, for subbituminous coals and lignite, a slag screen exit temperature of 1316°C (2400°F) may be adequate to maintain slag flow and prevent slag accumulation and slag screen plugging.

The slag screen typically makes use of six rows of three 3.8-cm (1.5-in.)-diameter vertical tubes mounted in an upwardly sloped duct (20 degrees) to facilitate slag flow from the slag screen into the furnace slag tap. The center line-to-center line tube spacing in each row is 9.5 cm (3.75 in.). Center line-to-center line spacing between individual rows is 10.2 cm (4 in.). Internal duct dimensions for the slag screen are 25 cm × 33 cm × 1.1 m (10 in. × 13 in. × 3.5 ft). The resulting flue gas velocity through the slag screen is roughly 28 m/s (91 ft/s). Depending on the fuel type or operating conditions, every other row of cooling tubes may be removed to ensure adequate temperature in the slag screen.

Slag screen tubes are fabricated using castable high-density refractory poured inside aluminum pipe. The aluminum pipe makes a structurally sound form during curing and eventually melts and runs into the slag pot as furnace temperatures rise. Water-cooled tubing inside the refractory tubes and the in floor of the furnace exit–slag screen inlet are intended to cool the refractory surfaces in order to minimize erosion and corrosion. Based on slag screen operating experience with bituminous, subbituminous, and lignite fuels, EERC personnel have determined that the high-density refractory is an acceptable tube material and that the size of the water-cooled tubes inside of the high-density refractory must be changed according to the type of fuel fired. During lignite- and subbituminous coal-fired tests, more cooling is necessary to build up a sufficiently thick frozen slag layer to protect the slag screen tubes from the severe erosion–corrosion attack that can occur within the slag screen. The diameter of the stainless steel water tubes inside the slag screen tubes is typically 1.3 cm (0.5 in.) o.d. in the first row and second row (depending on ash fusion temperature data), and 0.952 cm (0.375 in.) o.d. in the remaining four rows. However, it is necessary to reduce the size of the water tubes to 0.63 cm (0.25 in.) o.d. in all but the first row for Illinois No. 6 bituminous coal firing, with the o.d. of the water tubes in the first row reduced to 0.952 cm (0.375 in.). For fuels with more refractory ash, such as an eastern Kentucky bituminous coal, only three rows of tubes are used in order to maintain slag flow out of the screen section. The first row used 0.952-cm (0.375-in.)-o.d. water tubes, and the second and third rows used 0.63-cm (0.25-in.)-o.d. water tubes. The pilot-scale slag screen tubes will always require periodic replacement based on some level of erosion–corrosion and the fuels selected for testing. However, in a larger demonstration or commercial-scale unit, steam-cooled steel tubes could be used without a refractory coating, as long as a frozen slag layer can be maintained on the surface of the tubes.

For the coal–biomass cofiring tests, six rows of tubes were employed in the slag screen. The diameter of the stainless steel water tubes inside the slag screen tubes was 1.3 cm (0.5 in.) o.d. in the first and second rows, and 0.952 cm (0.375 in.) o.d. in the remaining four rows. Type S thermocouples, one each in the vicinity of the first and last row of tubes, are used to monitor slag screen temperature. However, these measured temperatures are believed to be lower than the actual flue gas temperatures because the thermocouples are located behind individual water-cooled slag

screen tubes and because of observed thermocouple deterioration by slag attack. Therefore, slag screen temperature control is based on an optical pyrometer measurement at the furnace exit–slag screen inlet. The EERC operates the slag screen at flue gas temperatures of at least 56°–112°C (100°–200°F) above the fluid temperature of the fuel ash to ensure slag flow from the slag screen to the slag tap. Thermocouple data are automatically logged on the data acquisition system. To monitor and record slag screen differential pressure, pressure taps were installed in the roof upstream and downstream of the tubes. As a backup to the data acquisition system, slag screen data periodically are recorded manually on data sheets. Mass balances are completed for all SFS operating periods in order to document the distribution of slag and ash in the system.

Dilution–Quench Zone

As the hot combustion gas leaves the slag screen, it is quenched with recirculated flue gas to 1010°C (1850°F) in order to reduce the stickiness of the remaining entrained ash to minimize deposition on the CAH tubes. Because of the stickiness of the ash and the high turbulence caused by the injection of the recirculated flue gas, the quench zone is the only region in the furnace where hard slag and ash deposits form. These deposits are removed online by knocking them into a hopper at the bottom of the zone.

The design of the dilution–quench zone was a cooperative effort between the EERC and UTRC. The zone has a circular cross section and is oriented vertically so that ash deposits can be easily removed. It has a 0.36-m (1.17-ft) diameter in the area of the FGR nozzles and then expands to 0.6 m (2 ft) to provide adequate residence time within duct-length constraints. The duct section containing the FGR nozzles is a water-cooled spool piece in order to permit changes to the size, number, and orientation of the FGR nozzles. The water-cooled wall appears to embrittle the slag deposits that form in this area, making them more prone to spontaneous shedding and generally easier to remove online. The vertically oriented dilution–quench zone is refractory-lined and located immediately downstream of the slag screen and upstream of the CAH duct. Routine cleaning of the dilution–quench zone is required during each weeklong coal- or lignite-fired test. A pressure transmitter is used to monitor and record differential pressure across the zone as an indication of slag deposition.

Process Air Preheaters

Process air required for operation of the CAH tube bank and the HTHX is preheated in five high-temperature alloy tube bundles located in the flue gas duct downstream of the CAH tube bank. The first tube bundle supports operation of the CAH tube bank, and the remaining four support the operation of the HTHX. Because of high flue gas temperatures (927°C [1700°F]) in the vicinity of the first three process air preheaters and a nominal operating air pressure of 10.3 bar (150 psig), all five tube bundles were fabricated using an RA253MA alloy rated for 899°C (1650°F) at 10.3 bar (150 psig) to maximize system flexibility and minimize the potential for material failure. An HR-160 alloy, rated for 955°C (1750°F) at 10.3 bar (150 psig), was selected to transfer the heated process air to the HTHX and CAH test sections. Use of the HR-160 alloy permitted the installation of electrical heaters to improve process air temperature control to the HTHX test section. The use of the two alloys in combination for the process air preheaters maximizes system flexibility.

The tube bundles are mounted in a refractory-lined, vertically oriented, square duct. Duct dimensions are 30.5 cm × 30.5 cm (12 in. × 12 in.), with an overall duct length of 6.2 m (20.5 ft). The refractory used in this section was a combination of Narco Cast 60 high-density refractory and Harbison-Walker 26 insulating refractory. All inlet and outlet process air lines supporting the CAH tube bank are insulated. Process air lines supporting the HTHX are insulated and electrically heated.

During coal firing, it is possible to obtain process air temperatures of 705°C (1300°F) at flow rates of 5.7 m^3/min (200 scfm), even though the heat-transfer rate degrades with ash deposition on the tube surfaces. Further heating of the process air entering the HTHX is achieved electrically and by recovering heat from the CAH tube bank. Air compressor system and power failures were encountered during previous projects to evaluate the performance of the CAH tube bank and HTHX, resulting in the use of the nitrogen backup system. The nitrogen backup system functioned as intended during these support system failures, supplying an emergency cooling medium to the process air preheaters and, ultimately, supporting the CAH tube bank and HTHX.

Flue Gas Heat Exchangers

The pilot-scale SFS has four tube-and-shell HXs for heat recovery and flue gas temperature control and two water-cooled HXs to reduce the heat load on system fans. Their location in the overall process layout is illustrated in Figure 3. The first two tube-and-shell HXs reduce flue gas temperature and preheat the secondary air for the main burner in the air-blown configuration. The third and fourth tube-and-shell HXs are used to control flue gas temperature at the inlet of the pulse-jet baghouse.

The tube-and-shell HXs have performed up to expectations during all test periods. In the air-blown configuration, the main burner secondary combustion air temperature is 316°–427°C (600°–800°F), depending on ambient air temperatures. During winter months, the secondary air temperature can be controlled at the lower end of the range, and during summer months, temperature control is limited to the higher end of the range. Tube-and-shell HXs 3 and 4 perform well, controlling the flue gas temperature at the baghouse inlet to <205°C (<400°F). Inspection during maintenance after each week of coal-fired operation indicates the presence of a scale-type ash layer on the surface of the tubes that must be removed in order to avoid deterioration of heat-transfer performance and corrosion of metal surfaces.

Two water-cooled HXs were fabricated and installed to reduce the load on the FD, induced draft, and process air fans and ambient temperature on the upper levels of the SFS support structure. A water-cooled heat exchange tube bundle was installed in the flue gas stream between the five high-pressure process air preheater tube bundles and the first tube-and-shell HX. This water-cooled tube bundle reduces the cooling load on the FD and process air fans. A water-jacketed HX was installed on the secondary air bypass line to the stack to reduce the amount of heat being emitted to the immediate area and the resulting ambient temperature in the high bay.

Emissions Control

A pulse-jet baghouse is used for final particulate control for the SFS. The baghouse design permits operation at both cold-side (121°–205°C [250°–400°F]) and hot-side (316°–371°C [600°–

700°F]) temperatures. The primary baghouse chamber and ash hopper walls are electrically heated and insulated to provide adequate temperature control to minimize heat loss and avoid condensation problems on start-up and shutdown. The main baghouse chamber was designed with internal angle iron supports to handle a negative static pressure of 37 mmHg (20 in. W.C.).

Flue gas flow rates to the baghouse can range from a low of 17.8 m^3/min (630 scfm) at 177°C (350°F) to a maximum of 30.1 m^3/min (1063 scfm) at 371°C (700°F). Therefore, the baghouse design was based on an average flue gas flow rate of 24.1 m^3/min (850 scfm) at 177°C (350°F) or 53.8 m^3/min (1900 acfm) at 371°C (700°F), based on a nominal furnace firing rate of 2.6×10^6 kJ/hr (2.5 MMBtu/hr). The baghouse is sized to accommodate a maximum of 36 bags mounted on wire cages with 5-cm (2-in.) bag spacing. Bag dimensions are nominally 15.2 cm (6 in.) in diameter by 3.0 m (10 ft) in length, providing a total filtration area of 52.5 m^2 (565 ft^2).

Each filter bag is secured to the tube sheet using a snap band sewn into the top cuff. Stainless steel (304 SS) wire cages with 20 vertical wires and 15-cm (6-in.) ring spacing provide bag support. The pulse-jet baghouse is a single compartment capable of either online or off-line cleaning. Pulse-jet cleaning can be triggered as a function of baghouse differential pressure or as a function of time. High-pressure–low-volume and low-pressure–high-volume cleaning options were included in the design of the pulse-air system. During heatup and off-line cleaning, flue gas flow is diverted directly to the stack or through a cyclone. One set of bags was used in support of this project: a 744-g/m^2 (22-oz/yd^2) woven glass bag with a polytetrafluoroethylene (PTFE) membrane.

The SFS does not have a flue gas desulfurization system for SO_2 control. Dispersion modeling data developed by the North Dakota Department of Health indicate that stack height, flue gas velocity at the stack exit, and the dilution effect of the system process air that is exhausted through the stack permit a maximum SO_2 emission rate of 9.4 kg/hr (20.8 lb/hr). However, based on operating experience with bituminous, subbituminous, and lignite fuels, the SFS has never exceeded a SO_2 emission rate of 7.7 kg/hr (17 lb/hr).

Instrumentation and Data Acquisition

The instrumentation and data acquisition components for the pilot-scale SFS address combustion air, flue gas, process air and water, temperatures, static and differential pressures, and flow rates. The data acquisition system is based on Genesis software and three personal computers. Two sets of flue gas instrumentation (O_2, CO_2, CO, SO_2, and NO_x) are dedicated to support the SFS in an air-blown mode. Flue gas is transferred from the sample point through a heated filter and sample line to the sample conditioner before it reaches the analyzers. Continuous flue gas sampling occurs between the slag screen and the dilution–quench zone to monitor and control slagging furnace operation. Flue gas is continuously sampled at the exit of the baghouse to monitor the SFS for air leaks as well as stack emissions. Total flue gas flow rate through the SFS is measured using a venturi.

High-Temperature Heat Exchanger

A key design feature of the furnace is accessibility for installation and testing of HTHX tubes. The HTHX panel was designed for testing material lifetimes and heat exchange coefficients and is

0.46 × 1.96 m (1.5 × 6.4 ft). This size was based on manufacturing constraints identified by UTRC, which designed and built the original HTHX, as well as a desire to minimize furnace heat losses. The HTHX contains three vertically oriented tubes originally made of MA754, a nickel-based ODS alloy. Process air for the HTHX is provided by an EERC air compressor system. Maximum air capacity available to support the HTHX is 11.3 m^3/min (400 scfm) at a delivery pressure of 10.3 bar (150 psig). As it passes through the HTHX, the process air is heated from nominally 538° to 705°C (1000° to 1300°F) to as high as 1094°C (2000°F).

A tie-in to an existing nitrogen system was also installed as a backup to the existing air compressor system to prevent the HTHX from overheating in the event of a power outage. In the event of a failure of inlet process air piping, a backflow emergency piping system was installed so that overheating of the HTHX could be avoided.

Concurrent to SFS modifications to permit coal–biomass cofiring, one of the MA754 alloy tubes in the HTHX was replaced with a tube manufactured using the new MA956 alloy. This is an iron-chromium-aluminum based ODS alloy that forms an alumina surface layer through oxidation that is typically much more resistant to corrosion than the chromia surface layer formed on the MA754 alloy. The MA956 alloy is described in more detail in the sections related to the bench-scale testing. Once the new alloy tube and connections were fabricated, the HTHX was hydraulically pressure tested to 103.4 bar (1500 psig) in order to verify that no leaks existed prior to its installation in the furnace wall. As was the case for previous air-blown tests without tile protection, the lower half of the HTHX was encased in insulation and refractory to limit furnace exposure to the top half of the HTHX because of process air limitations. In addition, it was necessary to encase the top 6 in. of the HTHX in low- and high-density insulating materials to protect the bolting materials and connections used in the installation of the MA956 alloy tube from furnace conditions. Therefore, only 39% of the HX surface was exposed to furnace conditions during the coal–biomass cofiring tests completed in support of this project. That represents an additional 22% reduction in exposed surface when compared to air-blown HTHX tests previously completed in support of other projects. Figure 7 is a photograph of the HTHX after the MA956 iron–chromium–aluminum ODS alloy tube was added and the HTHX was installed in the slagging furnace.

Convective Air Heater

The CAH design was a cooperative effort between the EERC and UTRC. It was constructed by UTRC and installed by the EERC in September 1997. The flue gas flow rate to the CAH tube bank has been calculated by the EERC to range from 101 to 131 m^3/min at 982°C (3553 to 4619 acfm at 1800°F), depending on the fuel and firing rate in the SFS. A rectangular inside duct dimension of 0.11 m^2 (1.17 ft^2) results in a flue gas approach velocity of 15–22 m/s (50–73 ft/s) to the CAH tube bank. Heat is recovered from the flue gas to meet process air temperature requirements for the CAH as well as the HTHX panel. The design process air exit temperature from the CAH is

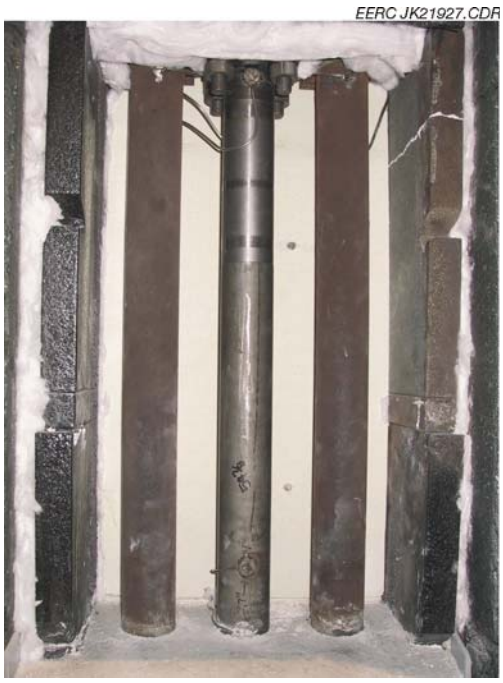

Figure 7. Photograph of the HTHX, modified to include a center tube of MA956 alloy, prior to Test SFS-XCEL1-0303.

649°C (1200°F) and is not permitted to exceed 705°C (1300°F). Process air flow is used to control process air exit temperature using a flow control valve.

The CAH tube bank consists of twelve tubes installed in a staggered three-row array. The first five tubes in the flue gas path are uncooled, with the remaining seven tubes cooled using heated air. Beginning in September 1998, the uncooled tubes consisted of three high-temperature alloys, each with a different pipe size. They were 3.8-cm (1.5-in.) Schedule 80 INCOLOY MA956, 2.5-cm (1-in.) Schedule 40 INCOLOY MA956HT, and 1.9-cm (0.75-in.) Schedule 40 PM2000. At the request of UTRC, two of these uncooled alloy tubes were removed from the CAH tube bank following a September 1999 test and returned to UTRC for characterization. The tubes removed from the CAH were composed of INCOLOY MA956HT and INCOLOY MA956. Replacement tubes were fabricated using 3.8-cm (1.5-in.) Schedule 40 stainless steel pipe.

The seven air-cooled tubes in the CAH tube bank were fabricated using 5-cm (2-in.) Inconel 625 tubing with a 0.478-cm (0.188-in.) wall thickness. Prior to an August 1998 test, fins were added to the air-cooled tubes in the CAH to improve heat transfer. The fins are 2.5-cm (1-in.) by 0.318-cm (0.125-in.) flat material and run the length of each tube on both the leading and trailing edges of the tube surface. Based on the subsequent data, it appears that the addition of the fins improved heat recovery during coal-fired test periods. The fins appear to have reduced the rate of heat-transfer degradation as ash deposits developed and helped to maintain a higher heat-transfer rate once the deposits had formed. However, no improvement in heat recovery was observed during NG-fired periods with clean tube surfaces. Figure 8 illustrates the position, size, and alloy type for the CAH

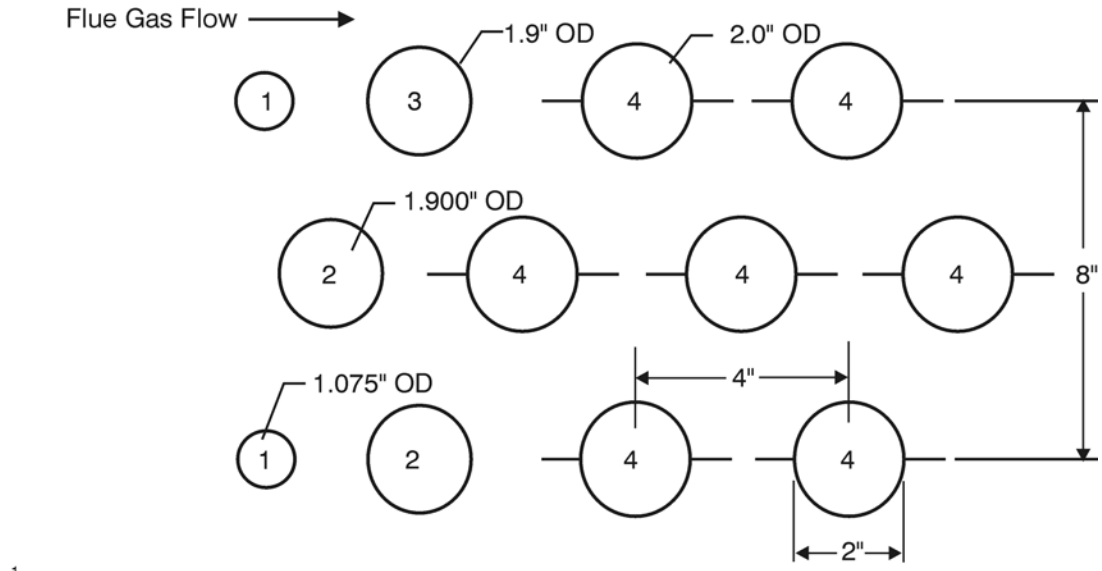

Figure 8. Illustration of the tubes in the CAH tube bank for Tests XCEL1–XCEL3.

tubes in place during the HTHX tests. Figure 9 is a photograph of the CAH tube bank showing the CAH tubes illustrated in Figure 8.

SFS Operations

Three pilot-scale SFS biomass cofiring tests were completed in support of this project. Each test involved cofiring biomass with North Antelope subbituminous coal on a nominal-firing-rate (kJ/hr or MMBtu/hr) basis of 80% coal and 20% biomass. The three biomass fuel types selected for these tests were hog fuel (a forest industry by-product) and two agriculture-based fuel sources (corn stover and switchgrass). Coal and biomass fuels were blended, on a mass basis, using two loss-in-weight gravimetric feeders, into the primary air line supporting the operation of a single burner. Only 39% of the HTHX alloy surface was exposed to furnace conditions during the biomass cofiring tests because of limitations on process air available to prevent overheating the alloy surfaces. Based on ash characterization, alloy tube surface temperature was limited to <1052°C (<1925°F) to minimize the potential for slag corrosion/erosion of the alloy tube surfaces. Table 4 summarizes some general information concerning the three test periods.

The approach used for each coal–biomass cofired test involved preheating the SFS while firing NG. During Test SFS-XCEL1-0303, the NG-fired period was somewhat longer in order to cure some new refractory in the furnace and slag screen. Test plans called for cofiring coal and biomass for nominally 85 hr on a continuous basis.

Figure 9. Photograph of the CAH tube bank used in support of Tests XCEL1–XCEL3.

Table 4. SFS Run Summary for the Coal–Biomass Cofiring Tests

Dates	10/9 to 10/17/03	11/14 to 11/21/03	12/12 to 12/19/03
Run Number	SFS-XCEL1-0303	SFS-XCEL2-0403	SFS-XCEL3-0503
Fuel Type	Natural gas North Antelope subbituminous coal Hog fuel	Natural gas North Antelope subbituminous coal Corn stover	Natural gas North Antelope subbituminous coal Switchgrass
Firing Rate Basis, kJ/hr or MMBtu/hr	80% coal 20% biomass	80% coal 20% biomass	80% coal 20% biomass
Convective Air Heater Use	Yes	Yes	Yes
HTHX Use	Yes	Yes	Yes
Natural Gas Firing, hr[1]	103	89	88
Coal Firing Rate, kg/hr Duration, hr	77.1 to 99.8 85	77.1 to 83.9 86	75.3 to 84.4 85
Biomass Firing Rate, kg/hr Duration, hr	23 to 41 83	26 to 29 86	23 to 27 85
Total Hours of Furnace Firing	188	175	173

[1] Natural-gas firing included heatup and cooldown and refractory curing when necessary. North Antelope subbituminous was the only coal fired in support of these biomass-cofired HTHX tests.

Slagging furnace operation was evaluated relative to furnace temperature (flue gas and refractory) and pressure measurements and online flue gas instrumentation readings (O_2, CO, CO_2, NO_x, and SO_2). A nominal coal–biomass cofiring rate of 2.3×10^6 kJ/hr (2.2 MMBtu/hr) at an air-to-fuel ratio of about 1.2:1 was anticipated to achieve furnace gas temperatures of nominally 1483°C (2700°F) near the furnace wall. The North Antelope subbituminous coal used for these tests is similar to other subbituminous coals fired in the SFS. Therefore, where appropriate, comparative data are presented for 100% coal-fired SFS tests for discussion purposes and development of conclusions concerning the impacts of biomass cofiring.

Special emphasis was placed on the collection of data to document the performance of the HTHX located in the furnace wall. Performance was evaluated relative to heat transfer from the furnace to the hot process air stream and the impact of slag on the high-temperature alloy heat-transfer surfaces. The furnace firing rate was adjusted during each test to achieve the desired HTHX surface temperature range for a nominal HTHX process air flow rate of 11.0 m^3/min (390 scfm). Temperature measurements were made at the surfaces of the alloy heat-transfer tubes as well as the bulk inlet and outlet process air. Photographs were taken to document observations before and after each test period. Ash and slag samples were recovered from the HTHX alloy surfaces for characterization.

Furnace exit, slag tap, and slag screen operating temperatures were a function of the main burner, auxiliary burner, and tap-hole burner firing rates, selected based on ash fusion data for the cofired subbituminous coal and biomass. These system temperatures are generally controlled at 56°–111°C (100°–200°F) above the fluid temperature of the slag under oxidizing conditions but can be higher when necessary to achieve desired furnace temperatures. The required FGR rate in the dilution/quench zone depends on the slag screen exit temperature. The FGR rate was controlled to achieve a flue gas temperature of 983°–1010°C (1800°–1850°F) entering the CAH tube bank.

Performance of the CAH tube bank was evaluated relative to heat transfer from the flue gas to the hot process air stream and the impact of ash deposition on the alloy tube surfaces. Temperature measurements were made to document the surface temperatures of the alloy heat-transfer surfaces as well as bulk inlet and outlet process air temperatures. Heat recovery from the CAH tube bank is integral to the preheating of process air for the HTHX panel in the furnace. However, it was not necessary to remove ash deposits from the CAH tube surfaces in order to achieve the process air conditions required to effectively support the operation of the HTHX. As a result, data concerning deposition rate on the CAH heat-transfer surfaces were estimated based on the weight of deposits collected and the duration of coal–biomass cofiring for each test period.

CAH ash deposits collected during each test were characterized to determine chemical composition and relative strength. Specific analyses included x-ray fluorescence (XRF), scanning electron microscopy (SEM) point count, and SEM morphology. Acquiring this information is important because biomass cofiring and the firing characteristics of the SFS concept represent a firing condition different from either pc or cyclone firing. Specifically, the flame is less turbulent, which increases its length and reduces NO_x formation, but flame and furnace temperatures are greater than in pc firing because of reduced radiant losses to the furnace walls. In addition, air-to-fuel ratios are higher than with cyclone firing.

Flue gas composition (O_2, CO, CO_2, NO_x, and SO_2) was monitored continuously using online instrumentation at the exit of the furnace and pulse-jet baghouse. SO_2 and nitrogen species data are reported on a g/10^6 kJ (lb/MMBtu) and concentration basis. Particulate sampling was completed at the inlet and outlet of the baghouse during each SFS test period. Sampling at the inlet of the baghouse documented particulate mass loading and size distribution. Sampling at the outlet of the baghouse documented particulate mass emissions. Particulate emissions are reported on a g/10^6 kJ (lb/MMBtu) and mass-per-unit-volume basis. Baghouse differential pressure was continuously monitored to document cleaning frequency and effectiveness of online cleaning.

Composite samples of coal, biomass, slag, and baghouse ash were collected for routine analysis. One composite coal and biomass sample was analyzed for each week of operation. Analyses included ultimate, proximate, Btu, dry sieve, ash fusion (oxidizing), XRF, computer-controlled SEM, and ash viscosity. Analysis of slag involved one composite sample for each week of operation and included ash fusion and composition. One baghouse ash composite sample was characterized for each week of operation. Analyses included Malvern particle size, carbon–hydrogen–nitrogen, major element composition, and SEM morphology. Composite samples of ash from other locations in the system were collected on an as-needed basis. Analyses of these samples depended on system performance observations and data analysis.

The balance of this report describes the SFS in some detail and summarizes process data and observations, sample analyses results, and conclusions for all three coal–biomass cofired tests (SFS-XCEL1-0303, SFS-XCEL2-0403, and SFS-XCEL3-0503). Where warranted, recommendations for future work are discussed.

Task 2 – Laboratory-Scale Testing

Joining

The ODS alloys used to construct the HTHX exhibit extremely high corrosion and creep resistance. These properties are imparted to the alloys because of the dispersion of the yttria particles throughout the alloy structure. However, because they must remain dispersed, the alloys cannot be welded because melting would allow the oxides to segregate in the joint, diminishing the usefulness of the metal. Therefore, the EERC is working with Oak Ridge National Laboratory (ORNL) to develop a method for joining the MA956 using transient liquid-phase (TLP) bonding. In the TLP method, a thin foil of a proprietary alloy is placed between the pieces to be joined, and the joint is heated, causing interdiffusion of the ODS and foil materials at temperatures well below the melting point of the ODS metal. If the oxides stay well-dispersed within the joint, then the joint should maintain a high fraction of the maximum usable temperature of the ODS material.

The pieces of MA956 used in these joining tests were one-in. lengths of 2 ½-in. diameter pipe cut from the same stock used to replace the center tube in the HTHX. Each 1-in. length was cut in half, and one cross section of each half was polished with a series of silicon carbide and diamond polishing compounds. The polished surface of one section of pipe was covered with the joining alloy foil, then the polished surface of the other was placed on top. The sandwich was then clamped together with a two-screw c-clamp configuration machined out of the same alloy to assure that there would not be a thermal expansion mismatch between the clamp and the pieces to be joined. The

clamped pipe sections were then heated in a tube furnace in various atmospheres and heating schedules. After each test the joined pieces were struck with a hammer, and if the pipe sections gave way the joints were deemed failures. Successful joints were cut perpendicularly to the join, polished, then examined in the SEM. In particular, determinations were made of how well the joining alloy had diffused into the ODS alloy, and how much porosity remained at the joint. Three of the joined pieces that showed good diffusion of the joining alloy and low porosity at the joints were sent to ORNL for tensile strength testing under the DOE Fossil Energy Materials Program. At the time of this report those tests had not yet been completed.

Slag Viscosity Measurements

The use of biomass alone or in combination with coal for power production in conventional coal-fired units is associated with a number of problems mainly created by the extremely reactive nature of its ash. These include slagging, fouling, corrosion, and erosion which can cause frequent unscheduled shutdowns, decreasing the availability and increasing the cost of the produced power. In particular, the flowing slag may severely corrode the HTHX if liquid slag is in contact with the alloy. To prevent corrosion, the surface of the HTHX must be operated below the solidus temperature of the slag. In order to determine the melting and rheological properties of the biomass and biomass–coal slags so that the solidus temperatures can be inferred, their viscosities were measured with a high-temperature rotational viscometer, and their crystallization behavior upon cooling was measured by heated-stage x-ray diffraction (XRD). These tests were performed by Dr. Stelios Arvelakis, a postdoctoral student from the Denmark Technical University, during the summer of 2003.

The coal–biomass ash mixtures were formed by mixing ash from the biomass fuels with coal ash on a basis of 20% thermal input of the correspondent coal–biomass blends. In the case of the hog fuel, one additional mixture was formed on the basis of 10% thermal input.

The viscosity measurements were performed using a Haake high temperature rotational viscometer shown in Figure 10a. The crucible stands on the top of a cylindrical alumina pedestal shown in Figure 10b, with a diameter of 39 mm (1.5 in.) and length of 152 mm (6 in.). Before the start of the measurement the ash material was preheated to 900°C (1700°F) in a porcelain dish to burn any residual carbon, and then was pre-melted in a Pt-Rh 80/20 dish using a muffle furnace for at least 2 hr to assure that it was at chemical thermodynamic equilibrium under the conditions of the viscometer. During this process the melting temperature of the slag and subsequently the working temperature of the viscometer was determined. After pre-melting, the material was cooled, then crushed with a hammer and used to fill the crucible used in the viscosity measurements. During the measurement the slag is heated up to a temperature 50°C (90°F) higher than its apparent liquidus temperature observed in the pre-melting step, and then the viscometer bob is submerged into the slag until the slag just covers its top. For standard test the bob was rotated at 45 rpm. In order to determine how the viscosity of the slag depended on the shear (rotational) rate, in some cases additional tests were also performed at higher rotational speeds. Slags that have viscosities which are relatively independent of shear are known as Newtonian slags. However, it is known that the viscosity of some liquids depends on the shear rate of the measuring apparatus. It would be of

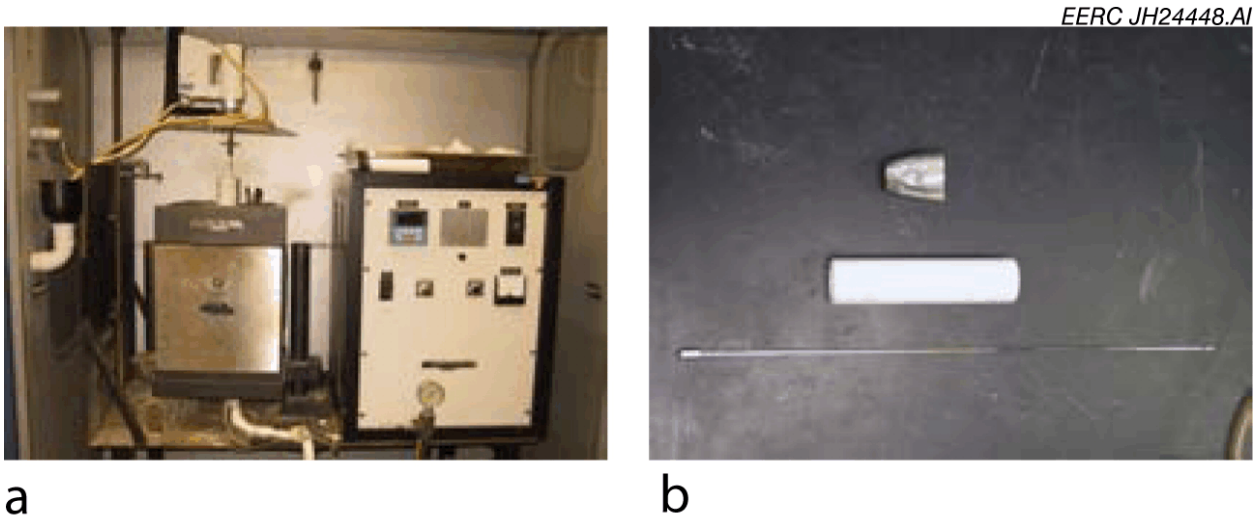

Figure 10. Experimental setup: a) test rig, b) test components.

particular interest if the slags tend to have a lower viscosity at higher shear rates, in other words, are shear-thinning. If this was the case, it may then be possible to clear a slag dam within a combustor simply by applying an external vibrator to the wall of the combustor at the point of the dam.

Flowing Slag Corrosion Testing of HTHX Alloy

Six flowing-slag corrosion tests were performed on MA956, the alloy used in the HTHX. The three SFS cofire slags was used, each at two temperatures. The EERC bench-scale dynamic slag application furnace (DSAF) was modified to permit measuring the corrosion rates of sections of cooled alloy pipe to flowing slag. Figure 11 shows a schematic of the system. During a test, the furnace is heated to 1500°C (2730°F) while the surface of the alloy tube section is cooled to the desired temperature by an internal air flow. The slag is screw-fed into the furnace system as sandlike grains where it drops into a platinum melting pan. The slag was collected from the SFS after each cofire test, when it was ground to a size range of 20 × 80 mesh. After melting in the platinum pan, the slag drips onto the surface of the cooled alloy tube section at approximately the 11 o'clock position. It is administered at a rate equal to the maximum expected in the pilot-scale system. It then flows around the cooled tube and drips off the alloy between the 6 and 7 o'clock positions, and out of the furnace through a hole in its bottom. After 100 hr of slag exposure, the DSAF is cooled, the alloy tube is removed and photographed, and its diameter is measured with a caliper. The surface is then sprayed with dilute epoxy to hold the remaining slag in place, and the tube section is cut into pieces, then embedded in epoxy, cross sectioned, and polished for analysis in a SEM.

The DSAF testing provides a worst-case-scenario type of test for the alloys because the corrosion mechanism is more severe than would be encountered by a HX in a power system. It is more severe because the slag is dripped directly onto the surface of the alloy whereas in a power system the surface would be coated with a thin layer of less reactive fly ash before building to the thickness at which the slag would become molten. The 100-hr tests were performed in the DSAF by

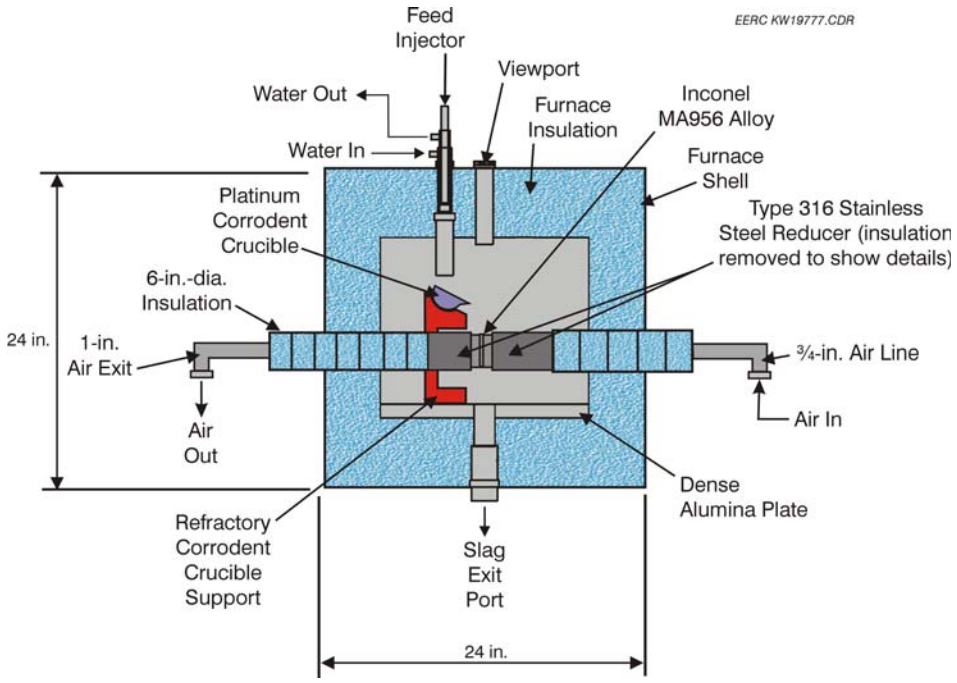

Figure 11. Schematic of the DSAF as modified for the flowing slag corrosion tests of air-cooled pipe section.

pouring slag at 1500°C (2730°F) onto pipe sections which were air-cooled to surface temperatures of 1050°C (1922°F) for the first three tests and 1150°C (2102°F) for the final three.

SEM analyses of one uncorroded and all of the corroded alloys were performed to determine if there was significant interaction between the alloy elements and the slag, and to measure any depletion of aluminum, the protective oxide layer-forming element, from the alloy. Figure 12 is an SEM image of a cross section of the surface of the MA956 tube as received from the manufacturer. The black layer on top is the epoxy used to mount the sample, and the white area on the bottom is the alloy. The thin gray portion in the middle is the protective alumina layer, less than 1 µm thick, that naturally forms on the surface of the alloy when heated above 1100°C (2010°F) as it is during manufacturing. The alumina forms by migration of aluminum metal from within the alloy to the surface where it oxidizes. Once it begins forming however, it prevents further transport of oxygen to the metal surface, thereby protecting the alloy from further oxidation. It is this same alumina layer that also protects the alloy from slag corrosion at high temperatures.

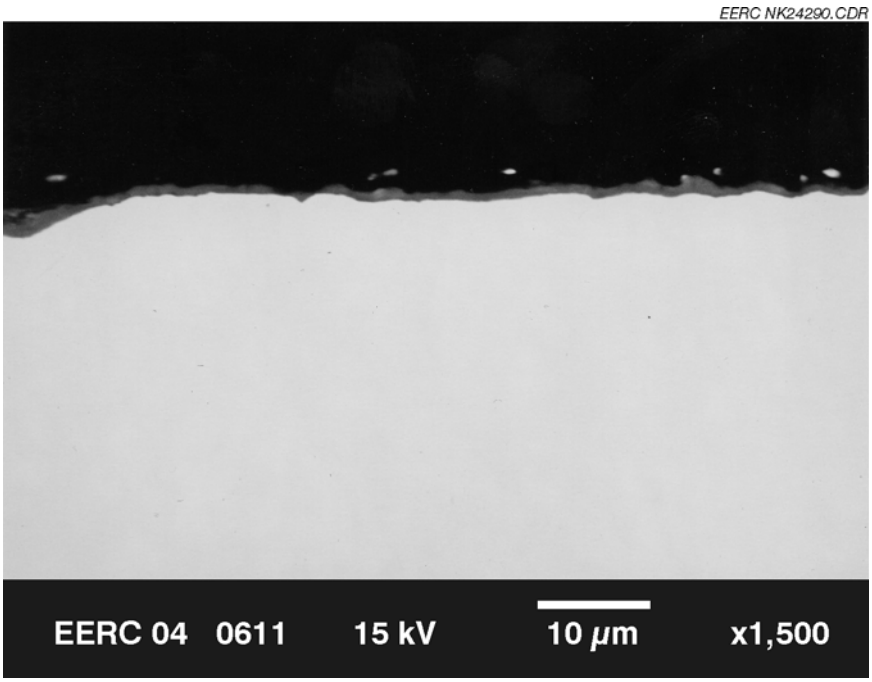

Figure 12. SEM photograph of a cross section of the MA956 alloy.

RESULTS AND DISCUSSION

Task 1 – Pilot-Scale Testing

The results of the three pilot-scale SFS coal–biomass cofiring tests are documented in this section of the report. The discussion is based on the data and observations from these tests as well as referenced information from previous projects, firing bituminous and subbituminous coal, related to development and testing of the HTHX (3, 39). SFS operation during each test involved NG firing during system heatup and cooldown, and nominally 85 hr of coal–biomass cofiring. Results are discussed with respect to fuel characteristics and SFS performance issues related to the slagging furnace, slag screen, dilution–quench zone, process air preheaters, and pulse-jet baghouse. Specific examples of process data for these subsystems are presented and discussed. In addition, CAH and HTHX heat-transfer and slag–ash data and observations are presented.

Fuel Characteristics

Discussions with Xcel Energy personnel in March 2003 addressed fuel selection; a truckload of the North Antelope subbituminous coal (18–23 × 10^3 kg [20–25 tons]) was delivered in May to support two coal–biomass cofiring tests. A second truckload of North Antelope subbituminous coal was acquired in December 2003 to support the third and final coal–biomass cofiring test. North Antelope subbituminous coal was selected for this project because it is used by Xcel Energy to power the Sherburne County Station.

Biomass fuel selections included hog fuel, corn stover, and switchgrass, which were acquired during May through June 2003 and stored for future use. Hog fuel was selected because wood residues are the most widely available biomass fuels and hog fuel currently is fired at Xcel's Ashland, Wisconsin, plant. Hog fuel consists of bark and wood remnants from the processing of trees. While sawdust is much more desirable because of its handling characteristics and typically small inorganic content, hog fuel is more abundant and cheaper because it has a higher inorganic content and requires further processing to feed into a combustion system. Corn stover, an agricultural by-product, was selected because of its availability in the upper Midwest; switchgrass was selected because it has been identified as a potential energy crop in a number of technical and economic biomass energy studies.

The potential need to air-dry the biomass to avoid handling, processing, and feed problems was verified upon inspection of the fuels. The hog fuel was the first biomass cofired followed by the corn stover and then switchgrass. Preparation of a 208-L (55-gal) drum of air-dried hog fuel through an existing EERC hammer mill, using a 3.18 mm (0.125 in.) screen, resulted in a product that could be successfully fed to the slagging furnace. Air drying and hammer mill tests also were successfully completed with the corn stover and switchgrass.

North Antelope coal feed rates typically ranged from 75 to 84 kg/hr (166 to 186 lb/hr). For a 2-hr period during the first test, the coal feed rate was increased to 100 kg/hr (220 lb/hr) to maintain furnace temperatures while correcting a plugging problem with the biomass feeder. Biomass feed rates typically ranged from 23 to 30 kg/hr (50 to 65 lb/hr) for the three coal–biomass cofiring tests.

However, during the last 24 hr of the first test, biomass feed rates were as high as 41 kg/hr (90 lb/hr) because of intermittent feeder plugging problems and resulting feed rate instability. Coal and biomass feed rates were adjusted and controlled to achieve a nominal 80%/20% coal–biomass cofiring contribution on a firing rate basis and to avoid exceeding a 1052°C (1925°F) temperature limit imposed for the HTHX alloy tube surfaces. Observations concerning furnace firing rate and temperature will be addressed in more detail later as part of the discussion of slagging furnace performance.

Table 5 summarizes the characteristics of all fuels. Note that these are as-fired properties and represent some drying of fuels during processing. Analysis of the composite coal samples collected during each of the three tests indicates that the as-fired coal contained 21–23 wt% moisture, 3.7–3.9 wt% ash, and 0.23–0.25 wt% sulfur, and a heating value of 21,625–21,978 kJ/kg (9306– 9458 Btu/lb). Coal ash was analyzed for ash fusion properties under oxidizing conditions. Results indicate a softening temperature of 1212°–1229°C (2213°–2244°F) and a fluid temperature of 1228°–1258°C (2241°–2296°F). Based on these data, the North Antelope subbituminous coal was similar to the two other subbituminous coals (Cordero Rojo and Rochelle) fired during previous projects evaluating the HTHX. However, moisture, ash, and sulfur content were slightly lower in the North Antelope coal resulting in a slightly higher heating value (HHV). Table 6 summarizes fuel analysis data for the Cordero Rojo and Rochelle subbituminous coals as well as two bituminous coals (Illinois No. 6 and Prater Creek) used extensively in earlier projects evaluating the HTHX (3, 39).

The final three columns in Table 5 summarize the analytical results for the biomass fuels fired during the tests. Analysis of the composite samples collected during each of the three tests indicates that the as-fired biomass fuels contained 7–12 wt% moisture, 5–7 wt% ash, and 0.04–0.13 wt% sulfur. The heating values ranged from 21,625 to 21,978 kJ/kg (7402 to 8036 Btu/lb) on an as-fired basis. The hog fuel was found to have the highest moisture content and heating value and the lowest sulfur and ash content. The two agricultural biomass sources had comparable sulfur levels, and the switchgrass was found to have the lowest moisture content and heating value. A comparison of the biomass fuels with the North Antelope coal shows the coal to have higher moisture, sulfur, and heating values, and a lower ash content.

Biomass ash was analyzed for ash fusion properties under oxidizing conditions. Results indicated softening temperatures ranging from 1245° to 1375°C (2273° to 2507°F) and fluid temperatures from 1288° to 1468°C (2350° to 2673°F). The ash fusion temperatures for all three biomass fuels were greater than for the North Antelope coal. However, the corn stover was more similar to the North Antelope coal than either of the other two biomass fuels. Fluid temperatures for the hog fuel and switchgrass were nominally 167°–208°C (300°–375°F) greater than those observed for corn stover and North Antelope coal, respectively.

Metal concentrations in the fuel ashes were determined by XRF analyses which are summarized in Table 5 and reported as wt% oxides. The coal ash primary components are calcium (26.3–26.9 wt% CaO), silica (25.9–27.2 wt% SiO_2), and alumina (17.0–18.3 wt% Al_2O_3). Alkaline-earth components (CaO, MgO, Na_2O, and K_2O) combined represent 34–36 wt% in the ash. These ash properties are similar to the Cordero Rojo and Rochelle subbituminous coals fired during previous tests evaluating the HTHX.

Table 5. Results of As-Fired Fuel and Ash Analysis for the Cofiring Tests

	North Antelope Subbituminous Coal[1]	Hog Fuel	Corn Stover	Switchgrass
Proximate Analysis, wt%				
Moisture	21.1–22.8	12.2	7.7	6.9
Volatile Matter	36.3–37.2	69.4	74.5	74.1
Fixed Carbon	37.2–37.9	13.4	10.6	13.6
Ash	3.7–3.9	5.0	7.1	5.4
Ultimate Analysis, wt%				
Hydrogen	6.0–6.1	6.2	6.1	6.0
Carbon	53.1–54.5	39.3	42.2	42.4
Nitrogen	0.9–1.0	0.5	0.8	1.2
Sulfur	0.23–0.25	0.04	0.12	0.13
Oxygen	34.6–36.1	49.0	43.6	44.9
Ash	3.7–3.9	5.0	7.1	5.4
Heating Value, kJ/kg	21,650–22,000	18,690	17,950	17,220
Percent as Oxides, wt%				
SiO_2	25.9–27.2	33.3	57.3	70.3
Al_2O_3	17.0–18.3	2.5	3.2	0.0
Fe_2O_3	7.2–7.6	3.2	1.4	0.25
TiO_2	1.5	0.3	0.3	0.03
P_2O_5	1.2	1.8	3.8	4.8
CaO	26.3–26.9	43.2	9.5	9.4
MgO	6.9–7.2	3.9	12.6	4.9
Na_2O	0.8–1.2	3.9	0.4	0.03
K_2O	0.2–0.3	7.9	10.0	7
SO_3	8.9–12.4	0.0	1.5	3.3
Ash Fusion Temp., °C				
Initial	1209–1224	1349	1232	1348
Softening	1212–1229	1375	1245	1353
Hemisphere	1218–1233	1417	1251	1448
Fluid	1227–1258	1467	1288	1459
Sieve Analysis				
Screen Mesh Size		Weight Percent Retained		
Coal 100, Biomass 16	6.5–7.2	2.3	9.1	4.2
Coal 140, Biomass 18	10.5–12.3	4.0	2.0	3.4
Coal 200, Biomass 20	14.0–14.9	4.6	3.0	3.4
Coal 230, Biomass 30	7.1–8.7	16.1	12.6	10.9
Coal 270, Biomass 40	1.2–7.2	17.8	22.2	21.0
Coal 325, Biomass 60	3.9–8.6	24.1	24.2	24.4
Pan	43.7–49.7	31.0	26.8	32.7
Total %	100.0	100.0	100.0	100.0
Bulk Density, kg/m^3	601–641	248	140	140

[1] These data represent the analysis results from composite samples collected during the three coal–biomass cofiring tests.

Table 6. Results of Fuel and Fuel Ash Analysis for Fuels Fired During Previous HTHX Tests[1, 2]

	Illinois No. 6 Bituminous Coal	Prater Creek Bituminous Coal	Cordero Rojo Subbituminous Coal	Rochelle Subbituminous Coal
Proximate Analysis, wt%				
Moisture	2.8–10.3	1.7–2.0	25.3–26.1	21.6–24.3
Volatile Matter	35.9–39.9	37.9–38.7	35.8–36.5	35.6–37.4
Fixed Carbon	43.3–46.3	54.5–55.3	32.7–32.9	35.8–36.7
Ash	10.6–11.7	4.7–5.1	5.3–5.4	4.3–4.7
Ultimate Analysis, wt%				
Hydrogen	4.7–5.8	5.3–5.4	6.3	6.1–6.4
Carbon	61.6–67.6	77.5–78.3	49.4–49.7	53.0–55.2
Nitrogen	0.8–1.9	2.3–2.4	1.2	0.6–0.7
Sulfur	3.2–4.1	0.8–0.9	0.45	0.3
Oxygen	10.6–17.6	8.4–8.7	37.1–37.2	32.9–33.4
Ash	10.6–11.7	4.7–5.1	5.3–5.4	4.3–4.7
Heating Value, kJ/kg	25,621–27,117	31,489–32,952	20,150–20,590	20,980–21,700
Percent as Oxides, wt%				
SiO_2	49.3–53.9	38.2–38.4	26.7–26.8	26.7–27.1
Al_2O_3	19.8–21.5	24.4–25.0	17.1–17.5	15.5–16.3
Fe_2O_3	13.6–17.5	22.5–23.0	6.8–7.2	6.3–6.6
TiO_2	0.9–1.0	0.9–1.0	1.6	1.2–1.4
P_2O_5	0.1–0.2	0.1–0.2	1.1	0.7–0.9
CaO	2.6–3.6	3.6–3.8	26.1–26.2	21.6–24.3
MgO	1.5–2.0	1.9–2.1	5.2	6.7–6.9
Na_2O	1.1–1.5	0.3–0.6	1.0	1.5
K_2O	1.9–2.3	2.2–2.3	0.3–0.4	0.1–0.4
SO_3	2.5–4.0	4.6–4.9	13.4–13.7	15.6–17.0
Ash Fusion Temp., °C				
Initial	1267–1311	1357–1362	1216	1206–1257
Softening	1283–1326	1366–1372	1232–1233	1207–1264
Hemisphere	1311–1342	1389–1396	1239–1241	1212–1266
Fluid	1366–1423	1411–1423	1252	1216–1274
Sieve Analysis				
Screen Mesh Size		Weight Percent Retained		
100	1.8–25.2	13.6–14.9	11.0–13.5	7.6–8.8
140	0–14.9	10.4–15.1	15.0–15.1	14.2–15.4
170	0–14.9	NA[3]	NA	NA
200	9.6–13.5	12.4–12.9	13.3–14.2	14.3–14.4
230	0–16.2	8.0–8.3	8.0–9.0	8.4–9.1
270	0.5–14.6	0.8–1.2	2.2–2.9	2.0–5.6
325	7.4–14.7	10.9–11.9	9.4–11.0	4.8–11.6
400	0–4.7	NA	NA	NA
Pan	29.7–57.8	38.8–40.7	37.6–38.0	39.7–43.4
Total %	99–100.2	99.9–100.0	100.0–100.2	98.6–100.6

[1] Analysis is presented on an as-fired basis.
[2] These data represent the range of analysis results from composite samples collected during multiple tests with each fuel type.
[3] Not available.

Analysis of the biomass fuel ash indicates that the primary components varied from fuel to fuel. The hog fuel ash was composed primarily of calcium (43.2 wt% CaO) and silica (33.3 wt% SiO_2) with combined alkaline-earth components (CaO, MgO, Na_2O, and K_2O) representing 59 wt% of the ash. The highest calcium and combined alkaline-earth content was observed for the hog fuel ash. Corn stover ash was composed primarily of silica (57.3 wt% SiO_2) with smaller quantities of magnesium (12.6 wt% MgO), potassium (10.0 wt% K_2O), and calcium (9.5 wt% CaO). Combined alkaline-earth components (CaO, MgO, Na_2O, and K_2O) represented 32 wt% of the corn stover ash. Switchgrass ash was composed of mostly silica (70.3 wt% SiO_2) with smaller quantities of calcium (9.4 wt% CaO), potassium (7.0 wt% K_2O), and magnesium (4.9 wt% MgO). Combined alkaline-earth components (CaO, MgO, Na_2O, and K_2O) represented only 21 wt% of the switchgrass ash, the lowest value for the four fuels fired in this project.

Dry-sieve analysis indicated that the pulverized Antelope coal used in the coal–biomass cofiring tests was 66–68 wt% −200 mesh (74 µm). The EERC attempts to pulverize fuel for the SFS to nominally 70 wt% −200 mesh (74 µm). Based on the dry-sieve data, the EERC generally achieved that objective. As previously stated, the biomass fuels were air-dried and processed through a hammer mill using a 3.18-mm (⅛-in.) screen. As a result, the biomass fuels were 73–78 wt% −30 mesh (540 µm). Although the particle size of the biomass fuels was significantly larger than the coal, overall carbon burnout during the coal–biomass cofiring tests was high as indicated by baghouse ash analysis that reported carbon values of 0.18–0.33 wt%. These values are consistent with previous tests firing bituminous, subbituminous, and lignite fuels in the SFS. The high degree of carbon burnout, >99.6%, observed in the SFS system for these tests is a direct result of adequate furnace temperature and residence time. Although carbon burnout was excellent for these tests and no biomass handling problems were encountered, the EERC is considering the acquisition of a smaller screen, 1.59 mm (0.0625 in.), for the hammer mill used to prepare the biomass fuels for future biomass combustion or gasification projects. A smaller screen should result in a more uniform product from the hammer mill, potentially improving biomass feed stability for the pilot-scale system. This issue will be discussed later in this report with respect to fuel feed rate data for each of the three coal–biomass cofiring tests.

Bulk density values were determined for each of the fuels fired in support of this project. As expected, the coal had the highest bulk density, 601–641 kg/m^3 (37.5–40.0 lb/ft^3). The lowest bulk density was observed for the corn stover, 136 kg/m^3 (8.5 lb/ft^3); switchgrass was similar. Of the three biomass fuels fired, hog fuel had the highest bulk density, 248 kg/m^3 (15.5 lb/ft^3).

Slagging Furnace Operation

The slagging furnace heatup rate during SFS tests completed in this and related projects was limited to 56°C/hr (100°F/hr) while NG was fired. This is the heatup rate recommended by the manufacturer for the high-density castable refractory in the furnace. Based on ash characterization (reported in under Task 2 results), the alloy tube surface temperature was limited to <1052°C (<1925°F) when cofiring coal and biomass to minimize the potential for slag corrosion–erosion of the alloy tube surfaces. Therefore, furnace firing rates and resulting furnace temperatures were adjusted to control alloy tube surface temperatures in the range of 1038°–1049°C (1900°–1920°F) for nominal process air flow rates of 11.0 m^3/min (390 scfm). Once this temperature range was achieved, NG firing was continued for at least 4 hr so that furnace refractory was approaching

thermal equilibrium. Subsequently, the main burner was switched from NG to coal–biomass cofiring, and feed rate adjustments were made to maintain alloy tube surface temperatures in the range of 1038°–1049°C (1900°–1920°F). After 12 hr of solid fuel firing, with the furnace reaching thermal equilibrium, most fuel feed adjustments were limited to the coal because it represented nominally 80% of the heat input.

XCEL1 (SFS-XCEL1-0303), cofiring coal and hog fuel, was completed the week of October 9–17, 2003. NG was initially fired in the main burner to preheat the furnace, cure new refractory in the slag screen and slag tap, and obtain HTHX performance data at full process air pressure (10.3 bar [150 psig]) and an alloy surface temperature limit of 1094°C (2000°F). The purpose of the NG-fired test was to establish a new baseline for the HTHX. A new baseline was required following modifications to the HTHX that resulted in a slight reduction of alloy tube surface area exposed to furnace conditions. After the NG-fired period, the cofiring of North Antelope subbituminous coal and hog fuel was initiated. Specific test objectives included 1) coal–biomass cofiring for a period of 85 hr to establish an ash–slag layer on the HTHX alloy tubes and obtain steady-state heat transfer data, 2) evaluating the impact of biomass cofiring on the performance of CAH and other SFS components, 3) determining a) flue-gas particulate mass loading and particle size at the baghouse inlet and b) baghouse particulate collection efficiency, 4) evaluating baghouse differential pressure control, and 5) documenting flue gas composition for SO_2, NO_x, CO_2, CO, and O_2. Following the solid fuel-fired test, main burner NG firing was employed to control cooldown.

As previously stated, when NG was fired, the surface temperature of the HTHX alloy tubes was limited to 1094°C (2000°F) to avoid overheating the alloy. As a result, during the NG-fired baseline test, furnace temperature was limited to 1535°C (2795°F) at a main burner firing rate of 2.90×10^6 kJ/hr (2.75 MMBtu/hr). After the baseline test was completed, the NG firing rate was reduced to 2.2×10^6 kJ/hr (2.1 MMBtu/hr), resulting in a furnace temperature of 1427°C (2600°F), in preparation for switching to coal–hog fuel cofiring.

Figures 13–15 illustrate the coal–hog fuel feed rate, firing rate, and furnace temperature data for Test XCEL1, respectively. The North Antelope subbituminous coal feed was continuous for 85 hr during the October 2003 test period. Spikes in coal feed rate observed in Figure 13 occurred during feed-hopper refill cycles. This also was true for the hog fuel feed rate during the first 60 hr of solid fuel firing. However, after 2 hr of coal–hog fuel cofiring, an electrical switch box supporting the biomass feeder failed, forcing an increase in the coal feed rate to maintain furnace temperature. The electrical switch box was replaced over a 2-hr period, and coal–hog fuel cofiring resumed for the balance of the test period. Coal feed rate ranged from 77 to 100 kg/hr (170 to 220 lb/hr). However, once the furnace reached thermal stability, the feed rate was typically 77 kg/hr (170 lb/hr). Minor adjustments to the coal feed rate were made to maintain the HTHX alloy surface temperature in the desired range. The hog fuel feed rate was nominally 32 kg/hr (70 lb/hr) during the test. However, during the final 24 hr of coal–hog fuel cofiring, the hog fuel feed rate became erratic, ranging from 23 to 41 kg/hr (50 to 90 lb/hr). Inspection of the biomass feeder during maintenance following the test determined that some wood debris had collected in the feeder. Once this debris was removed, a short operational test demonstrated that the previously observed feed rate stability was restored.

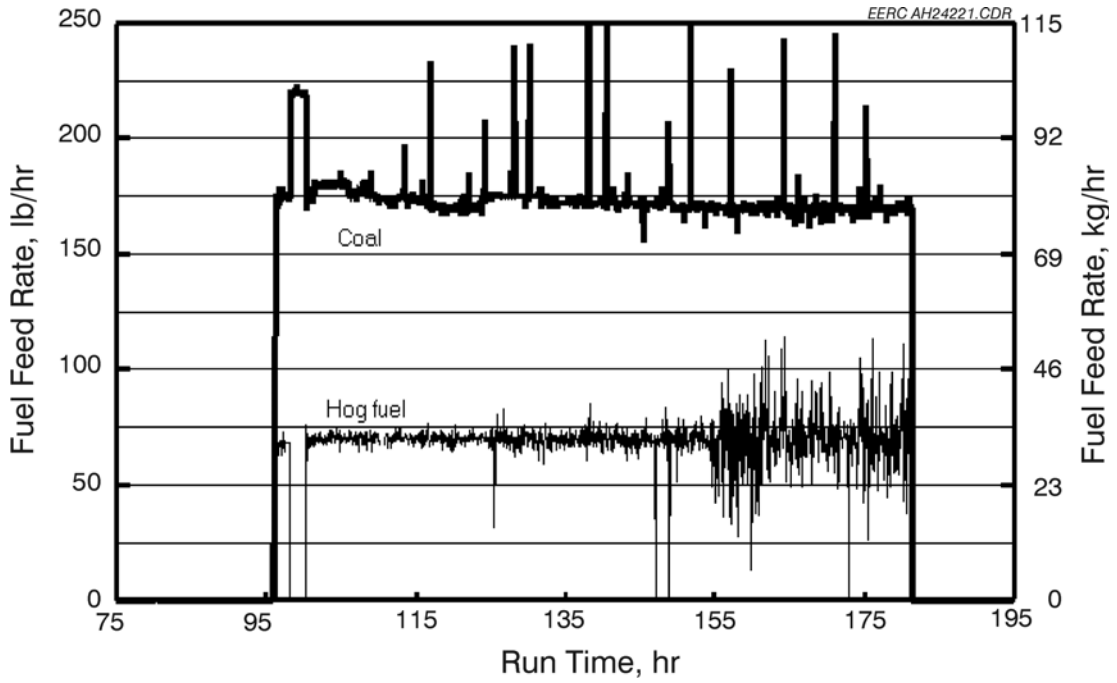

Figure 13. Fuel feed rate versus run time for Test SFS-XCEL1-0303.

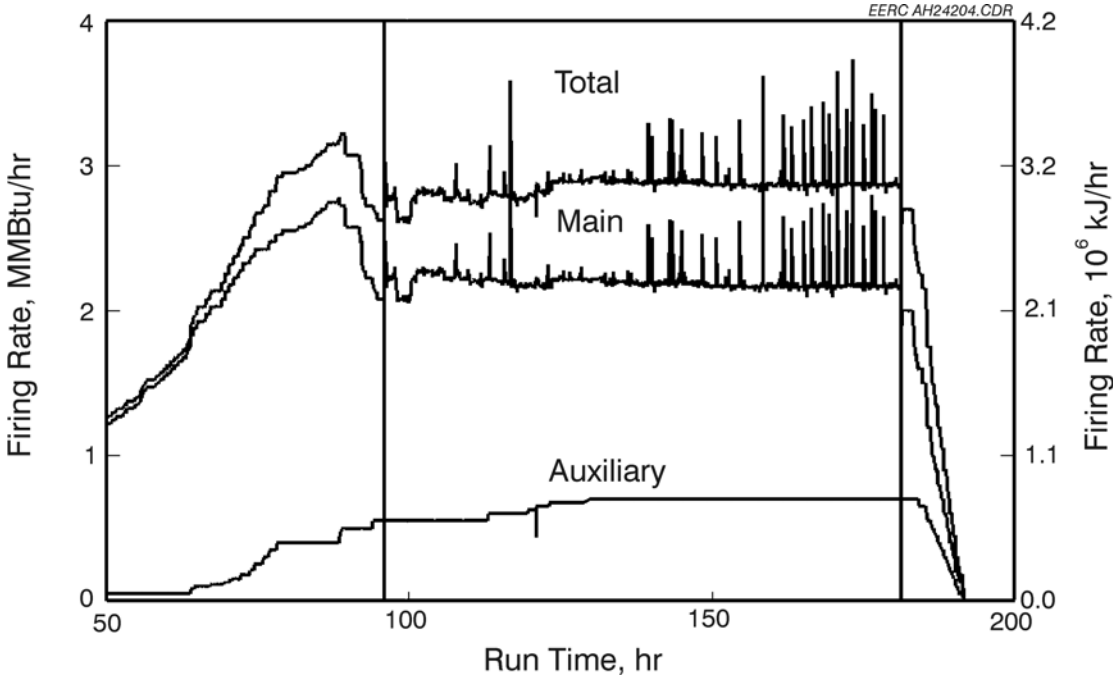

Figure 14. Slagging furnace firing rate versus run time for Test SFS-XCEL1-0303.

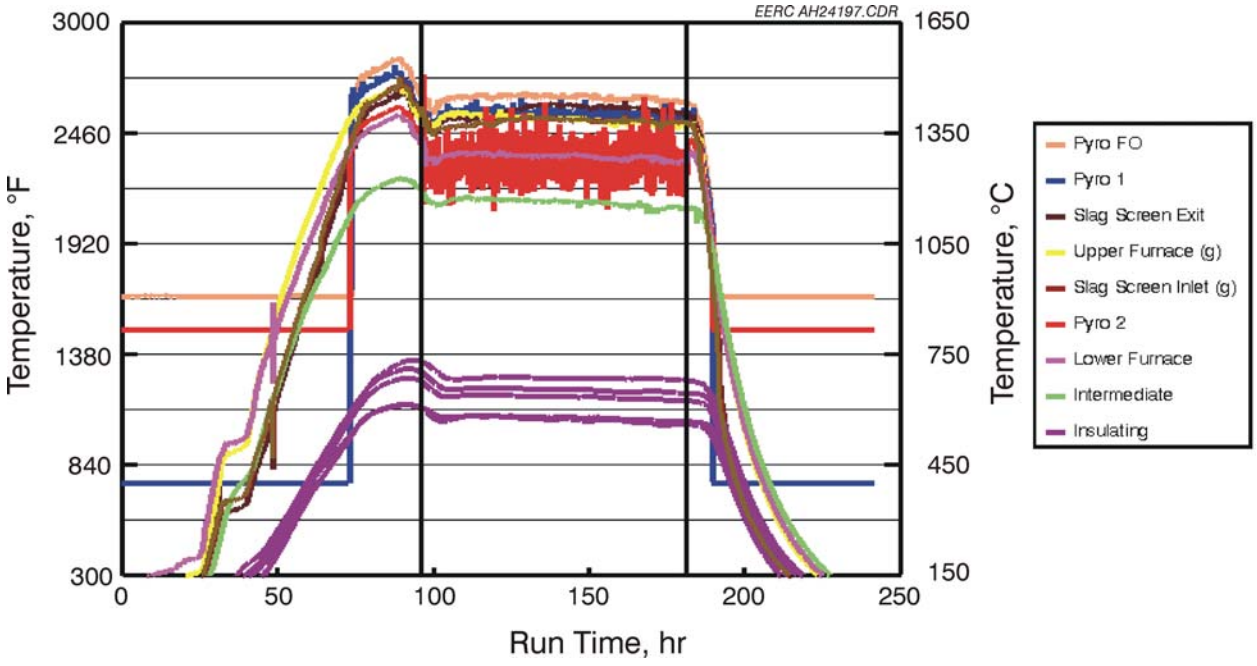

Figure 15. Furnace and slag screen temperatures versus run time for Test SFS-XCEL1-0303.

Furnace exit temperatures during the XCEL1 coal–hog fuel-fired test ranged from 1410° to 1455°C (2570° to 2650°F) as a result of main burner firing rates of 2.2–2.4 × 10^6 kJ/hr (2.1–2.3 MMBtu/hr). Once the furnace refractory reached thermal equilibrium, after nominally 12 hr of solid fuel firing, furnace exit temperature for the remainder of the test averaged 1445°C (2632°F) with a std. dev. of 6°C (11°F). Based on fuel feed rate and analysis data, coal firing represented 69%–100% and hog fuel firing represented 0%–31% of the heat input through the main burner as a result of the biomass feed problems previously discussed. For most of the test period, coal and hog fuel firing represented 74% and 26%, respectively, of the heat input through the main burner. Auxiliary burner firing rates ranged from 0.58 to 0.74 × 10^6 kJ/hr (0.55 to 0.70 MMBtu/hr), resulting in total furnace firing rates of 2.7–3.2 × 10^6 kJ/hr (2.6–3.0 MMBtu/hr). The main burner firing rate represented 76%–80% of the total firing rate during the coal–hog fuel-fired period. Normally, during air-blown operation the auxiliary burner firing rate is limited to 0.53 × 10^6 kJ/hr (0.50 MMBtu/hr) representing <20% of the total furnace firing rate. However, in this case it was necessary to fire the auxiliary burner at a higher rate to maintain a sufficiently high furnace exit temperature to avoid plugging problems in the slag screen. This was necessary because of the alloy surface temperature limit, <1052°C (<1925°F), imposed for the HTHX and the higher ash-fusion fluid temperature, 211°C (380°F) higher, observed for the hog fuel when compared to the coal.

Furnace refractory temperatures ranged from 610° to 730°C (1130° to 1345°F) for the hot side of the insulating refractory to as high as 1205°C (2200°F) for the cold side of the high-density refractory during the NG-fired period. Furnace refractory temperatures decreased somewhat during the coal–hog fuel-fired test as the firing rate decreased, resulting in values of 555°–685°C (1030°–1265°F) for the hot side of the insulating refractory to as high as 1169°C (2135°F) for the cold side

of the high-density refractory. No operating problems were encountered during the October 2003 test period beyond the biomass feed interruption and stability previously discussed.

Test XCEL2 (SFS-XCEL2-0403) cofiring coal and corn stover was completed the week of November 14–21, 2003. Main burner NG firing was limited to heatup, curing new refractory in the slag tap, and cooldown periods. After heatup and refractory curing, the cofiring of North Antelope subbituminous coal and corn stover was initiated. Specific test objectives were identical to those previously stated for Test XCEL1.

Figures 16–18 illustrate the coal–corn stover feed rate, firing rate, and furnace temperature data for Test XCEL2, respectively. The North Antelope subbituminous coal and corn stover feed was continuous for 86 hr during the November 2003 test. Coal feed rate ranged from 77 to 84 kg/hr (170 to 185 lb/hr). However, once the furnace reached thermal stability, the feed rate was nominally 82 kg/hr (180 lb/hr). The corn stover feed rate ranged from 26 to 30 kg/hr (58 to 65 lb/hr) and was nominally 30 kg/hr (65 lb/hr) during the test. Spikes in fuel feed rate observed in Figure 16 occurred during feed hopper refill cycles. During Test XCEL2, both the coal and corn stover feed rates were stable. Minor adjustments to the coal feed rate were made to maintain the HTHX alloy surface temperature in the desired range.

Furnace temperatures during the XCEL2 coal–corn stover-fired test ranged from 1477° to 1494°C (2690° to 2720°F) as a result of main burner firing rates of 2.3×10^6 kJ/hr (2.2 MMBtu/hr). Once the furnace refractory reached thermal equilibrium, after nominally 12 hr of solid fuel firing, furnace exit temperature for the remainder of the test averaged 1485°C (2704°F) with a std. dev. of 8°C (14°F). Based on fuel feed rate and analysis data, coal firing represented 76%–79% and corn

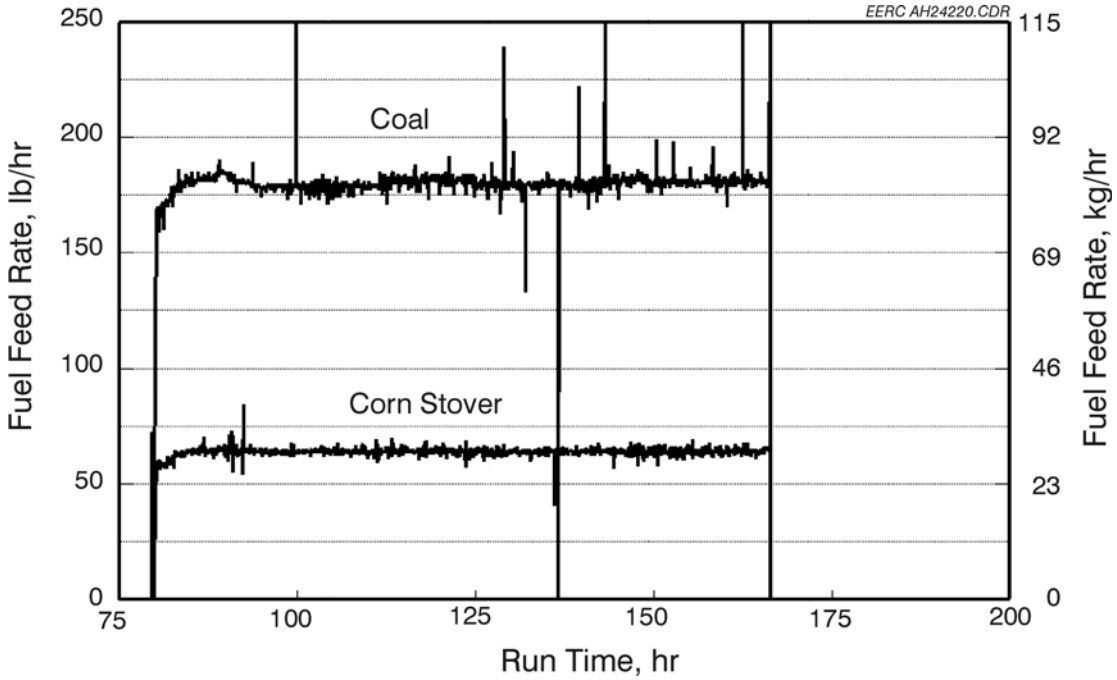

Figure 16. Fuel feed rate versus run time for Test SFS-XCEL2-0403.

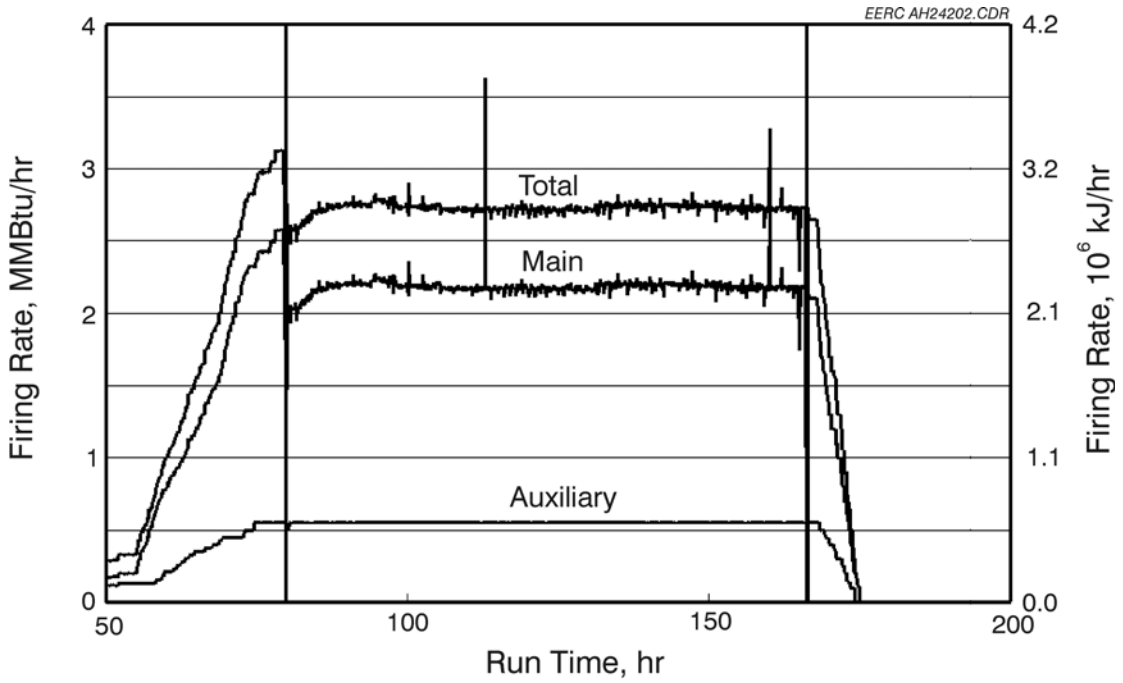

Figure 17. Slagging furnace firing rate versus run time for Test SFS-XCEL2-0403.

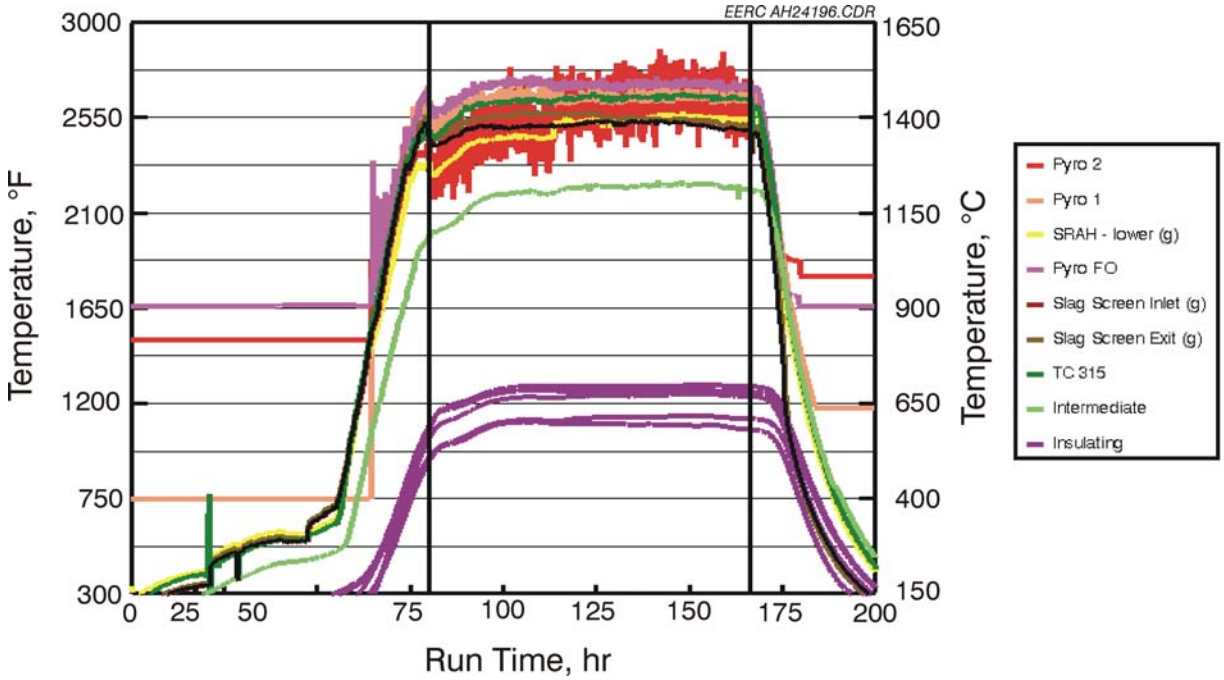

Figure 18. Furnace and slag screen temperatures versus run time for Test SFS-XCEL2-0403.

stover firing represented 21%–24% of the heat input through the main burner. Typically, coal and corn stover firing represented 77% and 23%, respectively, of the heat input through the main burner. The auxiliary burner firing rate was 0.58–0.74 × 10^6 kJ/hr (0.55 MMBtu/hr), resulting in a total furnace firing rate of 2.9 × 10^6 kJ/hr (2.75 MMBtu/hr). The main burner firing rate represented 80% of the total firing rate during the coal–corn stover-fired period. Normally, during air-blown operation the auxiliary burner firing rate is limited to 0.53 × 10^6 kJ/hr (0.50 MMBtu/hr) representing <20% of the total furnace firing rate. However, in this case it was necessary to fire the auxiliary burner at a slightly higher rate to maintain a sufficiently high furnace exit temperature to avoid plugging problems in the slag screen. This was necessary because of the alloy surface temperature limit, <1052°C (<1925°F), imposed for the HTHX and the higher ash fusion fluid temperature, 50°C (90°F) higher, observed for the corn stover when compared to the coal.

Furnace refractory temperatures ranged from 580° to 694°C (1075° to 1280°F) for the hot side of the insulating refractory to as high as 1216°C (2220°F) for the cold side of the high-density refractory during the coal–corn stover-fired test period. No operating problems were encountered during the November 2003 test period.

Test XCEL3 (SFS-XCEL3-0503) cofiring coal and switchgrass was completed the week of December 12–19, 2003. Main burner NG firing was limited to heatup, curing new refractory in the slag tap, and cooldown periods. Subsequent to completing heatup and refractory curing, the cofiring of North Antelope subbituminous coal and switchgrass was initiated. Specific test objectives were identical to those previously stated for Test XCEL1.

Figures 19–21 illustrate the coal–switchgrass feed rate, firing rate, and furnace temperature data for Test XCEL3, respectively. The North Antelope subbituminous coal and switchgrass feed was continuous for 85 hr during the December 2003 test period. Coal feed rate ranged from 75 to 84 kg/hr (166 to 186 lb/hr). A higher average coal feed rate was required during the last 40-plus hr of Test XCEL3 because it was necessary to switch to the second load of North Antelope coal acquired for this project. Based on fuel analysis, the heating value was slightly lower for the second load of coal because of higher moisture and ash content. The switchgrass feed rate ranged from 23 to 27 kg/hr (50 to 60 lb/hr) and was nominally 26 kg/hr (58 lb/hr) during the test. Spikes in coal feed rate observed in Figure 19 occurred during feed hopper refill cycles. However, during Test XCEL3 the switchgrass feed rate was less stable than the biomass feed rates observed during Tests XCEL1 (prior to the plugging problem) or XCEL2. The greater switchgrass feed rate instability is believed to be related to the cylindrical geometry of the material and the impact the geometry has on mass flow through the feed hopper. It likely tends to bridge more than the other two biomass materials. Also, inspection of the biomass feeder following Test XCEL3 indicated switchgrass packing around the screw within the housing which was not evident with the hog fuel or corn stover. During future coal–biomass cofiring tests with the SFS, the particle size of the biomass fuel should be further reduced to determine potential benefits with respect to feed rate stability and general operability of the SFS.

Furnace temperatures during the XCEL3 coal–switchgrass-fired test ranged from 1427° to 1494°C (2600° to 2720°F) as a result of main burner firing rates of 2.1–2.4 × 10^6 kJ/hr (2.0–2.3 MMBtu/hr). Once the furnace refractory reached thermal equilibrium, after 12 hr of solid fuel

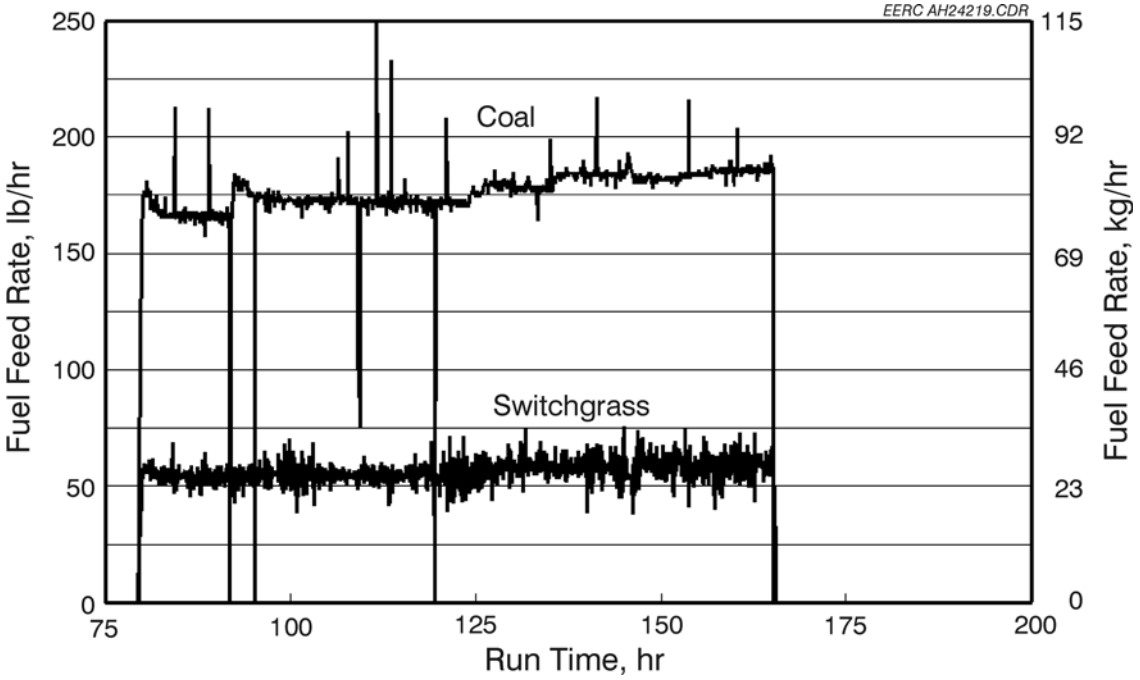

Figure 19. Fuel feed rate versus run time for Test SFS-XCEL3-0503.

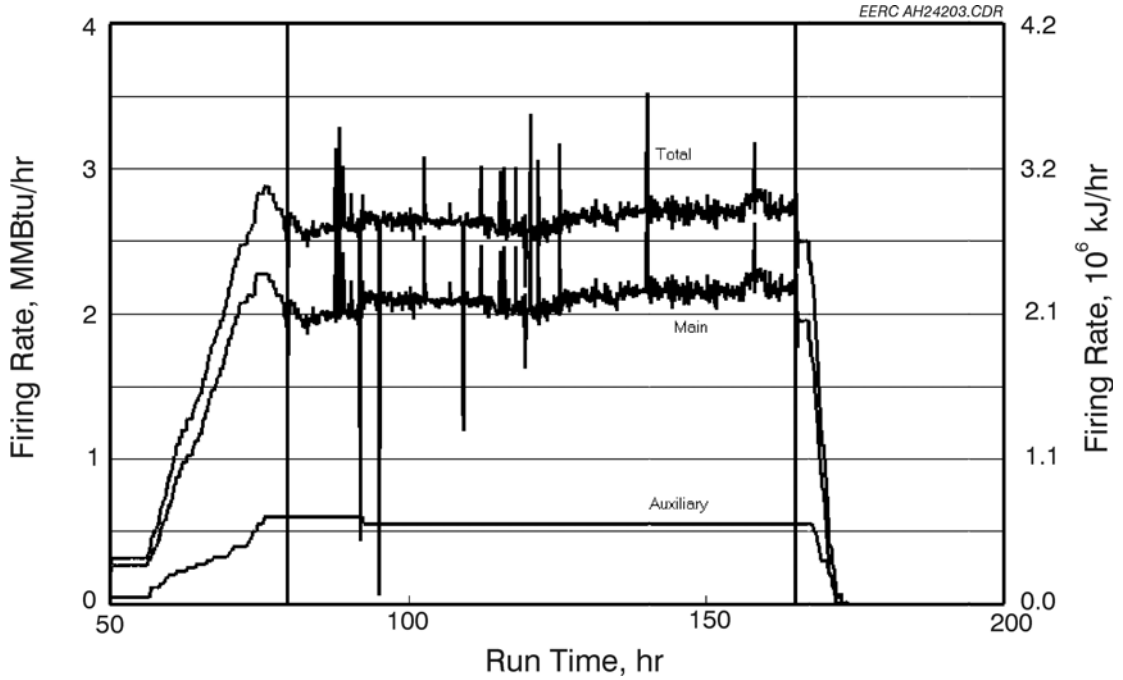

Figure 20. Slagging furnace firing rate versus run time for Test SFS-XCEL3-0503.

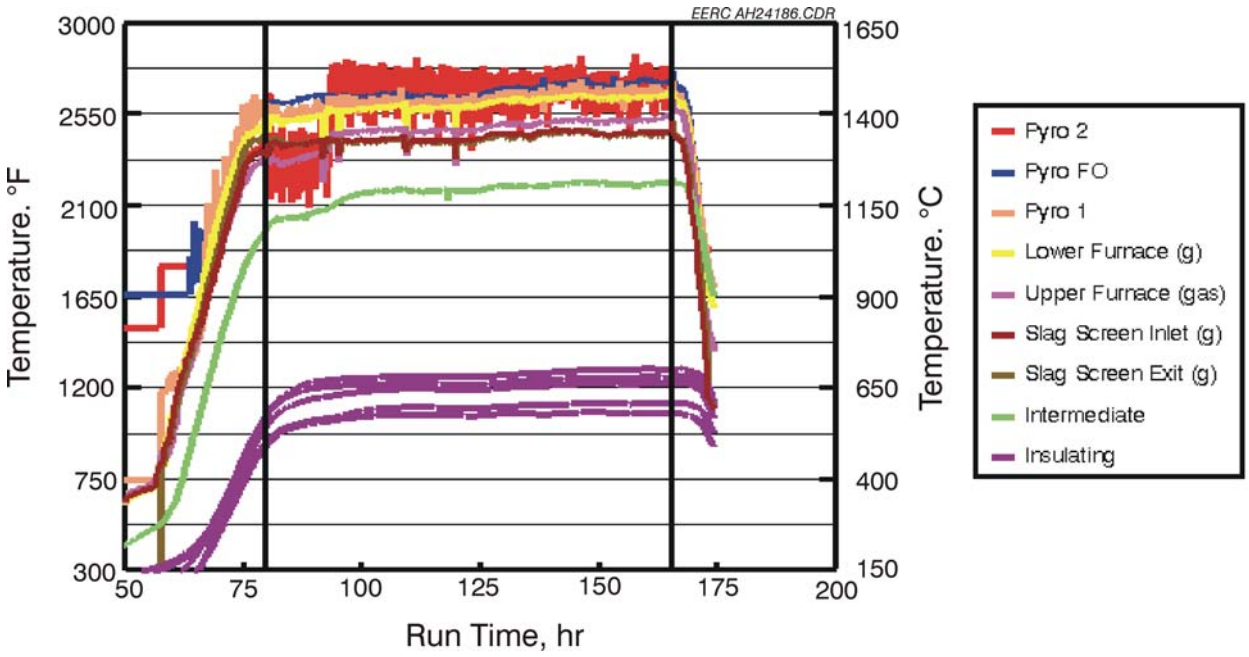

Figure 21. Furnace and slag screen temperatures versus run time for Test SFS-XCEL3-0503.

firing, furnace exit temperature for the remainder of the test averaged 1466°C (2671°F) with a std. dev. of 16°C (29°F). The higher furnace exit temperature std. dev. observed during XCEL3 is likely a direct result of the switchgrass feed rate instability. Based on fuel feed rate and analysis data, coal firing represented 78%–82% and switchgrass firing represented 18%–22% of the heat input through the main burner. Typically, coal and switchgrass firing represented 80% and 20%, respectively, of the heat input through the main burner. The auxiliary burner firing rate was 0.58×10^6 kJ/hr (0.55 MMBtu/hr) after the first 12 hr of coal–switchgrass cofiring, resulting in a total furnace firing rate of $2.7–3.0 \times 10^6$ kJ/hr (2.55–2.85 MMBtu/hr). The main burner firing rate represented 78%–80% of the total firing rate during the coal–switchgrass-fired test. Normally, during air-blown operation the auxiliary burner firing rate is limited to 0.53×10^6 kJ/hr (0.50 MMBtu/hr) representing <20% of the total furnace firing rate. However, in this case it was necessary to fire the auxiliary burner at a slightly higher rate to maintain a sufficiently high furnace exit temperature to avoid plugging problems in the slag screen. This was necessary because of the alloy surface temperature limit, <1052°C (<1925°F), imposed for the HTHX and the higher ash fusion fluid temperature, 233°C (420°F) higher, observed for the switchgrass when compared to the coal.

Furnace refractory temperatures ranged from 574° to 702°C (1065° to 1295°F) for the hot side of the insulating refractory to as high as 1216°C (2220°F) for the cold side of the high-density refractory during the coal–switchgrass-fired test period. No serious operating problems were encountered during the December 2003 test period. However, the compressor supplying process air to the HTHX tripped twice. The first trip forced a temporary reduction in coal feed rate to avoid overheating the HTHX alloy surfaces while the compressor was restarted and air pressure recovered over a 15-min period. The second trip was adequately handled by the nitrogen backup system while

the compressor was restarted; a reduction in coal feed rate was not necessary. The compressor trips are believed to have been caused by moisture that froze in a compressor instrument air line.

Furnace exit temperatures for the three coal–biomass-cofired tests were similar but not identical. One explanation may be the different moisture levels in the three biomass fuels. The hog fuel had the highest moisture of the three biomass fuels and resulted in the lowest average furnace exit temperature, even though in combination with the coal fired, it represented the highest average firing rate. However, based on the temperature and firing rate data and fuel characteristics, the differences in the furnace exit temperatures for the corn stover and switchgrass tests were likely a function of firing rate alone.

Minor pressure surges (a few tenths to 4 mmHg [a few tenths to 2 in. W.C.]) are not uncommon in the slagging furnace. They happen periodically as a result of baghouse cleaning, opening of access ports to clean the dilution–quench zone or view the HTHX, opening of access ports to insert or remove sampling probes or clean the CAH, and when flue gas flow distribution through the baghouse is altered. However, pressure surges in the furnace as a result of the activities identified did not cause any operating problems during the coal–biomass cofired SFS tests.

Inspection of the furnace refractory after completion of Test XCEL3 indicated that the high-density refractory was in good condition. The only area showing any deterioration was below the HTHX where slag from the tubes ran onto the horizontal surface below. However, no refractory repairs nor replacement were determined to be necessary. The only observed change in the high-density liner as a function of operation was that the color of the refractory surface darkened and became more glassy with each test, indicating a residual slag coating on the refractory. Figure 22 contains photographs illustrating the observation. The top photograph shows a newly cured refractory surface, with the bottom photograph showing the same refractory surface after completion of 751 hr of coal and coal–biomass cofiring representing 11 SFS tests.

The duration of solid fuel-fired tests completed in this and related projects ranged from 4 hr to nominally 200 hr. Several coal-fired tests were impacted in some way by fuel ash properties that affected the performance of the slag screen, slag tap, or both. In other cases, tests were terminated early because of a power failure, a compressor failure, the development of a process air leak in the HTHX–radiant air heater (RAH), the failure of RAH ceramic tiles, and a refractory failure in the bottom section of the furnace. However, no forced SFS shutdowns were experienced during this project. Overall, the slagging furnace has proven to be a reliable, relatively simple system to operate and modify in support of coal–biomass cofiring, HTHX evaluation, and other activities. Table 7 summarizes total operating time for the SFS in support of a variety of projects representing 39 tests and corresponding heating and cooling cycles.

Main and Auxiliary Burners

The main and auxiliary burners performed well. For the coal–biomass cofiring SFS tests, the main burner swirl was maintained at a minimum (nominally 20%), while the auxiliary burner swirl setting was nominally 80%. Carbon efficiency for all coal–biomass-cofired periods was >99.6% because of the high furnace operating temperature and adequate residence time. Based on its slagging

Figure 22. Photographs of the slagging furnace interior after high-density refractory curing (top) and after 751 hr of solid-fuel firing (bottom).

Table 7. Summary of SFS Operating Hours Through December 2003[1]

Natural Gas Firing, hr	Solid Fuel Firing, hr	Total Operation, hr
3795	2133	5928

[1] Natural gas firing represents heatup, cooldown, and test periods.

furnace operating experience, the EERC intends to continue minimum main burner swirl as necessary to establish a stable flame and uniform temperatures over the length of the furnace and minimize NO_x emissions for any future coal or coal–biomass-fired SFS tests.

Slag Screen Performance and Slag Analysis

Commercial slag screen design and the materials are application-specific. Therefore, the observations made in this report concerning slag screen performance are probably less relevant to the performance of a commercial power system design than the observations made with respect to other SFS components (HTHX, CAH, and pulse-jet baghouse). This is true regardless of the fuel type (bituminous coal, subbituminous coal, or lignite). Therefore, evaluating slag screen performance was not a priority for this project. However, the slag screen did impact the operation of the SFS in general and the dilution–quench zone and CAH tube bank specifically. Therefore, observations concerning the impact of coal–biomass cofiring on slag screen performance are relevant to the pilot-scale SFS and are discussed in this section of the report. As expected, fuel ash properties had a significant effect on slag screen performance. Slag screen operating temperature is selected on the basis of ash fusion data for the fuel to be fired. The EERC attempts to operate the slag screen at flue gas temperatures of 55°–111°C (100°–200°F) above the fluid temperature of the fuel ash to ensure slag flow from the slag screen through the slag tap. However, this is not possible for all fuel types. Therefore, it is sometimes necessary to modify the slag screen configuration to match fuel ash properties. For high-ash-fusion fuels, with fluid temperatures of >1427°C (>2600°F), it is generally necessary to reduce the number of tubes in the slag screen from 18 to nine thereby increasing the intertube spacing, as well as reduce the water-cooled surface in each 3.8-cm (1.5-in.) refractory tube to increase the surface temperature. These steps are necessary to prevent slag accumulation and plugging of the slag screen, which would result in a high slag screen differential pressure and a potential forced SFS shutdown. Other successful mitigation steps taken when firing a high-ash-fusion fuel have included the use of limestone to modify slag chemistry and higher-temperature operation of the furnace (1594°C [2900°F]) and slag screen (1483°C [2700°F]) to reduce slag viscosity.

North Antelope subbituminous coal was the primary fuel fired in this project. Based on past experience firing subbituminous coals, a six-row, 18-tube, slag screen configuration was believed to be optimal for fuel ash recovery as slag. In this project, the slag screen performed as intended while cofiring North Antelope subbituminous coal and biomass in the furnace. However, because of differences in the ash chemistry of the biomass fuels and the resulting ash fusion fluid temperatures, 1288°–1468°C (2350°–2673°F), it was necessary to adjust the auxiliary burner firing rate to achieve desired slag screen temperatures to avoid plugging problems.

Test XCEL1 (SFS-XCEL1-0303) involved NG firing to control heatup, refractory curing, and cooldown, and North Antelope subbituminous coal and hog fuel were cofired for 85 hr. Indicated

slag screen temperatures were raised to 1477°C (2690°F) as a result of NG firing and, during the coal–hog fuel-fired test, ranged from 1349° to 1430°C (2460° to 2605°F). Slag screen temperatures were somewhat limited as a result of necessarily low furnace temperatures, which were limited as a result of the <1052°C (<1925°F) surface temperature limit imposed to avoid slag erosion and corrosion of the HTHX alloy tubes. The ash fluid temperature (under oxidizing conditions) of the North Antelope subbituminous coal fired during this test was 1258°C (2296°F). However, the ash fluid temperature (under oxidizing conditions) of the hog fuel cofired was 1468°C (2673°F). During the initial 50 hr of coal–hog fuel cofiring, slag screen differential pressure increased from 1.3 mmHg (0.7 in. W.C.) to 3.9 mmHg (2.1 in. W.C.). In response, the auxiliary burner firing rate was increased from 0.58 to 0.74 × 10^6 kJ/hr (0.55 to 0.70 MMBtu/hr) between Run Hours 112 and 130. As a result, slag screen differential pressure decreased to <3.7 mmHg (<2 in. W.C.) by Run Hour 164. At the end of the coal–hog fuel cofiring test, slag screen differential pressure was nominally 3.2 mmHg (1.7 in. W.C.). Although increasing auxiliary burner firing rate effectively reduced slag screen differential pressure, inspection of the slag screen following Test XCEL1 revealed that the lower half of the slag screen contained a significant amount of accumulated slag.

Table 8 summarizes coal and hog fuel ash and slag composition and fusion temperature data for samples collected during Test XCEL1. Data are reported as oxides normalized to an SO_3-free basis, while the SO_3 numbers are reported as normalized with the other oxides. Reporting the numbers in this way makes it easier to see which elements become enriched or depleted in the slag because sulfur is vaporized during combustion and does not condense until the lower temperatures of the convective pass so it is not usually present in the slag. Slag recovered as it dripped into the slag pot during Test XCEL1 was found to have a fluid temperature (oxidizing conditions) of 1255°C (2291°F), essentially the same as the North Antelope coal ash. Slag composition data showed an increase in silica and alumina content when compared to both fuel ashes and a small decrease in calcia. The opposite trends occurred in the baghouse ash. The increases in silica and alumina in the slag were likely due to the fact that these elements were enriched in the larger mineral grains in the fuel. These larger grains separate from the gas flow more readily in the combustor and slag screen and so become more concentrated in the slag, and depleted in the baghouse ash. The opposite likely happened for the calcium-rich particles.

Although most of the slag flowed down into the slag pot, a significant amount remained frozen within the slag screen at the end of the test. Removal and analyses of the slag accumulated in the slag screen was not possible without damaging the slag screen. Therefore, the EERC elected to leave it to melt out during a subsequent test. Based on the high fusion temperature of the hog fuel ash, it may be that much of slag remaining in the slag screen originated from particles of the hog fuel that burned out within the slag screen. It is likely that if these fuels were cofired in a wet-bottom or cyclone-fired system, the high melting point ash could become problematic with respect to accumulation of slag on water walls and slag tapping from a cyclone if the hog fuel ash deposits separately from the coal ash.

In Test XCEL2 (SFS-XCEL2-0403) North Antelope subbituminous coal and corn stover were cofired for 86 hr. Prior to coal and corn stover cofiring, NG firing was adjusted to raise the furnace

Table 8. Fuel Ash, Slag, and Baghouse Ash Sample Analyses for Test XCEL1

Oxides,[1] wt%	North Antelope Coal	Hog Fuel	Slag	Baghouse Ash
SiO_2	30.4	33.3	37.7	13.9
Al_2O_3	19.1	2.5	20.1	11.9
Fe_2O_3	8.2	3.2	5.4	7.3
TiO_2	1.6	0.3	1.1	1.0
P_2O_5	1.3	1.8	0.9	2.5
CaO	30.1	43.2	28.0	26.6
MgO	7.8	3.9	4.4	5.6
Na_2O	1.2	3.9	1.2	5.8
K_2O	0.3	7.9	1.1	6.8
SO_3[2]	10.9	0.0	0.0	18.5
Fluid Temp., °C	1258	1467	1255	—

[1] Fuel and slag oxide concentrations normalized to an SO_3-free basis.
[2] Fuel and slag SO_3 concentrations normalized with other oxides.

and slag screen temperature to melt slag deposits formed during Test XCEL1. Once this was accomplished, as indicated by decreasing slag screen differential pressure, coal and corn stover cofiring was initiated. Slag screen temperatures were raised to 1410°C (2570°F) during NG firing and ranged from 1338° to 1416°C (2440° to 2580°F) during the coal–corn stover-fired test. The ash fluid temperatures (under oxidizing conditions) of the North Antelope subbituminous coal and the corn stover cofired during this test were 1236°C (2257°F) and 1288°C (2350°F), respectively. No slag screen-plugging problems were observed during the 86 hr coal–corn stover-fired period. In fact, slag screen differential pressure decreased from 2.1 to 1.1 mmHg (1.1 to 0.6 in. W.C.) during the coal–corn stover-fired test. Therefore, the auxiliary burner firing rate was maintained at 0.58×10^6 kJ/hr (0.55 MMBtu/hr) for the duration of solid fuel firing. Inspection of the slag screen following Test XCEL2 revealed that the slag that had accumulated during Test XCEL1 had melted and flowed from the slag screen to the slag tap and was recovered in the slag pot.

Table 9 summarizes coal and corn stover fuel ash and slag composition and fusion temperature data for samples collected during Test XCEL2. The slag sample characterized was recovered after the initial decrease in slag screen differential pressure, indicating that the slag accumulated in the slag screen during Test XCEL1 had flowed into the slag pot. Slag recovered as it dripped into the slag pot during Test XCEL2 was found to have a fluid temperature (oxidizing conditions) of 1299°C (2371°F), more than 38°C (100°F) higher than the coal ash but very similar to the corn stover ash. A greater percentage of the silica in the ash reported to the slag as well as smaller percentages of volatile alkali metals and calcium found in both fuels, leaving the baghouse ash with opposite enrichments/depletions. The enrichment of silica in the slag is likely due to the relatively larger size of silica-based minerals in the fuels causing them to deposit preferentially in the combustor and slag screen. The lower concentration of calcium in the slag is likely due to the fact that mineral particles enriched in that element were typically smaller and passed through the system to concentrate in the baghouse, along with the more volatile alkali metals. Based on the ash fusion temperature and slag

Table 9. Fuel Ash, Slag, and Baghouse Ash Sample Analyses for Test XCEL2

Oxides,[1] wt%	North Antelope Coal	Corn Stover	Slag	Baghouse Ash
SiO_2	29.5	58.2	45.5	20.5
Al_2O_3	20.0	3.3	18.6	14.9
Fe_2O_3	8.2	1.5	5.3	5.5
TiO_2	1.7	0.3	1.1	1.1
P_2O_5	1.4	3.9	1.0	5.2
CaO	30.1	9.6	20.3	28.6
MgO	7.9	12.8	5.9	6.9
Na_2O	1.0	0.4	0.9	2.3
K_2O	0.3	10.1	1.4	6.0
SO_3[2]	12.6	1.5	0.0	9.0
Fluid Temp., °C	1236	1288	1299	—

[1] Fuel and slag oxide concentrations normalized to an SO_3-free basis.
[2] Fuel and slag SO_3 concentrations normalized with other oxides.

composition data, the slag that was collected in the slag pot was slightly more refractory than either of the fuel ashes, consistent with composition of the slag. Based on the slag screen observations, cofiring North Dakota coal and corn stover in a low-temperature dry-ash system should not result in slag deposition or accumulation problems. Also, if these fuels were cofired in a wet-bottom or cyclone-fired system, the ash characteristics of the corn stover would not likely become problematic with respect to accumulation of slag on water walls and slag tapping from a cyclone.

Test XCEL3 (SFS-XCEL3-0503) involved NG firing to control heatup, refractory curing, and cooldown. North Antelope subbituminous coal and switchgrass were cofired for 85 hr. Indicated slag screen temperatures were raised to 1335°C (2435°F) as a result of NG firing and during the coal–switchgrass-fired test period ranged from 1327° to 1352°C (2420° to 2465°F). These temperatures may be lower than actual temperatures because of thermocouple deterioration as a result of slag erosion and corrosion. The ash fluid temperatures (under oxidizing conditions) of the North Antelope subbituminous coal and the switchgrass cofired during this test were 1236°C (2257°F) and 1288°C (2350°F), respectively. No slag screen-plugging problems were observed during the 85 hr coal– switchgrass-fired period as indicated by slag screen differential pressure ranging from 1.1 to 1.5 mmHg (0.6 to 0.8 in. W.C.). Therefore, although the auxiliary burner firing rate was initially set at 0.63×10^6 kJ/hr (0.60 MMBtu/hr) because the switchgrass and hog fuel ash fluid temperatures were similar, the auxiliary burner firing rate was reduced to 0.58×10^6 kJ/hr (0.55 MMBtu/hr) after 12 hr of solid fuel firing and maintained at that rate for the duration of test. Inspection of the slag screen following Test XCEL3 revealed that no slag had accumulated and that some erosion/corrosion of the tubes had occurred, indicating that auxiliary burner-firing rate and slag screen temperatures could have been reduced somewhat for these fuels.

Table 10 summarizes coal and switchgrass fuel ash and slag composition and fusion temperature data for samples collected during Test XCEL3. Slag recovered as it dripped into the slag

Table 10. Fuel Ash, Slag, and Baghouse Ash Sample Analyses for Test XCEL3

Oxides,[1] wt%	North Antelope Coal	Switchgrass	Slag	Baghouse Ash
SiO_2	29.8	72.7	51	21.0
Al_2O_3	20.1	0.0	15.2	14.7
Fe_2O_3	8.3	0.2	5.4	7.0
TiO_2	1.7	0.03	1	1.2
P_2O_5	1.3	4.9	1.1	5.6
CaO	29.4	9.7	18.9	28.2
MgO	7.9	5.1	5	6.4
Na_2O	1.3	0.03	0.8	2.1
K_2O	0.3	7.2	1.5	4.3
SO_3[2]	8.9	3.3	0	9.7
Fluid Temp., °C	1227	1459	1350	—

[1] Fuel and slag oxide concentrations normalized to an SO_3-free basis.
[2] Fuel and slag SO_3 concentrations normalized with other oxides.

pot during Test XCEL3 was found to have a fluid temperature (oxidizing conditions) of 1350°C (2462°F), 122°C (220°F) higher than the coal ash and 111°C (200°F) lower than the switchgrass ash. Composition data indicate that, as was true for the corn stover test, a greater percentage of the silica in the ash reported to the slag as well as smaller percentages of volatile alkali metals and calcium found in both fuels, leaving the baghouse ash with opposite enrichments/depletions. The enrichment of silica in the slag is likely due to the relatively larger size of silica-based minerals in the fuels causing them to deposit preferentially in the combustor and slag screen. The lower concentration of calcium in the slag is likely due to the fact that mineral particles enriched in that element were typically smaller and passed through the system to concentrate in the baghouse, along with the more volatile alkali metals. Based on the slag screen observations, cofiring North Antelope coal and switchgrass in a low-temperature dry-ash system should not result in slag deposition or accumulation problems. Also, if these fuels were cofired in a wet-bottom or cyclone-fired system, the ash characteristics of the switchgrass would not likely become problematic with respect to accumulation of slag on water walls and slag tapping from a cyclone.

Following each coal–biomass-cofiring test, slag and ash samples from system components and piping were collected and weighed in order to prepare a mass balance. A total theoretical ash quantity was calculated on the basis of the total fuel feed and the measured ash content of the composite fuel samples. Table 11 summarizes the ash mass balance data for each of the three test periods. Overall ash recovery ranged from 70% to 92%. Based on slag screen performance, previously discussed, the lower degree of closure observed for Test XCEL1 was the result of unrecoverable slag in the slag screen and the higher degree of closure observed for Test XCEL2 resulted from slag deposited in the slag screen during Test XCEL1 and recovered from the slag screen during Test XCEL2. Based on previous SFS tests firing bituminous and subbituminous coals, slag and ash recovery typically represents 80%–85% of the ash entering the system. Unrecoverable slag is typically lost to the furnace walls, in the bottom of the furnace, in the slag screen, and in the

Table 11. Ash Material Balance for the Coal–Biomass Cofiring Tests[1]

Test	XCEL1	XCEL2	XCEL3
Coal Ash In, kg	249	260	265
Biomass Ash In, kg	121	177	118
Total Solids In, kg	369	437	383
Slag–Ash Recovered			
Slag Pot, kg	173	273	232
Drawdown Ash, kg	0	0	0.9
Quench Zone Pot, kg	26	48.0	28
Quench Zone Walls, kg	1	9.1	4.5
CAH Probe–Duct Ash, kg	7.7	7.3	5.4
Air Preheater Surfaces, kg	3	8.2	4.5
Tube and Shell HX's 1 and 2, kg	3	5.0	4
Tube and Shell HX's 3 and 4, kg	3	3	2
Tube and Shell HX Elbows, kg	0.9	0.5	0.9
Baghouse Ash, kg	39	48.5	54.4
Miscellaneous Surfaces, kg	0	0	0.9
Total Slag/Ash Recovered, kg	258	403	337
Closure, %	70	92	88

[1] Solids recovered from the slag pot, quench zone, and drawdown subsystems are considered slag. Solids recovered from all other subsystems are classified as ash.

upper section of the dilution–quench zone. Some unrecoverable ash is lost to refractory-lined duct work even though these surfaces are brushed and to baghouse bags that are typically vacuumed.

Ash recovered as slag represented 54–76 wt%. Again, the range was affected by slag screen plugging during Test XCEL1. The 69 wt%, ash recovered as slag, a value observed for Test XCEL3 is comparable to data observed for previous subbituminous coal-fired SFS tests. Ash recovered in the CAH represented 1.4–2.1 wt% of the ash input with the fuel, consistent with past experience. Ash recovered in the baghouse represented 11–14 wt% of the ash input with the fuel, somewhat lower than values previously observed when firing subbituminous coal but within the range observed for bituminous and subbituminous coals for multiple slag screen configurations.

Dilution–Quench Zone

The dilution–quench zone functioned as expected. FGR was effectively used during all three coal–biomass cofiring tests to quench flue gas and entrained ash–slag particle temperatures upstream of the CAH tube bank. As a result, the flue gas temperature entering the CAH tube bank was nominally 983°C (1800°F). During each coal–biomass cofiring test, it was necessary periodically to clean the dilution–quench zone online to remove excessive slag deposits in the vicinity of the FGR nozzles and avoid the potential for significant increases in differential pressure and a potential forced shutdown. Periodic cleaning also improves the efficiency of the quench zone and enhances

the contribution of a water jacket to overall heat transfer, reducing the volume of recirculated flue gas required. About 7%–13% of the ash–slag recovered from the SFS was from the dilution–quench zone. This range is consistent with previous SFS tests firing subbituminous coal.

Process Air Preheaters

Process air for the CAH tube bank and the HTHX alloy tubes is heated using air preheater tube bundles located downstream of the CAH. The first air preheater tube bundle supplies process air for the CAH tube bank. Process air flow rates and temperature are adjusted and controlled to achieve desired process air temperatures at the inlet of the CAH tube bank and the inlet of the HTHX alloy tubes. Further heating of the process air entering the HTHX alloy tubes was achieved electrically and by recovering heat from the CAH tube bank. Although the process air preheater heat-transfer rate degraded as ash deposits developed on the tube surfaces during coal–biomass cofired tests, process air temperature and flow rate control were adequate to support operation of the CAH tube bank and HTHX alloy tubes.

Figure 23 illustrates process air preheater temperature data as a function of run time for Test XCEL2. In general, the data illustrated in the figure represent trends for all three coal–biomass cofiring test periods, showing that as the run progressed and the tubes became coated with ash, the process air temperatures exiting the HXs dropped. During Test XCEL2, process air exiting the first air preheater was controlled at temperatures ranging from 371° to 466°C (700° to 870°F) for a process air flow rate of 3.5–3.7 m^3/min (125–130 scfm). Process air temperatures at the exits of the other four preheater tube bundles were 493°–610°C (920°–1130°F) for flow rates totaling 7.2–

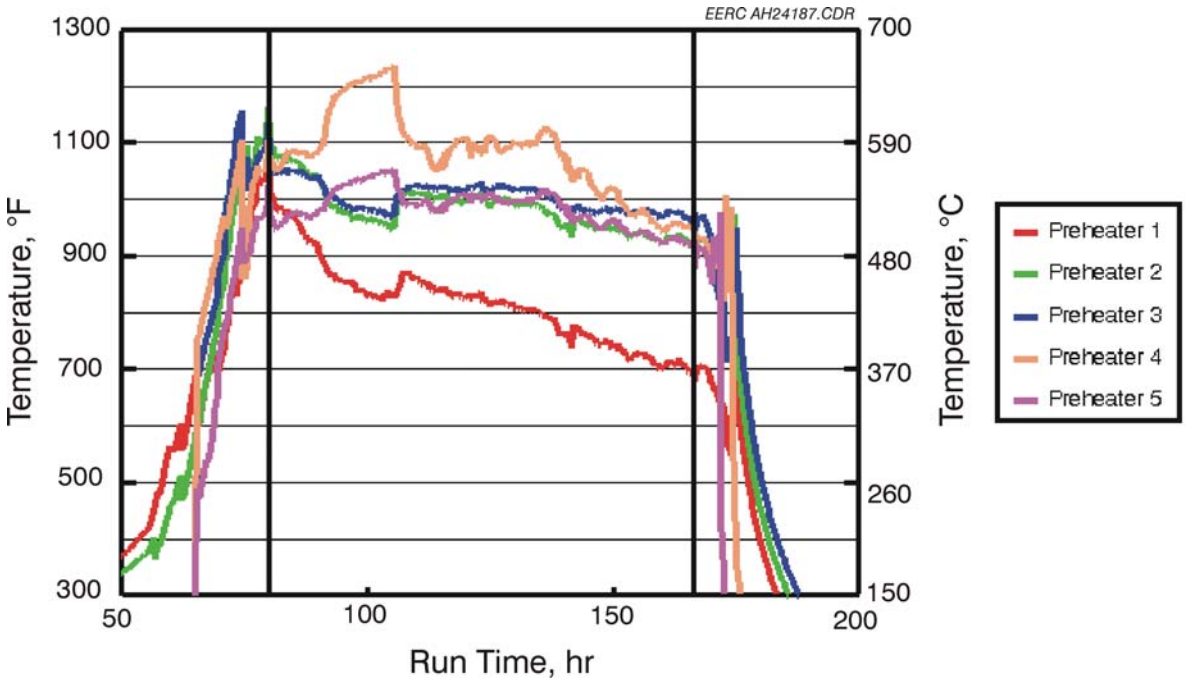

Figure 23. Process air preheater temperatures versus run time for Test SFS-XCEL2-0403.

7.6 m^3/min (255–270 scfm). During Tests XCEL1 and XCEL3, process air exiting the first preheater was controlled at temperatures ranging from 427° to 494°C (800° to 920°F) for process air flow rates of 3.4–4.2 m^3/min (120–150 scfm). Process air temperatures at the exits of the other four preheater tube bundles were 491°–652°C (915°–1205°F) for flow rates totaling 6.5–7.6 m^3/min (230–270 scfm).

Baghouse Performance

The characteristics of the fly ash generated in the high-temperature SFS are different than those observed for a given fuel fired in a conventional pc-fired system. Specific differences observed include a reduction in mass loading and particle size and a higher concentration of alkaline-earth components, and reductions in silica concentrations. This shift in ash properties was anticipated based on the use of a slag screen at the furnace exit to promote ash collection as slag. Ash passing through the slag screen is expected to represent smaller ash particles as well as ash components volatilized in the furnace and subsequently condensed at lower temperatures downstream. The clean-air plenum is routinely removed from the pulse-jet baghouse following SFS tests and the bags are inspected. In all cases, the tube sheet has been found to be clean, consistent with the low level of particulate emissions measured, and the bags pulled for inspection were found to be in good condition. When plans involve the firing of a different fuel, the bags are cleaned to avoid ash contamination from one test to another.

North Antelope subbituminous coal was the primary fuel fired in this project. However, the cofiring of three different biomass fuels impacted baghouse ash characteristics with the potential to affect baghouse performance. The bags used in support of this project were a woven glass–PTFE membrane-fabric combination. During previous projects firing bituminous and subbituminous coal, online cleaning was effective, and particulate control was good with this fabric type.

During coal–biomass cofired tests, baghouse temperatures and temperature profiles were as expected, and the electrical heaters worked well, limiting the potential for condensation on start-up and shutdown. Baghouse temperatures ranged from 166° to 174°C (330° to 345°F) for Test XCEL1, 163° to 174°C (325° to 345°F) for Test XCEL2, and from 152° to 166°C (305° to 330°F) for Test XCEL3. Figure 24 illustrates baghouse temperature versus run time for Test XCEL1. Baghouse temperature was intentionally reduced somewhat for Test XCEL3 to improve online bag cleaning. This issue will be addressed in more detail in the discussion of baghouse differential pressure.

Flue gas flow rates as a result of coal–biomass cofiring were 26.3–28.9 m^3/min (930–1020 scfm) for Test XCEL1, 22.1–26.6 m^3/min (780–940 scfm) for Test XCEL2, and 21.0–24.1 m^3/min (740–850 scfm) for Test XCEL3. Actual flue gas flow rates through the baghouse were 41.3–45.9 m^3/min (1460–1620 acfm), 34.7–41.8 m^3/min (1225–1475 acfm), and 31.7–37.7 m^3/min (1120–1330 acfm), respectively, for the three coal–biomass cofiring test periods. The higher flue gas flow rate observed for Test XCEL1 resulted from a higher auxiliary burner firing rate and higher hog fuel moisture content. The lowest flue gas flow rate was observed for Test XCEL3 because the switchgrass had the lowest moisture content and was fired at the lowest average rate.

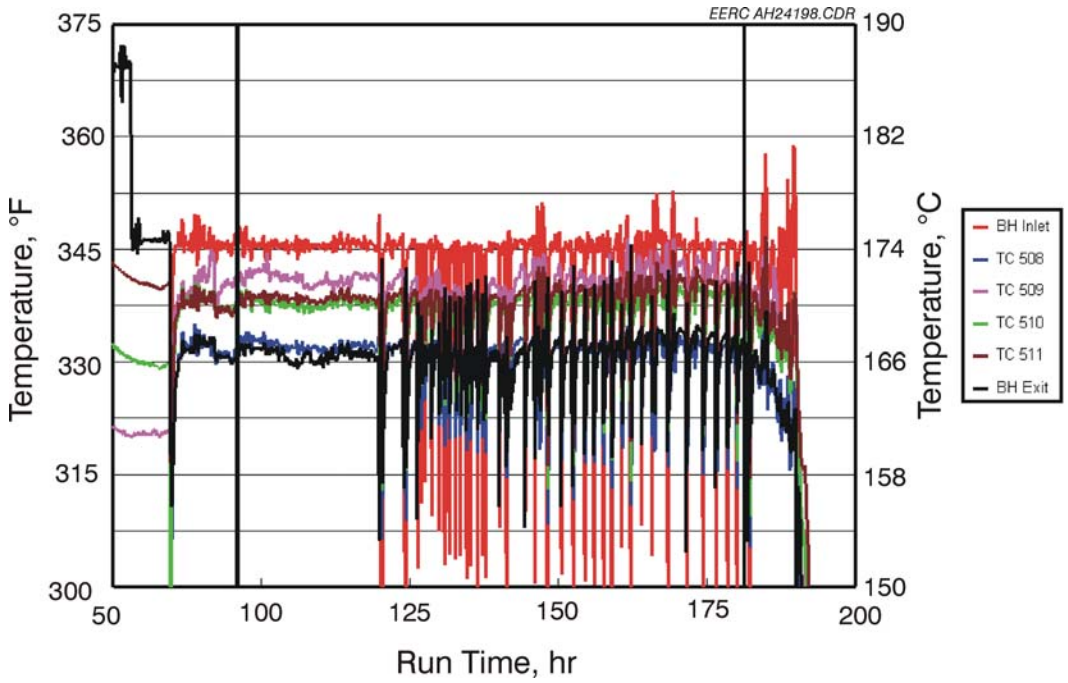

Figure 24. Baghouse temperature versus run time for Test SFS-XCEL1-0303.

The 36 bags (total filtration area of 52.5 m^2 [565 ft^2]) used in the baghouse were a 747 g/m^2 (22-oz/yd^2) woven glass with a PTFE membrane. The filter face velocities for the three coal–biomass cofiring tests were 0.70–0.85 m/min (2.0–2.9 ft/min). These filter face velocities are low compared to conventional pulse-jet filtration systems typically operating at or near 1.2 m/min (4 ft/min). Although evaluating baghouse performance was not a primary objective for this project, biomass cofiring had a significant impact on bag cleaning.

Online pulse cleaning of the PTFE membrane bags was accomplished using reservoir pulse-air pressures of 2.8–4.1 bar (40–60 psig) for previous bituminous and subbituminous coal-fired SFS tests (3). The baghouse differential pressure-cleaning set point was 11.2 mmHg (6 in. W.C.). Once the initial dust cake was formed, the cleaning frequency was 3–5 hr when firing an Illinois No. 6 bituminous coal (with and without CaO injection to control SO_3 emissions) and nominally 2 hr when firing a subbituminous coal. The bags were cleaned to a differential pressure of <5.6 mmHg (<3 in. W.C.) when firing bituminous coal and <7.5 mmHg (<4 in. W.C.) when firing subbituminous coal.

Figure 25 presents baghouse differential pressure as a function of run time for Test XCEL1. The online cleaning cycle trigger point was initially set at 11.2 mmHg (6 in. W.C.), and the first cleaning cycle occurred after nominally 6 hr of coal–hog fuel cofiring. However, this initial cleaning cycle only reduced the differential pressure to 8.4 mmHg (4.5 in. W.C.). Over the first 24 hr of coal–hog fuel cofiring, online cleaning became continuous and differential pressure control was erratic for reservoir pulse-air pressures ranging from 2.8 to 5.9 bar (40 to 85 psig). Therefore, the bags were cleaned off-line using a reservoir pulse air pressure of 4.1 bar (60 psig) and the cleaning-cycle trigger point was increased to 13.1 mmHg (7 in. W.C.). Online cleaning was again attempted and found to

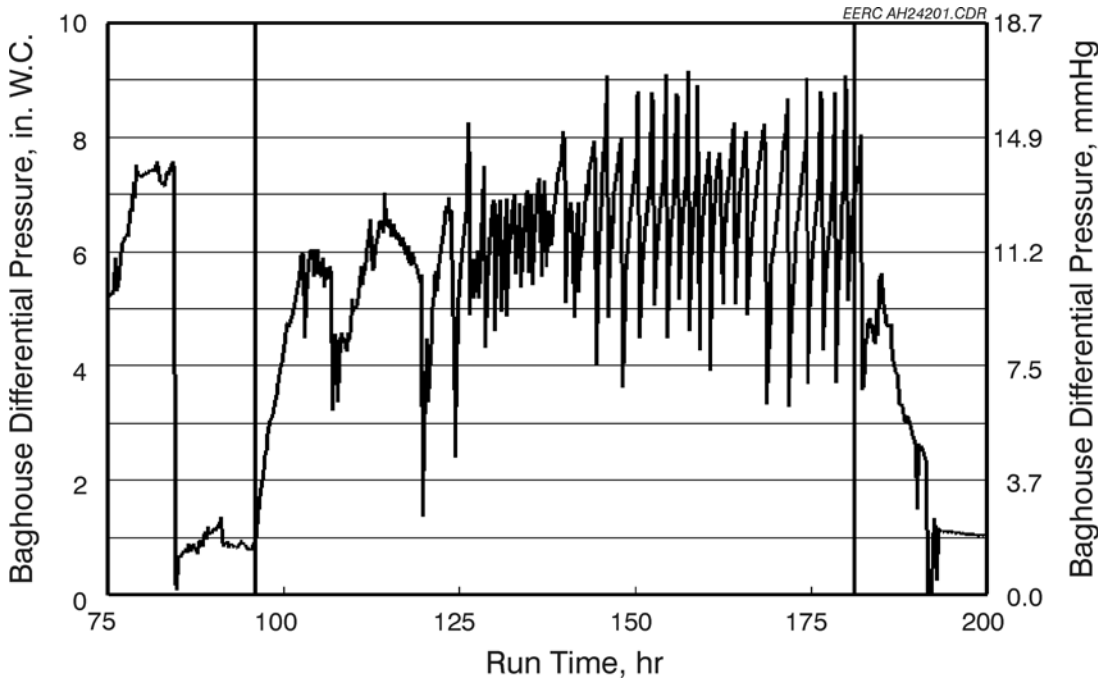

Figure 25. Baghouse differential pressure versus run time for Test SFS-XCEL1-0303.

be unsuccessful, forcing off-line cleaning. Increasing the trigger point to 14.9 and 16.8 mmHg (8 and 9 in. W.C.) also resulted in unsuccessful attempts to clean the bags online. Therefore, it was necessary to use off-line cleaning to control baghouse differential pressure during Test XCEL1, and cleaning frequency was 5–6 hr based on an off-line cleaning trigger point of 14.9 to 16.8 mmHg (8 to 9 in. W.C.).

Figure 26 presents baghouse differential pressure as function of run time for Test XCEL2. The online cleaning cycle trigger point was initially set at 9.3 mmHg (5 in. W.C.), and the first cleaning cycle only reduced the differential pressure to 7.5 mmHg (4 in. W.C.). Online cleaning was subsequently attempted at trigger points of 11.2 and 14.9 mmHg (6 and 8 in. W.C.) without success. Therefore, it was necessary to use off-line cleaning to control baghouse differential pressure when cofiring coal and corn stover during Test XCEL2. The off-line cleaning cycle trigger point was nominally 14.9 mmHg (8 in. W.C.) and cleaning frequency was 2–3 hr.

Figure 27 presents baghouse differential pressure as a function of run time for Test XCEL3. The online cleaning cycle trigger point was initially set at 11.2 mmHg (6 in. W.C.), baghouse temperature was reduced to nominally 154°C (310°F), and the first cleaning cycle successfully reduced the differential pressure to <3.7 mmHg (<2 in. W.C.). However, online cleaning became less effective with each subsequent cleaning cycle. After 26 hr of coal–switchgrass cofiring, it was necessary to use off-line cleaning to control baghouse differential pressure. The off-line cleaning-cycle trigger point was nominally 11.2 mmHg (6 in. W.C.) and cleaning frequency was 3–4 hr.

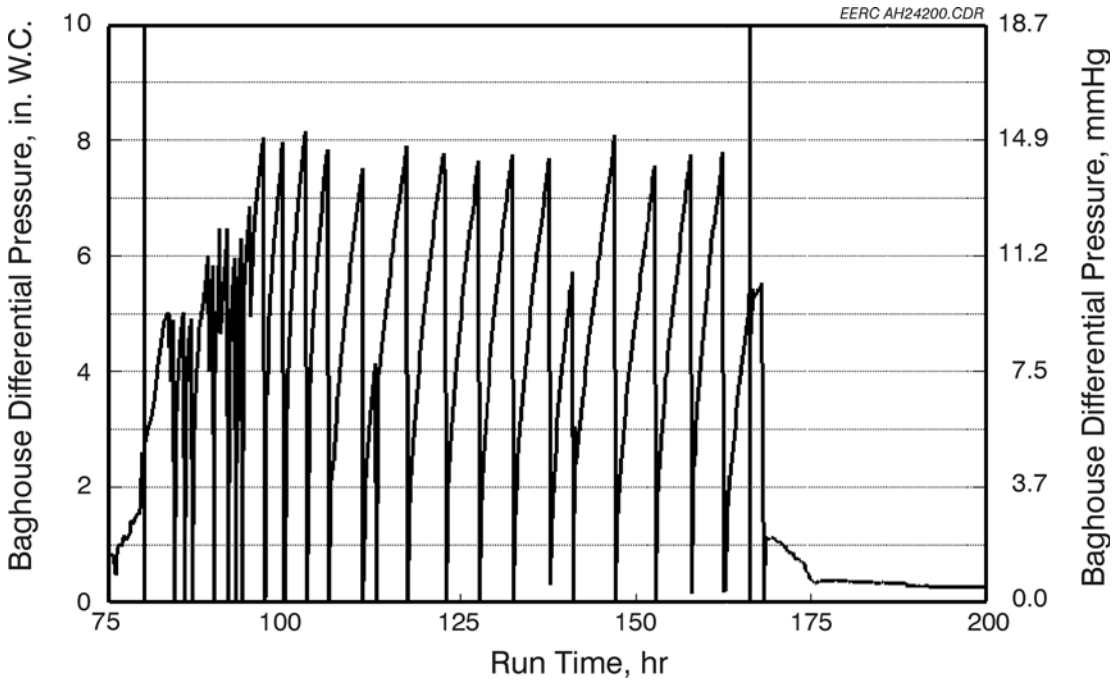

Figure 26. Baghouse differential pressure versus run time for Test SFS-XCEL2-0403.

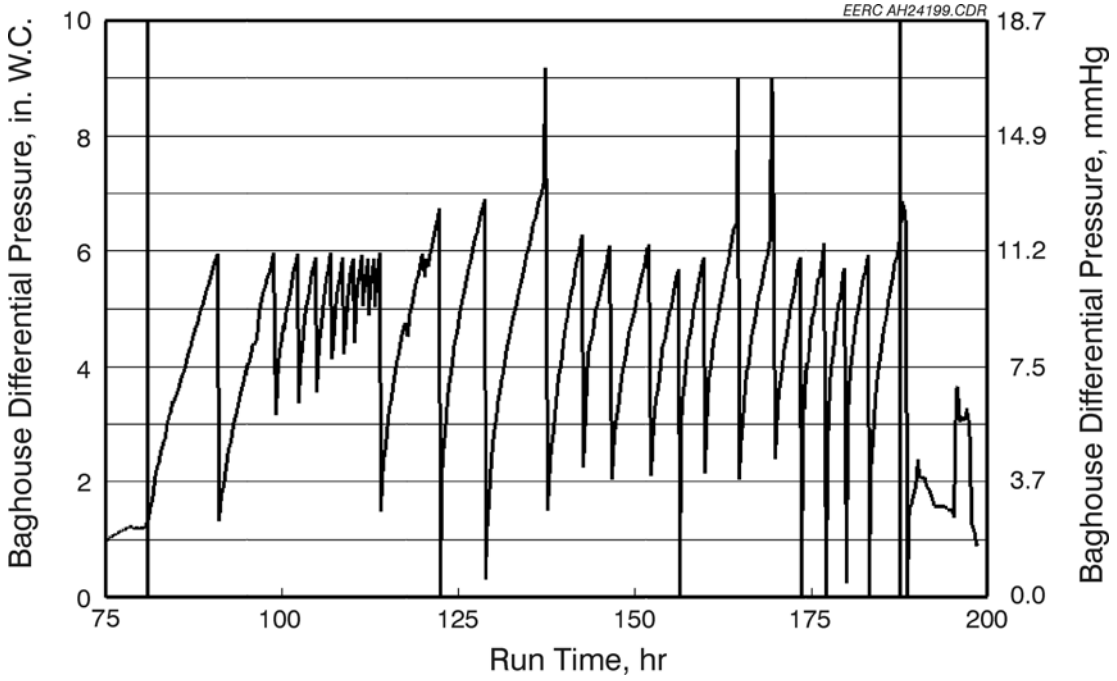

Figure 27. Baghouse differential pressure versus run time for Test SFS-XCEL3-0503.

Since online baghouse cleaning had not been a problem previously when firing a subbituminous coal, consideration must be given to the potential impact of biomass cofiring. Typically, 10%–15% of the ash in the fuels fired in the SFS reaches the baghouse. Baghouse ash recovered following the biomass cofiring tests represented 11%–14% of the total fuel ash. Particle-size and chemical composition analyses were completed for a composite ash sample collected from the baghouse hopper for each biomass cofiring test. Table 12 summarizes baghouse ash composition data for Tests XCEL1, XCEL2, and XCEL3 and a baghouse ash generated previously firing a Cordero Rojo subbituminous coal. Composition data for these samples show expected shifts in composition when baghouse ash is compared with the fuel ash for a slagging system. Specifically, concentrations of alkali and alkaline earth components increase, while silica and alumina concentrations decrease. In addition, the alkali components are not highly sulfated, typically <30 mole %.

Table 12. Baghouse Bulk Ash Sample Analyses for Tests XCEL1, XCEL2, and XCEL3 and a Previously Fired Subbituminous Coal

Oxides,[1] wt%	Cordero Rojo Coal	XCEL1	XCEL2	XCEL3
SiO_2	21.2–22.0	13.9	20.5	21.0
Al_2O_3	16.1–16.9	11.9	14.9	14.7
Fe_2O_3	6.7	7.3	5.5	7.0
TiO_2	1.4	1.0	1.1	1.2
P_2O_5	2.0	2.5	5.2	5.6
CaO	30.6–31.0	26.6	28.6	28.2
MgO	5.0	5.6	6.9	6.4
Na_2O	2.2–2.3	5.8	2.3	2.1
K_2O	0.6	6.8	6.0	4.3
SO_3	12.6–13.7	18.5	9.0	9.7

[1] Oxide concentrations normalized to 100% closure.

A comparison of the fuel ash composition data in Tables 5 and 6 for the North Antelope and Cordero Rojo subbituminous coals shows they are nearly identical. Therefore, any differences noted in the baghouse ash composition data in Table 12 would have to be a function of biomass cofiring. The primary difference in composition data is an order-of-magnitude or near-order-of-magnitude increase in the potassium content for the baghouse ash resulting from biomass cofiring. Phosphorus content is higher in two of the three biomass cofiring ash samples, and sodium is higher in the third. Therefore, one factor likely contributing to online baghouse-cleaning difficulties is an increase in the alkaline-earth content of the ash, specifically potassium and sodium, and the presence of phosphorus. The potassium and sodium constituents would be expected to be highly sulfated. However, the SO_3 content of the baghouse ash samples resulting from biomass cofiring is insufficient for sulfation levels of more than 16 (Test XCEL2) to 30 mole % (Test XCEL1) of the total alkali content based on calcium, sodium, and potassium. The low degree of alkali sulfation is a direct result of the low sulfur content of the coal (0.23–0.25 wt%) and biomass fuels (0.04–0.13 wt%) and the association of calcium with alumina and silicates.

SEM spot analyses were performed on representative ash particles in four composite baghouse ash samples, three resulting from the coal–biomass cofiring tests and one from a previous SFS test firing a Cordero Rojo subbituminous coal. Elemental results are summarized in Tables 13–16, and the corresponding SEM micrographs identifying the analysis points are contained in Figures 28–31. Based on the data, the elemental composition of point analyses for spherical ash particles in the 1–2-µm size range is dominated by the major components identified in the bulk fuel ash analyses. These elements include silica and calcia, with smaller concentrations of alumina, iron, and magnesium. Phosphorus appears to be associated with the calcium constituents. Single-point analyses of smaller nonspherical ash particles attached to the surface of the larger spherical particles or as a matrix between the larger ash particles showed a significant enrichment in potassium and sulfur for the coal–biomass-cofiring tests when compared to Test SFS-RH12-0200 firing the Cordero Rojo subbituminous coal. Some sodium enrichment also was observed in the case of hog fuel cofiring (Test XCEL1). The highest degree of potassium enrichment was observed for corn stover cofiring (Test XCEL2), consistent with the bulk fuel data showing the corn stover to have the highest ash content and the highest potassium content in the ash. Calculated mole ratios based on the elemental analysis data indicate that the potassium and sodium are present as sulfates. These data support the hypothesis that potassium sulfate formation and condensation were responsible for altering the cohesive properties of the baghouse ash resulting from coal–biomass cofiring when compared to previous subbituminous coal-fired tests and the difficulties encountered controlling differential pressure using online cleaning.

To determine if a change in baghouse ash cohesive properties occurred, baghouse hopper ash samples from the three coal–biomass cofiring tests and a previous test firing the Cordero Rojo subbituminous coal were evaluated using a Hosokawa Micron Powder Characteristics Tester. Data from several measurements are summarized in Table 17. The dispersibility measurement is an indication of how easily a sample disperses upon dropping onto a surface. The dispersibility data show that cofiring each of the three biomass types resulted in a baghouse ash with lower dispersibility than when firing coal alone, indicating a greater cohesive character for the baghouse ash resulting from coal–biomass cofiring.

The aerated density is the bulk density of the powder formed by sifting it into a cup. The packed density is the bulk density seen upon shocking of the previously sifted material. Together, these two density values are used to calculate the percent compressibility. A high compressibility value usually is associated with a less cohesive material, but this value also is dependent on particle size and shape. Aerated- and packed-density data must be interpreted with caution because the values also are dependent on the particle density of the individual materials. In this case, the compressibility values indicate that the baghouse ash samples resulting from coal–biomass cofiring are more cohesive than the sample resulting from coal firing alone.

The cohesiveness measurement involves the use of three sieves with openings of 75, 150, and 250 µm. Cohesiveness is calculated on the percentages of the sample mass retained on each screen. This measurement can be influenced by particle size. However, in this case, particle size was not a

Table 13. SEM Morphology Results for Test SFS-XCEL1-0303 Baghouse Ash

Element,[1] wt%	Point 1	Point 2	Point 3	Point 4	Point 5	Point 6
Si	15.5	2.1	3.6	4.6	1.3	8.1
Al	4.6	5.4	4.4	4.7	6.3	3.8
Fe	2.4	5.9	5.4	4.2	10.3	7.5
Ti	3.4	0.0	0.0	0.0	0.9	1.4
P	0.7	1.0	1.7	1.7	1.8	1.4
Ca	41.8	49.6	19.0	20.4	17.4	30.1
Mg	5.7	6.2	1.8	2.5	2.2	3.0
Na	0.9	2.0	4.8	7.0	5.2	3.7
K	0.8	2.0	20.1	11.3	11.3	9.9
S	1.2	6.8	18.5	16.4	14.9	12.0
Cl	0.0	0.0	0.2	0.7	0.3	0.6
Cr	0.3	0.0	0.5	0.0	0.0	0.0
Ba	0.0	0.0	1.5	1.1	0.0	0.7
O	22.7	19.0	18.5	25.4	28.1	17.8

[1] Element concentrations normalized to 100% closure.

Table 14. SEM Morphology Results for Test SFS-XCEL2-0403 Baghouse Ash

Element,[1] wt%	Point 1	Point 2	Point 3	Point 4	Point 5	Point 6
Si	21.3	8.2	4.2	3.4	3.2	2.6
Al	19.2	8.8	5.4	7.1	1.7	2.6
Fe	2.8	9.9	7.4	6.2	2.4	6.4
Ti	0.3	1.7	1.0	1.3	0.4	0.6
P	0.4	3.4	2.1	0.9	1.5	1.6
Ca	14.7	26.9	33.1	27.3	19.7	34.1
Mg	4.1	4.5	2.6	4.6	2.7	1.7
Na	2.6	1.2	0.8	0.6	1.0	0.4
K	5.2	2.9	12.9	10.7	15.5	20.5
S	0.9	4.0	14.8	14.1	16.8	18.8
Cl	0.0	0.6	1.1	1.1	1.1	0.9
Cr	0.3	0.1	0.2	0.0	0.0	0.0
Ba	1.7	2.6	0.8	0.7	2.0	1.4
O	26.5	25.2	13.6	22.0	32.0	8.4

[1] Element concentrations normalized to 100% closure.

Table 15. SEM Morphology Results for Test SFS-XCEL3-0503 Baghouse Ash

Element,[1] wt%	Point 1	Point 2	Point 3	Point 4
Si	3.4	10.4	7.2	7.5
Al	9.4	8.9	6.4	7.8
Fe	13.0	4.0	3.9	5.6
Ti	1.6	4.0	1.1	1.4
P	6.3	1.9	3.4	4.4
Ca	40.2	23.2	29.5	30.2
Mg	6.7	3.2	3.7	3.5
Na	1.2	2.5	1.9	1.6
K	1.4	5.8	9.4	7.6
S	2.9	8.4	14.7	9.4
Cl	0.1	0.3	0.3	0.4
Cr	0.0	0.3	0.3	0.0
Ba	0.3	1.1	0.4	2.6
O	13.5	26.0	17.8	18.0

[1] Element concentrations normalized to 100% closure.

Table 16. SEM Morphology Results for Test SFS-RH12-0200 (Cordero Rojo) Baghouse Ash

Element,[1] wt%	Point 1	Point 2	Point 3	Point 4	Point 5	Point 6
Si	10.4	11.1	11.6	8.6	9.6	9.0
Al	15.3	11.8	11.4	7.9	9.6	8.4
Fe	5.9	11.2	5.4	7.3	7.2	9.4
Ti	0.6	0.3	0.6	0.7	1.8	0.0
P	1.1	1.0	1.2	1.4	0.9	1.8
Ca	39.9	39.4	27.9	34.3	36.4	44.5
Mg	2.8	3.6	3.6	2.7	3.1	1.8
Na	0.6	0.3	1.3	1.8	1.6	0.7
K	0.0	0.0	1.2	0.4	1.0	0.9
S	2.7	2.4	11.7	13.6	10.3	10.8
Cl	0.1	0.1	0.4	0.3	0.1	0.0
Cr	0.0	0.0	0.0	0.0	0.0	0.0
Ba	2.1	2.5	1.2	2.1	0.6	4.5
O	18.5	16.3	22.5	18.9	17.8	8.2

[1] Element concentrations normalized to 100% closure.

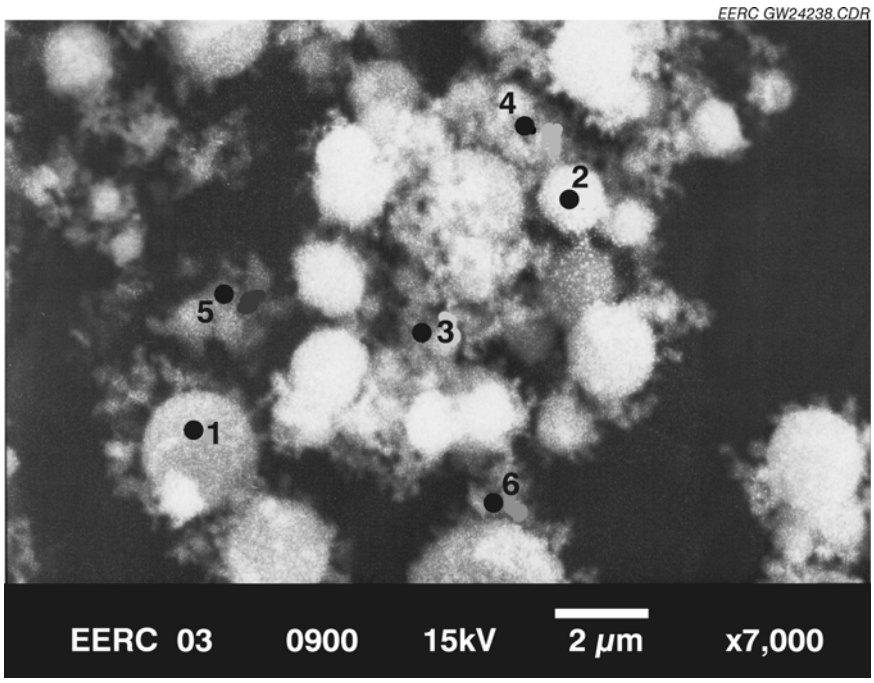

Figure 28. SEM micrograph of Test SFS-XCEL1-0303 baghouse ash.

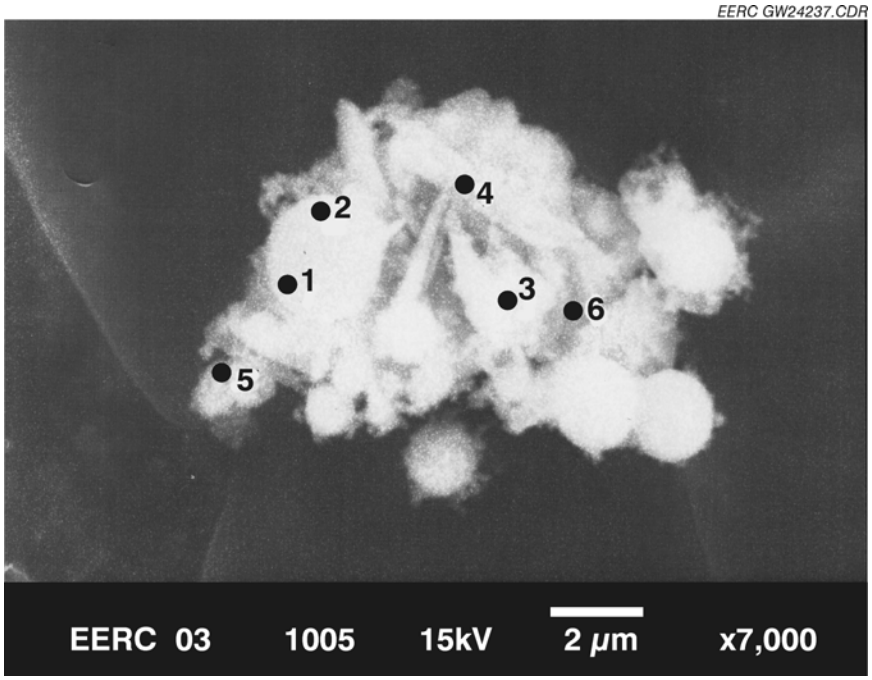

Figure 29. SEM micrograph of Test SFS-XCEL2-0403 baghouse ash.

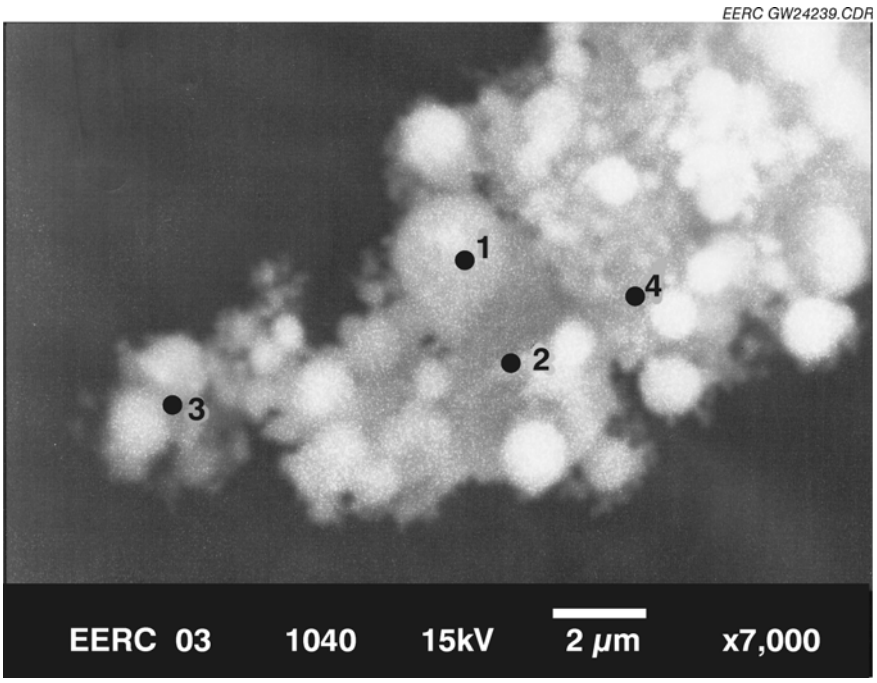

Figure 30. SEM micrograph of Test SFS-XCEL3-0503 baghouse ash.

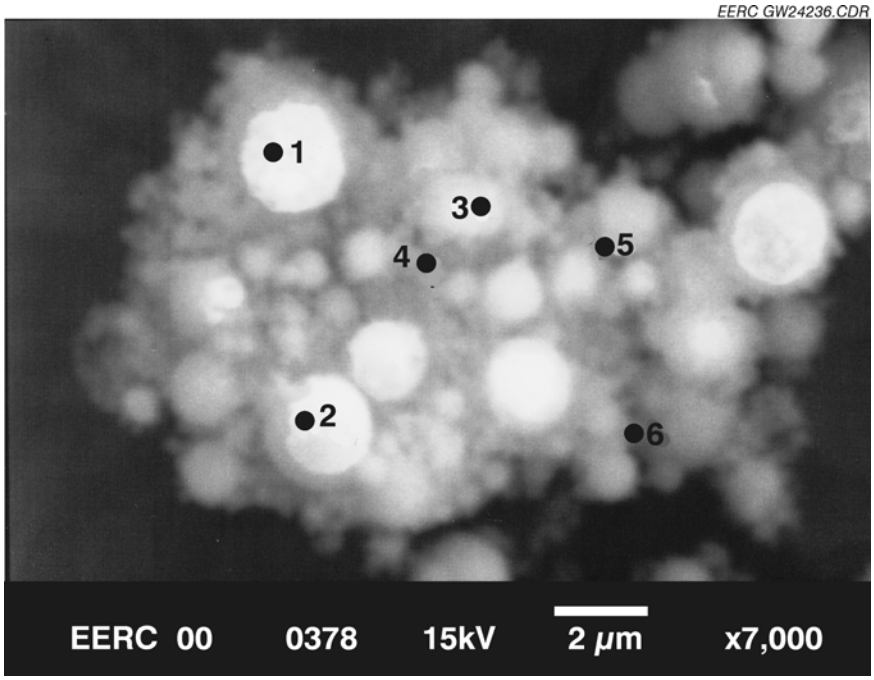

Figure 31. SEM micrograph of Test SFS-RH12-0200 (Cordero Rojo) baghouse ash.

Table 17. Cohesive Characteristics of Baghouse Ash Samples for Tests XCEL1, XCEL2, XCEL3 and a Previously Fired Subbituminous Coal

Sample	Dispersibility, %	Aerated Bulk Density, g/cm^3	Packed Bulk Density, g/cm^3	Compressibility, %	Cohesiveness, %
XCEL1	9.9	0.41	0.73	43.6	53.7
XCEL2	14.4	0.42	0.7	40.5	41.4
XCEL3	12.6	0.45	0.81	44.7	47.9
RH12	23.5	0.42	0.79	47.1	21.6

factor because the four ash samples had a similar particle size, as discussed later in this report. Results from this measurement also indicate that the baghouse ash samples resulting from coal–biomass cofiring are more cohesive than the sample resulting from coal firing alone.

All of the data presented support the conclusion that baghouse ash samples resulting from coal–biomass cofiring are more cohesive than the sample resulting from coal firing alone. However, these measurements were made at ambient conditions using samples that were cooled and exposed to air. Also, the baghouse ash sample resulting from coal firing alone used for comparison was generated and stored 45 months prior to completion of the coal–biomass cofiring tests. Therefore, these measurements may not be indicative of differences in ash properties at baghouse temperature in a flue gas environment, potentially overstating or understating the effect of biomass cofiring on baghouse ash cohesive properties. Assuming these qualitative measurements accurately represent the cohesive character of the baghouse ash resulting from coal–biomass cofiring, in addition to the difficulty encountered with online cleaning, the baghouse ash also may have poor flow characteristics resulting in hopper bridging requiring significant remediation measures.

Another ash characteristic that can affect baghouse performance is particle size distribution (PSD). Figure 32 summarizes bulk ash particle size data, based on Malvern analyses, for the three biomass cofiring tests and a baghouse ash resulting from the firing of the Cordero Rojo subbituminous coal, designated RH12. The data in the figure show that the baghouse ash PSD was slightly larger for the three ash samples resulting from biomass cofiring, 100 wt% <8–11 µm versus 100 wt% <7 µm, 80 wt% <5–7 µm versus 80 wt% <4.5 µm, and 50 wt% <3–4 µm versus 50 wt% <2.5 µm. The slightly larger particle size for the ash resulting from biomass cofiring is likely related to the larger particle size of the biomass fuels previously discussed. Figure 33 summarizes aerodynamic particle-size data, based on multicyclone sampling, for the three biomass cofiring tests and a SFS test firing Cordero Rojo subbituminous coal, designated RH12. The data in the figure show that the aerodynamic PSD resulting from biomass cofiring is within the range of values observed for subbituminous coal alone. Therefore, neither bulk ash or aerodynamic PSD appears to be a contributing factor to the online baghouse cleaning difficulties when biomass is cofired.

However, SEM micrographs in Figures 28–31 indicate that nearly all of the ash particles were 2 µm or less. Therefore, the particle-size data based on Malvern analyzes and multicyclone sampling may have been affected by the cohesive character of the ash particles and the formation of particle agglomerates.

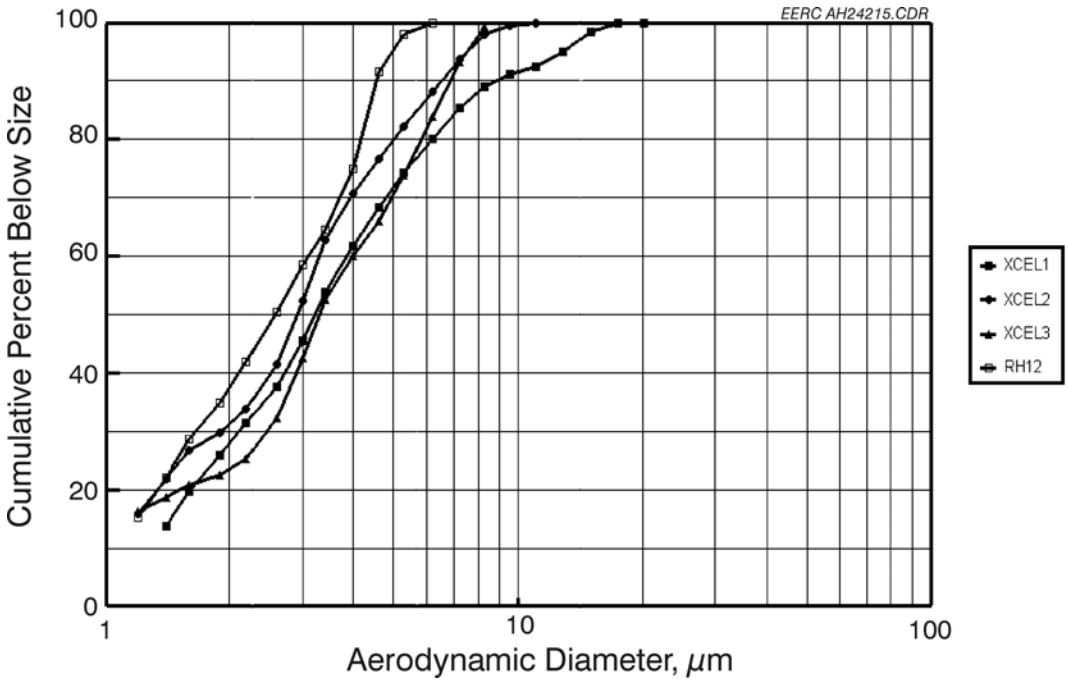

Figure 32. Baghouse ash Malvern particle-size data for the three coal–biomass cofiring tests and a Cordero Rojo coal-fired test (SFS-RH12-0200).

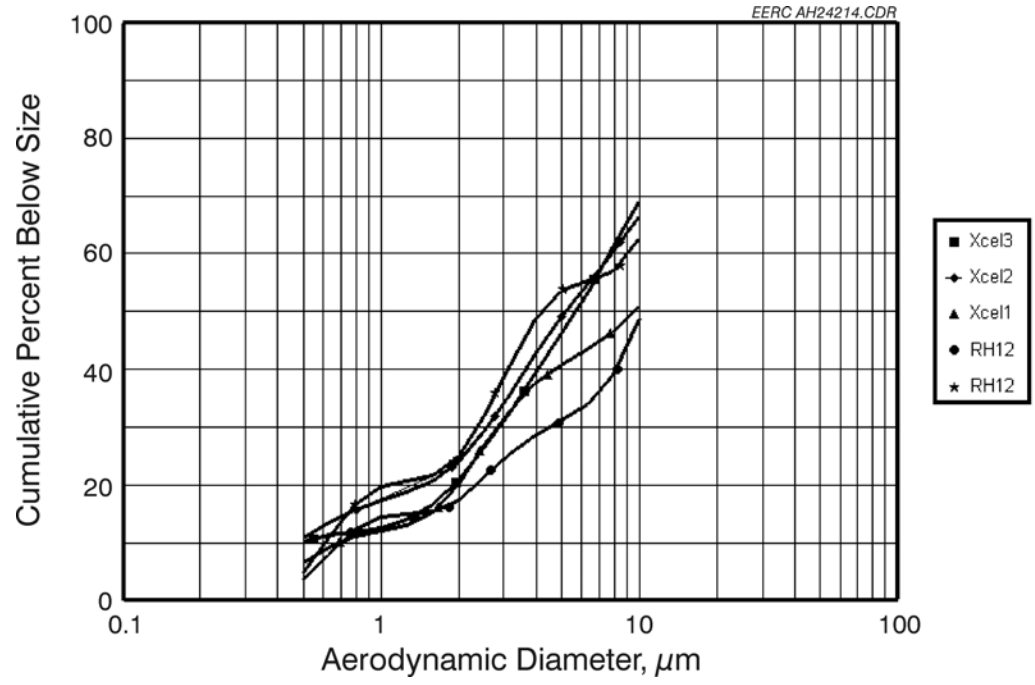

Figure 33. Multicyclone ash particle-size data for the three coal–biomass cofiring tests and a Cordero Rojo coal-fired test (SFS-RH12-0200).

Based on the fly ash data reviewed, online cleaning difficulties appear to be related to ash chemistry and a resulting inability to dislodge the dust cake from the bag surface. The slagging system magnifies the problem because of the reduced total mass loading to the baghouse and the enrichment of alkali sulfates in the baghouse ash. In order to successfully control baghouse differential pressure with online cleaning, substantially more energy would have to be employed during online cleaning (pulse pressures of >4.1 bar [>60 psig]) or biomass cofiring would have to be reduced from the 20% rate used during these tests. Further testing would be required to determine if online cleaning would be effective at higher pulse pressures or 15%, 10%, or 5% biomass cofiring rates.

Coal–biomass cofiring in a conventional pc-fired system, resulting in a dry ash condition, may not present online baghouse cleaning difficulties for 20% biomass cofiring. The greater overall mass loading would result in a much lower degree of ash enrichment in alkali sulfates, and the larger average particle size would likely reduce particle cohesion characteristics. However, specific tests would be required to verify this observation. The SFS produces a fly ash more representative of a cyclone-fired system than a conventional pc-fired system.

This project did not address the potential impacts of biomass cofiring on the performance of an electrostatic precipitator (ESP). However, based on the observations concerning baghouse performance, potential impacts on ESP performance can be identified. If an ESP had been used during these slagging furnace tests, plate rapping might have been negatively affected by the cohesive character of the alkali sulfates. Also, the small particle size of the fly ash generated might have resulted in a higher level of particulate emissions. Again, in a nonslagging system, increased mass loading and larger particle sizes might permit 20% biomass cofiring without negatively impacting ESP performance. Therefore, the EERC would recommend the completion of tests specifically to evaluate dust cake release characteristics during plate rapping, potential emission spikes because of rapping reentrainment, and bulk ash resistivity characteristics to determine the impact of coal–biomass cofiring on ESP performance.

Particulate mass loading measurements were made at the inlet and outlet of the baghouse. These data are summarized in Table 18 along with data from a previous test firing Cordero Rojo subbituminous coal. Baghouse inlet mass loading values for the three biomass cofiring tests ranged from 0.2918 to 0.3920 g/m^3 (0.1275 to 0.1713 gr/scf). These values are at least 1 order of magnitude lower than would be expected in a conventional pc-fired system. This is primarily the result of ash removal as slag in the slag screen, but other contributing factors are slag–ash removal in the dilution–quench zone and downstream heat-transfer surfaces (CAH tubes, process air preheaters, and tube-and-shell HXs). The lowest baghouse inlet mass loading was observed for Test XCEL1, consistent with the hog fuel having the lowest ash content of the three biomass fuels cofired and Test XCEL1 having the highest flue gas flow rate as a result of hog fuel moisture content and auxiliary burner firing rate. The highest baghouse inlet mass loading was observed for Test XCEL3, consistent with this test having the lowest flue gas flow rate as a result of a low switchgrass moisture content and auxiliary burner firing rate. Differences in baghouse inlet mass loading were mostly the result of differences in flue gas volumetric flow rate. Baghouse inlet mass loading ranges were found to overlap when the biomass cofiring tests were compared with a previous test where Cordero Rojo subbituminous coal was fired.

Table 18. Particulate Mass Loading Data for Tests XCEL1, XCEL2, XCEL3 and a Previously Fired Subbituminous Coal

Test No.	XCEL1	XCEL2	XCEL3	RH12
Baghouse Inlet Data:				
Sample Point Temp., °C	174	174	166	172 and 178
Flue Gas Moisture, vol%	11.5	11.5	11.0	11.8 and 11.5
Total Mass Sampled, mg	34.785	50.739	68.2631	53.753 and 42.202
Mass Loading, g/m^3	0.2918	0.3082	0.3920	0.4650 and 0.3554
Baghouse Outlet Data:				
Sample Point Temp., °C	162	166	154	156 and 156
	162	166	156	161 and 160
Flue Gas Moisture, vol%	11.0	11.1	10.6	12.4 and 12.5
	10.9	11.2	10.4	11.0 and 11.3
Total Mass Sampled, mg	0.46	0.00000	0.00000	0.309 and 0.180
	0.47	0.00000	0.00000	0.155 and 0.146
Mass Loading, g/m^3	0.0025	0.0000	0.0000	0.002 and 0.001
	0.0025	0.0000	0.0000	0.0009 and 0.0009
Mass Collection Efficiency, %	99.14	100	100	99.61 to 99.74
Mass Emissions, $g/10^6$ kJ	1.9	0.0000	0.0000	0.60 to 1.2

Baghouse outlet mass loading values for the three biomass cofiring tests ranged from 0.0000 to 0.0025 g/m^3 (0.0000 to 0.0011 gr/scf). The lowest baghouse outlet mass loadings were observed for Tests XCEL2 and XCEL3, both resulting in no measurable particulate emissions. Based on postrun maintenance, the particulate emissions rate measured for Test XCEL1 may have been affected by one bag that was improperly mounted in the tube sheet, potentially creating a minor flue gas leak through the tube sheet. The sampling results for Tests XCEL2 and XCEL3 showing no mass emissions at the outlet of the baghouse were not expected.

As indicated in the table, although low mass emissions have been previously observed, zero values have not. Possible contributing factors to the zero mass-loading values include high differential pressures, low filter face velocities; off-line cleaning requirements mean that sampling periods do not reflect spikes in mass emissions as a function of cleaning cycles. The lowest mass loading and emission rate previously observed were 0.0002 g/m^3 (0.0001 gr/scf) and 0.1720 $g/10^6$ kJ (0.0004 lb/MMBtu) when a Rochelle subbituminous coal was fired. Therefore, if the baghouse differential pressure control problem observed during the biomass cofiring tests is solved, online cleaning will likely result in mass loadings of <0.002 g/m^3 (<0.001 gr/scf) and mass emissions of <1.29 $g/10^6$ kJ (<0.003 lb/MMBtu).

Assuming baghouse differential pressure can be controlled using online pulse cleaning as a result of operating parameter changes or a reduced biomass cofiring rate in the SFS, the cohesive character of the ash may be beneficial. Specifically, it may reduce emission spikes as a function of the cleaning cycle. This benefit also would be likely in a conventional dry-ash pc-fired system.

Carbon content was measured in the baghouse ash to determine combustion efficiency. The carbon content of the baghouse ash was found to be <0.40 wt% when the North Antelope coal was cofired with each of the three biomass fuels. The high carbon burnout consistently observed in the slagging furnace is a function of the residence time and high operating temperature of the slagging furnace.

CO Concentrations

Table 19 shows the average flue gas composition data for each coal–biomass cofiring test as well as a range of data for previous subbituminous coal-fired tests. The data are based on furnace exit measurements made immediately downstream of the slag screen tubes. The CO concentration (dry basis) ranged from 0 to 500 ppmv for the three biomass cofiring tests. However, typically no CO was observed at the baghouse outlet sampling location, indicating that the CO is oxidized in the dilution– quench zone and CAH section. Typical CO concentrations measured in the slag screen were <10 ppmv. Values >10 ppmv were intermittent spikes related to fluctuations in fuel feed rate as a function of refill cycles, momentary fuel hang-up in the feeder, or low excess air levels related to flow control problems. More frequent and higher CO concentration spikes were observed in the slag screen for the biomass cofiring tests when compared to previous subbituminous coal-fired tests because of biomass feed rate instability and the significantly larger particle size of the biomass fuel versus the pc. When elevated CO concentrations are observed at the exit of the baghouse, it is the result of operating the slag tap burners in a fuel-rich condition. When this condition is observed, it is corrected by either increasing the air flow or reducing the NG flow to the slag tap burners.

NO_x Concentrations and Emissions

Measured NO_x concentrations in the flue gas ranged from 355 to 490 ppmv (dry basis) during the biomass cofiring tests with no significant differences observed among the biomass fuels. Total NO_x emissions (reported as NO_2) were determined to range from 230 to 340 g/10^6 kJ (0.54 to 0.79 lb/MMBtu). NO_x emissions varied somewhat as a function of fuel firing rate and excess air levels. The auxiliary burner firing condition is also believed to have affected the NO_x concentrations and emissions during the biomass cofiring tests. The higher average NO_x emissions observed for Test XCEL1 were likely the result of a higher auxiliary burner firing rate. However, no specific tests have been conducted to document the effect of the auxiliary burner on SFS NO_x emissions. Based on fuel nitrogen content, Test XCEL1 should have resulted in the lowest average NO_x emissions. However, that was not the case. Therefore, NO_x emissions from the SFS are likely dominated by a combination of the lower swirl firing condition of the main burner and the moderate to high swirl condition of the NG-fired auxiliary burner.

SO_2 Concentrations and Emissions

No attempt at controlling SO_2 emissions was made during the coal–biomass cofiring tests. Measured flue gas SO_2 concentrations during the coal–biomass cofiring test tests ranged from 40 to 380 ppmv (dry basis). Calculated SO_2 emissions, based on measured SO_2 in the flue gas, flue gas flow rate, and the coal–biomass-cofiring rate, resulted in values ranging from 40 to 430 g/10^6 kJ (0.1 to 1.0 lb/MMBtu). The variation in these values is a direct result of the variation in the fuel sulfur content, 0.23–0.25 wt% in the coal and 0.04–0.13 wt% in the biomass, and coal and biomass firing

Table 19. Flue Gas Composition Data for the Coal–Biomass Cofiring Tests and Previously Fired Subbituminous Coals (dry basis)

	Concentration	g/10^6 kJ
XCEL1		
O_2	3.4–5.1 vol%	
CO_2	10.4–13.3 vol%	
CO	0–250 ppmv	
NO_x	430–490 ppmv	310–340
SO_2	40–380 ppmv	40–430
H_2O	11.5 vol%	
XCEL2		
O_2	3.2–5.0 vol%	
CO_2	12.5–14.1 vol%	
CO	0–500 ppmv	
NO_x	355–465 ppmv	240–300
SO_2	50–100 ppmv	40–100
H_2O	11.5 vol%	
XCEL3		
O_2	3.1–4.7 vol%	
CO_2	13.1–14.5 vol%	
CO	0–500 ppmv	
NO_x	360–475 ppmv	230–310
SO_2	50–140 ppmv	40–200
H_2O	11.0 vol%	
Subbituminous Coals		
O_2	3.0–5.8 vol%	
CO_2	12.6–14.7 vol%	
CO	5–80 ppmv	
NO_x	440–605 ppmv	300–430
SO_2	150–320 ppmv	300–300
H_2O	11–12 vol%	

rates during the individual tests (2.1–2.4 × 10^6 kJ/hr [2.0–2.3 MMBtu/hr]). Specifically in the case of Test XCEL1, the high end of the SO_2 concentration and emission ranges resulted from a short period of 100% coal firing, previously discussed, required to mitigate the effects of an electrical problem encountered in the biomass feeder.

Based on fuel feed rates and sulfur content, average flue gas SO_2 concentration (dry basis and 3 vol% O_2) should have been 111 ppmv for Test XCEL1, 213 ppmv for Test XCEL2, and 218 ppmv

for Test XCEL3. Except for the 100% coal-fired period during Test XCEL1, measured SO_2 concentrations (dry basis, corrected to 3 vol% O_2) were less than the predicted values, implying inherent sulfur capture by fly ash alkaline-earth components. Calculated inherent sulfur capture during Tests XCEL1, XCEL2, and XCEL3 ranged from 32%–58%, 49%–71%, and 25%–74%, respectively. The values at the high end of the range may have been affected by SO_2 capture on filters in the sample train. However, no moisture problems were encountered with the sample train filters and SO_2 sulfation reactions at the filter temperatures used (<149°C [<300°F]) are very slow.

CO_2 Concentrations

Measured CO_2 concentrations in the flue gas ranged from 10.4 to 14.5 vol% (dry basis) during the biomass cofiring tests as a result of coal–biomass cofiring in the main burner, NG firing in the auxiliary burner, and a range of excess air levels in the flue gas. The lowest CO_2 concentrations were observed during Test XCEL1, which represented the highest auxiliary burner NG-firing rate.

H_2O Concentrations

Measured H_2O concentrations in the flue gas ranged from 11.0 to 11.5 vol% during the coal–biomass cofiring tests as a result of coal–biomass cofiring in the main burner and NG firing in the auxiliary burner. These measurements were the result of particulate sampling at the inlet of the baghouse. If NG firing in the auxiliary burner were eliminated, these values would be lower, nominally 10 vol%.

CAH Results

CAH tube bank performance has met all objectives relative to heat transfer and its support of the HTHX panel during this as well as previous projects. Performance differences relative to fuel ash properties were as expected. Table 20 summarizes total operating hours for the CAH tube bank, representing 37 thermal cycles.

Table 20. Summary of CAH Tube Bank Operating Hours Through December 2003[1]

Natural Gas Firing, hr	Solid Fuel Firing, hr	Total Operation, hr
3480	2100	5580

[1] Natural gas firing represents heat-up, cooldown, and refractory curing.

Figure 34 illustrates the location of thermocouples originally installed in the CAH tube bank, and Table 21 presents a list of thermocouple descriptions. When the coal–biomass cofiring tests began, only two of the five surface thermocouples were functioning properly and a third was functioning intermittently. However, the remaining three surface thermocouples had failed by the end of Test XCEL2.

The potential effectiveness of sootblowing was not addressed during this project because the EERC elected to permit the formation of ash deposits on CAH tube bank surfaces in order to develop

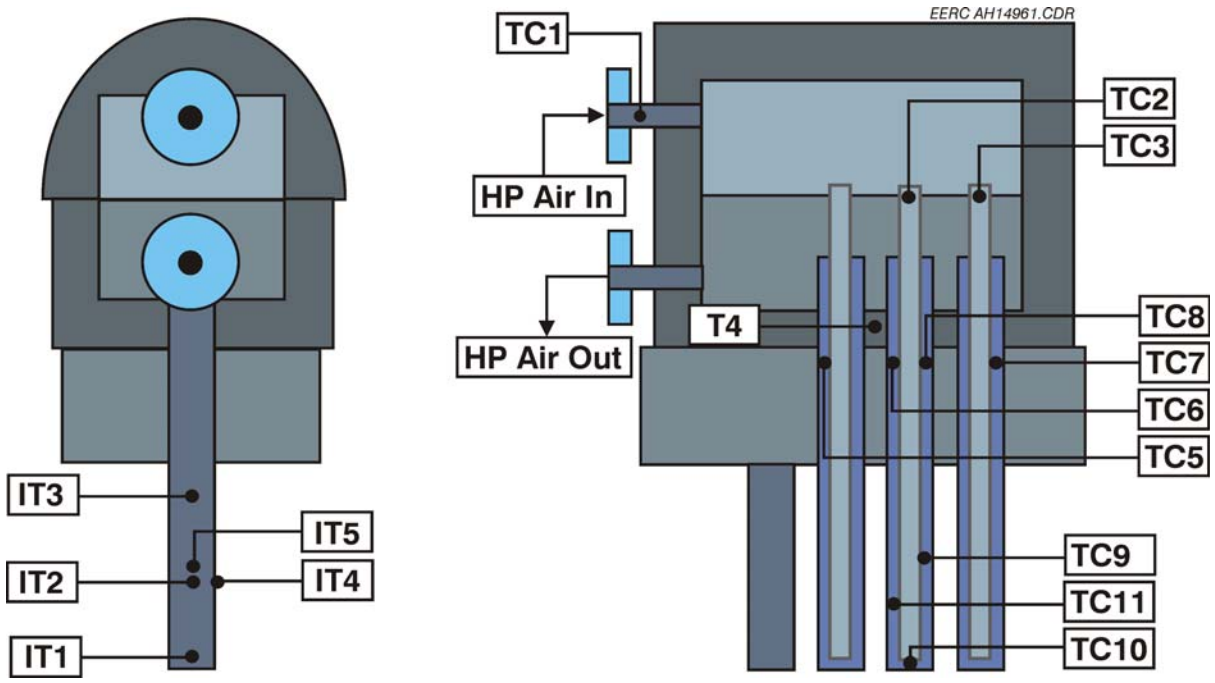

Figure 34. Thermocouple locations in the CAH tube bank.

Table 21. Description of CAH Thermocouple Locations[1]

Category	No.	Label	Description
Air Inlet	1	TC1	Bulk flow entering the inlet header
	2	TC2	Air entering center tube
	3	TC3	Air entering most downstream tube
Air Outlet	4	TC6	Air leaving center tube
	5	TC7	Air leaving most downstream tube
	6	TC5	Air leaving most upstream tube (failed)
	7	TC8	Air leaving side tube
Air in Active Region	8	TC10	Bottom of center tube
	9	TC11	4 in. up outside annulus, center tube
	10	TC9	8 in. up outside annulus, center tube
Tube Surface	11	IT1	1 in. up center tube, facing upstream (failed)
	12	IT2	5 in. up center tube, facing upstream (failed)
	13	IT3	8 in. up center tube, facing upstream (failed)
	14	IT4	5 in. up center tube, facing to side (failed)
	15	IT5	5 in. up center tube, facing downstream (failed)
Header Shell	16	TC4	Next to shell on outside, between return

[1] Thermocouple locations are illustrated in Figure 30.

deposits for subsequent recovery and characterization. Based on CAH operating experience in other projects, an 8-hr sootblowing frequency is adequate for an eastern Kentucky bituminous coal fired in the SFS. However, all of the other fuel types (bituminous, subbituminous, and lignite coals), including the North Antelope subbituminous coal fired in this project, require more frequent (4-hr cycle) sootblowing to achieve comparable results. Also, improved sootblowing effectiveness in the SFS may require a modification to the method employed to increase the tube surface area affected by each sootblowing event. For the balance of this discussion, the performance of the CAH tube bank is analyzed with respect to the operation of the SFS while cofiring North Antelope subbituminous coal and three biomass fuels (hog fuel, corn stover, and switchgrass).

CAH operating data (bracketed data in the figures) from cofiring North Antelope coal and the biomass fuels are summarized in Figures 35 (tube bank surface and flue gas temperatures), 36 (process air temperatures), and 37 (process air flow rates) for Test SFS-XCEL1-0303. Based on the single thermocouple measurement (IT2), the leading-edge clean tube surface temperatures were nominally 721°C (1330°F) during an initial NG-fired test and reduced to 688°C (1270°F) prior to initiating solid-fuel firing. As a result of coal–hog fuel cofiring, surface temperature decreased from 688°C (1270°F) to 521°C (970°F) as ash deposits developed and adjustments were made to the process air flow rate. As previously stated, in order to permit development and recovery of samples for characterization, no attempt was made to sootblow the CAH tube bank during the coal–biomass cofiring tests.

While NG was fired and the tubes were clean, heat recovery from the CAH tube bank was roughly 43,255 kJ/hr (41,000 Btu/hr). This result was observed for the following conditions:

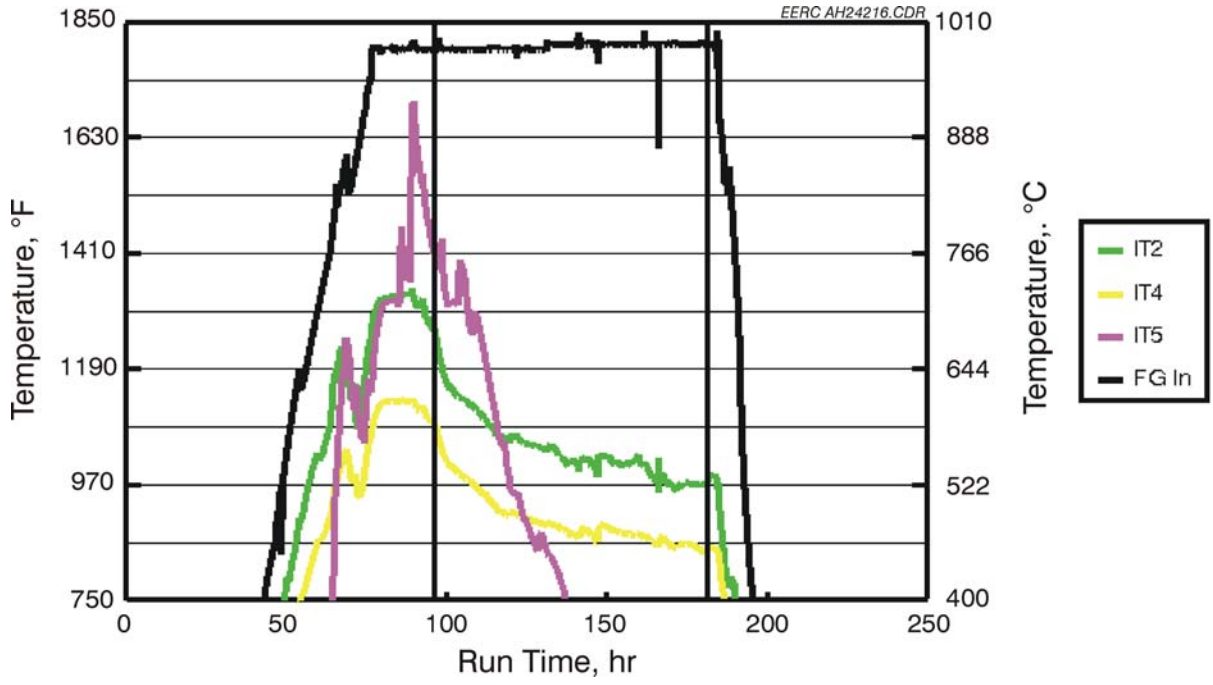

Figure 35. CAH tube surface and flue gas temperatures versus run time for Test SFS-XCEL1-0303.

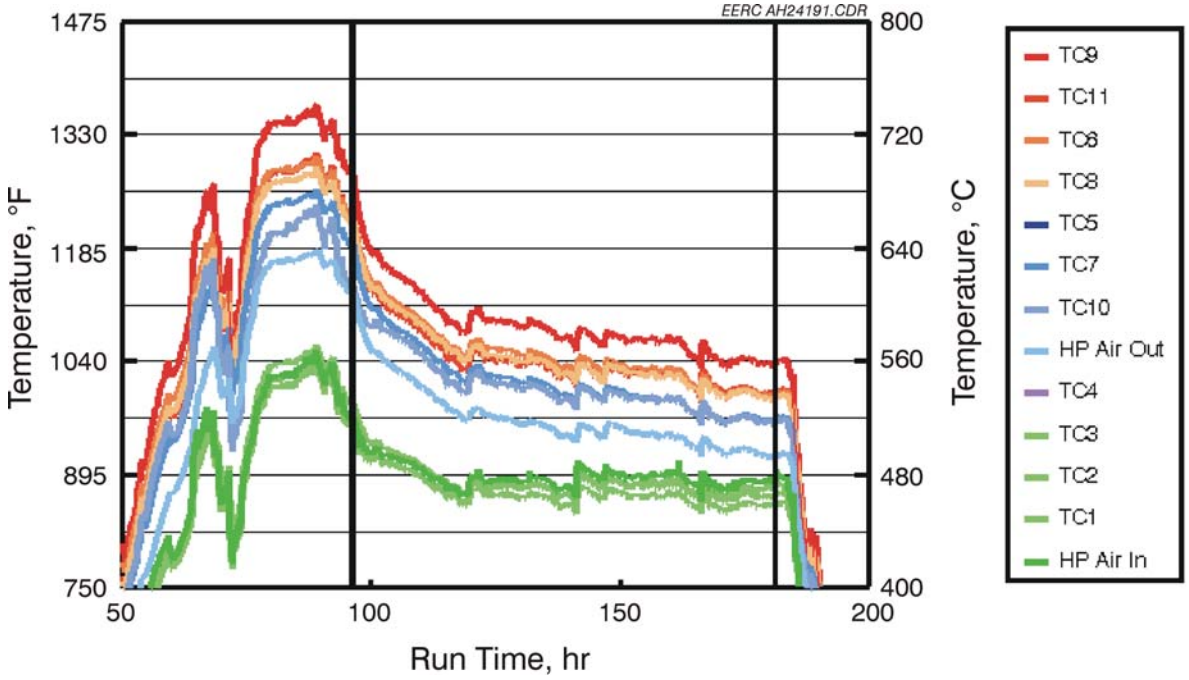

Figure 36. CAH process air temperatures versus run time for Test SFS-XCEL1-0303.

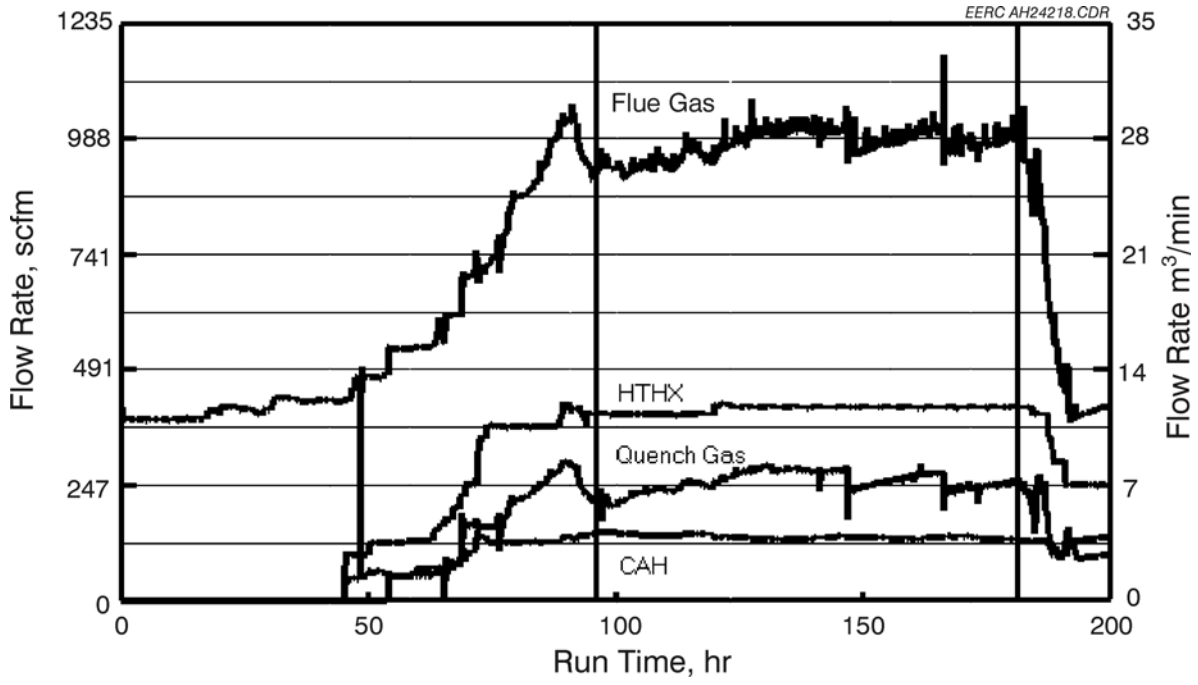

Figure 37. CAH process air, HTHX process air, quench gas, and flue gas flow rates versus run time for Test SFS-XCEL1-0303.

- Process air flow rate of 3.5 m^3/min (125 scfm)
- Inlet process air temperature of 538°C (1000°F)
- Outlet process air temperature of 633°C (1170°F)
- Flue gas temperature of 983°C (1800°F) entering the CAH tube bank

Figure 38 presents heat recovery in the CAH as a function of run time for Test XCEL1.

When coal–hog fuel cofiring began (Run Hour 96), leading-edge surface temperatures initially decreased at a rate of 4°C/hr (8°F/hr) over 25 hr as ash deposits developed on the surface of the tubes. Because sootblowing was not employed during this test, surface temperatures continued to trend lower until stabilizing at nominally 521°C (970°F) after 76 hr of coal–hog fuel cofiring. Process air flow rates were adjusted during the coal–hog fuel-cofired test to maintain process air exit temperature in the range of 480°–540°C (900°–1000°F). The maximum and minimum process air flow rates through the CAH tube bank were 4.2 m^3/min (150 scfm) and 3.7 m^3/min (130 scfm), respectively. As ash deposits developed on the tube surfaces, heat recovery from the CAH tube bank decreased from a maximum of nominally 47,897 kJ/hr (45,400 Btu/hr), for inlet and outlet process air temperatures of 513°C (955°F) and 660°C (1220°F), to a minimum of 19,306 kJ/hr (18,300 Btu/hr), for inlet and outlet process air temperatures of 457°C (855°F) and 540°C (1000°F).

The CAH deposits that formed during Test XCEL1 were limited to the leading and trailing edges of the tubes. Figure 39 is a photograph of ash deposits (without sootblowing) on the surface of the tubes following Test XCEL1. The photograph shows substantial leading-edge deposition on uncooled and cooled tubes in the gas path with significantly less trailing-edge deposition. The cooled tubes visible in the photograph (two tubes on the right side of the photograph) show the leading-edge

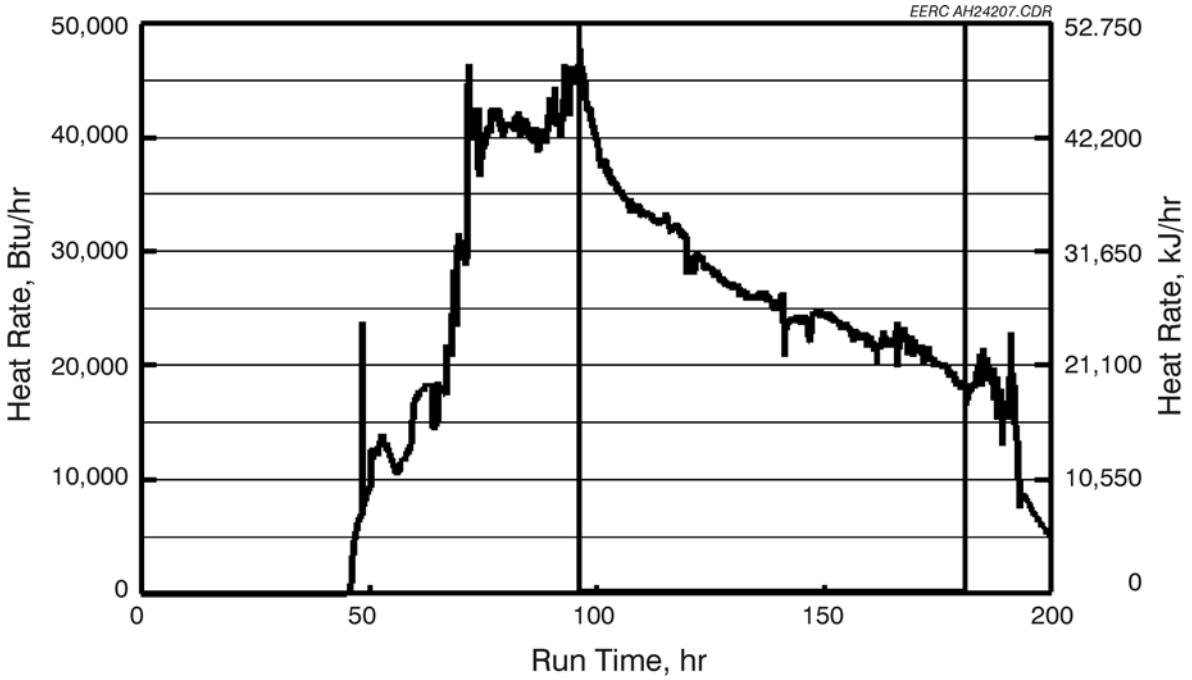

Figure 38. CAH heat recovery versus run time for Test SFS-XCEL1-0303.

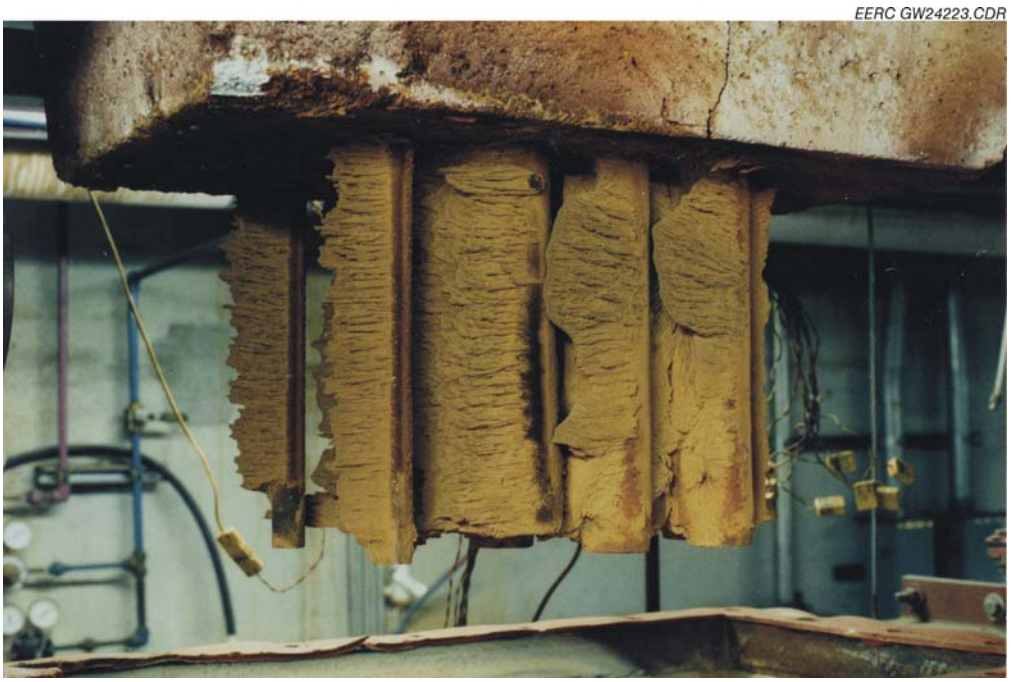

Figure 39. Photograph of ash deposits on the CAH tubes following Test SFS-XCEL1-0303.

deposits to be nonuniform. However, these deposits were found to be friable, and the lower portions of these leading-edge deposits fell off when the tube bank was removed from the refractory-lined duct. CAH tube bank plugging was not a problem when cofiring the North Antelope coal and hog fuel. No deposits were observed bridging the flue gas path between the tubes.

Deposit strength is a function of ash chemistry, particle size, and temperature history. The relative strength of the deposits formed when cofiring the North Antelope coal and hog fuel was indicated when portions of the deposits on the cooled tube surfaces fell off when the tube bank was removed from the refractory-lined duct. In addition, the friability of the deposits was evident when attempting to recover ash deposits from tube surfaces for characterization: the deposits tended to break up even with careful handling. Because sootblowing was not attempted during Test XCEL1, a total mass was determined for the ash deposits associated with the CAH tubes. The total weight of the deposits collected from the CAH tubes and duct was 7.7 kg (17 lb). The total weight of the deposits collected from the CAH tubes was 3.2 kg (7 lb). On a mass-per-unit-time basis, the ash deposition rate for the cofiring of North Antelope coal and hog fuel was 36.3 g/hr (0.082 lb/hr). Incorporating the surface area of the tube bank (0.58 m^2 [6.28 ft^2]) results in a value of 62.6 g/hr-m^2 (0.013 lb/hr-ft^2). On a coal–hog fuel-cofiring-rate basis, the CAH ash deposition rate would be 15.8 g/10^6 kJ (0.036 lb/MMBtu). These calculated values are slightly lower, yet comparable, to results for previous subbituminous coal-fired SFS tests. The slightly lower ash deposition rate for Test XCEL1 was likely a function of slag screen plugging observed during the test, which resulted in a lower ash mass loading reaching the CAH tube bank.

As a result of coal–corn stover cofiring during Test SFS-XCEL2-0403 CAH surface temperature decreased from 716°C (1320°F) to 457°C (855°F) as ash deposits developed and

adjustments were made to the process air flow rate. As previously stated, to permit development and recovery of samples for characterization, no attempt was made to sootblow the CAH tube bank during the coal–biomass cofiring tests. The clean tube surface temperature at the beginning of Test XCEL2 was higher than that observed for Test XCEL1 because of a lower initial air flow rate, 120 versus 150 scfm, and a slightly higher flue gas temperature, 1010°C (1850°F) versus 983°C (1800°F), entering the CAH tube bank.

Figure 40 presents heat recovery in the CAH as a function of run time for Test XCEL2. When coal–corn stover cofiring firing began (Run Hour 80), leading-edge surface temperatures initially decreased at a rate of 6°C/hr (10°F/hr) over 25 hr as ash deposits developed on the surface of the tubes. Because sootblowing was not employed during this test, surface temperatures continued to trend lower, decreasing to nominally 457°C (855°F) after 86 hr of coal–corn stover cofiring. It is possible but not obvious that tube surface temperatures had stabilized by the end of the test. In order to maintain a relatively constant process air exit temperature, process air flow rates were not adjusted. As a result, the process air flow rate was typically 3.5 m^3/min (125 scfm) and ranged from 3.4 to 3.7 m^3/min (120 to 130 scfm). As ash deposits developed on the tube surfaces, heat recovery from the CAH tube bank decreased from a maximum of nominally 43,466 kJ/hr (41,200 Btu/hr), for inlet and outlet process air temperatures of 544°C (1010°F) and 688°C (1270°F), to a minimum of 24,476 kJ/hr (23,200 Btu/hr), for inlet and outlet process air temperatures of 368°C (695°F) and 443°C (830°F).

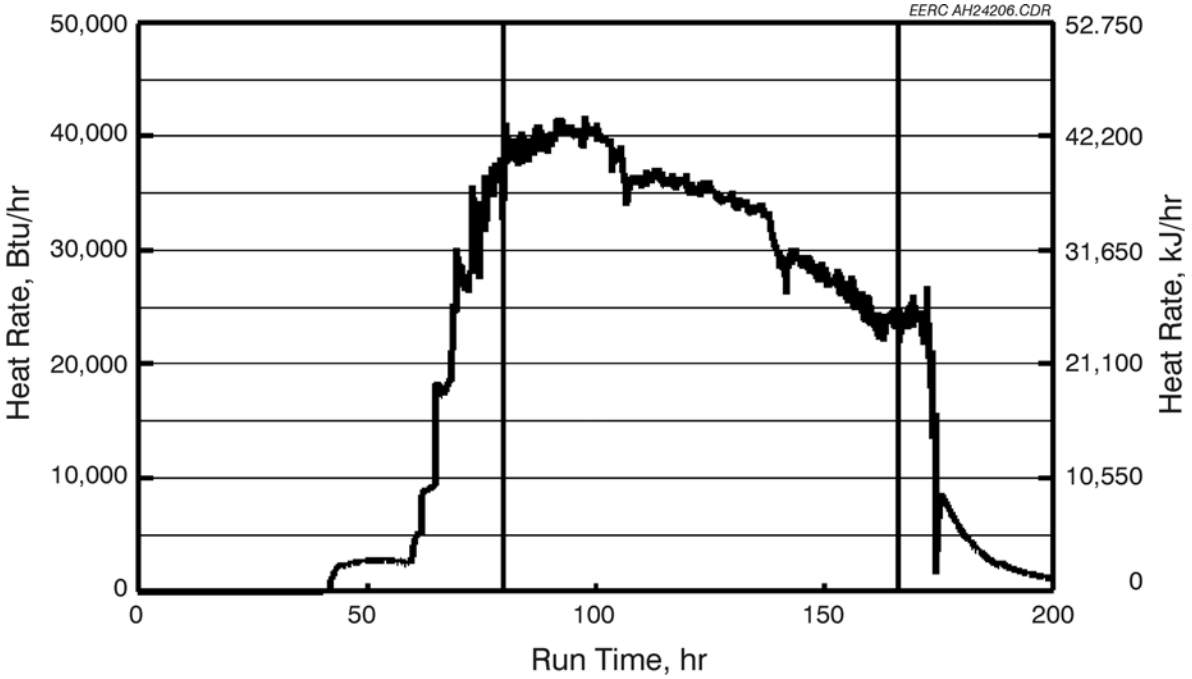

Figure 40. CAH heat recovery versus run time for Test SFS-XCEL2-0403.

The CAH deposits that formed during Test XCEL2 were limited to the leading and trailing edges of the tubes. Figure 41 is a photograph of ash deposits (without sootblowing) on the surface of the tubes following Test XCEL2. The photograph shows substantial leading-edge deposition on uncooled and cooled tubes in the gas path with less trailing-edge deposition. The cooled tubes visible on the right side of the photograph show the leading-edge deposits to be continuous over the length of the tubes; these deposits remained intact when the CAH tube bank was removed from the duct. However, deposits on the first two uncooled surfaces did fall off the tubes when the tube bank was removed from the duct, indicating a degree of friability. CAH tube bank plugging was not a problem when cofiring the North Antelope coal and corn stover. No deposits were observed bridging the flue gas path between the tubes.

Deposit strength is a function of ash chemistry, particle size, and temperature history. The relative strength of the deposits was demonstrated as the deposits remained intact on the cooled tube surfaces when the tube bank was removed from the refractory-lined duct. However, the friability of the deposits was evident when attempting to recover ash deposits (they tended to fall apart) from tube surfaces for characterization. Because sootblowing was not attempted during Test XCEL2, a total mass was determined for the ash deposits associated with the CAH tubes. The total weight of the deposits collected from the CAH tubes and duct was 7.3 kg (16 lb). The total weight of the deposits collected from the CAH tubes was 4.5 kg (10 lb). On a mass-per-unit-time basis, the ash deposition rate for the cofiring of North Antelope coal and corn stover was 52.8 g/hr (0.116 lb/hr). Incorporating the surface area of the tube bank (0.58 m^2 [6.28 ft^2]) results in a value of 91.0 g/hr-m^2 (0.018 lb/hr-ft^2). On a coal–corn stover-cofiring-rate basis, the CAH ash deposition rate would be 23.0 g/10^6 kJ (0.053 lb/MMBtu). These calculated values are essentially the same as results for previous subbituminous coal-fired tests, 78.3 g/hr-m^2 (0.017 lb/hr-ft^2). The slightly higher ash

Figure 41. Photograph of ash deposits on the CAH tubes following Test SFS-XCEL2-0403.

deposition rate for Test XCEL2 when compared to Test XCEL1 was a function of fuel ash content observed during Test XCEL2 as well as slag screen performance resulting in a higher ash mass loading reaching the CAH tube bank. Specifically, the corn stover ash content was 7.1 versus 5.0 wt% for the hog fuel during Test XCEL1, and there was no slag screen plugging observed during Test XCEL2.

As a result of coal–switchgrass cofiring during Test SFS-XCEL3-0503, CAH surface temperature likely decreased in a manner similar to Tests XCEL1 and XCEL2 as ash deposits developed and adjustments were made to the process air flow rate. However, there were no surface thermocouples working reliably during Test XCEL3.

Figure 42 presents heat recovery in the CAH as a function of run time for Test XCEL3. When coal–switchgrass cofiring began (Run Hour 80), leading-edge surface temperatures likely decreased at a rate similar to those observed during the previous coal–biomass-cofiring tests, 4°–6°C/hr (8°–10°F/hr) over 25 hr as ash deposits developed on the surface of the tubes. Because sootblowing was not employed during this test, surface temperatures likely continued to trend lower, as indicated by decreasing process air temperatures and CAH heat recovery. Based on process air temperatures and CAH heat recovery, it does not appear that tube surface temperature had stabilized by the end of the coal–switchgrass-cofiring test period. Process air flow rate was 3.4–3.5 m^3/min (120–125 scfm) and ranged from 3.4 to 3.7 m^3/min (100 to 135 scfm) as a result of flow rate adjustments and two compressor trips. As ash deposits developed on the tube surfaces, heat recovery from the CAH tube bank decreased from a maximum of nominally 44,943 kJ/hr (42,600 Btu/hr), for inlet and outlet

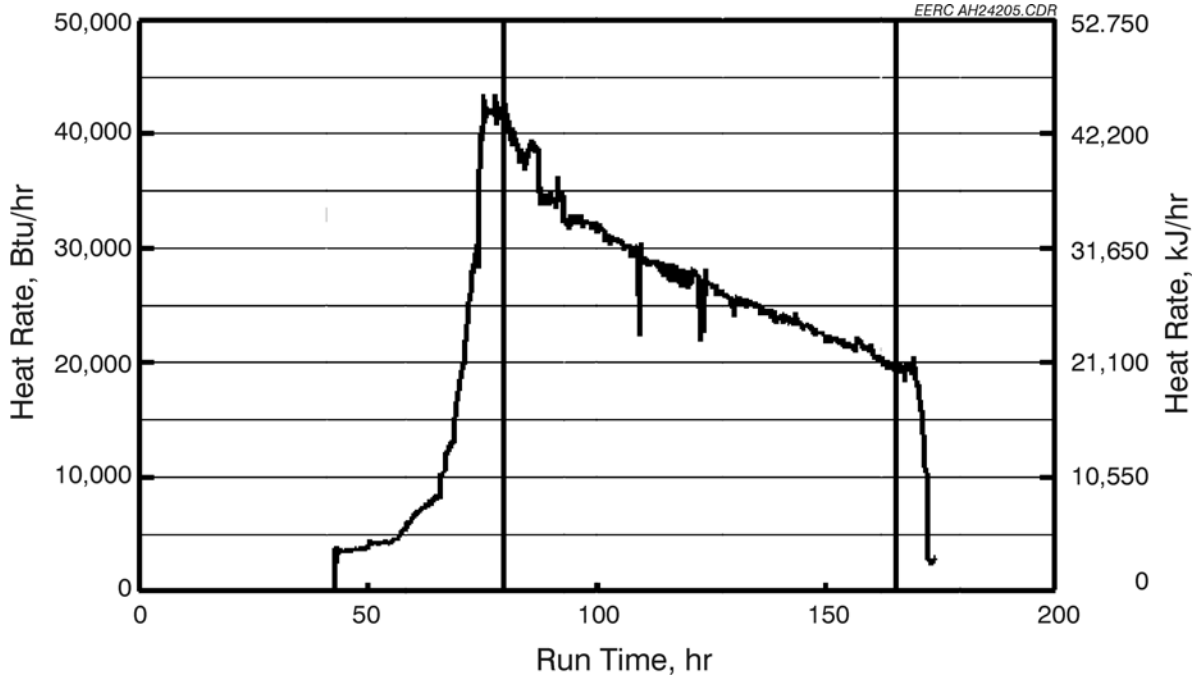

Figure 42. CAH heat recovery versus run time for Test SFS-XCEL3-0503.

process air temperatures of 499°C (930°F) and 666°C (1230°F), to a minimum of 20,572 kJ/hr (19,500 Btu/hr), for inlet and outlet process air temperatures of 421°C (790°F) and 488°C (910°F).

The CAH deposits that formed during Test XCEL3 were limited to the leading and trailing edges of the tubes. Although a photograph of the ash deposits on the surface of the tubes following Test XCEL3 was unavailable, the deposits were similar to those illustrated in the photographs in Figures 39 and 41. There was substantial leading-edge deposition on uncooled and cooled tubes in the gas path with less trailing-edge deposition. CAH tube bank plugging was not a problem when cofiring the North Antelope coal and switchgrass. No deposits were observed bridging the flue gas path between the tubes.

Deposit strength is a function of ash chemistry, particle size, and temperature history. The relative strength, or friable nature, of the deposits was evidenced as they fell apart when we attempted to recover ash deposits from tube surfaces for characterization. Because sootblowing was not attempted during Test XCEL3, a total mass was determined for the ash deposits associated with the CAH tubes. The total weight of the deposits collected from the CAH tubes and duct was 5.4 kg (12 lb). The total weight of the deposits collected from the CAH tubes was 3.6 kg (8 lb). On a mass-per-unit-time basis, the ash deposition rate for the cofiring of North Antelope coal and switchgrass was 42.7 g/hr (0.094 lb/hr). Incorporating the surface area of the tube bank 0.58 m^2 (6.28 ft^2) resulted in a value of 73.6 g/hr-m^2 (0.015 lb/hr-ft^2). On a coal–switchgrass-cofiring-rate basis, the CAH ash deposition rate would be 18.8 g/10^6 kJ (0.044 lb/MMBtu). These calculated values are essentially the same as results for previous subbituminous coal-fired tests, 78.3 g/hr-m^2 (0.017 lb/hr-ft^2). The slightly higher ash deposition rate for Test XCEL3 when compared to Test XCEL1 was a function of fuel ash content observed during Test XCEL3 as well as slag screen performance resulting in a higher ash mass loading reaching the CAH tube bank. Specifically, the switchgrass ash content was 5.4 versus 5.0 wt% for the hog fuel during Test XCEL1, and there was no slag screen plugging observed during Test XCEL3. Test XCEL3 resulted in a lower CAH ash deposition rate when compared to Test XCEL2 because the fuel ash content was lower during Test XCEL3.

Based on previous experience firing subbituminous coal, if sootblowing had been employed during these coal–biomass-cofiring tests, it is likely that CAH heat recovery would have been maintained at 34,290–42,200 kJ/hr (32,500–40,000 Btu/hr). A comparison of the CAH heat-transfer data for the three coal–biomass-cofiring tests indicates that the results for cofiring hog fuel and switchgrass are similar. When cofiring corn stover, the initial increase in CAH heat recovery after initiating solid fuel cofiring resulted from increasing furnace firing rate and the subsequent increase in furnace exit temperature and flue gas flow rate. During this same period, slag screen differential pressure was decreasing as the slag accumulated during Test XCEL1 began to flow from the slag screen to the slag tap. However, the CAH heat recovery rate when cofiring corn stover did not degrade to <21,100 kJ/hr (<20,000 Btu/hr) as was observed for the hog fuel and switchgrass. There is no obvious explanation for this difference based on flue gas or process air temperatures and flow rates. One possible explanation may be related to the density of the ash deposits formed.

As with the other fuels fired in the SFS, the data support the conclusion that the addition of the fins to the air-cooled tubes improves heat recovery during the coal–biomass-cofiring tests. The fins appear to reduce the rate of heat-transfer degradation as ash deposits develop and help to maintain

a higher heat-transfer rate once the deposits have formed. However, no improvement in heat recovery was observed during NG-fired periods with clean tube surfaces.

Routine sootblowing was not used during these tests. Based on previous SFS tests, routine sootblowing of the finned tubes will maintain CAH heat recovery in the range of 31,650–42,200 kJ/hr (30,000–40,000 Btu/hr). However, if the fins were removed from the tubes, an effective sootblowing method might result in a similar level of CAH heat recovery. The only way to prove an advantage for finned tubes would be to complete a series of tests to specifically address that question.

One of the standards of success identified for this project in the original proposal was the production of clean pressurized air at 705°C (1300°F) with the CAH while limiting convective pass flue gas temperature to 1010°C (1850°F). Based on the temperature measurements made during the three coal–biomass cofiring tests, clean pressurized air temperatures generally stabilized at 510°–538°C (950°–1000°F) near the end of each test. At face value, these data indicate that the proposed standard of success was not achieved. However, this result was a function of several factors:

1) The CAH was originally designed to preheat 3.4 m^3/min (100 scfm) of process air from 538° to 705°C (1000° to 1300°F) in support of the original tubes-in-a-box HTHX configuration. When the EERC elected to focus on evaluation of the bare-tube HTHX configuration and increase the volume of process air supporting the HTHX, the CAH surface area was not increased to handle the additional process air volume because there was nothing new to be learned from the CAH in terms of heat transfer. During the coal–biomass cofiring tests the CAH process air flow rates were 3.4–4.2 m^3/min (120–150 scfm), 20%–50% greater than the original design basis.

2) No attempt was made to routinely sootblow the CAH surfaces in order to develop ash deposits for characterization; therefore, CAH outlet process air temperatures decreased as a function of ash deposition on heat-transfer surfaces.

3) CAH inlet process air temperatures were nominally 167°C (300°F) lower than the design basis and data observed during tests evaluating the tubes-in-a-box configuration because of the higher process air flow rates through existing preheater surface.

Therefore, based on previous HTHX tests and the data generated during the coal–biomass cofiring tests, reducing the process air flow rate to design volumes or adding sufficient CAH surface and surface to adequately preheat process air upstream of the CAH would easily result in CAH outlet process air temperatures of 700°C (1300°F).

Tables 22–24 show the composition data for deposits that formed on the cooled tubes during the three coal–biomass cofiring tests as compared to the bulk fuel ash compositions and the average slag compositions. The CAH deposit data is a combination of XRF and SEM data but reported on the same basis. The deposits were typically split into two categories, the inner powder layer, and an outer sintered layer. The inner layer is typically composed of very small ash particles that deposit on the tubes through thermophoresis, a process by which small particles are driven from a hot gas to a

Table 22. CAH Deposit Samples from the Coal–Hog Fuel Cofiring Test SFS-XCEL1-0303

Oxides,[1] wt%	North Antelope Coal	Hog Fuel	Slag	Outer Sinter Layer	Inner Layer
SiO_2	25.9–27.2	33.3	37.7	22.0	22.6
Al_2O_3	17.0–18.3	2.5	20.1	16.0	17.4
Fe_2O_3	7.2–7.6	3.2	5.4	8.3	8.8
TiO_2	1.5	0.3	1.1	1.5	1.6
P_2O_5	1.2	1.8	0.9	1.5	1.6
CaO	26.3–26.9	43.2	28.0	34.2	34.3
MgO	6.9–7.2	3.9	4.4	7.0	7.5
Na_2O	0.8–1.2	3.9	1.2	3.8	2.8
K_2O	0.2–0.3	7.9	1.1	5.6	3.4
SO_3[2]	8.9–12.4	0.0	0.0	15.3	26.0

[1] Oxide concentrations normalized to an SO_3- and ClO-free basis.
[2] SO_3 and ClO concentrations normalized with other oxides.

Table 23. CAH Deposit Samples from the Coal–Corn Stover Cofiring Test SFS-XCEL2-0403

Oxides,[1] wt%	North Antelope Coal	Corn Stover	Slag	Outer Sinter Layer	Inner Layer
SiO_2	25.9–27.2	57.3	45.5	26.7	27.2
Al_2O_3	17.0–18.3	3.2	18.6	16.5	15.8
Fe_2O_3	7.2–7.6	1.4	5.3	6.8	6.1
TiO_2	1.5	0.3	1.1	1.6	1.3
P_2O_5	1.2	3.8	1.0	2.7	2.8
CaO	26.3–26.9	9.5	20.3	30.3	19.4
MgO	6.9–7.2	12.6	5.9	7.7	6.6
Na_2O	0.8–1.2	0.4	0.9	2.5	6.1
K_2O	0.2–0.3	10.0	1.4	5.1	14.7
SO_3[2]	8.9–12.4	1.5	0.0	20.9	27.7

[1] Oxide concentrations normalized to an SO_3-free basis.
[2] SO_3 concentrations normalized with other oxides.

Table 24. CAH Deposit Samples from the Coal–Switchgrass Cofiring Test SFS-XCEL3-0503

Oxides,[1] wt%	North Antelope Coal	Switchgrass	Slag	Outer Sinter Layer	Inner Layer
SiO_2	25.9–27.2	70.3	51.0	26.6	28.1
Al_2O_3	17.0–18.3	0.0	15.2	17.3	15.6
Fe_2O_3	7.2–7.6	0.25	5.4	6.9	6.2
TiO_2	1.5	0.03	1.0	1.5	1.4
P_2O_5	1.2	4.8	1.1	3.9	4.1
CaO	26.3–26.9	9.4	18.9	31.3	28.6
MgO	6.9–7.2	4.9	5.0	7.4	6.6
Na_2O	0.8–1.2	0.03	0.8	1.4	2.2
K_2O	0.2–0.3	7.0	1.5	3.7	7.0
SO_3[2]	8.9–12.4	3.3	0.0	15.4	24.6

[1] Oxide concentrations normalized to an SO_3-free basis.
[2] SO_3 concentrations normalized with other oxides.

cool surface. These particles are often much smaller than typical ash particles, and may contain significant amounts of alkali metal, alkaline earth, sulfur or chlorine because these elements often vaporize to a certain extent at the high temperatures in the main furnace, then condense as or onto small particles in cooler zones such as around the CAH. The outer layer consists primarily of larger particles that deposit on the tubes via inertial impaction. That is, they separate from the gas stream as the gas diverges around the tube. Because of their higher inertia, then continue toward the tube, impacting on other ash particles. Because the incoming particles are insulated from the cooled tube by other ash particles, they remain somewhat soft and can sinter, or stick together, into massive deposits.

Table 22 shows that the inner and outer layers of the CAH deposit have similar compositions except that the inner layer is more sulfated than the outer layer. The similarity in compositions indicates that there was little difference in the deposition mechanisms of the ash particles in each layer making them much less distinct than is often seen in CAH deposits. Both layers are somewhat depleted in silica as compared to the fuels, most likely because more of the silica-rich ash had deposited in the main furnace and slag screen. SEM analyses showed that most of the silicate material is complex calcium alumina silicate, which is a common ash particle type for Powder River Basin coals. The deposits are also highly enriched in sulfur, indicating that a large proportion of the alkali metals and alkaline earth elements in the deposits have sulfated, the inner layer more so than the outer by virtue of its lower temperature and longer residence time in the furnace.

Table 23 shows that the inner layer of the CAH deposit formed while cofiring coal and corn stover is very enriched in sodium and potassium, and depleted in calcium relative to the outer sintered layer of the deposit or the fuels fired. It is also much more highly sulfated. The higher alkali content of this inner layer would make it more corrosive toward the CAH alloy than that formed while cofiring coal and hog fuel. It is enriched in these elements because they vaporize during combustion, and condense at lower temperatures as or on smaller particles that preferentially deposit on the relatively cool bare CAH tubes. The reason for the lower calcium content is not clear. The

outer layer, which is formed more from larger particles, and is at a higher temperature, more reflects the composition of the coal ash, except that it too contains a higher potassium concentration and is relatively highly sulfated.

Table 24 shows that the inner dusty layer and outer sintered layer of the CAH deposits formed while cofiring coal and switchgrass are very similar except for some enrichment of sodium and potassium, and especially sulfur in the inner layer. This trend was also seen while cofiring with corn stover and occurs because these alkali metals vaporize during combustion and recondense preferentially on or as smaller particles that tend to form the inner layers of ash on cooled surfaces. As was also true for the deposits formed during the other tests, the high sulfur concentrations indicate strong sulfation of the alkaline metal and alkali earth elements on the cooled tubes. As compared to the fuel ashes, the deposits have similar compositions to the coal ash because it forms a much larger proportion of the ash, except for the enrichment of the potassium which predominantly originates from the switchgrass. As was true for the deposits formed while cofiring the other fuels, SEM analyses show that the sulfated materials are relatively complex mixtures dominated by calcium sulfate, whereas the silicates are also complex and dominated by calcium aluminosilicate material. These results are consistent with deposits formed during other tests firing only Powder River Basin coals.

HTHX Test Results

Initial shakedown and testing of the HTHX panel took place in December 1997 and continued through September 2000 in support of a previous project (3). In the original design of the HTHX, 1" thick ceramic tiles were placed between the tubes and the flame to protect the tube from direct impact by the fuel slag. Although the performance of the HTHX panel during the previous project met or exceeded all heat-transfer performance goals, it was determined that the tiles were prone to thermal shock failure, and the heat-transfer rate was too low to be commercially acceptable. Toward the end of the project, laboratory tests showed that as long as the surface temperature of the tubes was kept below the solidus temperature of the slag, the corrosion rates were very low. Therefore, a subsequent project was completed to evaluate the performance of the HTHX alloy surfaces without ceramic tile protection, fully exposing the alloy surfaces to slagging furnace conditions (40). These tests showed that without the ceramic tiles the slag layer developed on the tubes was very thin and essentially self-cleaning, and that heat transfer rates were increased by a factor of five. The heat transfer rate was so high that the available cooling air compressor capacity was exceeded, so that full furnace temperatures could not be achieved unless the upper and lower sections of the HX tubes were embedded in insulating alumina board and refractory.

Table 25 summarizes the operating hours for the HTHX through December 2003 (the end of the current test cycle), representing 28 thermal cycles. The HTHX has been exposed to a range of furnace firing conditions for a total of 4054 hr, representing operation with and without tiles. NG firing represents 2194 hr (including heatup, cooldown, and refractory curing), and solid fuel firing represents 1860 hr.

Table 25. Summary of HTHX–RAH Panel Operating Hours Through December 2003[1]

Natural Gas Firing, hr	Coal–Lignite Firing, hr	Total Operation, hr
2194	1860	4054

[1] Natural gas firing includes heatup, cooldown, and refractory curing.

Three coal–biomass cofiring tests were completed while firing the SFS in an air-blown configuration in this project. Figure 43 illustrates the location of thermocouples in the HTHX, and Table 26 describes the HTHX thermocouples used during the air-blown SFS tests. These thermocouples represent process air and alloy tube surface temperature measurements. For the coal–biomass cofiring tests, only the alloy tube surface thermocouple T2 was directly exposed to furnace conditions. All remaining alloy surface thermocouples, as well as the lower half and upper 11% of the HTHX, were encased in insulation and refractory, shielding them from furnace conditions.

Figures 44 and 45 summarize the HTHX tube surface temperatures and process air temperatures for Test SFS-XCEL1-0303. HTHX process air flow rates during the test were controlled at set points of 10.6–11.2 m^3/min (375–395 scfm), but were typically 10.9–11.2 m^3/min (385–395 scfm) during the coal–hog fuel-cofiring period. Changes in process air flow rate were minimized during Test XCEL1 to achieve thermal stability during the 85-hr coal–biomass cofired test. During Test XCEL1, only minor adjustments were made to the process air flow rate and furnace firing rate to maintain a specified HTHX tube surface temperature. The original test plan limited the maximum HTHX tube surface temperature to <1052°C (<1925°F) while cofiring coal and biomass. However, early in the test while firing NG, the EERC determined that the designated control thermocouple was reading high relative to other HTHX thermocouples based on previous operating experience. This differential indicated the thermocouple would likely fail prior to completion of Test XCEL1. Therefore, other thermocouples, both process air and tube surface, were used to control furnace-firing rate and process air flow rate to avoid overheating the HTHX. As a result, indicated maximum HTHX tube surface temperatures were controlled at 1091°C (<1995°F) and typically ranged from 1071° to 1082°C (1960° to 1980°F).

During a 16-hr NG-fired test prior to initiating coal–hog fuel cofiring, process air temperatures of 766°–799°C (1410°–1470°F) were achieved at the HTHX exit based on process air flow rates of 10.5–10.9 m^3/min (370–386 scfm), furnace firing rates of 3.2–3.4 × 10^6 kJ/hr (3.0–3.2 MMBtu/hr), and a furnace exit temperature of 1499°–1535°C (2730°–2795°F). Inlet process air temperatures were 577°–596°C (1070°–1105°F). HTHX heat recovery in this case was 418,200–464,100 kJ/hr (396,400–439,900 Btu/hr) when corrected for surface area. These values are consistent with data observed for other NG-fired tests at comparable firing rates and furnace temperatures.

During the coal–hog fuel-cofiring test, Run Hours 96 through 181, the HTHX process air flow rate was controlled at 10.9–11.2 m^3/min (385–395 scfm). However, as the data in the figures demonstrate, alloy tube surface and process air temperatures decreased with time before apparently stabilizing during the final 12 hr of the coal–hog fuel-firing test. These decreasing temperatures were the result of ash deposition on heat-transfer surfaces, HTHX alloy tube surfaces, CAH surfaces, and process air preheater surfaces. Deposition on the HTHX alloy tube surfaces began with a low-density sintered layer, followed by a higher-density intermediate layer, and finally a high-density molten slag

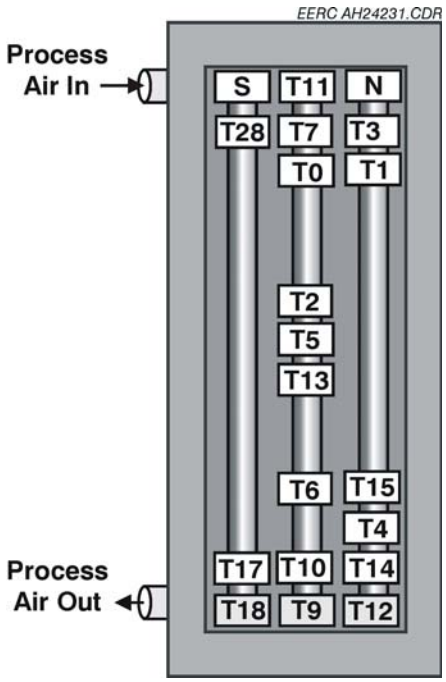

Figure 43. Thermocouple locations in the HTHX for the coal–biomass cofiring tests.

Table 26. Description of HTHX Thermocouple Locations for the Coal–Biomass Cofiring Tests[1]

Category	No.	Label	Description
Air Inlet	1	HP Air In	Provided by the EERC, in pipe before inlet header
	2	T11	Air entering HTHX through center tube
Air Outlet	3	T18	Air leaving left (south) tube
	4	T9	Air leaving middle tube
	5	T12	Air leaving right (north) tube
MA Tube Surface	6	T0	Top of middle tube facing cold side
	7	T1	Top of north tube facing cold side
	8	T2	Middle of middle tube facing toward furnace
	9	T3	Top of north tube facing toward furnace
	10	T4	Bottom of north tube facing cold side
	11	T5	Middle of middle tube facing toward furnace
	12	T6	Bottom of middle tube facing cold side
	13	T7	Top of middle tube facing toward furnace
	14	T10	Bottom of the middle tube facing toward furnace
	15	T13	Middle of middle tube facing cold side
	16	T14	Bottom of north tube facing toward furnace
	17	T15	Bolting material on bottom of middle tube
	19	T17	Bottom of south tube facing toward furnace
	20	T28	Top of south tube facing toward furnace

[1] Thermocouple locations are illustrated in Figure 43.

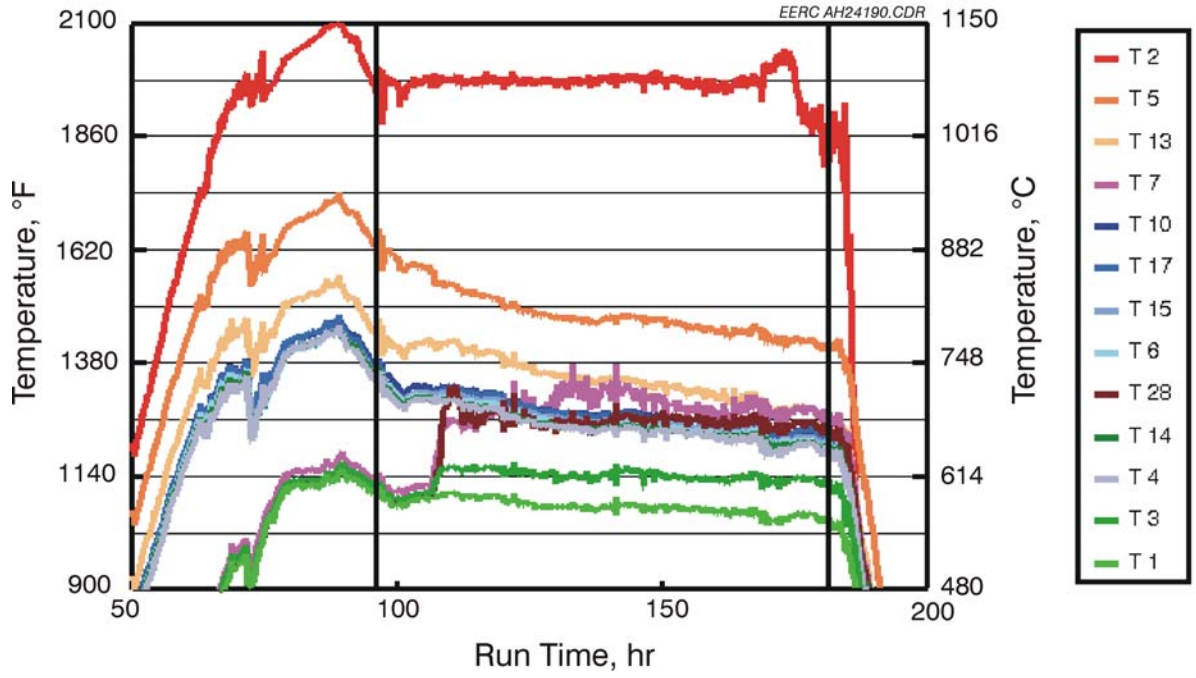

Figure 44. HTHX tube surface temperatures versus run time for Test SFS-XCEL1-0303.

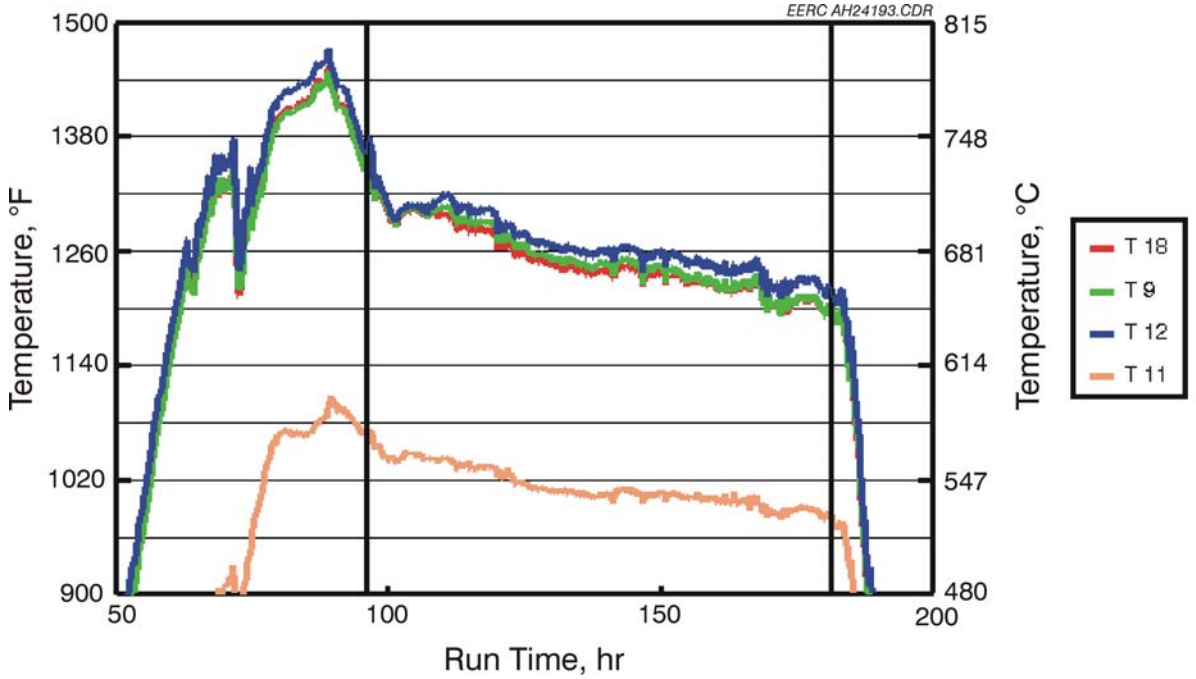

Figure 45. HTHX process air temperatures versus run time for Test SFS-XCEL1-0303.

layer. However, there was no evidence of slag flow down the surface of the alloy tubes. Based on these observations, a higher tube surface temperature limit could have been employed without causing an alloy corrosion problem while firing the coal–hog fuel combination. The composition and thickness of the ash–slag layers that developed during Test XCEL1 are discussed later in this section.

As a result of ash–slag deposition, HTHX alloy surface temperatures decreased during the coal–hog fuel-cofiring test for the first 70 hr and appeared to stabilize during the last 10–15 hr. The exception to this observation was tube surface Thermocouple T2, the only one directly exposed to furnace conditions. Alloy surface temperatures indicated by Thermocouple T2 were stable for the first 70 hr before gradually increasing and then dramatically decreasing. This observation is a result of Thermocouple T2 failing during the last 12 hr of coal–hog fuel cofiring. During the coal–hog fuel-cofiring test, the range of measured alloy surface temperatures protected from furnace conditions decreased from 605° to 905°C (1120° to 1660°F) to 571° to 771°C (1060° to 1420°F). This decrease is a direct result of decreasing heat transfer as a function of ash/slag deposition on alloy tube surface exposed to furnace conditions and the decreasing process air inlet temperature resulting from ash deposition on CAH and air preheater surfaces.

The low end of these temperature ranges represents the back side of the tube surfaces near the process air inlet, with the high end of the temperature ranges representing the front side of the tube surfaces near the midpoint immediately beneath the insulating material and high-density refractory used to isolate the lower half of the HTHX. The front-to-back tube surface temperature differential was nominally 8°C (15°F) at the process air exit and 83°–111°C (150°–200°F) near the middle of the HTHX. The low front-to-back temperature differential at the process air exit is the result of the insulating material and high-density refractory used to isolate the lower half of the HTHX from furnace conditions. A similar observation was made for the process air inlet prior to the insulating materials shifting. Tube surface temperatures during Test XCEL1 were generally lower than values observed for previous HTHX tests (167°–222°C [300°–400°F]) because of the lower alloy surface temperature limit selected for the coal–biomass cofiring tests. A lower temperature limit was selected because of the biomass ash properties to avoid the potential for alloy corrosion by the slag.

The alloy surface temperature step change observed for Thermocouples T28, T7, and T3 (representing the furnace side of the top of each alloy tube) at Run Hour 107 was a result of a shift in the insulating board and fibrous insulation used to isolate those thermocouples from furnace conditions. Inspection of the HTHX following Test XCEL1 confirmed that a gap developed in the insulating material, exposing these thermocouples to a small amount of radiation from the furnace. However, no effect on HTHX heat recovery was observed.

During the coal–hog fuel-cofiring test the range of measured process air temperatures at the exit of the HTHX decreased from 733° to 749°C (1350° to 1380°F) to 649° to 666°C (1200° to 1230°F). This decrease is the direct result of decreasing heat transfer caused by ash–slag deposition on HTHX alloy tube surfaces as well as ash deposition on downstream heat-transfer surfaces (CAH and air preheater surfaces). After achieving apparent thermal stability, process air temperatures of 649°–666°C (1200°–1230°F) were maintained at the HTHX exit based on a process air flow rate of 11.1 m^3/min (393 scfm), a furnace-firing rate of 3.1×10^6 kJ/hr (2.9 MMBtu/hr), and a furnace

temperature of 1433°C (2610°F). Inlet process air temperatures decreased from 577° to 530°C (1070° to 985°F) during the coal–hog fuel-cofiring test.

Heat recovery data from the HTHX for Test XCEL1 are presented as the lower line in Figure 46. Heat recovery decreased from 146,010 kJ/hr (138,400 Btu/hr) to nominally 120,590 kJ/hr (114,300 Btu/hr) during the coal–hog fuel-firing test period as a result of ash and slag deposition on the HTHX alloy tube surfaces. Correcting the XCEL1 data to account for isolation of the lower half and upper 11% of the HTHX from furnace conditions results in an equilibrium heat recovery value of 292,450 kJ/hr (277,200 Btu/hr) as shown by the upper line in the figure.

The corrected HTHX heat recovery rate for Test XCEL1 is only 66% of that observed for Test HTHX3, a test performed with Illinois No. 6 bituminous coal during a previous program. The primary reason for this difference is furnace temperature, 1433°C (2610°F) for Test XCEL1 versus 1571°C (2860°F) for Test HTHX3, and a lower HTHX tube temperature during XCEL1. Again, furnace and tube surface temperatures during Test XCEL1 were limited because of fuel ash–slag properties and a desire to avoid alloy corrosion. At an equivalent furnace temperature, HTHX heat recovery during Test XCEL1 was comparable to previous HTHX tests. Comparisons of air-blown HTHX heat recovery data for this and previous projects are summarized later in this discussion.

Figure 47 presents photographs of the HTHX before (top) and after (bottom) completion of Test XCEL2 (SFS-XCEL2-0403), which involved 90 hr of NG firing (heatup, some refractory curing, and cooldown) and 86 hr of coal–corn stover cofiring. The top photograph shows the interior of the slagging furnace and the clean, oxidized alloy surfaces of the HTHX tubes prior to Test XCEL2. The lower half of the tubes is encased in insulating material and high-density

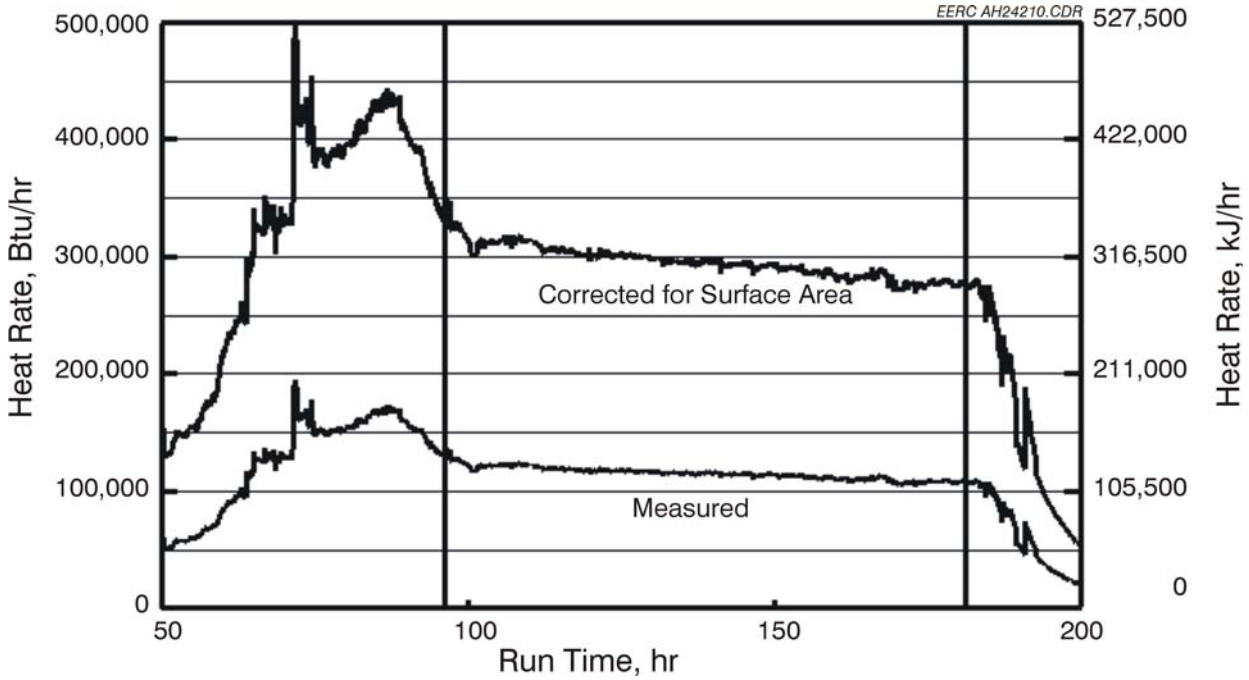

Figure 46. HTHX heat recovery versus run time for Test SFS-XCEL1-0303.

Figure 47. Photographs of the HTHX prior to (top) and after (bottom) completion of Test SFS-XCEL2-0403.

refractory, and the upper 11% is protected from furnace conditions using a combination of fibrous insulation and fiberboard insulation. One tube surface thermocouple is visible on the center tube several inches above the high-density refractory. The bottom photograph illustrates the impact of coal–corn stover cofiring on the interior of the slagging furnace and HTHX alloy tubes. No significant change is apparent concerning the furnace refractory. However, ash and slag deposits are evident on the HTHX alloy tubes. The bottom photograph illustrates that a molten slag layer had formed on the surface of the tubes. However, during cooldown, the slag layer fractured on the surface of the alloy tubes. As a result, most of the slag layer fell off the left tube, appears cracked on the center tube, and has partially fallen off the right tube. Visual examination of the tube surfaces beneath the slag layer reveals a sintered ash layer. No real evidence of slag flow down the surface of the alloy tubes is apparent in the photographs. Based on these observations, a higher tube surface temperature limit could have been employed without causing an alloy corrosion problem while firing the coal–corn stover combination. Samples of the slag layer and the sintered ash layer beneath the slag were recovered for analysis, and the results are discussed later in this report.

Figures 48 and 49 summarize the HTHX tube surface temperatures and process air temperatures for Test XCEL2. HTHX process air flow rates during the test were controlled at set points of 10.8, 11.0, and 11.2 m^3/min (380, 390, and 395 scfm). During Test XCEL2, only minor adjustments were made to the process air flow rate and furnace firing rate in an attempt to achieve thermal stability during the 86-hr coal–corn stover cofired test period and to maintain a specified HTHX tube surface temperature. The original test plan limited the maximum HTHX tube surface temperature to <1052°C (<1925°F) while cofiring coal and corn stover. Prior to Test XCEL2, a new T2 thermocouple was installed on the center tube for the purpose of maintaining the <1052°C (<1925°F) alloy tube surface temperature limit. However, after 70 hr of coal–corn stover cofiring, thermocouple T2 failed. The balance of the test was completed while maintaining relatively constant furnace temperatures and process air flow rates. Other thermocouples, both process air and tube surface, were used to adjust process air flow rate to avoid overheating the HTHX. As a result, indicated maximum HTHX tube surface temperatures were controlled at 1055°C (<1930°F) and typically ranged from 1033° to 1049°C (1890° to 1920°F).

During the coal–corn stover cofiring test, Run Hours 81 through 167, HTHX process air flow rate was generally controlled at 11.0 m^3/min (390 scfm). However, as the data in the figures demonstrate, alloy tube surface and process air temperatures decreased with time and did not appear to have stabilized after 86 hr of coal–corn stover cofiring. These decreasing temperatures were the result of ash deposition on heat-transfer surfaces, HTHX alloy tube surfaces, CAH surfaces, and process air preheater surfaces. Deposition on the HTHX alloy tube surfaces began with a low-density sintered layer, followed by a higher-density intermediate layer, and finally a high-density molten slag layer. However, there was no evidence of slag flow down the surface of the alloy tubes. Based on these observations, a higher tube surface temperature limit could have been employed without causing an alloy corrosion problem while firing the coal–corn stover fuel combination. The composition and thickness of the ash–slag layers that developed during Test XCEL2 are discussed later in this section.

As a result of ash–slag deposition, HTHX alloy surface temperatures decreased during the coal–corn stover-cofiring test period. The exception to this observation was tube surface

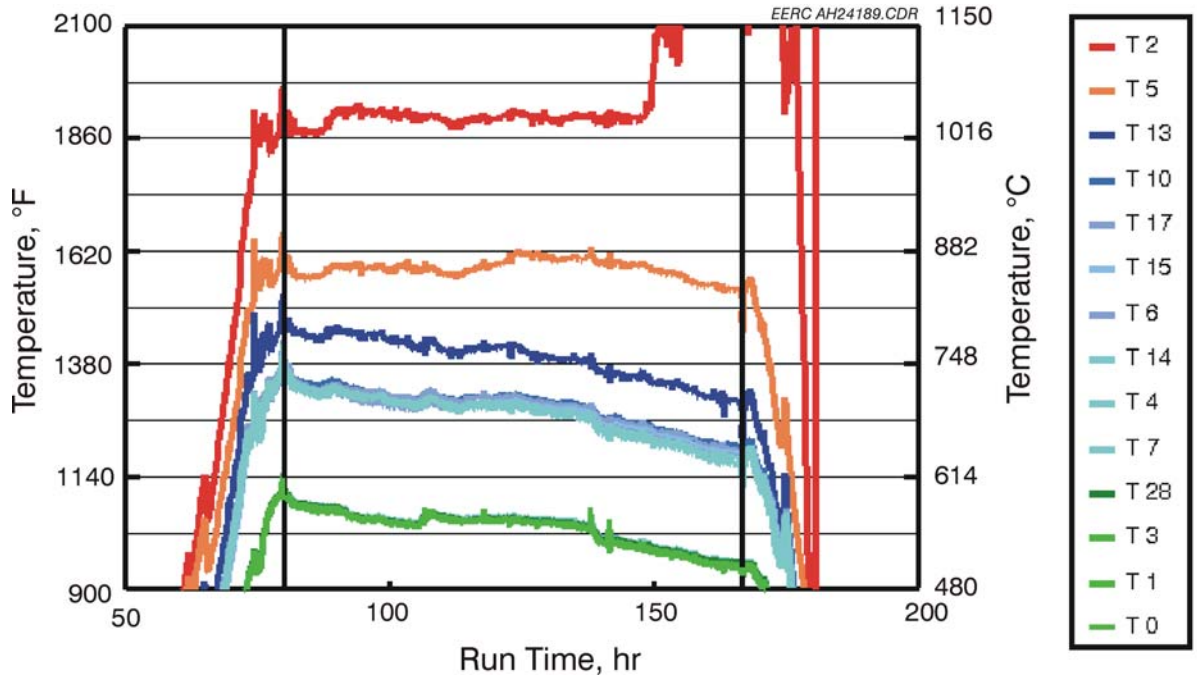

Figure 48. HTHX tube surface temperatures versus run time for Test SFS-XCEL2-0403.

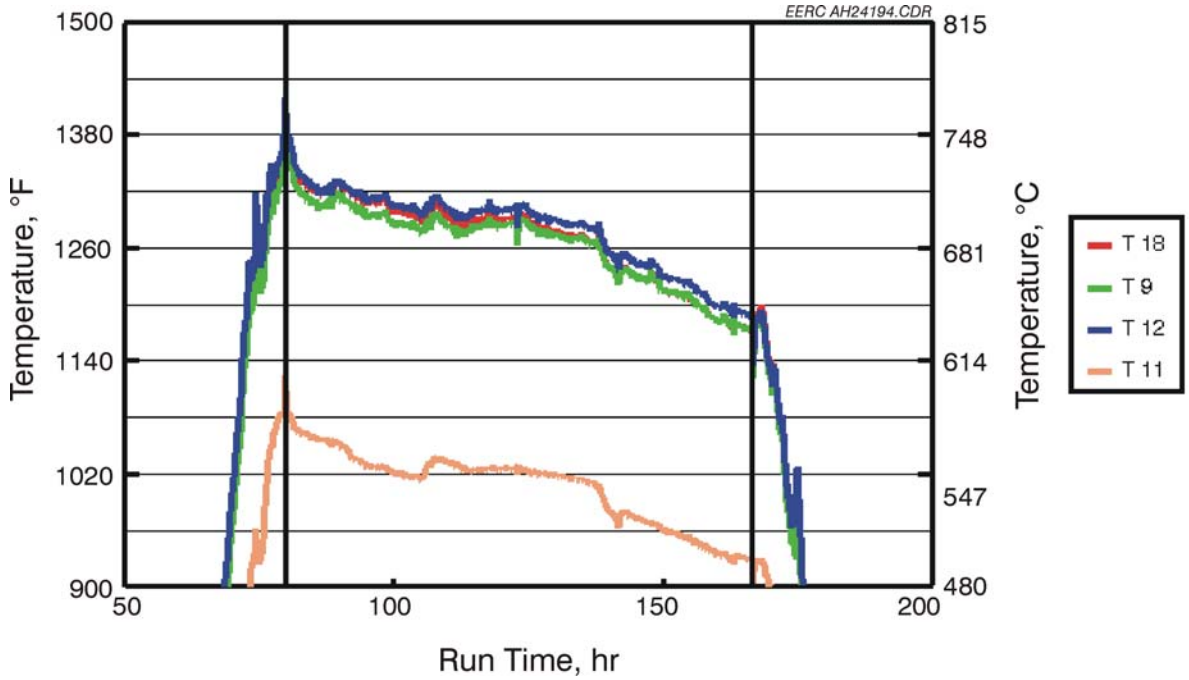

Figure 49. HTHX process air temperatures versus run time for Test SFS-XCEL2-0403.

Thermocouple T2, the only thermocouple directly exposed to furnace conditions. Alloy surface temperature indicated by Thermocouple T2 was reasonably stable for the first 70 hr before dramatically increasing. This observation is a result of the failure of Thermocouple T2 caused by slag corrosion of the thermocouple sheath. During the coal–corn stover-cofiring test the range of measured alloy surface temperatures protected from furnace conditions decreased from nominally 596° to 880°C (1105° to 1615°F) to 510° to 838°C (950° to 1540°F). This decrease is a direct result of decreasing heat transfer as a function of ash–slag deposition on alloy tube surface exposed to furnace conditions and the decreasing process air inlet temperature resulting from ash deposition on CAH and air preheat surfaces.

The low end of these temperature ranges represents the back side of the tube surfaces near the process air inlet, with the high end of the temperature ranges representing the front side of the tube surfaces near the midpoint immediately beneath the insulating material and high-density refractory used to isolate the lower half of the HTHX. The front-to-back tube surface temperature differential was <8°C (<15°F) at the process air inlet,<14°C (<25°F) at the process air exit, and 69°–133°C (125°–240°F) near the middle of the HTHX. The low front-to-back temperature differential at the process air inlet and exit is the result of the insulating material used to isolate the upper 11% and lower half of the HTHX from furnace conditions. Tube surface temperatures during Test XCEL2 were generally lower than values observed for previous HTHX tests (167°–222°C [300°–400°F]) because of the lower alloy surface temperature limit selected for the coal–biomass-cofiring tests. A lower temperature limit was selected because of the biomass ash properties to avoid the potential for alloy corrosion by the slag.

Tube surface temperatures during Test XCEL2 were generally lower than values observed for Test XCEL1 because of lower process air inlet temperatures. Process air temperatures decreased from 735° to 749°C (1355° to 1380°F) to 635° to 644°C (1175° to 1190°F) at the HTHX exit during the coal–corn stover-cofiring test. Inlet process air temperatures decreased from 585° to 499°C (1085° to 930°F) during the test period. The lower process air inlet temperatures observed at the conclusion of Test XCEL2, when compared to Test XCEL1, are consistent with the higher ash deposition rate observed in the CAH for Test XCEL2. However, these differences would likely be mitigated if routine sootblowing were applied to the CAH and process air preheat surfaces.

Heat recovery data from the HTHX are presented in Figure 50 for Test XCEL2. Heat recovery decreased from 152,130 kJ/hr (144,200 Btu/hr) to nominally 141,580 kJ/hr (134,200 Btu/hr) during the coal–corn stover-firing test as a result of ash and slag deposition on the HTHX alloy tube surfaces, although it is uncertain that HTHX thermal stability was achieved during the last 12 hr of the test period. Correcting the Test XCEL2 data to account for isolation of the lower half and upper 11% of the HTHX from furnace conditions results in a minimum heat recovery value of 363,030 kJ/hr (344,100 Btu/hr).

A comparison of Tests XCEL2 and XCEL1 heat recovery data for the coal–biomass-firing test periods shows that for a process air flow rate of 11.0 m^3/min (390 scfm), heat recovery was 24% greater for Test XCEL2. The reason for the greater heat recovery rate during Test XCEL2 was the higher furnace temperature, 1477°C (2690°F) versus 1433°C (2610°F), for Test XCEL1. The corrected HTHX heat recovery rate for Test XCEL2 is only 82% of that observed for Test HTHX3

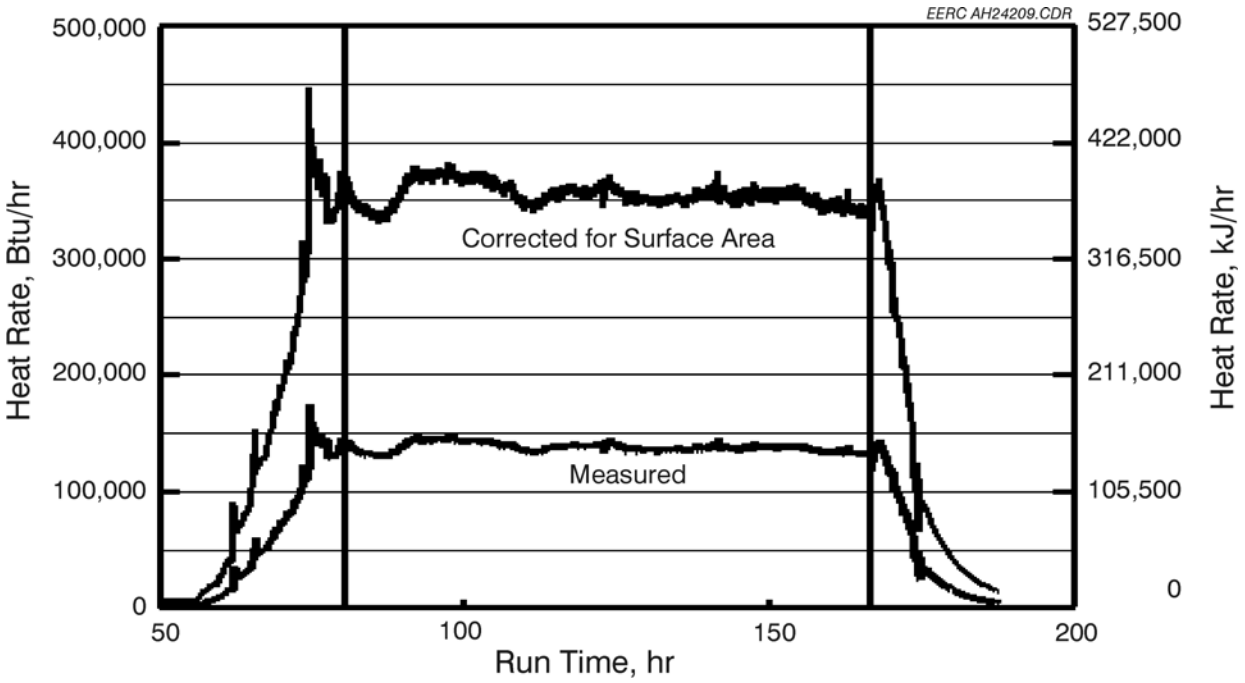

Figure 50. HTHX heat recovery versus run time for Test SFS-XCEL2-0403.

(a previous test performed with Illinois No. 6 coal), 363,030 versus 440,990 kJ/hr (344,100 versus 418,000 Btu/hr). The primary reason for this difference is the lower furnace temperature, 1477°C (2690°F) for Test XCEL2 versus 1571°C (2860°F) for Test HTHX3 firing an Illinois No. 6 bituminous coal, and the lower HTHX tube temperature during XCEL2. Again, furnace and tube temperatures during Test XCEL2 were limited because of fuel ash–slag properties and a desire to avoid any potential alloy corrosion. At an equivalent furnace temperature, HTHX heat recovery during Test XCEL2 was comparable to previous HTHX tests (40). Comparisons of air-blown HTHX heat recovery data for this and previous projects are summarized later in this discussion.

Figure 51 presents a photograph of the HTHX after completion of Test XCEL3 (SFS-XCEL3-0503) which involved 88 hr of NG firing (heatup, some refractory curing, and cooldown) and 85 hr of coal–switchgrass cofiring. The interior of the slagging furnace and the clean oxidized alloy surfaces of the HTHX tubes prior to Test XCEL3 looked nearly identical to the top photograph in Figure 47. Again, the lower half and upper 11% of the tubes were protected from furnace conditions using a combination of fibrous insulation, fiberboard insulation, and high-density refractory. One new alloy surface thermocouple was installed on the center tube several inches above the high-density refractory prior to Test XCEL3. The photograph in Figure 51 illustrates the impact of coal–switchgrass cofiring on the interior of the slagging furnace and HTHX alloy tubes. No significant change is apparent concerning the furnace refractory other than some refractory deterioration above the HTHX and on the upper half of the high-density refractory encasing the lower half of the HTHX.

Ash and slag deposits are not evident on the HTHX alloy tubes. The photograph illustrates that any molten slag and most of the sintered ash layer that had formed on the surface of the tubes fell

Figure 51. Photograph of the HTHX after completion of Test SFS-XCEL3-0503.

off, likely as a function of cooldown. Visual examination of the tube surfaces revealed a light sintered ash layer remaining after Test XCEL3. No evidence of slag flow down the surface of the alloy tubes was seen. Samples of molten slag and sintered ash material were recovered for analysis, and the results are discussed later in this report.

Figures 52 and 53 summarize the HTHX tube surface temperatures and process air temperatures for Test XCEL3. HTHX process air flow rates during the test were controlled at set points of 10.6, 10.8, 11.0, and 11.2 m^3/min (375, 380, 390, and 395 scfm). During Test XCEL3, only minor adjustments were made to the process air flow rate and furnace firing rate to achieve thermal stability during the 85 hr coal–switchgrass-cofiring test and to maintain a specified HTHX tube surface temperature. The original test plan limited the maximum HTHX tube surface temperature to <1052°C (<1925°F) while cofiring coal and switchgrass. As previously stated, prior to Test XCEL3, a new T2 thermocouple was installed on the center tube for the purpose of maintaining the <1052°C (<1925°F) alloy tube surface temperature limit. However, after 17 hr of coal–switchgrass cofiring, Thermocouple T2 failed. The balance of the test was completed while maintaining relatively constant furnace temperatures and process air flow rates. Other thermocouples, both process air and tube surface, were used to adjust process air flow rate to avoid overheating the HTHX. As a result, indicated maximum HTHX tube surface temperatures were controlled at <1055°C (<1930°F).

A step change in alloy surface and process air temperatures is evident at Run Hour 93. This step change resulted from an adjustment to the main burner swirl setting. Burner swirl was increased slightly to reduce the temperature differential over the length of the furnace; this resulted in more

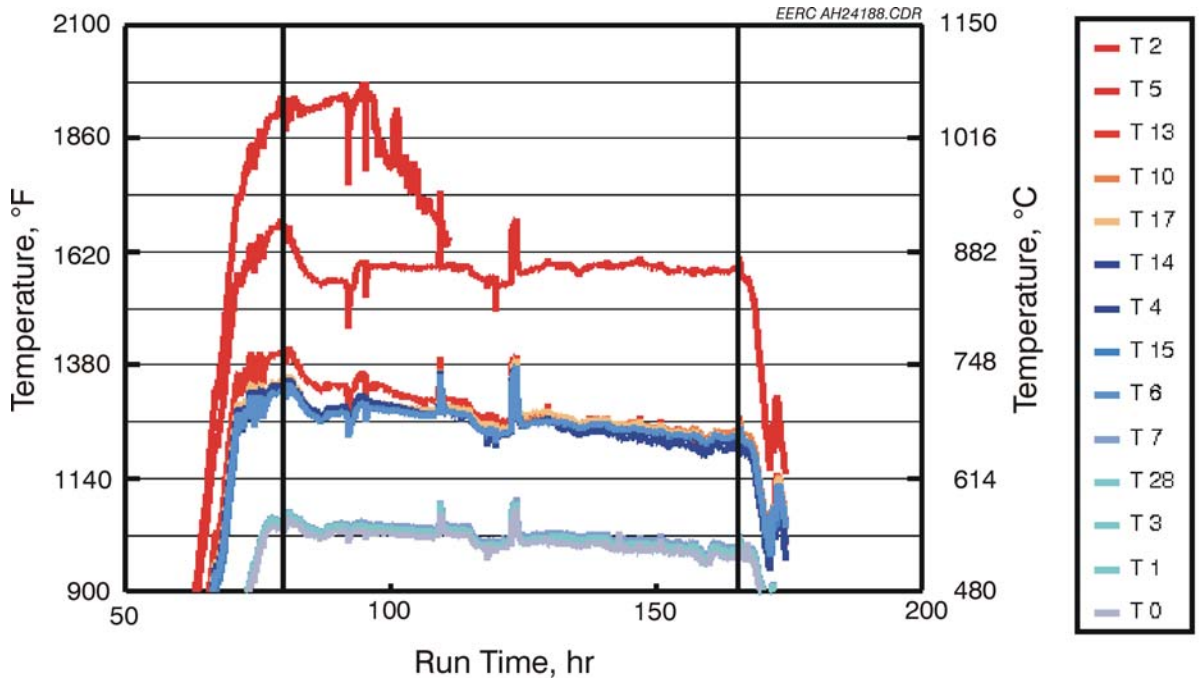

Figure 52. HTHX tube surface temperatures versus run time for Test SFS-XCEL3-0503.

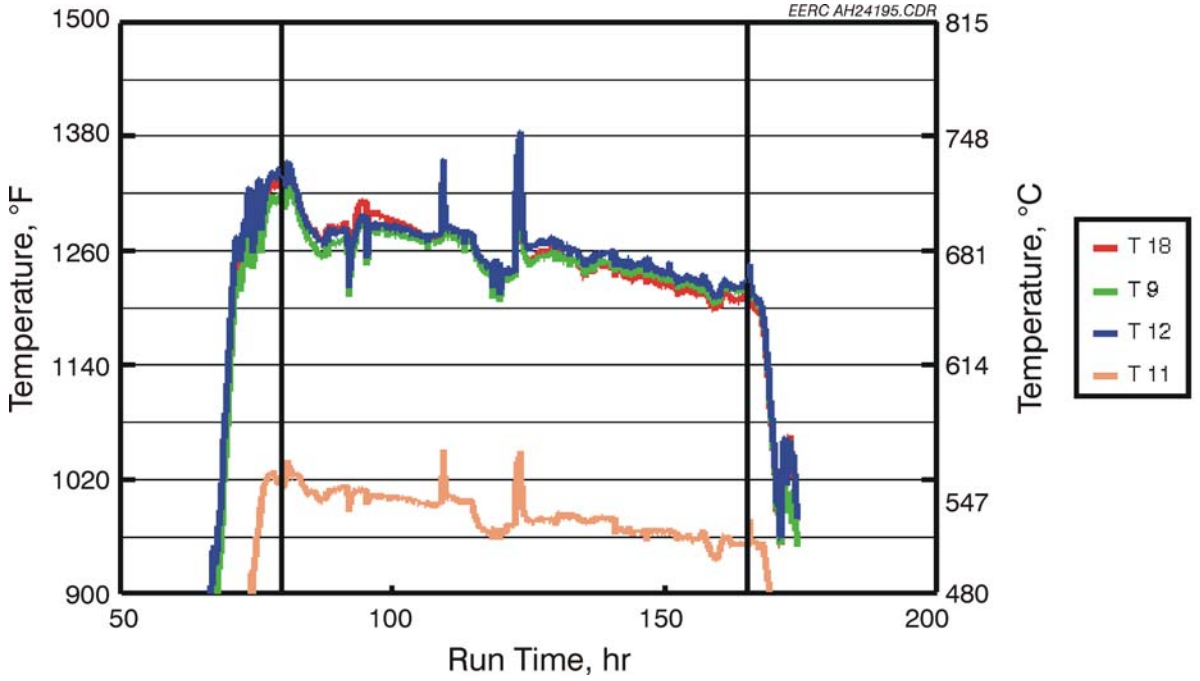

Figure 53. HTHX process air temperatures versus run time for Test SFS-XCEL3-0503.

uniform furnace temperatures. Spikes in alloy surface and process air temperatures are evident at Run Hours 109 and 123. These temperature spikes resulted from compressor trips and a temporary loss of process air flow. In both cases, the nitrogen backup system functioned as intended to avoid overheating the HTHX alloy tubes.

During the coal–switchgrass-cofiring test, Run Hours 80 through 165, HTHX process air flow rate was generally controlled at 11.0 m^3/min (390 scfm). However, as the data in the figures demonstrate, alloy tube surface and process air temperatures decreased with time and may have stabilized during the last 8 hr of coal–switchgrass cofiring. These decreasing temperatures were the result of ash deposition on heat-transfer surfaces, HTHX alloy tube surfaces, CAH surfaces, and process air preheater surfaces. Deposition on the HTHX alloy tube surfaces began with a low-density sintered layer, followed by a higher-density intermediate layer, and, finally, a high-density molten slag layer. However, there was no evidence of slag flow down the surface of the alloy tubes. Based on these observations, a higher tube surface temperature limit could have been employed without causing an alloy corrosion problem while firing the coal–switchgrass fuel combination. The composition and thickness of the ash–slag layers that developed during Test XCEL3 are discussed later in this section.

As a result of ash–slag deposition and decreasing process-air temperature, HTHX alloy surface temperatures decreased during the coal–switchgrass-cofiring test period. Exceptions to this observation were tube surface Thermocouples T2 and T5. Thermocouple T2, the only tube surface thermocouple directly exposed to furnace conditions, was slowly increasing with furnace temperature until it failed as a result of slag corrosion of the thermocouple sheath. Thermocouple T5, located within a few inches of T2 yet protected from furnace conditions, was generally stable during the coal–switchgrass-cofiring test except for the step change associated with a burner swirl adjustment and the spikes resulting from compressor trips. During the coal–switchgrass-cofiring test, the range of measured alloy surface temperatures protected from furnace conditions decreased from nominally 577° to 910°C (1070° to 1670°F) to 521° to 869°C (970° to 1595°F). This decrease is a direct result of decreasing heat transfer as a function of ash–slag deposition on alloy tube surface exposed to furnace conditions and the decreasing process air inlet temperature resulting from ash deposition on CAH and air preheat surfaces.

The low end of these surface temperature ranges represents the back side of the tube surfaces near the process air inlet, with the high end of the temperature ranges representing the front side of the tube surfaces near the midpoint immediately beneath the insulating material and high-density refractory used to isolate the lower half of the HTHX. The front-to-back tube surface temperature differential was <8°C (<15°F) at the process air inlet and exit and 125°–200°C (225°–360°F) near the middle of the HTHX. The low front-to-back temperature differential at the process air inlet and exit is the result of the insulating material used to isolate the upper 11% and lower half of the HTHX from furnace conditions. Tube surface temperatures during Test XCEL3 were generally lower than values observed for previous HTHX tests (128°–222°C [230°–400°F]) because of the lower alloy surface temperature limit selected for the coal–biomass-cofiring tests. A lower temperature limit was selected because of the biomass ash properties to avoid the potential for alloy corrosion by the slag.

Tube surface temperatures during Test XCEL3 were comparable to Test XCEL1 and generally higher than values observed for Test XCEL2 because of higher process air inlet temperatures.

Process air temperatures decreased from 721° to 733°C (1330° to 1350°F) to 658° to 666°C (1215° to 1230°F) at the HTHX exit during the coal–switchgrass-cofiring test. Inlet process air temperatures decreased from 558° to 510°C (1035° to 950°F) during the test period. The process air inlet temperatures observed at the conclusion of Test XCEL3 were lower than Test XCEL1 and higher than Test XCEL2. These process air temperature differences are consistent with the ash deposition rates observed in the CAH for Tests XCEL1 (15 g/10^6 kJ [0.036 lb/MMBtu]), XCEL2 (23 g/10^6 kJ [0.053 lb/MMBtu]), and XCEL3 (19 g/10^6 kJ [0.044 lb/MMBtu]). However, these differences would likely be mitigated if routine sootblowing were applied to the CAH and downstream process air preheat surfaces.

Heat recovery data from the HTHX are presented in Figure 54 for Test XCEL3. Heat recovery decreased from 164,580 kJ/hr (156,000 Btu/hr) to nominally 145,270 kJ/hr (137,700 Btu/hr) during the coal–switchgrass-firing test period as a result of ash and slag deposition on the HTHX alloy tube surfaces, although it is uncertain that HTHX thermal stability was achieved during the last 16 hr of the test period. Correcting Test XCEL3 data to account for isolation of the lower half and upper 11% of the HTHX from furnace conditions results in a minimum heat recovery value of 372,630 kJ/hr (353,200 Btu/hr).

A comparison of Tests XCEL3 and XCEL1 heat recovery data for the coal–biomass-firing tests shows that for a process air flow rate of 11.0 m^3/min (390 scfm), heat recovery was 27% greater for Test XCEL3. The reason for the greater heat recovery rate during Test XCEL3 was the higher furnace temperature,1488°C (2710°F) versus 1433°C (2610°F), for Test XCEL1. A similar

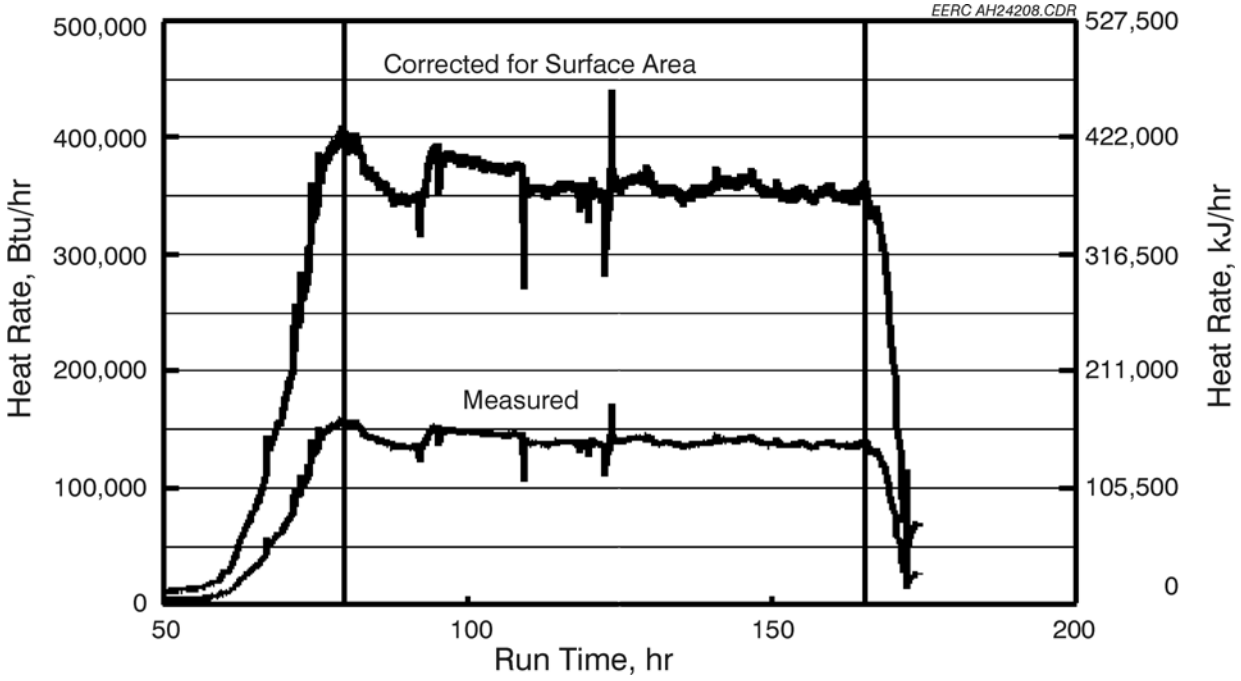

Figure 54. HTHX heat recovery versus run time for Test SFS-XCEL3-0503.

comparison with Test XCEL2 data indicates that Test XCEL3 HTHX heat recovery was 3% greater. The reason for the higher heat recovery rate during Test XCEL3 was also higher furnace temperature, 1488°C (2710°F) versus 1477°C (2690°F), for Test XCEL2.

The corrected HTHX heat recovery rate for Test XCEL3 is only 84% of that observed for Test HTHX3, a previous test performed with Illinois No. 6 coal, 372,630 versus 440,990 kJ/hr (353,200 versus 418,000 Btu/hr). The primary reason for this difference is furnace temperature, 1488°C (2710°F) for Test XCEL3 versus 2860°F (1571°C) for Test HTHX3 firing an Illinois No. 6 bituminous coal, and the lower allowed HTHX tube surface temperature. Again, furnace and tube temperatures during Test XCEL3 was limited because of fuel ash–slag properties and a desire to avoid alloy corrosion. At an equivalent furnace temperature, HTHX heat recovery during Test XCEL3 was comparable to previous HTHX tests (40).

Figure 55 summarizes the air-blown heat recovery data on an equivalent-surface-area basis for the biomass-cofiring tests (Tests XCEL1, XCEL2, and XCEL3) and several previous air-blown tests evaluating the HTHX while firing other coals. Data resulting from Tests XCEL1, XCEL2, and XCEL3 are represented by closed diamond symbols. The data from previous NG-fired tests are represented by open symbols connected by lines. Previous data from coal-fired tests are simply open symbols.

Short-term coal-fired tests indicated that the more radiant coal flame resulted in higher heat recovery rates than when firing NG. However, ash and slag deposition on the alloy tubes appears to degrade the heat recovery rate to a level equivalent to NG firing.

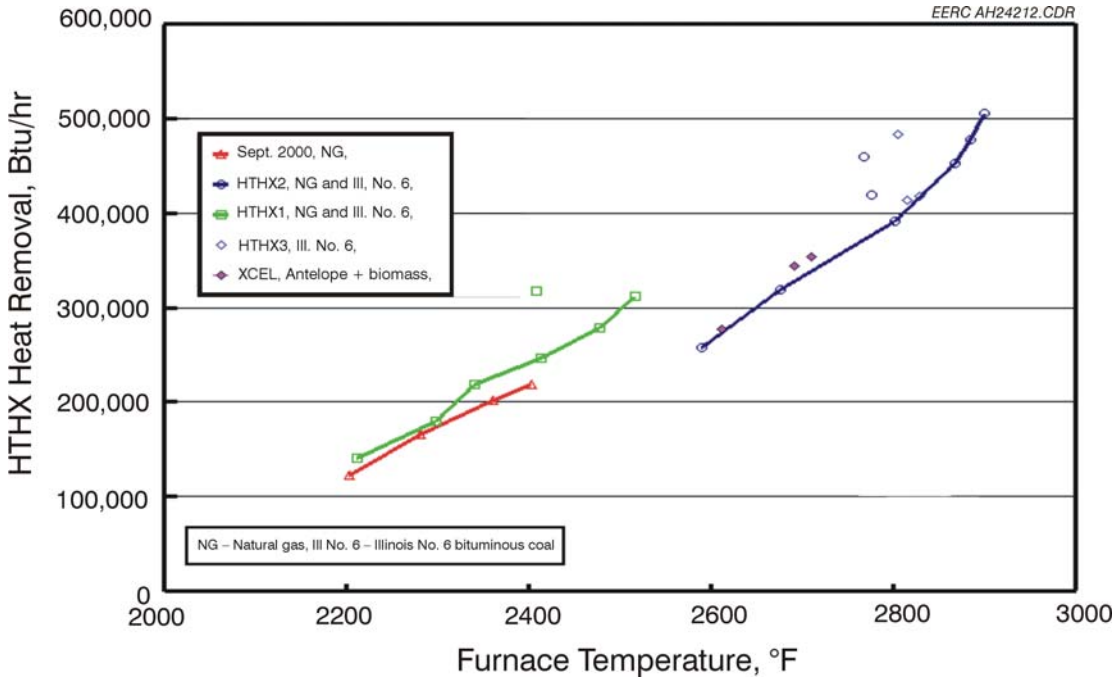

Figure 55. Heat recovery as a function of furnace temperature on an equivalent-surface-area basis for the biomass cofiring tests as well as previous air-blown HTHX tests.

Even at the lower furnace temperatures resulting from coal–biomass cofiring, HTHX heat recovery (on an equivalent-surface-area basis) was consistent with previous tests firing NG and bituminous coal. Therefore, at comparable furnace temperatures, coal–biomass cofiring does not present any unique impediments to HTHX heat recovery. However, biomass ash–slag properties will limit furnace and HTHX alloy surface temperatures. In that event, it is not likely that HTHX heat recovery rates observed for bituminous coal can be practically achieved when cofiring biomass.

One of the standards of success identified for this project in the original proposal was the production of clean pressurized air at 927°C (1700°F) while the slagging furnace was operated at a temperature of no more than 1566°C (2850°F). Based on the temperature measurements made during the three coal–biomass-cofiring tests, clean pressurized air temperatures generally stabilized at 635°– 666°C (1175°–1230°F) near the end of each test. At face value, these data indicate that the proposed standard of success was not achieved. However, this result was a function of several factors. First, 61% of the HTHX surface was isolated from furnace conditions limiting the heat-transfer surface available to raise air temperature because of limited process air capacity. Second, alloy surface temperature was limited to <1052°C (<1925°F) and, as a result, furnace temperature did not exceed 1494°C (2720°F). Finally, no attempt was made to routinely sootblow the CAH and air preheater surfaces in order to develop ash deposits for characterization, resulting in HTHX inlet process air temperatures 167°C (300°F) lower than those observed during tests evaluating the tubes-in-a-box configuration. Therefore, based on previous HTHX tests and the data generated during the coal– biomass cofiring tests, the EERC is confident that process air temperatures of >927°C (>1700°F) can be achieved and maintained if the entire surface of the HTHX is exposed to furnace conditions, the alloy tube surface temperature limit is raised to 1090°C (2000°F), and routine sootblowing of CAH and air preheat surfaces is employed.

Tables 27–29 summarize the composition data for deposits that formed on the HTHX alloy tubes during the coal–biomass-cofiring tests. The inner layer of the deposit has a composition very much like that of the slag except that it is somewhat depleted in calcium and enriched in magnesium, potassium, sodium and sulfur. SEM analyses show that most of the alkali and alkaline earth elements are associated with aluminosilicate ash particles, and that a large fraction of these elements, along with the calcium, have sulfated. This sulfation does not occur when the surface temperature of the HTHX is maintained at higher temperatures. The sulfation implies that running the HTHX at the lower temperature not only significantly reduces the heat removal rate of the unit, but opens the alloy to a new corrosion pathway based on sulfur. Although MA956 is known to be highly resistive to sulfur-based corrosion, other alloys may not be so resistive. The outer layers of the HTHX deposits is highly enriched in silica which dilutes the concentrations of the other elements, indicating that most of those elements were collected in the slag screen rather than on the main furnace walls. This differentiation likely occurred because the alumina is associated with medium-sized clay particles in the coal which do not separate from the gas flow in the low turbulence main furnace, but do deposit in the high velocity slag screen. In addition, some of the alumina in the slag may have come from dissolution of newly added alumina refractory which was not yet coated with slag from earlier tests. Because of the much higher temperature of the outer sintered layer of ash, no sulfation of the ash has occurred.

Table 27. HTHX Ash and Slag Samples from the Coal–Hog Fuel Cofiring Test

Oxides,[1] wt%	North Antelope Coal	Hog Fuel	Slag	Outer Sintered Layer	Inner Powdered Layer
SiO_2	25.9–27.2	33.3	37.7	51.5	35.6
Al_2O_3	17.0–18.3	2.5	20.1	10.3	17.0
Fe_2O_3	7.2–7.6	3.2	5.4	4.3	7.3
TiO_2	1.5	0.3	1.1	0.8	1.3
P_2O_5	1.2	1.8	0.9	1.0	1.4
CaO	26.3–26.9	43.2	28.0	23.2	20.1
MgO	6.9–7.2	3.9	4.4	2.6	6.6
Na_2O	0.8–1.2	3.9	1.2	3.5	7.1
K_2O	0.2–0.3	7.9	1.1	2.9	3.7
SO_3[2]	8.9–12.4	0.0	0.0	0.0	16.2

[1] Oxide concentrations normalized to an SO_3-free basis.
[2] SO_3 concentrations normalized with other oxides.

Table 28. HTHX Ash and Slag Samples from the Coal–Corn Stover Cofiring Test

Oxides,[1] wt%	North Antelope Coal	Corn Stover	Slag	Fused Outer Slag Layer	Intermediate Sintered Ash	Low-Density Inner Powder
SiO_2	25.9–27.2	57.3	45.5	68.2	66.7	41.9
Al_2O_3	17.0–18.3	3.2	18.6	7.8	7.7	14.5
Fe_2O_3	7.2–7.6	1.4	5.3	3.0	3.1	5.4
TiO_2	1.5	0.3	1.1	0.5	0.5	1.2
P_2O_5	1.2	3.8	1.0	1.2	1.0	3.5
CaO	26.3–26.9	9.5	20.3	8.9	9.5	18.9
MgO	6.9–7.2	12.6	5.9	6.5	6.4	7.8
Na_2O	0.8–1.2	0.4	0.9	1.0	1.3	3.1
K_2O	0.2–0.3	10.0	1.4	2.8	3.7	3.6
SO_3[2]	8.9–12.4	1.5	0.0	0.0	0.0	12.4

[1] Oxide concentrations normalized to an SO_3-free basis.
[2] SO_3 concentrations normalized with other oxides.

Table 29. HTHX Ash and Slag Samples from the Coal–Switchgrass Cofiring Test

Oxides,[1] wt%	North Antelope Coal	Switch-grass	Slag	Fused Outer Slag Layer	Intermediate Sintered Ash	Low-Density Inner Powder
SiO_2	25.9–27.2	70.3	51.0	70.5	72.4	40.3
Al_2O_3	17.0–18.3	0.0	15.2	5.5	5.9	17.6
Fe_2O_3	7.2–7.6	0.25	5.4	3.6	3.5	8.4
TiO_2	1.5	0.03	1.0	0.4	0.5	1.6
P_2O_5	1.2	4.8	1.1	1.2	1.3	3.4
CaO	26.3–26.9	9.4	18.9	9.7	10.0	12.2
MgO	6.9–7.2	4.9	5.0	3.1	3.3	5.2
Na_2O	0.8–1.2	0.03	0.8	2.0	0.9	5.6
K_2O	0.2–0.3	7.0	1.5	4.0	2.3	5.8
SO_3[2]	8.9–12.4	3.3	0.0	0.0	0.0	10.0

[1] Oxide concentrations normalized to an SO_3-free basis.
[2] SO_3 concentrations normalized with other oxides.

Table 28 shows that, as was true for the inner powder deposits formed on the HTHX when cofiring coal and hog fuel, the inner layer of the deposit formed during the coal-corn stover coal firing has a composition very much like that of the slag except that it is enriched in magnesium, potassium, sodium and sulfur. SEM analyses show that most of the alkali and alkaline earth elements are associated with aluminosilicate ash particles, and that a large fraction of these elements, along with the calcium, have sulfated. This sulfation does not occur when the surface temperature of the HTHX is maintained at higher temperatures. As the deposit builds, and therefore reaches higher temperatures leading to sintering, sulfation no longer occurs, and the deposits become highly enriched in silica which dilutes the concentrations of the other elements. The silica enrichment most likely occurs because the temperature of the deposit is so high that silica-rich ash particles are softened and become more sticky than at lower temperatures.

Table 29 shows that, as was true for the inner powder deposits formed on the HTHX when cofiring the other fuels, the inner layer of the deposit formed during the coal-switchgrass cofiring has a composition very much like that of the slag except that it is enriched in potassium, sodium and sulfur. SEM analyses show that most of the alkali and alkaline earth elements are associated with aluminosilicate ash particles, and that a large fraction of these elements, along with the calcium, have sulfated, although for this test there is also more of the complex nonsilicate sulfate material.. This sulfation does not occur when the surface temperature of the HTHX is maintained at higher temperatures. As the deposit builds, and therefore reaches higher temperatures leading to sintering, sulfation no longer occurs, and the deposits become highly enriched in silica which dilutes the concentrations of the other elements. In fact, the composition of the outer layers of the deposit take on a composition very similar to that of the switchgrass ash. It is unlikely, however, that only switchgrass ash deposited on the HTHX tubes. It is more likely that the high silica contents reflect preferential deposition of larger mineral grains which are rich in silica in both the coal and the switchgrass. As was also true for the other tests, the relatively low alumina content in the outer deposits relative to the slag composition indicates that only a relatively small fraction of the

aluminosilicate-rich clay particles in the coal deposit in the main combustor. Instead, they appear to be preferentially removed in the slag screen.

Economic Analyses of IFCC Systems

A brief study was performed to identify the performance and the first-order economics of an IFCC employing a bare-tube HTHX. The study was performed by Dr. Fred Robson of kraftWorks Systems, a consultant hired by the EERC. Dr. Robson served as the primary systems analyst for UTRC under the original HiPPS program. The results were compared to a variety of systems including typical pc-fired plants, integrated gasification combined cycles (IGCCs), and NGCCs. Since the pilot-scale testing of coal–biomass cofiring showed no significant influence of biomass cofiring on the operation of the combustor, and since the cost of biomass is only slightly less than that of coal, it was assumed that costs for cofiring would be essentially the same as for just firing coal so no separated calculations were included for cofiring. Two main IFCC firing scenarios were investigated; coal-fired with air and coal-fired with O_2. Because IFCC systems have a high potential for operation as zero-emission power plants, special focus was placed on firing with O_2, and including CO_2 recovery. Three main IFCC energy cycles were investigated:

- Commercially available GT with coal-fired HTHX with 927°C (1700°F) exit and NG-boost fuel.

- Advanced aeroderivative GT with coal-fired HTHX with 1489°C (2100°F) exit and NG-boost fuel.

- Commercially available aeroderivative GT with using only a coal-fired HTHX with 1489°C (2100°F) exit, i.e., all-coal IFCC.

When firing a fuel in an IFCC with O_2, it was assumed that flue gas, consisting primarily of CO_2 and H_2O, would be recycled to replace a portion of the N_2 normally found in the primary and secondary air used in a pc-burner. Recycling would be done in order to keep the flame temperature from becoming too high. In all cases it was assumed that the amount of O_2 supplied would be 20% greater than that required to completely burn the fuels, but that the amount of recycled flue gas would be less than the amount of N_2 excluded so that the total concentration of O_2 in the flue gas, before fuel combustion, would be approximately 50%. By using a reduced flue gas recycle rate relative to the N_2 replaced, the overall size of the furnace and pollution control devices can be reduced. Each of these configurations had two variations: 1) 50% O_2 (vol.) in oxidant with all the oxidant and coal for the HTHX supplied at the combustor entrance; and 2) 50% O_2 (vol.) in oxidant with the oxidant and coal supplied incrementally along the combustor. This case variation is denoted by A (Cases 1A, 2A, and 3A). In the first variation, the HTHX resembles closely the configuration developed in the HiPPS Program, the DOE sponsored program completed in 2001 (41) under which the SFS and HTHX were originally constructed. Unlike the HiPPS, however, in which and HTHX with ceramic tiles was used, a bare tube HTHX was included as was tested under the XCEL program. In the second variation, coal and oxidant are introduced sequentially along the length of the combustor section of the HTHX, thereby allowing a reduction of recycle gas required for temperature moderation. All systems used an advanced cryogenic air separation unit (ASU) to supply 98% O_2 for combustion. Also, the exhaust for each, consisting essentially of only H_2O and

CO_2, was cooled, the H_2O removed, and the CO_2 compressed to 140 bar (2000 psia) for pipeline recovery so that the plant would operate with essentially zero emissions.

A simplified schematic of the generic IFCC analyzed is shown in Figure 56. The simulations were carried out using the Advanced Performance Simulation Analysis Tool developed under the auspices of the National Fuel Cell Research Center, Advanced Power and Energy Programs, University of California at Irvine. This simulation tool has been used in a number of programs including the recently completed *Vision 21 Systems Methodology* sponsored by DOE.

Case 1

The configuration in Case 1 (and Case 1A) is based on the power plant defined in the HiPPS study (41). The heat and mass balances for Case 1 are presented in Table 30. In this configuration, a Siemens–Westinghouse V84-type industrial GT is used in conjunction with a coal-fired (Table 31) combustor that heats the compressor discharge air to 927°C (1700°F). The heated air then goes to a specially designed low-NO_x GT combustor where NG (Table 32) is burned to boost the temperature to the desired GT entrance temperature of 1368°C (2495°F). The heated air is expanded in the turbine and the exhaust goes to a heat recovery steam generator (HRSG) where boiler

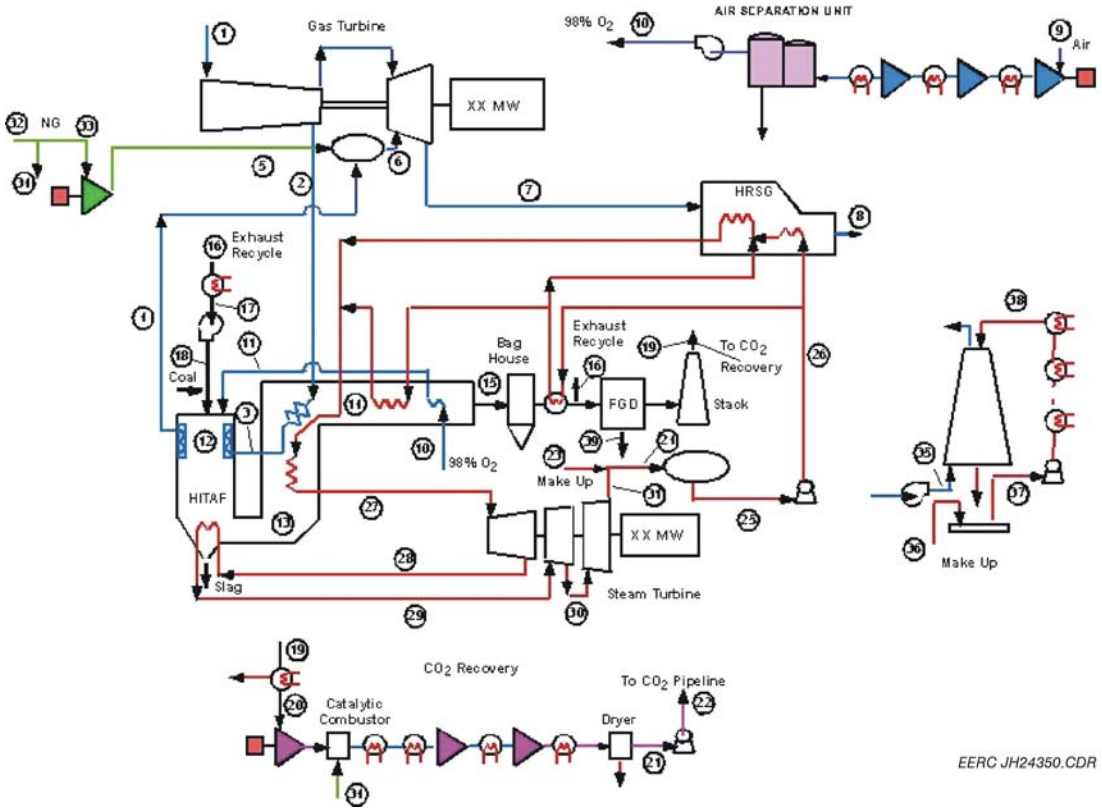

Figure 56. Simplified schematic of the IFCC.

Table 30. Case 1 – Heat and Mass Balance

	Stream Number					
	1	2	3	4	5	6
Flow Rate, kg/sec	416.31	329.44	329.44	329.44	4.09	333.53
Pressure, bar	1.014	15.920	15.603	15.293	25.000	14.527
Temperature, °C	15	389	704	927	5.056	1368
Composition, mol%						
H_2O	0.99	0.99	0.99	0.99		5.19
N_2	77.34	77.34	77.34	77.34	1.10	75.71
O_2	20.74	20.74	20.74	20.74		16.06
CO_2						2.14
SO_2						
SO_3						
H_2S						
CH_4					96.70	
C_2H_6					1.80	
C_3H_8					0.11	
Ar	0.93	0.93	0.93	0.93		0.91

	Stream Number					
	7	8	9	10	11	12
Flow Rate, kg/sec	420.39	420.16	215.33	43.07	43.07	279.36
Pressure, bar	1.076	1.062	1.014	2.220	2.179	1.058
Temperature, °C	538.9	100	15	7.000	320	1592
Composition, mol%						
H_2O	4.23	4.23	0.99			14.35
N_2	76.04	76.04	77.34	0.50	0.50	1.08
O_2	17.02	17.02	20.74	98	98	2.06
CO_2	1.70	1.70				80.99
SO_2						0.12
SO_3						0.01
H_2S						
CH_4						
C_2H_6						
C_3H_8						
Ar	0.91	0.91	0.93	1.50	1.50	1.38

Continued. . .

Table 30. Case 1 – Heat and Mass Balance (continued)

	Stream Number					
	13	14	15	16	17	18
Flow Rate, kg/sec	279.36	279.36	279.36	220.44	209.97	209.97
Pressure, bar	1.047	1.037	1.027	1.021	1.016	1.5
Temperature, °C	1209.83	667.611	330.78	100	30	65.167
Composition, mol%						
H_2O	14.35	14.35	14.35	14.35	4.31	4.31
N_2	1.08	1.08	1.08	1.08	1.20	1.20
O_2	2.06	2.06	2.06	2.06	2.30	2.30
CO_2	80.99	80.99	80.99	80.99	90.49	90.49
SO_2	0.12	0.12	0.12	0.12	0.14	0.14
SO_3	0.01	0.01	0.01	0.01	0.02	0.02
H_2S						
CH_4						
C_2H_6						
C_3H_8						
Ar	1.38	1.38	1.38	1.38	1.55	1.55

	Stream Number					
	19	20	21	22	23	24
Flow Rate, kg/sec	58.817	56.041	54.703	54.699		142.70
Pressure, bar	1.016	0.9963	85.2606	138.995		0.048
Temperature, °C	100	30	30	48.667		32.17
Composition, mol%						
H_2O	14.37	4.40				100
N_2	1.08	1.20	1.29	1.29		
O_2	2.06	2.30				
CO_2	81.08	90.52	97.04	97.04		
SO_2	0.01	0.01	0.03	0.03		
SO_3	0.01	0.02				
H_2S						
CH_4						
C_2H_6						
C_3H_8						
Ar	1.38	1.55	1.64	1.64		

Continued. . .

Table 30. Case 1 – Heat and Mass Balance (continued)

	Stream Number					
	25	26	27	28	29	30
Flow Rate, kg/sec	142.70	142.70	142.70	142.70	142.70	142.70
Pressure, bar	0.048	129.994	101.0	25.986	25.986	4.7
Temperature, °C	32	45.056	510	301	509.39	256.61
Composition, mol%						
H_2O	100	100	100	100	100	100
N_2						
O_2						
CO_2						
SO_2						
SO_3						
H_2S						
CH_4						
C_2H_6						
C_3H_8						
Ar						

	Stream Number							
	31	32	33	34	35	36	37	38
Flow Rate, kg/sec	142.70	4.34	4.09	0.25	125.97	48.580	2519.43	2519.43
Pressure, bar	0.048	3.682	3.682	3.682	1.100	4.1	1.014	3.599
Temperature, °F	32.17	1.333	1.333	1.333	23.61	−9.611	15	26.78
Composition, mol%								
H_2O	100				0.99	100	100	100
N_2		1.10	1.10	1.10	77.34			
O_2					20.74			
CO_2								
SO_2								
SO_3								
H_2S								
CH_4		96.70	96.70	96.70				
C_2H_6		1.80	1.80	1.80				
C_3H_8		0.11	0.11	0.11				
Ar					0.93			

Table 31. Coal Characteristics, North Antelope Subbituminous Coal*

Proximate Analysis, wt%	Range
Moisture	21.1–22.8
Volatile Matter	36.3–37.2
Fixed Carbon	37.2–37.9
Ash	3.7–3.9
Ultimate Analysis, wt%	
Hydrogen	6.0–6.1
Carbon	53.1–54.5
Nitrogen	0.9–1.0
Sulfur	0.23–0.25
Oxygen	34.6–36.1
Ash	3.7–3.9
HHV, kJ/kg	21,650–22,000

*As-fired.

Table 32. Natural Gas Composition

Ultimate Analysis, wt%		
C		73.25
H		24.26
N		1.87
O		0.62
	Total	100.00
Composition, mol%		
CH_4		96.67
C_2H_6		1.8
C_3H_8		0.11
CO_2		0.32
H_2S		0.0004
N_2		Balance
	Total	100.00
Average Molecular Weight		16.55
Higher Heating Value		
(dry gas at 16°C [60°F], 1.0 bar [30 in. Hg])		
kJ/m^3		37,740
kJ/kg		53,938

feedwater is heated and boiled prior to going to steam-cooled HXs in the downstream portion of the coal combustor where the steam is superheated and reheated. Some feedwater heating also occurs in this area.

In this configuration, the total coal and oxidant mixed with recycle gas from the combustor exhaust are fed into the firebox of the combustor. The recycle amount is based on moderating the combustion temperature to 1593°C (2900°F) when using a 50% (vol.) O_2 content. Heat is transferred to the bare-metal HTHX by radiation and convection. The gas exits this HTHX at 1204°C (2200°F) and passes through several steam HXs before entering a second compressor discharge air heater. This HX is convective. Before exiting, the combustion air is further cooled by feedwater heating and oxidant preheating. The combustion products, mainly CO_2 and H_2O, then go through a baghouse to remove particulates, further cooling against feedwater, and then to a flow splitter where recycle gas is taken off and recycled to the combustor to moderate combustion temperature.

Heat from the GT exhaust and from the combustion products in the HTHX is used to raise steam for the steam turbine. In this case, as in all the cases considered, the steam system uses a 100 bar/ 501°C/501°C (1450 psi/950°F/950°F) turbine. This steam system is not necessarily the optimum for each of the cases considered; however, the level of effort limited the number of bottoming cycle variations that could be considered. Thus this system was a good compromise for the brief analyses. Further parametric evaluations would no doubt identify steam systems that would increase overall performance by as much as several percentage points.

In Case 1, approximately 79% of the exhaust is recycled to the combustor. This requires about 7250 kW of fan power. The remaining exhaust goes to a limestone scrubber for S removal and then to the CO_2 recovery system.

The CO_2 recovery system consists of a series of coolers to condense out approximately 75% of the water prior to the first compressor. Following the compressor is a catalytic combustor where a small amount of NG is burned to remove essentially all of the remaining O_2 (2% vol). The burner is necessary to condition the CO_2 recovery stream to meet pipeline specifications. The gas is further compressed, cooled with glycol added to remove the remaining water, and pumped to the 140-bar (2000-psi) level. A total of 24,133 kW is required.

The Case 1 IFCC produces approximately 375 MW gross power and 295 MW net power, the majority of the losses due to the CO_2 recovery system, with recycle fan power also contributing. The net efficiency is 36.48% (HHV). This value is attractive for a coal-fired power plant (coal supplies over 72% of the energy input), especially when it has a CO_2 recovery system for the coal combustor.

In this configuration, 84% of the total CO_2 is recovered. In the coal stream, essentially 97% of the CO_2 is recovered. Only a small fraction of the CO_2 from methane stream is recovered. That fraction is represented by the methane used in the catalytic combustor in the CO_2 recovery system. No CO_2 from the GT boost combustor is recovered.

Case 1A

The configuration for Case 1A differs from Case 1 in that the oxidant (recycle gas with 50% [vol.] O_2) and coal are now injected along the axis of the HTHX combustor (see Figure 57 for a conceptual diagram of one suggested variation of this combustor). For the same temperature conditions (1593°C [2900°F]) the total amount of recycle gas is reduced to 50% of the combustor exit flow. This requires 1910 kW, a significant reduction in fan power. Also, because of the differing flow rates in the HTHX, the heat available for steam raising shifts somewhat resulting in a 1-MW gain in steam turbine power. The overall effect is a gain in the net power of 7 MW and an efficiency increase to 37.36 % (HHV), nearly a point better.

The change in the way the recycle is handled has a beneficial effect and makes this configuration even more attractive versus the pc plant with CO_2 recovery. Because the CO_2 concentration in the exhaust is somewhat less, not quite as much CO_2 is recovered as in Case 1, 83% vs. 84 %.

Case 2

The Case 2 configuration differs from Case 1 in two areas: the GT is an advanced intercooled aeroderivative engine; and the compressor discharge air outlet temperature from the HTHX is 1489°C (2100°F). This requires an aggressive material development for the metallic HTHX tubes. The remainder of the system is similar to the Case 1 configuration.

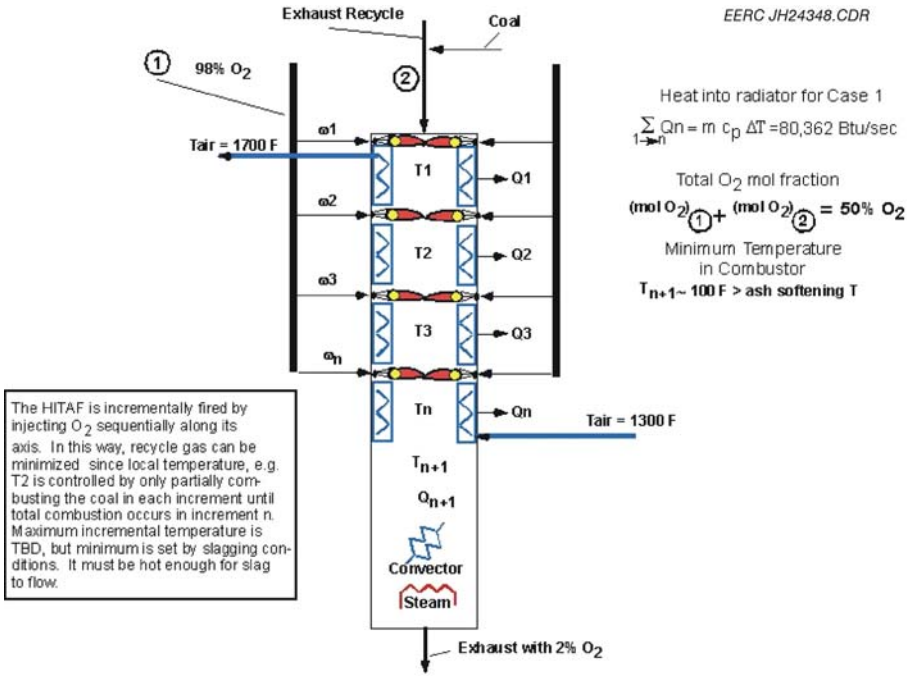

Figure 57. Simplified conceptual design for the sequential combustor.

In Case 2, again, approximately 79% of the exhaust is recycled to the combustor. This requires about 4550 kW of fan power. The other major power consumer is the CO_2 recovery system. Here, 18,776 kW are used in the recovery of 87% of the total CO_2. The net power for this configuration is nearly 170 MW and the net efficiency of this system, 35.31% (HHV), is well above the efficiencies of the pc systems with CO_2 recovery.

As in Case 1, essentially 97% of the CO_2 in the coal stream is recovered. Only a small fraction of the CO_2 from methane stream is recovered. That fraction is represented by the methane used in the catalytic combustor in the CO_2 recovery system. No CO_2 from the GT-boost combustor is recovered.

Case 2A

The Case 2A configuration differs from Case 2 in that the oxidant (recycle gas with 50% [vol.] O_2) and coal are now injected along the axis of the HTHX combustor. For the same temperature conditions (1593°C [2900°F]), the total amount of recycle gas is reduced to 50% of the combustor exit flow. This requires 1197 kW, a significant reduction in fan power. Also, because of the differing flow rates in the HTHX, the heat available for steam raising shifts somewhat resulting in a 1-MW gain in steam turbine power. The overall effect is a gain in the net power slightly over 4 MW and an efficiency increase to 36.27 % (HHV), nearly a point better.

As in Case 2, essentially 97% of the CO_2 in the coal stream is recovered. Only a small fraction of the CO_2 from methane stream is recovered. That fraction is represented by the methane used in the catalytic combustor in the CO_2 recovery system. No CO_2 from the GT boost combustor is recovered. Overall, 87% of the CO_2 is recovered.

Case 3

The configuration in Case 3 is conceptually similar to Cases 1 and 2 with the exception that the GT is based on a commercially available nominal 25-MW aeroderivative GT. In Case 3 (and 3A), four of these are used. However, the use of a single GT of this type could be the basis of a utility-scale demonstration of the entire IFCC concept. Like Case 2, the HTHX outlet temperature is 1489°C (2100°F), a value only about 55°C (100°F) less than the design temperature of the GT. Thus, no boost combustor is used in this configuration—it is essentially an all-coal configuration. Some small amount NG (approximately 2% of the heat input) is used in the catalytic combustor in the CO_2 recovery system.

In Case 3, again, approximately 79% of the exhaust is recycled to the combustor. This requires about 5977 kW of fan power. The other major power consumer is the CO_2 recovery system. Here, 19,818 kW are used in the recovery of 97% of the total CO_2. The net power for this configuration is nearly 149 MW and the net efficiency of this system, 30.74% (HHV), is above the efficiencies of the pc systems with CO_2 recovery.

Case 3A

The Case 3A configuration differs from Case 3 in that the oxidant (recycle gas with 50% [vol.] O_2) and coal are now injected along the axis of the HTHX combustor. For the same temperature conditions (1593°C [2900°F]) the total amount of recycle gas is reduced to 50% of the combustor exit flow. This requires 1571 kW, a significant reduction in fan power. The other major power consumer is the CO_2 recovery system. Here, 19,544 kW are used in the recovery of 97% of the total CO_2. Also, because of the differing flow rates in the HTHX, the heat available for steam raising shifts somewhat resulting in a 1-MW gain in steam turbine power. The overall effect is a gain in the net power of nearly 7 MW and an efficiency increase to 31.88 % (HHV), more than a point better.

The performance of the Case 3 systems is enough better than the O_2-blown pc plant (approximately 8%) to warrant use of that configuration as the basis of a first of a kind demonstration. While the single-engine system would have an output of only about 35 MW, it would serve to point out any requirements for further HTHX research and development. All other components are essentially off-the-shelf.

Alternative Configurations

The ASU for the O_2-blown IFCC represents a significant power consumption, on the order 15%–17% of the gross system power. The IFCC is unique in its potential to adapt transport membrane technology for O_2 production. One alternative configuration that appears to be worth future consideration is shown in Figure 58.

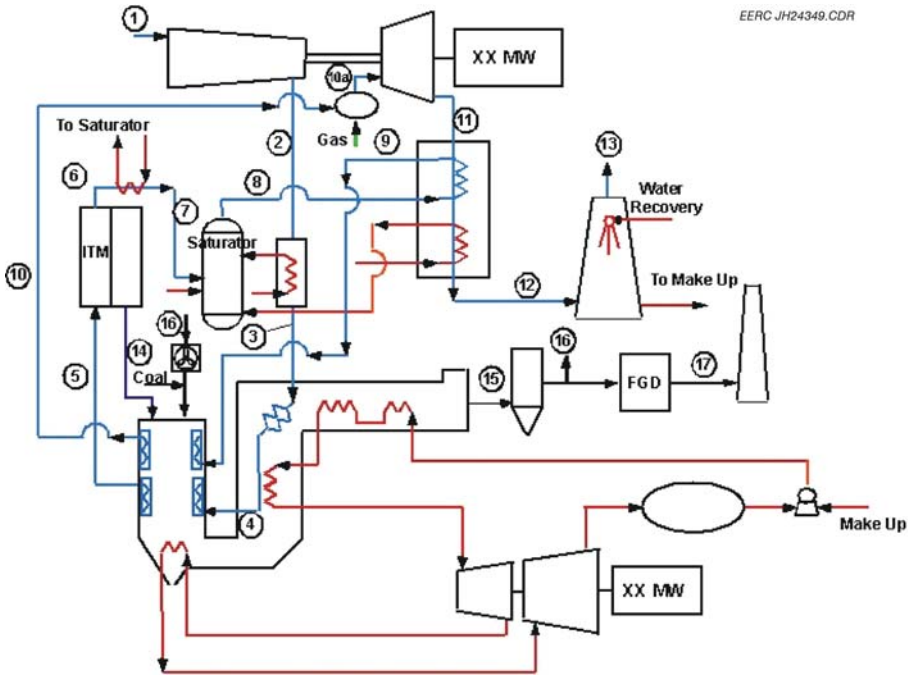

Figure 58. O_2-blown IFCC with ion transport membrane/oxygen transport membrane and humidification.

The operating temperature of O_2 transport membranes—ion transport membrane/oxygen transport membrane (ITM/OTM)—is in the range of 815°C–910°C (1550°–1700°F). In the IFCC, the HTHX could be configured so that one HTHX would take the compressor discharge air from the 700°C (1300°F) convective heater outlet to the ITM/OTM temperature. Since the ITM/OTM will remove a large part of the O_2, it would be possible to add mass to the compressor discharge equal to the O_2 fraction removed. This is done in a saturator and the resulting configuration looks much like a humid air turbine (HAT) cycle. However, in this configuration, the GT expander sees a mass flow that closely resembles its design flow and no gas path changes are required, a benefit compared to the more usual HAT cycle configurations. The humidified air is recuperated and then goes to the HTHX where it is heated to 1489°C (2100°F) before expansion. The humidified air provides additional work in the turbine.

The O_2 pressure drop through the ITM/OTM is essentially equal to the GT pressure ratio and since the oxidant supply to the HTHX is at near atmospheric pressure, little on no oxidant compression is needed, a large benefit. While no analysis of this configuration has been done, analyses of HAT cycles with CO_2 recovery indicate increased performance even though oxidant compression is required in those cycles.

A summary of the assumptions and the projected performances of these systems are presented in Table 33. Also included in Table 33 for comparative purposes are the estimated performances of: 1) a standard configuration steam station with CO_2 recovery by means of an amine separation unit; and 2) an O_2-blown steam station with CO_2 recovery. It can be seen that the IFCC units have better estimated performance.

Economic Analysis

A high-level economic analysis was carried out for the IFCC systems and comparisons made to other systems with CO_2 recovery. The intent of the analysis was not to provide detailed costing but to put the IFCC configurations into context with available information on the COE for other systems. Only Cases 1A and 3A were used in the economic analyses.

The first step was to select a method of cost comparison. Because the information on the cost of the IFCC plants was based on costs developed by Bechtel (now Nexant) in 1998 (41), it was decided to use the cost normalization approach. In this approach, a baseline plant is selected as the norm, i.e., the plant whose cost will be the denominator of the normalization fraction. The cost of the other plant(s) is divided by the norm and if greater than unity, the plant is more expensive and if less, it is less expensive. By doing this, plants from different information sources can be compared, if a similar type plant can be selected as the norm. In the case of the IFCC, Bechtel had costed out a contemporary pc plant, a 165 bar/538°C/538°C (2400 psi/1000°F/1000°F)-system. Under the auspices of DOE, Parsons had compared a variety of technologies with and without CO_2 recovery (42), including a 165 bar/538°C/538°C (2400 psi/1000°F/1000°F) pc system.

Thus, the IFCC data and the Parsons data could be normalized against a similar plant. While there may be some differences between the Bechtel and Parsons costing procedures, by using what

Table 33. Performance of O_2-Blown IFC Systems with CO_2 Recovery

Case	1	1A[1]	2	2A[1]	3	3A[1]	Steam 1[2]	Steam 2[3]
Type GT	V84	V84	FT4000IC	FT4000IC	4xFT8	4xFT8	NA	NA
Coal Input, metric ton/day	2281	2281	1430	1430	1875	1875	3369	3223
10^6 kJ/h (HHV)	2074	2074	1300	1300	1705	1705	3809	3275
Nat. Gas Input, 10^6 kJ/h (HHV)	842	841.3	419.49	419.07	40.20	39.64		
Total Energy Input, 10^6 kJ/h (HHV)	2916	2915.54	1719.32	1719.32	1745.17	1744.61	3809	3275
GT Power, MW	157.5	157.50	128.30	128.30	81.20	81.20	NA	NA
ST Power, MW	217.1	218.20	90.50	91.10	132.50	133.50	348.50	417.60
Total Gross Power, MW	374.6	375.70	218.80	219.40	213.70	214.70	348.50	417.60
Aux Power, MW	79.2	73.30	50.20	46.50	64.70	59.80	65.40	109.20
Net Power, MW	295.4	302.40	168.60	172.90	149.00	154.90	283.10	298.40
CO_2 Captured, metric ton/day (Pure Basis)	4614	4550	2894	2853	3789	3743.8	7543	7577
Overall Thermal Efficiency, % HHV (Coal + NG)	36.48	37.36	35.31	36.27	30.74	31.88	26.76	29.48

[1] Sequential firing with 50% O_2 (vol).
[2] Amine CO_2 removal @ 103 bar (1500 psi).
[3] O_2-blown CO_2 removal @ 103 bar (1500 psi).

Assumptions:
1. Coal composition and HHV taken as average of the range.
2. Both hot-end and cold-end temp. approaches in CAH held at 260°C (500°F).
3. GT generator efficiency = 98.5%.
4. ST generator efficiency = 98%.
5. Steam cycle 100 bar/501°C/501°C (1450 psig/950°F/950°F).
6. Vacuum condenser of the deaerating type in use.
7. O_2 Purity (from ASU) = 98% vol.
8. O_2 conc. in combustion products = 2% vol.
9. CO_2 pressure at plant fence line = 138 bar (2000 psig).

Bechtel calls Total Direct Cost and Parsons calls Process Plant Costs, a reasonable normalization can be assumed.

The second step was to review the costs of the IFC system defined in the HiPPS program (41) and update the costs to account for the use of bare-tube HTHX. In that study, Bechtel developed detailed costs for the IFCC. Because the bare-tube HTHX is one-fifth the area of the HiPPS furnace (43) and because it weighs much less since massive amounts of refractory are not used, the sections impacted are HTHX cost and foundations and structural steel cost. It was assumed that the other sections were unaffected. The HTHX cost was reduced by 75% compared to the HiPPS furnace and the concrete and structural steel requirements were reduced by 10%.

The third step was to determine the cost factors for the ASU and the CO_2 recovery system, which required a more detailed analysis.

ASU and CO_2 Recovery Cost

The cost of the ASU for the Parsons O_2-blown pc is $111.1 million for 303,230 kg/hr (668,508 lb/hr) of 95.5% O_2 (42). For 98% pure O_2, a 10% increase in cost was assumed. For the V84 IFCC, the flow is 43.07 kg/sec (94.95 lb/sec) or 155,047 kg/hr (341,820 lb/hr) for ~375 MW or 165,383 kg/hr (364,608 lb/hr) for ~400 MW plant. The ASU would cost $66.4 million. When this cost is normalized to the Parsons' pc capital cost, the factor is 0.188. As described above, because this is normalized against the same basic plant type (both against the pc without CO_2 recovery), the 0.188 can be used for the V84-based IFCC. For the FT8 IFCC, the flow is 35.40 kg/sec (78.04 lb/sec) for 214.7 MW or ~66.2 kg/sec (~146 lb/sec) for ~400 MW plant. The ASU cost factor on a normalized basis would be 0.289.

The cost of the CO_2 compression system for the Parsons O_2-blown pc is $34.21 million for 353,385 kg/hr (779,080 lb/hr) (42). This is ~$97/kg/hr at 103 bar (~$44/lb/hr at 1500 psi). Assume conservatively that recovery system costs scale at the one-half power of compression ratio, then cost at 138 bar (2000 psi) would be $(138/103)^{½}$ ($[2000/1500]^{½}$) or 1.15 higher at ~$110/kg/hr (~$51/lb/hr). For the V84 IFC, the costs would be $58.2/kW. For the FT8 IFC, the costs would be ~$84/kW. These normalize to 0.045 and .067 respectively for the V84 and FT8 plants.

The cost factors for the IFCC plants are given in Table 34.

Levelized Cost of Electricity

The levelized cost of electricity (LCOE) is widely used to compare alternative power systems. EPRI developed the most widely used methodology for determining LCOE (44). This procedure was the basis of the LCOE presented by Parson (42). These values are used to compare the 10-year LCOE with the O_2-blown IFCCs with CO_2 recovery. The Parsons values (42) are listed in Table 35. To develop the LCOE for the IFCC plants, the levelized capital cost for the pc plant (42) was multiplied by the normalizing factor from Table 34 for each of the IFCC plants. The fuel costs were estimated by applying the different system heat rates and pro-rating the value for the coal and gas fractions. To determine the levelized fuel cost. The Table 35 fuel costs are based on the 2002 fuel costs of $0.99/$10^6$ kJ ($1.04/MMBtu) for coal and $3.08/$10^6$ kJ ($3.25/MMBtu) for NG used in Reference 42. Costs for consumables, and fixed and variable operating and maintenance (O&M) were assumed the same for the IFCC plants as for the O_2-blown pc plant. The results for the coal-fired plants and the IFCCs are shown in Figure 59.

Effect of Fuel Cost

The fuel costs shown in Table 35 and Figure 60 are those used by Parsons (42), $0.99/$10^6$ kJ ($1.04/MMBtu) for coal and $3.08/$10^6$ kJ ($3.25 MMBtu) for NG. The most recent DOE/Energy Information Agency (June 2004) gas price (http://tonto.eia.doe.gov/dnav/ng/ng_pri_sum_dcu_nus_m.htm) for utility use is $6.18/$10^6$ kJ ($6.52/MMBtu). Thus the cost for the V84 IFC would be 23.9 mills/kWh and for the FT8 IFC, 14.1 mills/kWh. Note that for the NGCC, the fuel cost would be 45.6 mills/kWh and for the NGCC with CO_2 recovery, 49.3 mills/kWh. The effect of fuel cost on the NGCC and IFCC plants is shown in Figure 61. At NG prices between $4.50

Table 34. Normalized Capital Costs for O_2-Blown IFCC Systems

Code of Accounts	PC – Bechtel	IFC Refractory V84	IFC Bare Tube V84	IFC Bare Tube FT8	IFC O_2 V84	IFC O_2 FT8
Power Generation			% of PC Capital Cost $/kW			
1.0 Steam Generation/HTHX						
1.1 HTHX		0.14	0.04	0.08	0.04	0.08
1.2 HRSG		0.047	0.047	0.047	0.047	0.047
1.3 Boilers/Heaters	0.237	0.01	0.01	0.01	0.01	0.01
2.0 Gas Turbine System						
2.1 Gas Turbine Generator		0.164	0.164	0.328	0.164	0.328
2.2 Gas Turbine HRSG		0.037	0.037	0.037	0.037	0.037
2.3 Natural Gas Supply		0.002	0.002	0.002	0.002	0.002
3.0 Steam Turbine System						
3.1 Steam Turbine Generator	0.13	0.07	0.07	0.07	0.07	0.07
3.2 Condensor	0.009	0.005	0.005	0.005	0.005	0.005
3.3 Pumps	0.022	0.013	0.013	0.013	0.013	0.013
4.0 Flue-Gas Emissions Control						
4.1 SO_x, NO_x, Particulate Control	0.239	0.107	0.107	0.107	0.107	0.107
Balance of Plant						
5.0 Coal and Ash Handling	0.053	0.029	0.029	0.029	0.029	0.029
6.0 Water Treatment	0.034	0.019	0.019	0.019	0.019	0.019
7.0 HVAC, Tanks, Insulation, Stack	0.025	0.034	0.034	0.034	0.034	0.034
8.0 Other Process Systems						
8.1 Piping	0.055	0.036	0.036	0.036	0.036	0.036
8.2 Instruments and Controls	0.018	0.019	0.019	0.019	0.019	0.019
8.3 Electrical Equipment	0.02	0.02	0.02	0.02	0.02	0.02
8.4 Electrical Materials	0.011	0.011	0.011	0.011	0.011	0.011
9.0 Civil and Structural						
9.1 Concrete	0.022	0.022	0.017	0.017	0.017	0.017
9.2 Steel and Site Preparation	0.125	0.132	0.106	0.106	0.106	0.106
Subtotal Direct Costs	1	0.917	0.786	0.99	0.786	0.99
10.0 ASU					0.188	0.287
11.0 CO_2 Recovery					0.045	0.067
Total Direct Costs					1.019	1.344

Table 35. LCOE for Plants with CO_2 Recovery

Case	Base PC	PC Amine	O_2 PC	IGCC	IGCC/CO_2	V84 IFC	FT8 IFC	NGCC	NGCC/CO_2
Contribution to LCOE									
Capital Charges	25.3	47.3	45	27.4	37.8	25.7	34	10.3	18.2
Fuel Costs	9	12.6	11.5	7.5	8.7	15.2	12.8	20.9	24.2
Consumables	2	6.4	2.6	0.5	0.6	2.6	2.6	0.2	0.2
Fixed O&M	5.1	8.7	8.3	5.2	6.8	8.3	8.3	2.9	4.9
Variable O&M	0.9	1.5	1.5	0.9	1.2	1.5	1.5	0.5	0.9
Total	42.3	76.5	68.9	41.5	55.1	53.3	59.2	34.8	48.4
Normalized Value	1	1.81	1.63	0.98	1.30	1.26	1.40	0.82	1.14

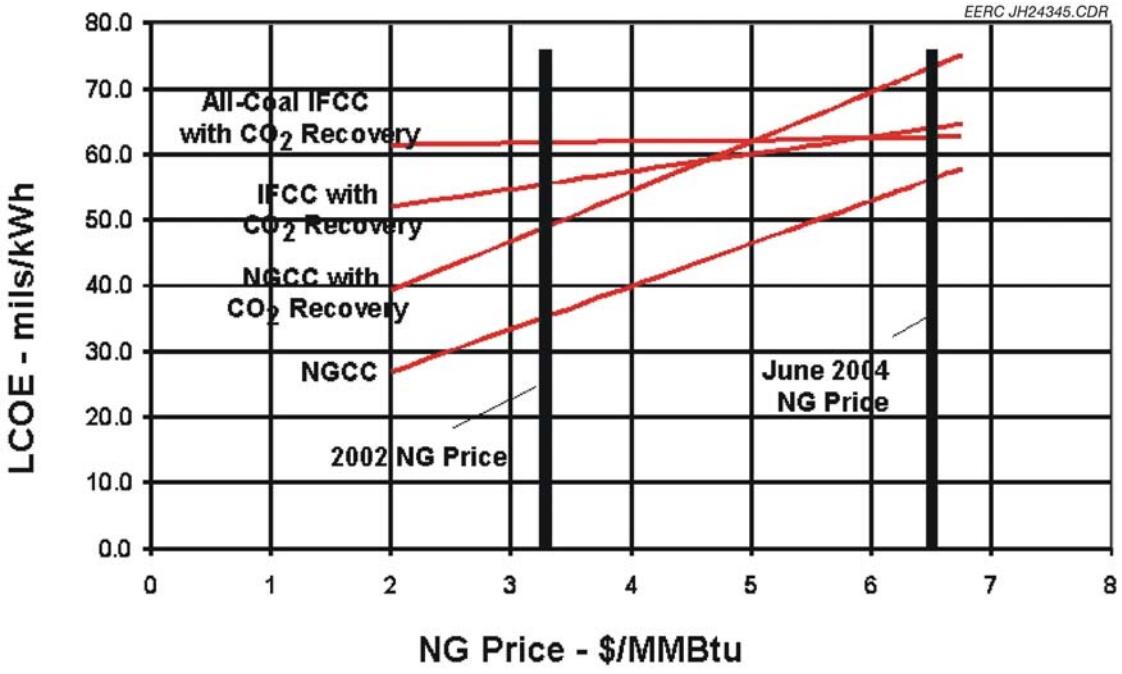

Figure 59. The effect of NG price on LCOE.

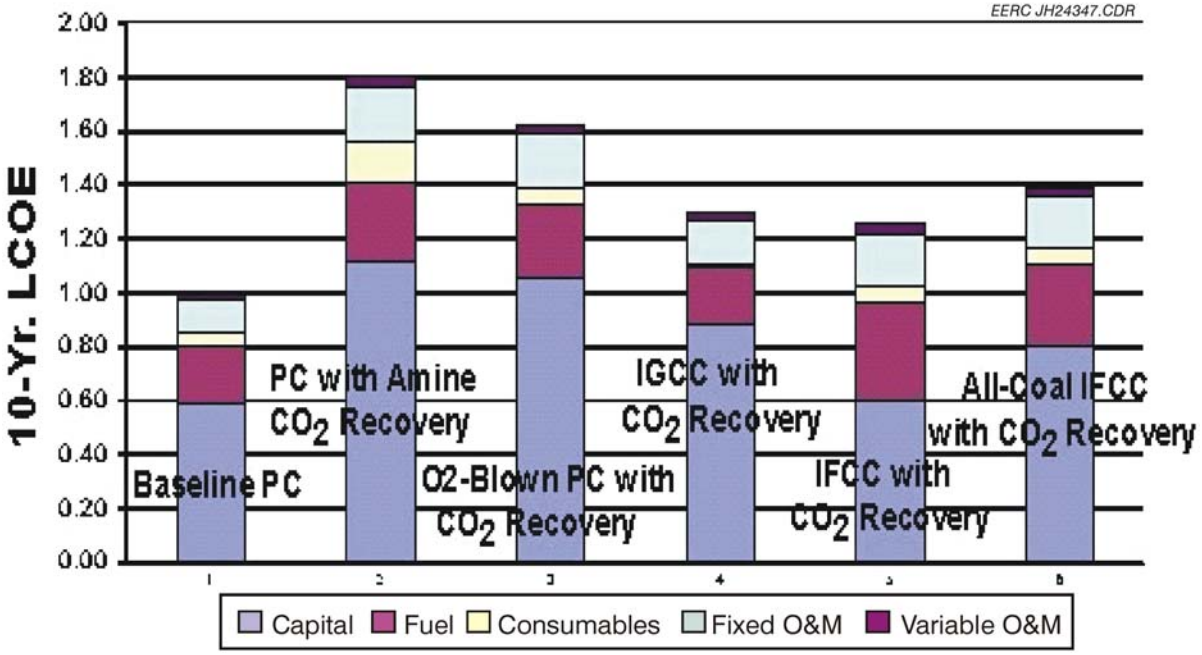

Figure 60. Normalized LCOE for coal-fired plants.

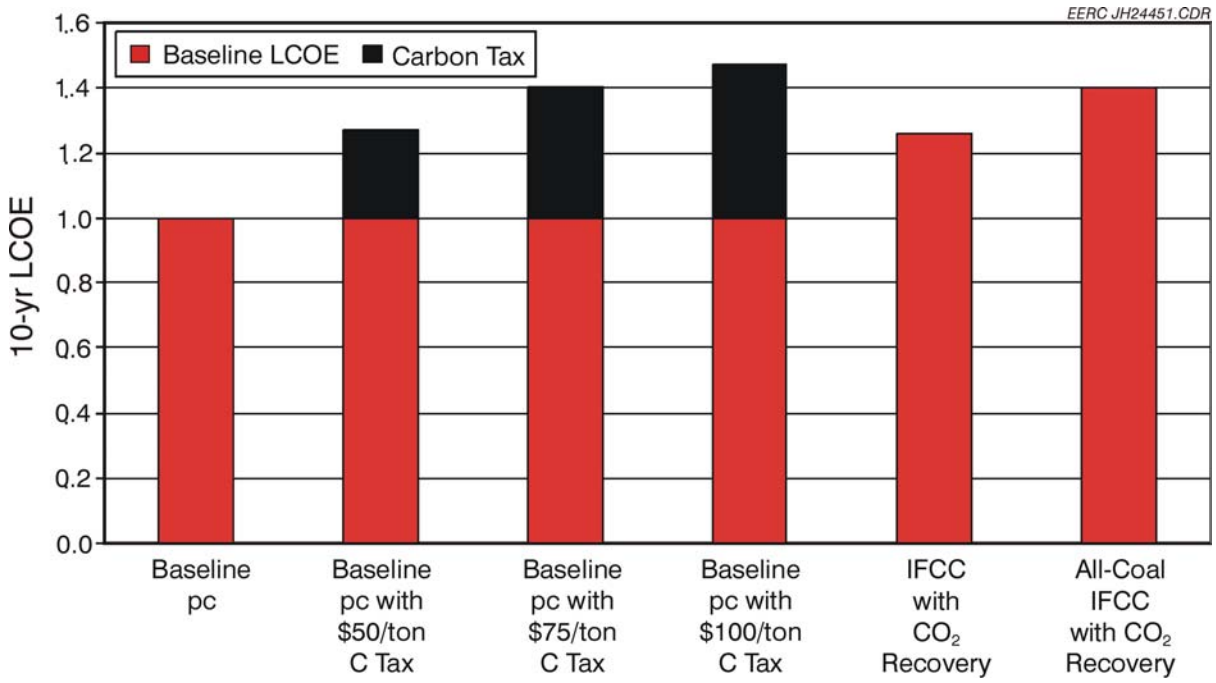

Figure 61. Effect of carbon tax.

and \$4.74/10^6 kJ (\$4.75 and \$5.00/MMBtu), the IFCC plants are more attractive than the NG plants with CO_2 recovery.

Carbon Tax

An alternative to CO_2 recovery would be to add a carbon tax (e.g., Reference 45). The tax increases the COE by increasing the cost of the fuel. For example, a carbon tax of \$83/metric ton (\$75/ton) C emitted (3.32 metric ton [3.67 ton] CO_2) would increase the price of coal by the fraction of coal which is carbon multiplied by \$83 (\$75). For the coal used in Reference 42, that would be 0.58 metric ton carbon/metric ton (0.58 ton carbon/ton) as-received coal, which would increase the coal cost by \$48/metric ton (\$43/ton) from the assumed price of \$28/metric ton (\$25/ton). If the baseline pc plant were to have a carbon tax, it would raise the LCOE as shown in Figure 61.

As can be seen in Figure 61, it would take a carbon tax somewhat under \$55/metric ton (\$50/ton) carbon to raise the LCOE of the baseline pc to a level higher than the LCOE for the IFCC with CO_2 recovery and to a value around \$83/metric ton (\$75/ton) carbon to be higher than the all-coal IFCC with CO_2 recovery. Given the propensity of the utility industry to use trade-off credits rather than invest in new technology, the introduction of CO_2 recovery technology becomes very much dependent on the carbon tax rate with a value of approximately \$55/metric ton (\$50/ton) carbon being the threshold, and \$44/metric ton (\$40/ton) if 20% biomass cofiring is used. If rules for CO_2 similar to the best available control technology for other pollutants are implemented, then CO_2 recovery will be required and the IFCC would be an attractive alternative power system.

Conclusions

Even with the limited number of configurations analyzed, it is apparent that the IFCC with CO_2 recovery offers better performance and lower COE than pc plants with CO_2 recovery. This is also true with the lower-performing all-coal IFCC. The IFCC also has competitive COE's to IGCC plants. At NG prices above \$4.70/10^6 kJ (\$5.00/MMBtu), the IFCC systems are attractive alternatives NGCC systems with CO_2 recovery while maintaining the standard operations of a pc plant. A near zero-emission IFCC is also cheaper to operate than a modern pc system if a carbon tax of more than \$55/metric ton (\$50/ton) C is imposed. If 20% biomass cofiring is employed, the breakeven point would be \$44/metric ton (\$40/ton) of carbon.

Recommendations

A more detailed analysis allowing wider evaluation of alternative IFCC configurations and lower level cost analysis should be performed. For example, the IFCC is uniquely suitable for use with membrane transfer oxygen units and such a system should have significantly higher performance and lower costs. More detailed design and accompanying cost analysis, especially for alternative firing sequences for the HTHX and also the entire furnace assembly and enclosure, would identify critical issues and supply better cost estimates for this unique enabling technology. The EERC is in discussions with the DOE National Energy Technology Laboratory to them perform these calculations in a manner consistent with their previous analyses of other advanced power system concepts.

Task 2 – Laboratory Scale Testing

MA956 Joining

Laboratory testing has shown that MA956 is highly resistant to corrosion by the products of coal combustion. However, because of the dispersion of small oxide particles within its structure, it can not be welded because this would lead to segregation of the dispersed oxide. Therefore, the EERC investigated TLP bonding of the alloy. In these tests, one TLP metal foil type provided by ORNL was used to join pieces of MA956 under three different processing conditions. Both the TLP metal type and processing conditions remain proprietary and so cannot be described here, but the three conditions will be labeled as A, B, and C for the purposes of this report. The three TLP-bonded samples were cross-sectioned and examined by SEM.

An SEM micrograph of Joint A is shown in Figure 62. The TLP metal migrated approximately 150 µm into the ODS alloy, but left relatively large areas of highly concentrated TLP metal within the ODS alloy. Minor porosity was detected at the joint interface. An yttrium/aluminum-rich particle phase was formed at the interface, with a concentration of 45/25 wt%, respectively, that contained small amounts of chromium and iron. Oxygen content was very low and, in many instances, not detected, so the particles are not oxides. The particle diameter was approximately 4 µm. The yttrium/aluminum particles were also detected away from the interface but always adjacent to an area of TLP metal. This relationship is not fully understood and is being researched. The large TLP metal concentrations were centered at about 70 µm from the interface. It is difficult to tell during SEM examination, but the metal appears to be traveling between ODS alloy grains. The metal contains

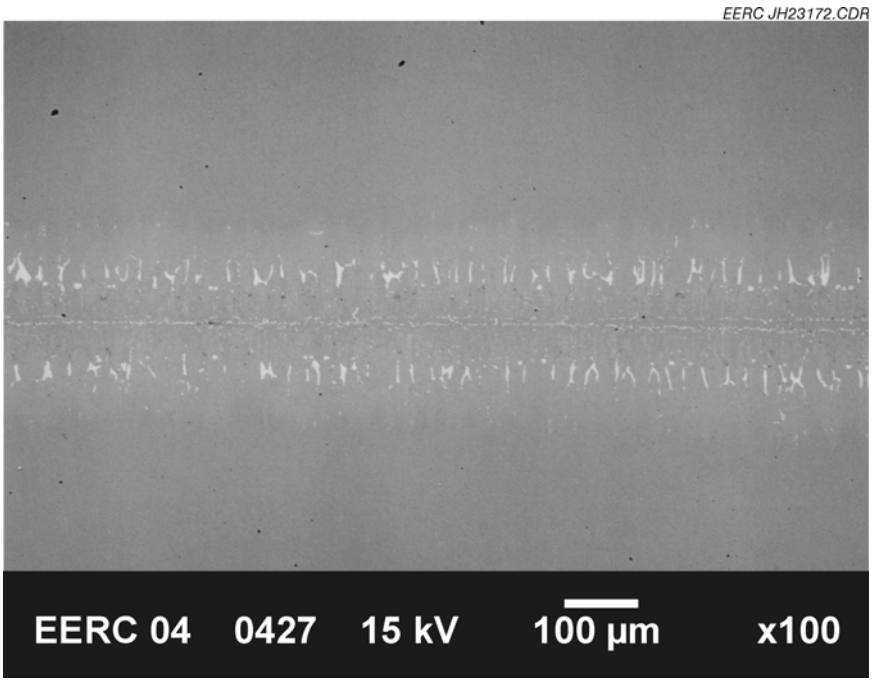

Figure 62. SEM micrograph of Joint A. The light area is the TLP metal diffusion.

elevated levels of aluminum and titanium, with small amounts of iron and chromium. The titanium concentration was triple that of the base alloy, which implies that the surrounding alloy was slightly deficient in aluminum and titanium.

TLP Joint B is shown in Figure 63. Porosity at the interface is minor. Migration of TLP metal from the interface was detected to a distance of approximately 350 µm, or roughly twice that of Joint A. Concentrations of TLP metal can still be observed; however, they are smaller, thinner, and at the outer limits of the metal migration. The TLP metal concentration at the joint interface is much less than that found in Joint A. The same yttrium/aluminum-rich phase was observed adjacent to areas rich in TLP metal. The particle size of this phase was about half that of the previous sample. A new TLP metal phase was detected which has titanium levels eight times that of the base alloy. The phase appears as small, 2 µm and less, particles dispersed in the TLP-affected zone of the alloy. This is a curious, unexpected phase that is also being investigated.

Joint C is shown in Figure 64. Migration of the TLP metal is approximately the same as that of Joint B, but the dispersion is even greater. The porosity at the interface was low but higher than that of the two previous joints. The yttrium/aluminum-rich phase was still present, but the particle size was found to be approximately 1–2 µm. The titanium-rich phase was found in the sample, with titanium concentrations now reaching 75 wt%, but the particle size is roughly the same as for Joint B. The TLP metal-rich areas of this sample have iron and titanium concentrations which are roughly double that of Joint B.

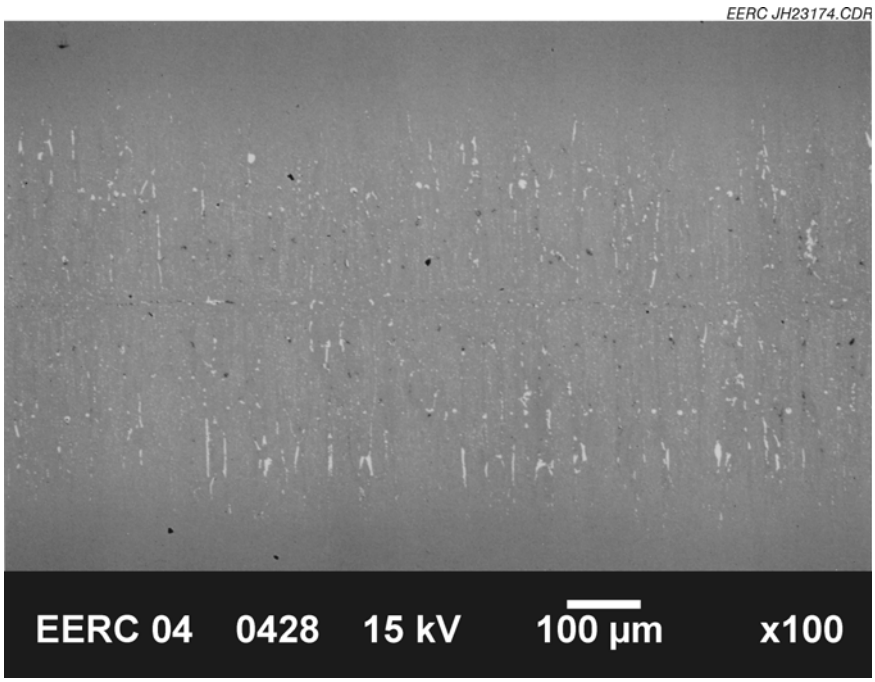

Figure 63. SEM micrograph of Joint B.

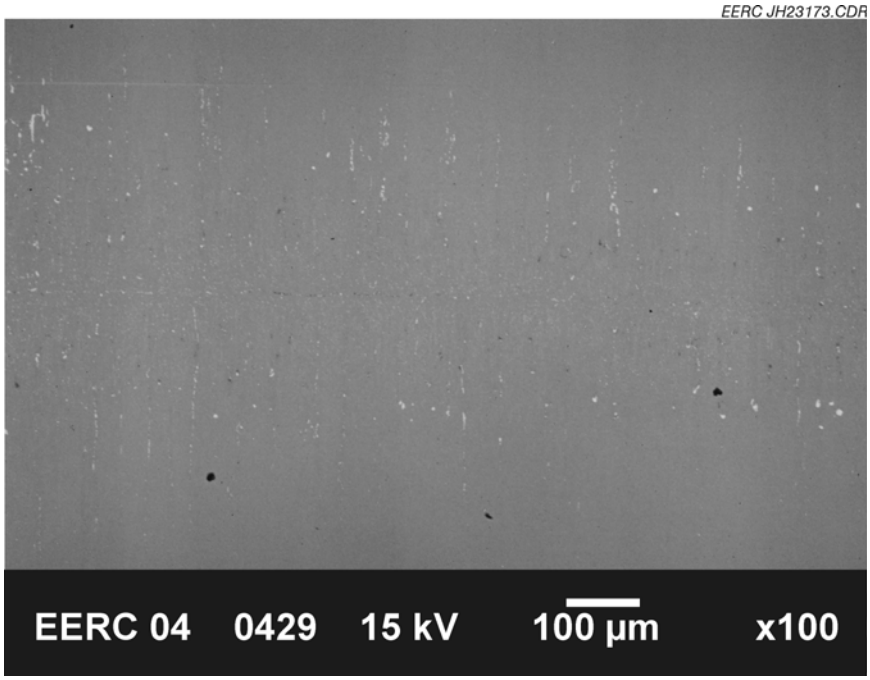

Figure 64. SEM micrograph of Joint C.

A summary of the SEM results is shown in Table 36. TLP metal migration and dispersion improved with joining temperature. At the higher temperatures, an unexpected secondary titanium-enriched phase was formed and is being investigated. Porosity was very low but increased slightly with temperature. Residual TLP metal in the joint was enriched in aluminum, titanium, iron, and a little chromium. This proved to be the opposite of what was expected. It was believed that the metal would disperse into the iron but it appears that the iron is actually dispersing into the TLP metal. This is also being further investigated. The migration of the metal appears to be between the grain boundaries. Overall these TLP results appear promising, but ultimately it is the strength of the joints that is of utmost importance. Therefore, portions of each of the joints have been sent to ORNL for tensile strength testing.

Table 36. Summary of SEM Examinations of the TLP Joints

	TLP Metal Migration	Metal Dispersion	Residual Metal	Porosity	Y/Al Phase	Metal/Ti Phase
A	150 μm	Poor	Thick – concentrated near midpoint of dispersion	Minor	Present	Not present
B	300 μm	Better	Thin – concentrated at edge of dispersion	Minor	Present ≤2 μm particle size	Present ≤2 μm particle size
C	300 μm	Best	Very thin – concentrated at edge of dispersion	Minor, but higher than the others	Present ≤2 μm particle size	Present ≤2 μm particle size, much higher Ti content

Viscosity Measurements of Coal–Biomass Blends

To prevent rapid corrosion of the HTHX, the surface must be operated below the solidus temperature of the slag. In order to determine the melting and rheological properties of the biomass and biomass–coal slags so that the solidus temperatures can be inferred, their viscosities were measured with a high-temperature rotational viscometer, and their crystallization behavior upon cooling was measured by heated-stage XRD. These tests were performed by Dr. Arvelakis during the summer of 2003. He performed the tests with several sample types. They consisted of melted slags made from pure and blended fuel ashes, as well as samples of the slags created in the SFS during the pilot scale tests, although due to time constraints he was not able to include the slag created during the pilot-scale test of the coal and switchgrass.

Table 37 gives the results regarding the elemental analysis of the various coal, biomass and coal–biomass slags used in the viscosity studies. The coal ash contains large amounts of silica, alumina and calcium, while significant amounts of iron, magnesium and sulfur are also present. The presence of alkali metals and other elements such as titanium and phosphorus is limited. Hog fuel ash contains mainly calcium as the dominant element. The amount of silica and alkali metals is rather low while the amounts of elements such as iron, aluminum, magnesium titanium and sulfur is below 2% on ash basis. A large amount of unknown fraction observed during the analysis of the

Table 37. Elemental Analysis of Coal, Biomass and Coal–Biomass Ash and Slag Samples

Mass Basis %	K_2O	Na_2O	CaO	MgO	SiO_2	Al_2O_3	Fe_2O_3	TiO_2	SO_3	P_2O_5
Coal Slag[1]	0.4	1.6	26.0	5.5	35.3	17.7	6.7	1.4	0.0	1.1
Hog Fuel Ash	5.3	3.5	41.5	3.6	25.0	2.9	2.2	0.2	1.2	1.7
Hog Fuel Slag[1]	0.3	1.0	45.1	3.6	28.6	3.1	2.6	0.3	0.0	1.9
Coal–Hog Fuel (6/1) Slag[1]	1.0	1.7	28.0	5.5	32.9	15.8	6.6	1.2	0.0	1.2
Coal–Hog Fuel Slag[2]	1.1	1.2	28.0	4.4	37.7	20.1	5.4	1.1	0.0	0.9
Corn Stalks Slag[1]	9.3	2.0	11.4	11.6	51.7	3.1	2.6	0.4	0.0	2.9
Coal–Corn Stalks (1.86/1) Ash	2.8	1.2	17.1	6.2	36.7	11.5	4.7	0.9	3.1	1.4
Coal–Corn Stalks (1.86/1) Slag[1]	2.5	1.1	16.9	6.5	42.8	12.9	5.2	1.0	0.0	1.4
Coal–Corn Stalks Slag[2]	1.4	0.9	20.3	5.9	45.5	18.6	5.3	1.1	0.0	1.0
Coal–Switchgrass Slag[1]	2.7	1.5	19.5	4.9	47.8	14.3	6.4	1.1	0.0	2.0

[1] Slag after the viscosity measurement.
[2] Slag from the cocombustion tests.

specific sample is due to the high amount of calcium carbonates present in the ash. The corn stover is primarily silicate with medium amounts of calcium and alkali metals, while the amount of magnesium appears to be among the highest observed in biomass samples reaching 11% on an ash basis. Some enrichment of the specific sample in magnesium due to extraneous factors is suspected. Mixing of the coal ash with the biomass ashes lowers the amounts of silica, iron and aluminum and increases the amounts of calcium, alkali metals, sulfur and phosphorus compared to the coal ash in the case of the coal–hog fuel mixture. In the case of the coal–corn stalks mixture the amount of magnesium also increases significantly together with the amounts of silica and alkali metals, while the amounts of calcium, aluminum and iron decreases.

Coal

During premelting the coal ash forms two separate phases, a glassy dark phase and a yellow nonglassy phase floating on top of the glassy phase consisting of alkali and calcium sulfates. The composition of the glassy phase, given in Table 37, shows that it is primarily a calcium aluminosilicate glass with no sulfur. Figure 65 shows the heated stage XRD data for the coal ash while heating to a melt. It shows that a substantial amount of quartz and anhydrite ($CaSO_4$) exists in the coal ash, along with small amounts of brownmillerite ($Ca_2Al_2O_5$). These largely react between 950° and 1000°C (1740° and 1830°F), along with some of the aluminosilicate glass material, to form gehlenite ($Ca_2Al_2SiO_7$) which slowly dissolves at higher temperatures. Figure 66a presents the results from the viscosity measurements performed on the coal slag while cooling below 1300°C (2370°F).

Two tests are repetitions at the same rotational speed, while the third was performed using higher rotational speed of 107.8 rpm. The curves show good reproducibility in the tests. The melt appears to reach the temperature of critical viscosity (T_{cv}), below which it rapidly solidifies, at 1190°C (2174°F). The T_{250}, the temperature where the slag viscosity reaches 250 poise and therefore does not flow well, is approximately 1170°C (2138°F).

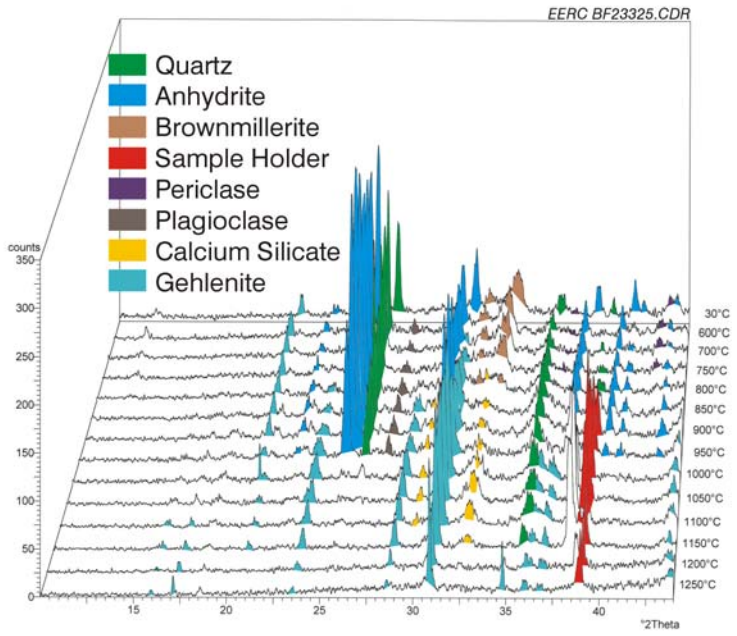

Figure 65. Heated-stage XRD data for the coal ash while being heated to a melt.

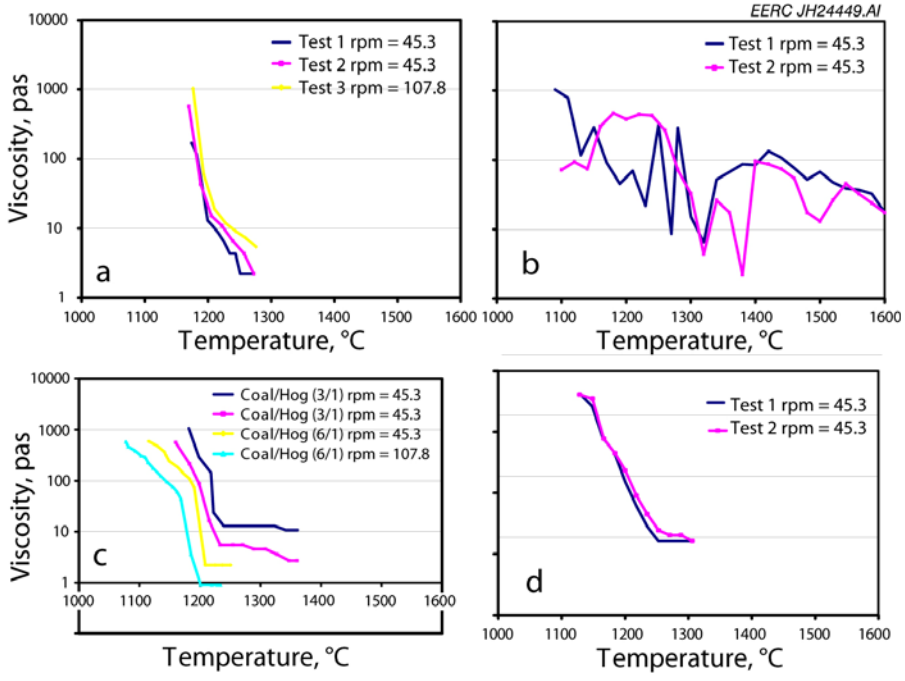

Figure 66. Viscosity characteristics of a) coal ash, b) hog fuel ash, c) coal–hog fuel, d) coal–hog fuel slag.

The use of a higher rotational speed (107.8 rpm) leads to a slight shift of the curve to higher temperatures most likely because friction of the slag with the walls of the crucible creates more of a drag on the viscometer bob at higher rotation rates, which is measured as a slight increase in viscosity. However, the increase is relatively small, indicating that the edge effects, especially at the lower rotation rate, are not significant in interpreting the results. Figure 67 shows the heated stage XRD data for the coal slag while cooling. It shows that there is a small amount of gehlenite in the molten slag even at 1250°C (2282°F), increasing as the slag cools. However, there is not a strong increase in peak area on cooling, indicating that most of the solidification of the slag is simple hardening of the amorphous glass phase, and not the formation of large quantities of solid crystals.

Hog Fuel

The premelting of the material results in a non-glassy slag that does not flow well even at 1500°C (2730°F). The heated stage XRD data shown in Figure 68 indicates that the ash contains high levels of calcite ($CaCO_3$) and quartz, which appear to decompose and react to form calcium- and magnesium-rich silicates such as calcium silicate (Ca_2SiO_4), merwinite ($Ca_3Mg(SiO_4)_2$, and akermanite ($Ca_2MgSi_2O_7$), undoubtedly also along with calcium aluminosilicate glass (which can not be detected by XRD because it is not crystalline). The apparent disappearance of crystalline forms above 1050°C (1922°F) in the data is most likely due to an experimental problem such as the slag flowing out of the sample holder, rather than a true melting of the crystals since their melting points are in the 1450°–1575°C (2642°–2867°F) range, and because no crystallization occurred during cooling. It is likely that high concentrations of these minerals are present at 1500°C (2730°F) which is why the slag does not flow well at that temperature. Figure 66b shows that during cooling, the hog fuel slag viscosity is highly erratic as a function of temperature. The measured viscosity is

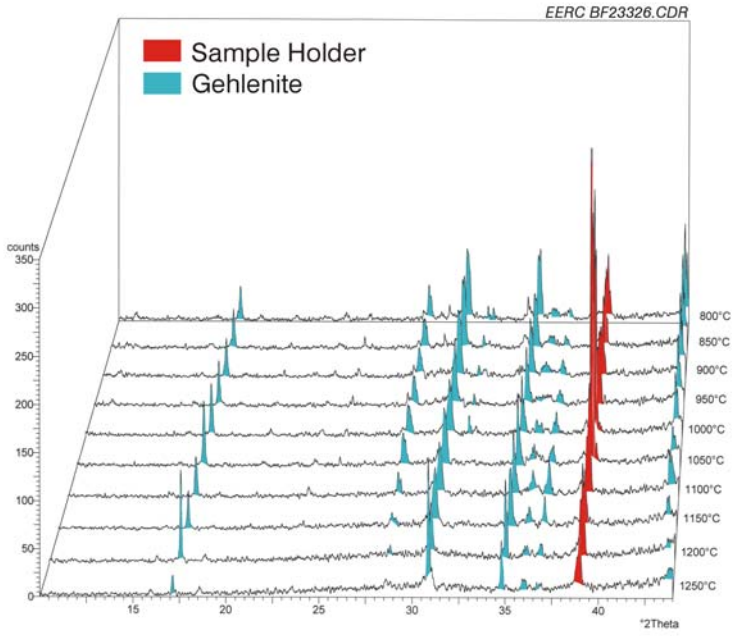

Figure 67. Heated-stage XRD data for the coal slag while cooling from the melt.

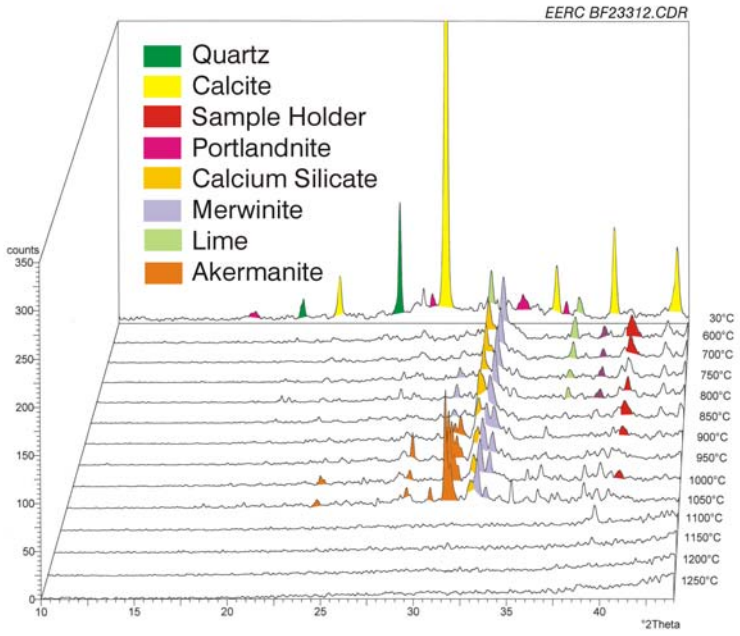

Figure 68. Heated-stage XRD data for the hog fuel ash while being heated to a melt.

characterized by large variations probably due to the periodic formation and segregation of crystals along the side of the viscometer crucible. The results from the two different viscosity measurements differ substantially between them though they were both conducted under the same experimental conditions.

During the first test, the material appears to reach its T_{cv} at the level of 1130°C (2066°F), where the slag solidifies rapidly. In the second test the T_{cv} appears to shift down to temperatures below 1100°C (2010°F). However, as seen by the heated stage XRD data, there is probably very little liquid material present in the slag. As it is seen from Table 37, the slag after the end of the viscosity measurements appears to be depleted in alkali metals and sulfur through vaporization, while the amounts of Ca, Si, Al, as well as of the other elements increase compared to the premelted slag. The low amounts of alkali metals, Si and Al in the slag and the high amounts of Ca and Mg lead to the formation of the Ca- and Mg-rich silicates which are crystalline even at 1500°C (2730°F). This would lead to a great deal of difficulty in operating a slagging system firing only the hog fuel, but may simplify the operation of a pc-fired boiler because the ash would be relatively non-sticky.

Figure 66c presents the results from the viscosity measurements performed using the two coal–hog fuel ash mixtures prepared in the laboratory, and 66d, the slag generated from the combustion test of the coal–hog fuel mixture in the pilot-scale slagging furnace. As seen in Figure 66c, the mixing of hog fuel ash in a ratio of 1/6 with the coal ash leads to a material that has a slightly lower T_{cv} than the coal ash as it begins to solidify completely at around 1200°C (2190°F). The lower viscosity of this slag is likely due to the increase calcium content, due to the addition of the hog fuel, which breaks up the silicate networks. With more hog fuel ash added, the T_{cv} is increased to approximately 1230°C (2246°F), with a T_{250} of around 1190°C (2174°F), similar to that of the coal.

Heated stage XRD data shows that it is principally akermanite that crystallizes out of the slag upon cooling, and the rest of the material is amorphous glass that hardens upon cooling. Apparently, when this level of hog fuel is added the presence of the solid akermanite crystals in the slag increases its viscosity more than the breakup of silicate networks can decrease it.

Figure 66d presents the results from the viscosity measurements performed using the slag generated after the combustion test using the coal–hog fuel mixture. The generated slag appears to be a dark glass as in the case of the coal and the synthetic coal–hog fuel slags. According to Figure 66d the slag has a low viscosity and flows well until approximately 1250°C (2282°F) below which it slowly thickens, reaching a T_{250} of about 1180°C (2156°F), similar to the coal slag alone. The measured viscosity appears to be close to the measurements from the second synthetic slag mixture. The comparison of the elemental composition of the artificial coal–hog fuel slag and the slag resulted from the co-combustion test shows that the co-combustion slag appears to be enriched in Si and Al and slightly depleted in alkali metals, Fe, Mg, Ti and P compared to the synthetic slags. This observation appears to be in good agreement with the results from the viscosity measurements and explains the shifting of the viscosity curves to higher temperatures in the case of the slag from the cocombustion test.

Corn Stover

The corn stover ash contains the highest amount of alkali metals and chlorine compared to all the biomasses and the coal, while it also contains high amounts of silica, and substantial amounts of calcium, magnesium, phosphorus and sulfur. The formation of a yellow 1-mm thick sulfate layer on the top of the slag material was observed during the pre-melting stage at 1400°C (2550°F). Heated stage XRD data, shown in Figure 69, indicates that the ash contains primarily quartz with some hannerbachite ($CaSO_3$) initially, which melts together on heating, most likely with the loss of sulfur from the melt. Some periclase (MgO) crystallizes out of the melt during heating, but then redissolves above 1050°C (1922°F). Unlike the hog fuel ash heated stage XRD however, there are crystalline phases seen in the cooling curve for the slag, to it could not have run out of the sample holder in this case.

Figure 70 shows the viscosity curves for the corn stover ash and mixtures upon cooling from a melt. In 70a the viscosity of the corn stover slag reaches its T_{cv} at 1130°C (2066°F) where the viscosity increases sharply and the slag solidifies rapidly. Repetition of the viscosity measurement using higher rotational speed (107.8 rpm) shows general agreement with the lower rotational rate but with a slightly higher T_{cv} of 1150°C (2102°F), after which the slag solidifies rapidly. As it is seen from Table 37, the elemental analysis of the corn stover slag after the end of the viscosity tests shows that the slag contains large amounts of alkali metals, and Mg, in combination with low amounts of Ca and Al and large amounts of Si. This results a slag with lower melting temperature alkali silicates compared to the other biomass, coal and coal–biomass slags. Figure 71 shows the heated stage XRD data for the slag as it cools, indicating the formation of diopside ($CaMg(SiO_3)_2$) crystals in the slag between 1150° and 1100°C (2102° and 2010°F) as the slag begins to solidify.

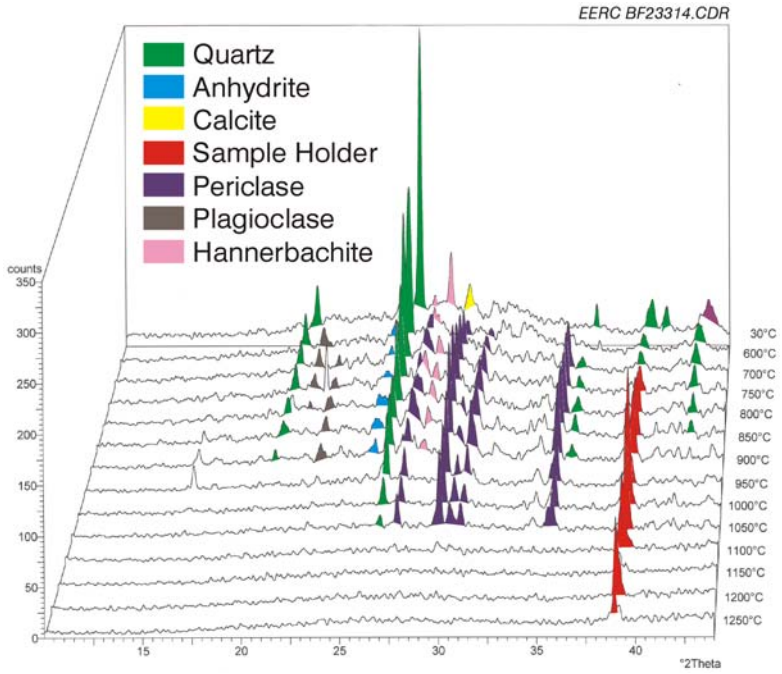

Figure 69. Heated-stage XRD data for the corn stover ash while being heated to a melt.

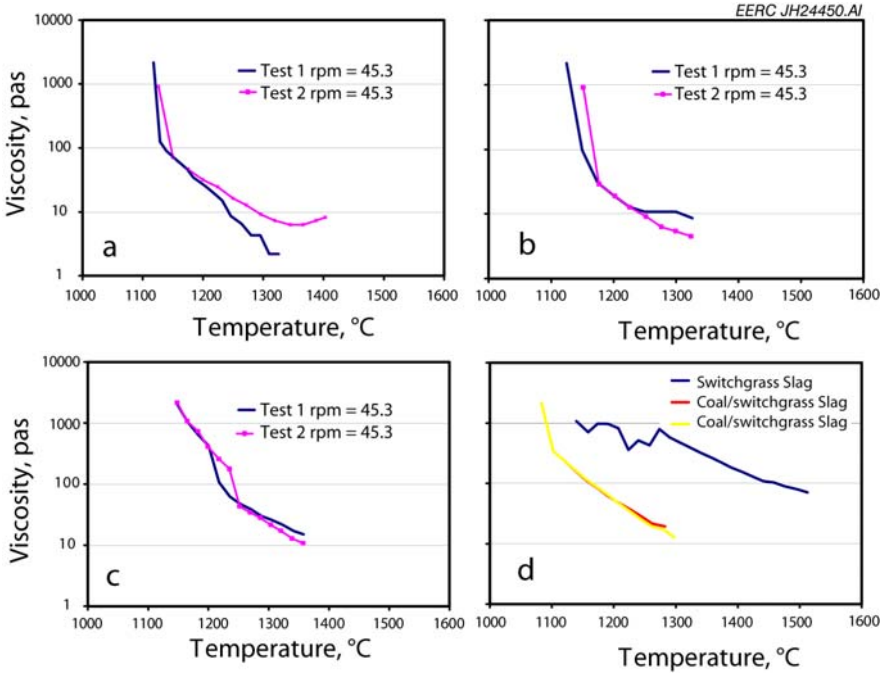

Figure 70. Viscosity characteristics of a) corn stover ash, b) corn stover and coal ash, c) coal and corn stover slag d) switchgrass and switchgrass and coal slag.

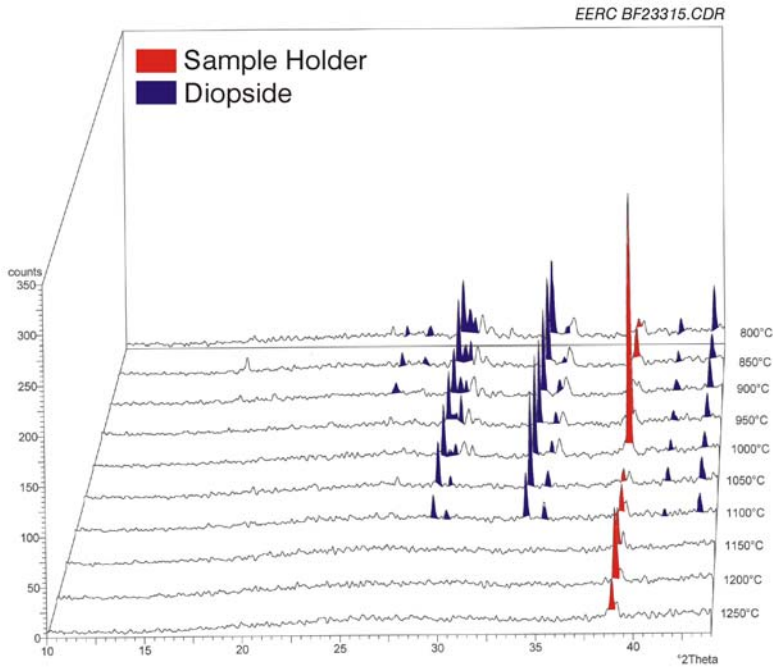

Figure 71. Heated-stage XRD data for the corn stover ash while being cooled from a melt.

Figure 72 shows the heated stage XRD data for the synthetic mixture of coal and corn stover ash while heating. It indicates that the anhydrite in the coal ash reacts with the silicates in the ashes to form akermanite and diopside at 700°C (1300°F), then completely melting between 850° and 900°C (1560° and 1650°F). As seen in Figure 70b the viscosity of the molten synthetic slag made from corn stover and coal ash is very low as it cools until the T_{cv} of 1180°C (2156°F), about the same as for the coal slag. The crystallization of the melt appears to progress gradually in the first steps after the T_{cv} point until the temperature of 1150°C (2102°F) where the viscosity curve slope increases dramatically, and the melt solidifies rapidly. The use of higher rotational speed during the second viscosity test results in a viscosity curve that is in good agreement with the lower rotational rate curve. Heated-stage XRD data show that crystals do not form in the melt until the temperature is lowered to 950°C (1740°F), although the peaks could not be identified with the data reduction software.

The viscosity pattern of the coal–corn slag from the co-combustion test in the SFS is different compared to the synthetic coal–corn ash slag. Figure 70c shows that the slag generally has a higher viscosity and T_{cv} than the synthetic ash melt (1240° vs. 1180°C [2264° vs. 2156°F]). The T_{250} for the slag is approximately 1220°C (2228°F), about 40°C (72°F) higher than for the coal and hog fuel slag. The use of higher rotational speed in the viscosity measurement appears to have the same effects as in the case of the synthetic slag measurements, but generally the two curves are in good agreement. The elemental analysis of both the synthetic coal–corn slag as well as the coal–corn slag from the cocombustion test appears to be in good agreement with the results obtained from the viscosity measurements. As it is seen from Table 37, the synthetic coal–corn ash slag appears to be enriched in alkali metals and depleted in Al, even after the end of the viscosity measurement, compared to the

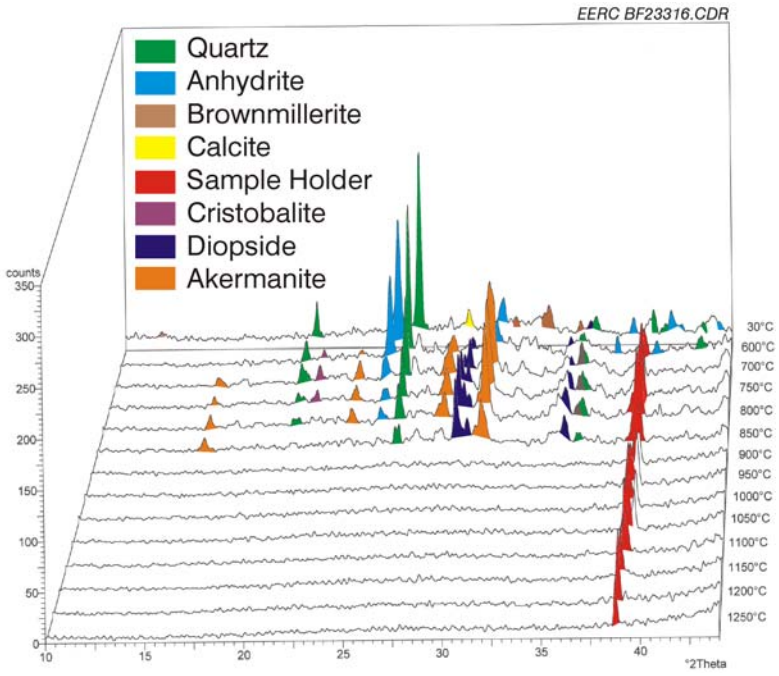

Figure 72. Heated-stage XRD data for the synthetic coal and corn stover ash while being heated to a melt.

slag from the combustion test which should reduce both the viscosity and T_{cv} of the synthetic slag relative to the combustor slag. The variations occur because at the high temperatures in the combustor the alkalis tend to vaporize. Also, there is preferential deposition of the larger mineral grains in the combustor. These differences indicate that making a synthetic slag from the fuel ashes only roughly approximates the slag that actually forms in the combustor.

Switchgrass

Figure 70d presents the results from the viscosity measurements with the synthetic switchgrass slag and the synthetic coal–switchgrass mixture slag. As it is seen from Figure 70d the switchgrass slag appears to melt at significantly higher temperature (>1500°C [>2730°F]) compared to all the other biomass and coal–biomass slags. The slag was seen to have white color while even at 1550°C (2822°F) it formed a relatively viscous melt with limited flow characteristics. This is probably due to the high concentration of silica in the slag, as well as the low amounts of alkali metals, calcium and alumina. The material has a significantly higher viscosity compared to the other biomass and coal–biomass slags, which increases logarithmically as temperature decrease until reaching a region of instability below 1270°C (2318°F). Figure 73 shows the heated stage XRD data for the switchgrass ash as it cools from a melt. The data indicate that in the temperature range of the instability cristobalite (a high temperature version of SiO_2), nepheline ($NaAlSiO_4$) and crystals begin to form in the melt. The instability in the viscosity curve that develops when these crystals form is likely due to their segregation within the melt. Figure 70d also shows that the addition of switchgrass ash to the coal ash, (32/68 %wt), produces a slag that has a viscosity versus temperature behavior

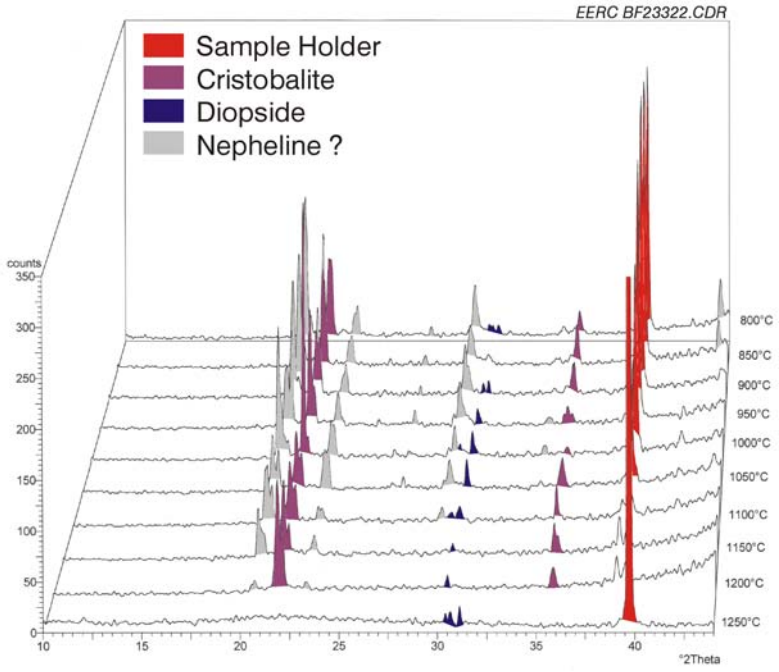

Figure 73. Heated-stage XRD data for the synthetic coal and switchgrass ash while being cooled from a melt.

very similar to that of the coal and corn stover ash slag except shifted to lower temperatures because the T_{cv} for the coal–switchgrass blended ash slag is the lowest of any of the three mixtures, around 1100°C (2010°F), which is actually lower than the T_{250} of 1120°C (2048°F). It is surprising that this synthetic slag would have a significantly lower T_{250} than the other cofire test slags because of its similar composition, although it does have somewhat higher alkali metal and lower alumina contents. Due to time constraints, Dr. Arvelakis was not able to include the actual slag created during the pilot-scale test of the coal and switchgrass in the viscosity tests.

Conclusions of Slag Behavior Testing

The slags resulted from the cocombustion of the coal–biomass mixtures in the slagging furnace have similar viscosity characteristics compared to the synthetic ash mixtures. The combustor slags contain higher amounts of silica and alumina and lower of alkali metals, while the viscosity shifts to slightly higher values and the solidification of the slags appear now to proceed at slightly higher temperatures. The T_{250} for the coal slag is similar to that of the coal–hog fuel slag, slightly lower than the T_{250} for the coal–corn stover slag, but higher than that of the coal–switchgrass slag, although only the synthetic coal–switchgrass ash slag was tested (i.e., not the actual SFS slag). It is somewhat surprising that the synthetic coal–switchgrass slag would have a significantly lower T_{250} than the other cofire test slags because of its similar composition, although it does have somewhat higher alkali metal and lower alumina contents.

Generally, the determination of the viscosity characteristics of the synthetic coal–biomass ash mixtures behave similarly to the SFS slags, and so their behaviors can be used to provide rough

approximations of the flow behavior of the slags within the SFS. In addition, the similarity of the curves made when using different rotational rates for the viscometer bob indicate that the slags are newtonian in that they are not prone to shear thinning or thickening. However, the compositions of the synthetic and even actual slags do not approximate the compositions of the ash and slag initially depositing on the HTHX, and therefore can not be used to predict the solidus temperatures of the HX deposits in order to determine the appropriate operating temperature of the HTHX so as to reduce corrosion of the alloy by the slag. This implies that instead of performing simple laboratory experiments to determine the appropriate operating temperature, it will be necessary to either employ computer models of ash formation and deposition, or perform pilot-scale tests of the fuels using air-cooled probes on which to form ash deposits for further analysis.

Flowing Slag Corrosion Testing of MA956 Alloy

In order to determine the rates and mechanisms of corrosion of MA956 alloy used in the HTHX by the coal-biomass slags, flowing slag corrosion tests were performed on coupons of the material in the DSAF. The DSAF testing is a worst-case-scenario type of test for the alloys because the corrosion mechanism is more severe than would be encountered by a HX in a power system. It is more severe because the slag is dripped directly onto the surface of the alloy whereas in a power system the surface would be coated with a thin layer of fly ash before building to the thickness at which the slag would become molten. The fly ash would most likely be less reactive to the alloy than the slag because it is relatively solid upon deposition. However, it also has a different composition than the slag as was seen in the analyses of the deposits formed on the HTHX reported under the Task 1 results. Six 100-hour corrosion tests were performed on the MA956. They were performed by pouring slag at 1500°C (2730°F) onto pipe sections which were air-cooled to surface temperatures of 1050°C (1922°F) for the first three tests and 1150°C (2102°F) for the final three. The lower temperature was chosen because it was substantially below the temperature of critical viscosity measured for the synthetic slags made by mixing appropriate ratios of the fuel ashes, as reported in the previous section of this report. This means that the slag would freeze to the surface of the alloy; therefore, the rate of reaction between the slag and the alloy or oxide scale on the surface of the alloy would be relatively low. The higher temperature was chosen because it was closer to, but still below, the temperature of critical viscosity for the hog fuel and corn stover blends, but slightly above the T_{250} for the synthetic switchgrass blend so that the slag would not freeze at the point at which it dropped on to the surface of the alloy for that slag. Because the switchgrass slag is more molten at 1150°C (2102°F), we expect that it would be more reactive toward the alloy than the frozen slags. The slag compositions used in the DSAF tests are shown in Table 38.

Figure 74 shows the surfaces of the alloy tube sections after the six tests. In all cases, the surface recessions due to slag corrosion were too small to measure with a caliper. During the 1150°C (2102°F) tests the slag wetted the surface more broadly and flowed farther around the circumference before dripping off than at the lower temperature. In all tests, the ribbon of slag frozen to the surface fell off upon cooling. With the exception of the switchgrass test at 1150°C (2102°F), the frozen slag broke from the alloy surface within the slag itself, leaving behind a thin layer of slag on the surface of the alloy. For the switchgrass test at 1150°C (2102°F), the slag broke off near where the slag

Table 38. Slag Analyses

Oxides[1], wt%	80% North Antelope 20% Hog Fuel	80% North Antelope 20% Corn Stover	80% North Antelope 20% Switchgrass
SiO_2	37.7	45.5	51
Al_2O_3	20.1	18.6	15.2
Fe_2O_3	5.4	5.3	5.4
TiO_2	1.1	1.1	1
P_2O_5	0.9	1.0	1.1
CaO	28	20.3	18.9
MgO	4.4	5.9	5.0
Na_2O	1.2	0.9	0.8
K_2O	1.1	1.4	1.5
SO_3[2]	0	0	0

[1] Fuel and slag oxide concentrations normalized to an SO_3-free basis.
[2] Fuel and slag SO_3 concentrations normalized with other oxides.

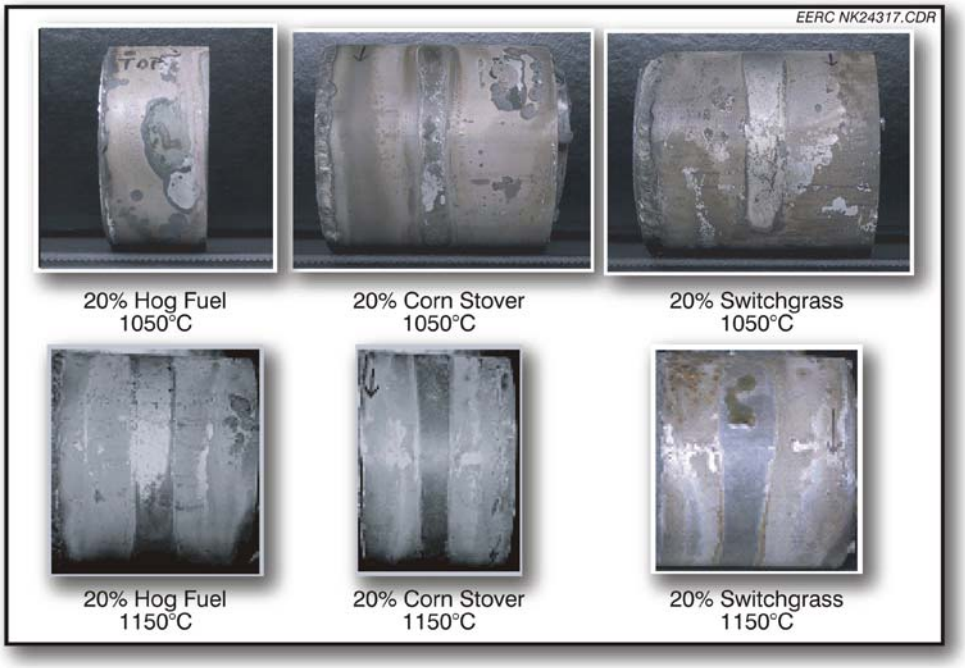

Figure 74. MA956 tube sections after 100 hours of exposure to flowing slag.

dripped on to the alloy, taking any remaining alumina scale with it. During temperature cycling this remaining slag serves as a protective layer that reduces the attack on the alloy by the initial contact with the molten slag. Since the slag layer did not remain attached for the switchgrass test at 1150°C (2102°F), the protective layer would not remain, and corrosion could be unacceptably high at that temperature for that slag. As the switchgrass slag flowed around the tube, it cooled due to radiation

losses from the tube and uneven heating so that some of the slag near the point where it dripped off of the alloy remained attached. Because of the cooling, the alloy temperature near the point where the slag drips off of the alloy is typically 100°C (180°F) cooler than where the slag drips on to the alloy.

SEM analyses of one uncorroded and all of the corroded alloys were performed to determine if there was significant interaction between the alloy elements and the slag, and to measure any depletion of aluminum, the protective oxide layer-forming element, from the alloy. Figure 75 is an SEM image of a cross section of the surface of the MA956 tube as received from the manufacturer. The black layer on top is the epoxy used to mount the sample, and the white area on the bottom is the alloy. The gray portion in the middle is the protective alumina layer, less than 1 μm thick, that naturally forms on the surface of the alloy when heated above 1100°C (2010°F) as it is during manufacturing. The alumina forms by migration of aluminum metal from within the alloy to the surface where it oxidizes. Once it begins forming, however, it prevents further transport of oxygen to the metal surface, thereby essentially stopping further oxidation. It is this same alumina layer that also protects the alloy from slag corrosion at high temperatures.

Figure 76 shows a cross section of the surface of the MA956 tube immediately above the point upon which the slag was dripped (no slag) for the 20% hog fuel test at 1050°C (1922°F). The gray layer in the middle is alumina. The white spots are composed of various combinations of phosphorous, chromium, yttrium, gold and platinum. The alloy is the source of the chromium and yttrium, while the crucible is the source of the gold and platinum. In this test the alumina layer ranges

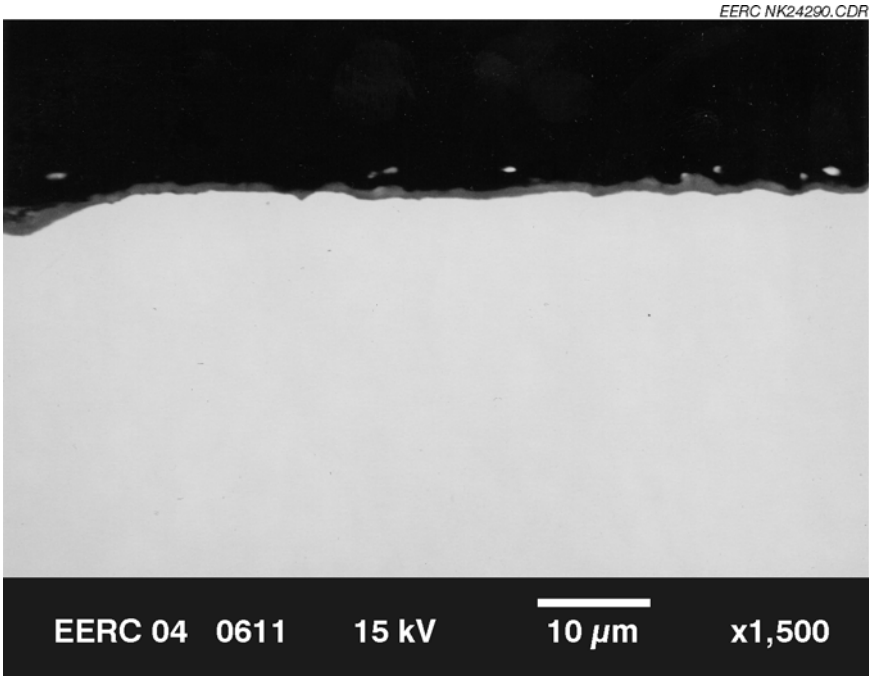

Figure 75. SEM image of a cross section of the surface of the MA956 tube as received.

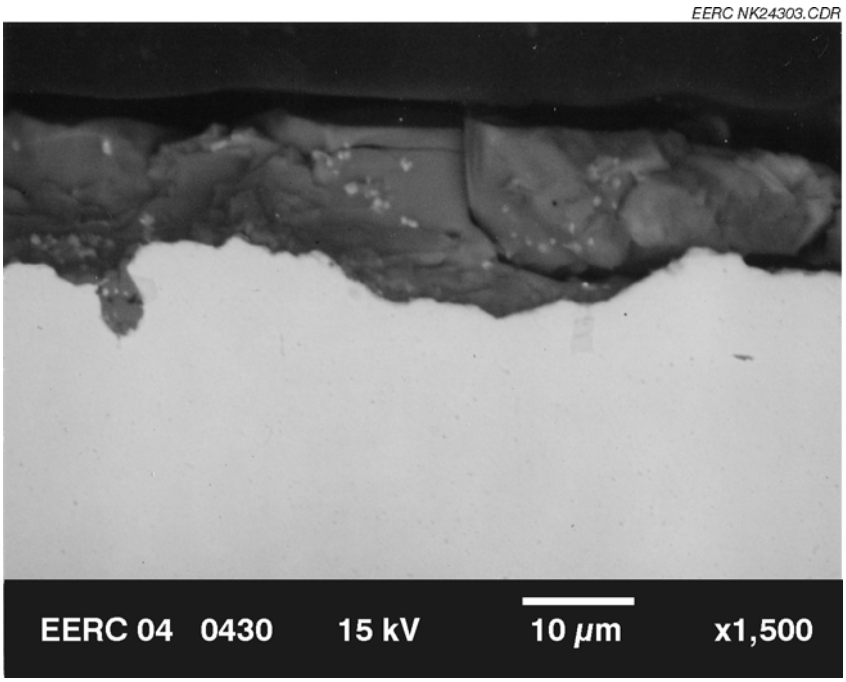

Figure 76. SEM image of a cross section of the surface of MA956 tube for 20% hog fuel at 1050°C (no slag).

from 6 to 21 μm thick indicating that the thickness of the alumina layer increased significantly during testing.

In addition to imaging the slag–scale interface, the SEM was used with energy dispersive x-ray analysis to measure the depletion of scale-forming elements as a function of depth within the alloys. The analyses were performed in 10-μm-square areas starting at the top of the alumina layer and moving into the alloy perpendicular to the surface. The measurements were made at three places within each corroded coupon, slightly above the spot upon which the slag dripped onto the alloy (no slag), at the spot where the slag landed on the coupon (at application) and at the spot where the slag dripped off of the alloy. As previously described, because of radiant energy losses, the spot at which the slag dripped off of the alloy was typically up to 100°C (180°F) cooler that the first two spots. Figure 77 is a semilog plot of the concentration of aluminum within the MA956 sample exposed to the 20% hog fuel at 1050°C (1922°F) as a function of depth. The increase in aluminum near the surface reveals the presence of the protective alumina layer (scale). The graph shows that below the scale and the slag there is no significant depletion of aluminum in the alloy in 100 h when compared to the as received sample. In contrast, for the region of the sample upstream of where the slag was dropped, there is a small but measurable depletion of aluminum down to a depth of 200 μm. This may indicate that the slag actually protects the alloy from oxidation by reducing the oxygen activity at the surface of the alloy. SEM analyses showed that the slag remaining attached to the surface was significantly enriched in alumina, indicating that a portion of the protective alumina layer had dissolved into the slag. However, the slag ribbon that spalled off was only enriched slightly in the region immediately adjacent to the slag that did not spall off. The fact that some of the slag remained

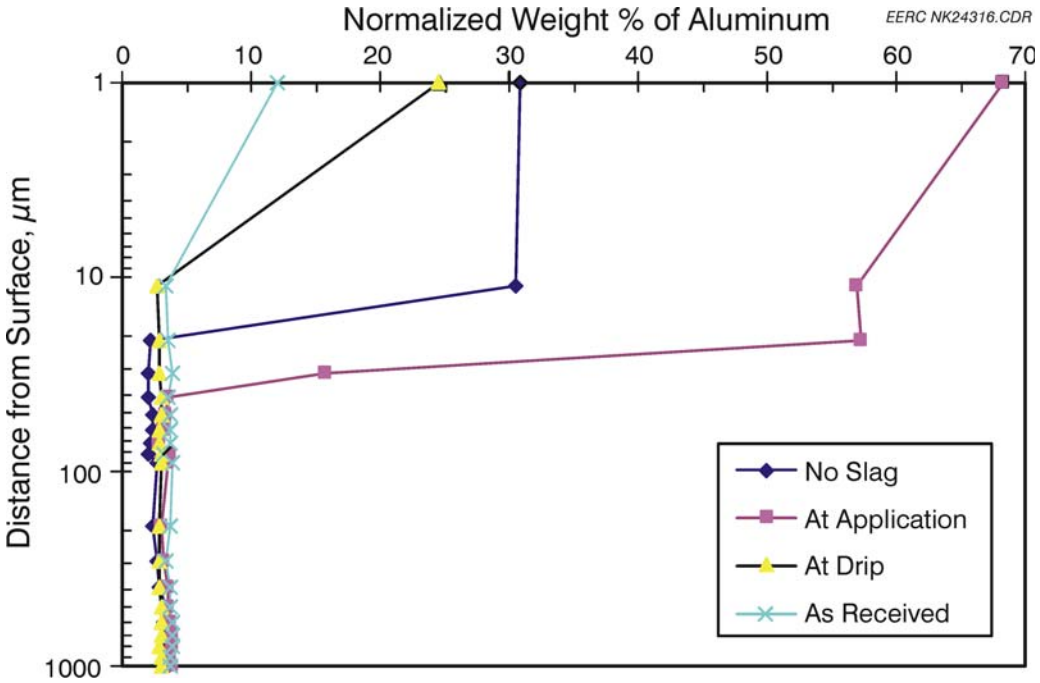

Figure 77. Aluminum content in MA956 as a functions of depth for 20% hog fuel at 1050°C.

attached to the MA956 surface shows that the protective oxide layer was not lost through spallation during thermal cycling.

Figure 78 is an SEM image of the inside surface of the slag ribbon at the drip for the 20% hog fuel test at 1050°C (1922°F). The grainy texture visible within the slag ribbon is the result of the crystallization within the slag that occurs during freezing. At the bottom of the slag layer, which would have been adjacent to the slag that remained attached to the alloy, dark crystals with compositions similar to the mineral anorthite ($CaAl_2Si_2O_8$) have formed. This is in contrast to the heated stage XRD results which showed primarily calicum and magnesium rich silicates crystallizing out of the slag upon cooling. The formation of anorthite in the DSAF slag may indicate a slightly higher aluminum content next to the alloy caused by a small amount of dissolution of the alumina-scale from the alloy into the spalled slag, even though the spalled slag as a whole was not enriched in alumina. Or it may indicate that the slag simply cooled more slowly than in the XRD, allowing time for the more viscous alumina-rich minerals to crystallize. The lighter areas are more calcium-rich and alumina-poor glasses or solid solutions.

The alumina layer ranges from 3 to16 µm thick for the 20% corn stover test at 1050°C (1922°F). Figure 79 is a semilog plot of the concentration of aluminum within the MA956 samples. The graph shows that there is no significant depletion of aluminum at the no slag and at drip locations. However, it appears there may be a slight depletion of aluminum at the application site, possibly because it may become slightly hotter than the surrounding alloy because of the heat of the slag as it contacts the metal. Unlike the hog fuel test, there does not appear to be a depletion of

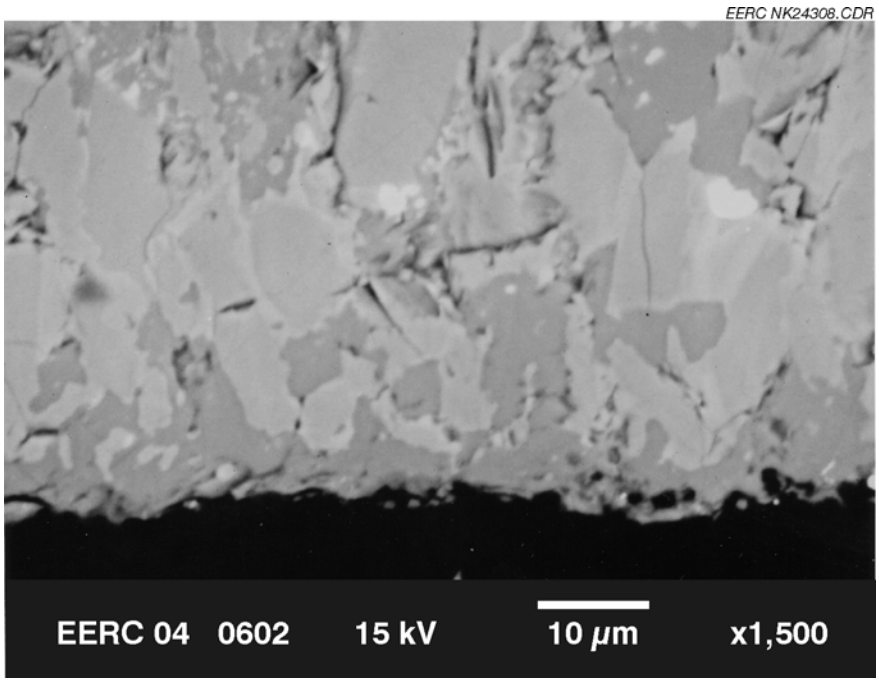

Figure 78. SEM image of a cross section of the inside surface of the slag ribbon for 20% hog fuel at 1050°C (at drip).

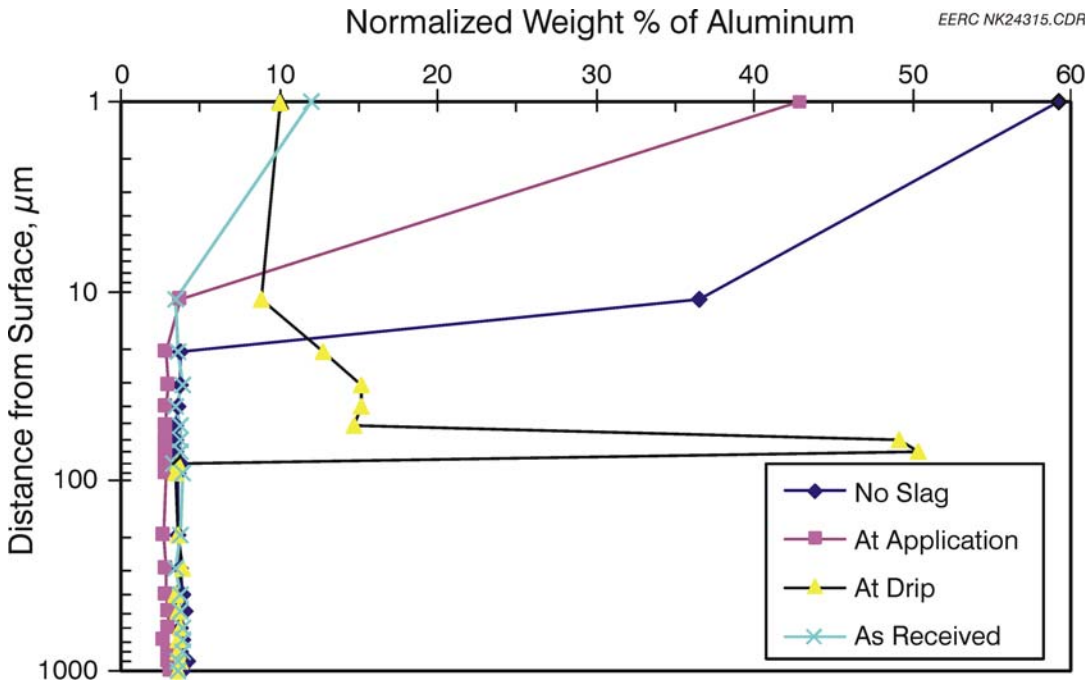

Figure 79. Aluminum content in MA956 as a function of depth for 20% corn stover at 1050°C.

aluminum in the alloy above the slag application point. Again, the slag remaining on the surface was enriched in alumina, while the slag ribbon that spalled off was not.

The alumina layer ranges from 3 to 26 µm thick for the 20% switchgrass test at 1050°C (1922°F). Figure 80 is a semilog plot of the concentration of aluminum within the MA956 samples. The graph shows that there is no significant depletion of aluminum at the no slag and at application sites. However, it appears there may be significant depletion of aluminum at the drip site, the area from which the slag dripped off of the alloy. This is an unlikely result since this portion of the alloy coupon is up to 100°C (180°F) cooler than the upper part of the coupon at which the slag is dripped. Therefore, the apparent depletion of aluminum at this point may be an artifact of a heterogeneous alloy composition, or demonstrate the range of error in the sample preparation and analysis techniques. Although SEM analysis was unable to detect any slag remaining on the surface, the protective alumina layer was not lost through spallation. The slag ribbon that spalled off was not enriched in alumina.

The alumina layer ranges from 3 to 17 µm thick for the 20% hog fuel test at 1150°C (2102°F). Figure 81 is a semilog plot of the concentration of aluminum within the MA956 samples. The graph shows no significant depletion of aluminum at all three sites. The slag remaining on the surface was enriched in alumina, while the slag ribbon that spalled off was not.

The alumina scale layer ranges from 3 to 11 µm thick for the 20% corn stover test at 1150°C (2102°F). Figure 82 is a semilog plot of the concentration of aluminum within the MA956 samples. The graph shows no significant depletion of aluminum from the alloy at all three sites. Again, the slag remaining on the surface was enriched in alumina, while the slag ribbon that spalled off was not.

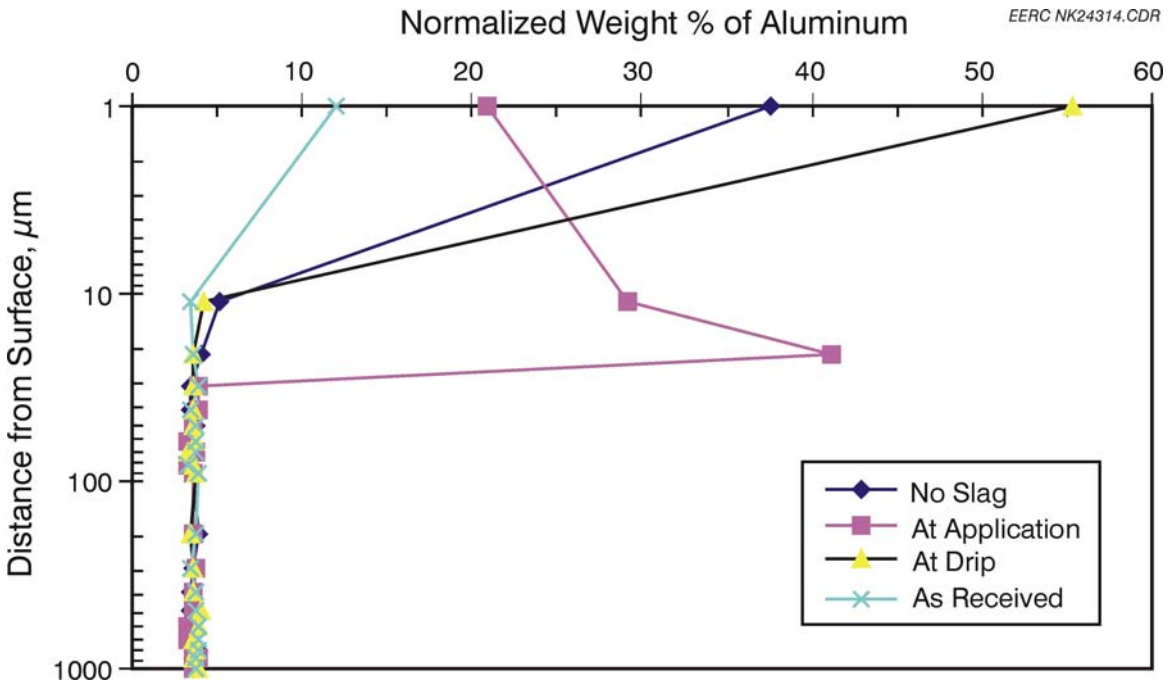

Figure 80. Aluminum content in MA956 as a function of depth for 20% switchgrass at 1050°C.

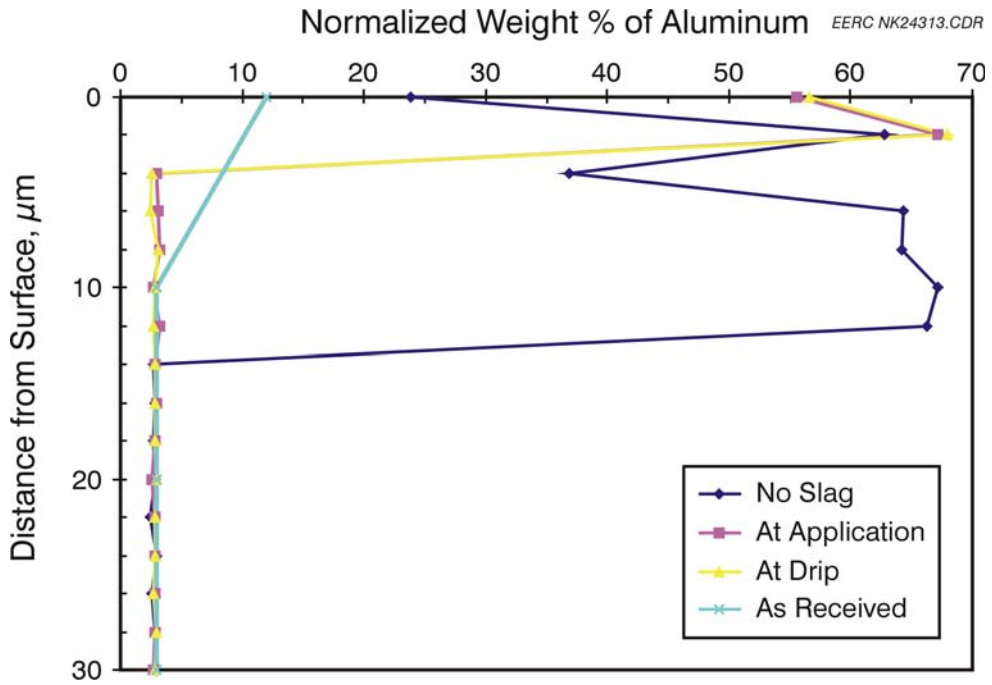

Figure 81. Aluminum content in MA956 as a function of depth for 20% hog fuel at 1150°C.

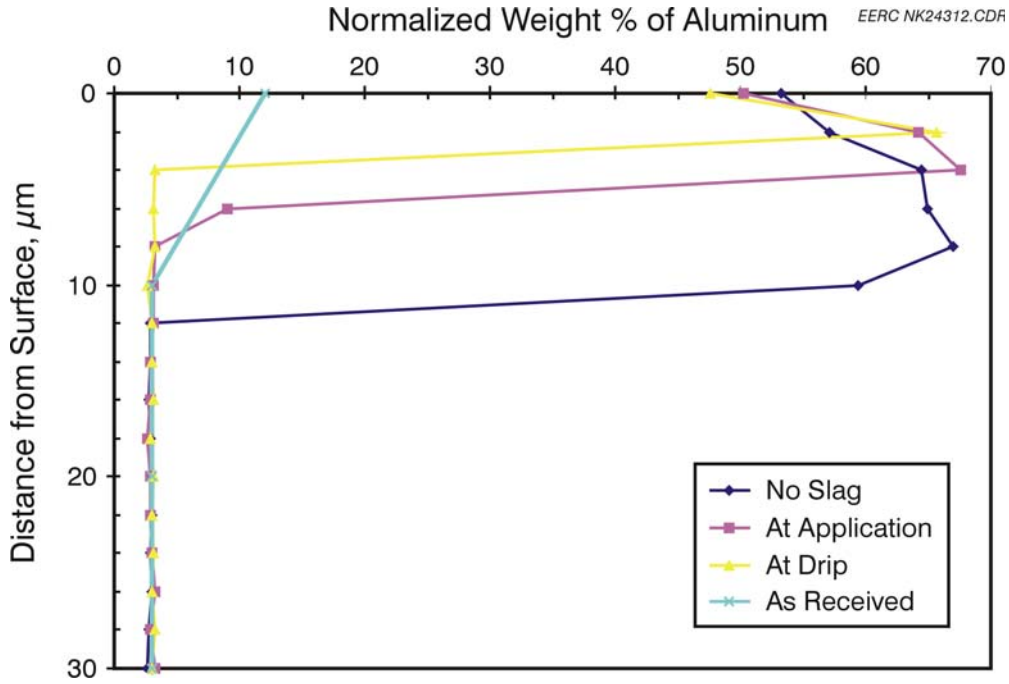

Figure 82. Aluminum content in MA956 as a function of depth for 20% corn stover at 1150°C.

Figure 83 is an SEM image of the MA956 tube at the drip for the 20% switchgrass test at 1150°C (2102°F). For this test the alumina layer ranges from 0 µm at the slag application site, to 19 µm thick near where the slag dripped off of the alloy. The slag near the drip off point was solid because of radiation cooling of the alloy near the drip off point. The slag remaining on the surface of the drip site was enriched in alumina, while the slag ribbon that spalled off of that site was not. However, around the slag application site the slag remained molten after dripping onto the alloy, dissolving the alumina scale from the alloy surface. Also, the spalled slag at this site was shown to be enriched in alumina. This could potentially lead to relatively rapid loss of aluminum from the alloy. Figure 84 is a semilog plot of the concentration of aluminum within the MA956 samples. The graph shows no significant depletion of aluminum at all three sites. The lack of depletion near the site where the slag dripped onto the alloy may indicate that the molten slag itself lowered the oxygen activity near the surface of the alloy. Even so, the fact that the slag dissolved the alumina scale and did not remain attached during cooling shows that this temperature is most likely too high for use of the MA956 when firing the coal–switchgrass blend, at least in situations when molten slag directly impacts the alloy.

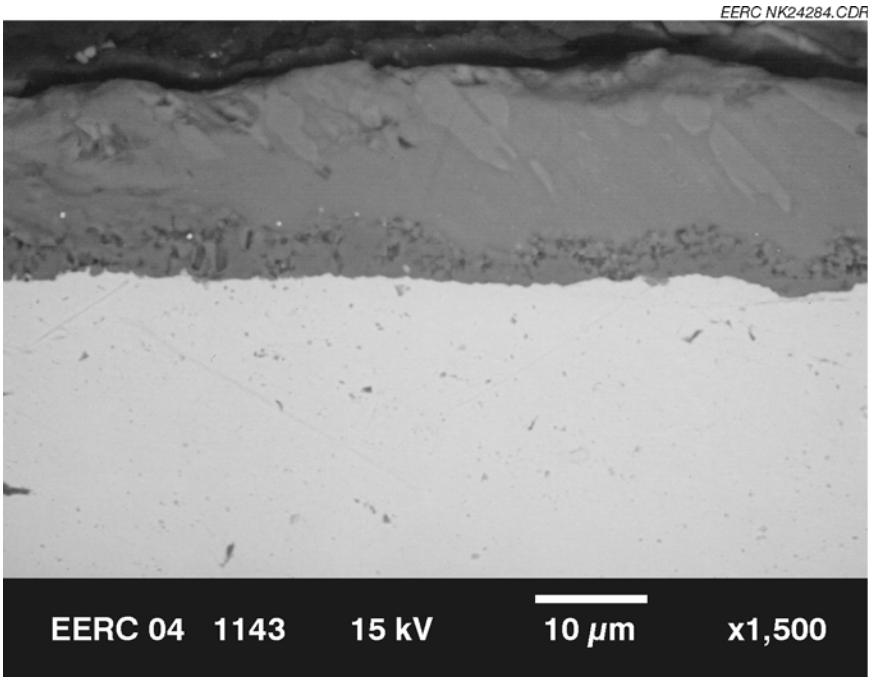

Figure 83. SEM image of a cross section of the surface of the MA956 tube for 20% switchgrass at 1150°C (at drip).

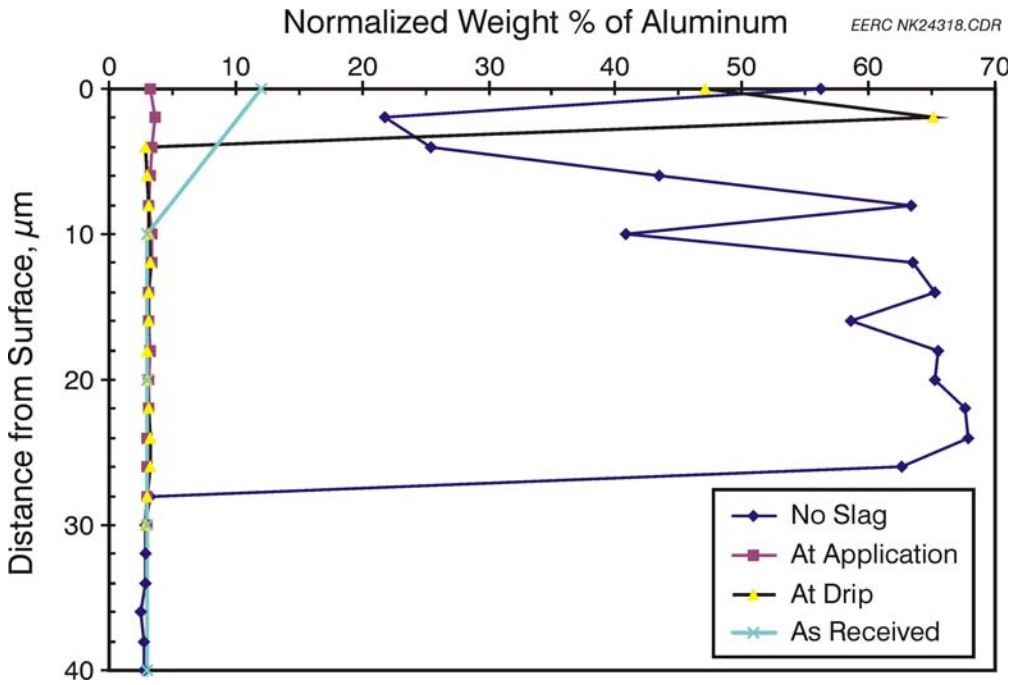

Figure 84. Aluminum content in MA956 as a function of depth for 20% switchgrass at 1150°C.

CONCLUSIONS AND RECOMMENDATIONS

Task 1 – Pilot-Scale Testing

The three pilot-scale coal–biomass-cofiring tests were completed during the weeks of October 9–17 (XCEL1), November 14–21 (XCEL2), and December 12–19 (XCEL3), 2003. Conclusions based on the data and recommendations for further work are presented here.

Fuel Characteristics

The potential need to air dry the biomass fuels to avoid handling, processing, and pilot-scale feed problems was verified upon inspection. The preparation of air-dried hog fuel, corn stover, and switchgrass through an existing EERC hammer mill, using a 3.18-mm (0.125-in.) screen, resulted in an acceptable biomass fuel that could be fed to the pilot-scale slagging furnace. Biomass moisture content would be expected to be less problematic in commercial systems as a function of smaller surface-to-volume ratios.

A comparison of the North Antelope coal with the biomass fuels showed the coal to have a higher moisture and sulfur content and heating value and a lower ash content. For the biomass fuels, the hog fuel was found to have the highest moisture content and heating value and the lowest sulfur and ash content. The two agricultural biomass sources had comparable sulfur levels and the switchgrass was found to have the lowest moisture content and heating value.

Ash fusion temperatures for all three biomass fuels were greater than those observed for the North Antelope coal. Hog fuel and switchgrass fluid temperatures were 167°–208°C (300°–375°F) greater than those observed for the corn stover and North Antelope coal.

The primary components of the North Antelope coal ash were calcium, silica, and alumina. Alkaline-earth components (CaO, MgO, Na_2O, and K_2O) combined represent 34–36 wt% in the ash. Biomass fuel ash primary components varied from fuel to fuel. Hog fuel ash was primarily composed of calcium and silica with combined alkaline-earth components representing 59 wt% of the ash. Corn stover ash was composed of primarily silica with combined alkaline-earth components representing 32 wt% of the ash. Switchgrass ash was composed of mostly silica with combined alkaline-earth components representing only 21 wt% of the ash, the lowest value for the four fuels fired in this project.

Dry sieve analysis indicated that the pulverized Antelope coal used in the coal–biomass-cofiring tests was 66–68 wt% −200 mesh (74 µm), slightly larger than the objective of 70 wt% −200 mesh (74 µm). Biomass fuels were 73–78 wt% −30 mesh (540 µm) as a result of processing through a hammer mill using a 3.18-mm (0.125-in.) screen.

As expected, the coal had the highest bulk density, 601–641 kg/m^3 (37.5–40.0 lb/ft^3). The lowest bulk density was observed for the corn stover, 136 kg/m^3 (8.5 lb/ft^3), although switchgrass was similar. Hog fuel was found to have the highest bulk density, 248 kg/m^3 (15.5 lb/ft^3), of the three biomass fuels.

Slagging Furnace Operation

North Antelope subbituminous coal feed was continuous for a minimum of 85-hr during the biomass-cofiring tests. Coal and biomass feed rates were adjusted and controlled to achieve a nominal 80%–20% coal–biomass cofiring contribution on a firing-rate basis and to avoid exceeding a 1052°C (1925°F) temperature limit imposed for the HTHX alloy tube surfaces. North Antelope coal feed rates ranged from 75 to 84 kg/hr (166 to 186 lb/hr). Biomass feed rates typically ranged from 27 to 32 kg/hr (60 to 70 lb/hr) for the three coal–biomass-cofiring tests.

Generally, both the coal and biomass feed rates were stable. Momentary spikes in the feed rates were observed during feed hopper refill cycles. The switchgrass feed rate was less stable than the hog fuel or corn stover, possibly related to the cylindrical geometry of the material and the impact that geometry has on mass flow through the feed hopper. It likely bridges more than the other two biomass materials. Inspection of the biomass feeder indicated switchgrass packing around the screw within the housing, which was not evident with the hog fuel or corn stover.

Furnace exit temperatures during the coal–biomass-cofiring test periods ranged from 1410° to 1494°C (2570° to 2720°F) as a result of main burner firing rates of 2.1–2.4 × 10^6 kJ/hr (2.0–2.3 MMBtu/hr). The hog fuel had the highest moisture level of the three biomass fuels and resulted in the lowest average furnace exit temperature, even though in combination with the coal fired, it represented the highest average firing rate. Based on the temperature and firing rate data and fuel characteristics, the differences in the furnace exit temperatures for the corn stover and switchgrass tests were likely a function of firing rate alone.

Based on fuel feed rate and analysis data, biomass cofiring represented nominally 26% (hog fuel), 23% (corn stover), and 20% (switchgrass) of the heat input through the main burner, respectively for Tests XCEL1, XCEL2, and XCEL3. Normally, during air-blown operation the auxiliary burner firing rate is limited to 0.53 × 10^6 kJ/hr (0.50 MMBtu/hr) representing <20% of the total furnace firing rate. However, it was necessary to fire the auxiliary burner at a slightly higher rate (20%–24%) to maintain a sufficiently high furnace exit temperature to avoid plugging problems in the slag screen. This was necessary because of the alloy surface temperature limit, <1052°C (<1925°F), imposed for the HTHX.

No forced SFS shutdowns or serious operating problems were encountered during any of the three pilot-scale combustion tests. However, the compressor supplying process air to the HTHX tripped twice while cofiring switchgrass. Frozen moisture in a compressor instrument air line is believed to have been the cause.

Although the particle size of the biomass fuels was significantly larger than the coal, overall carbon burnout during the coal–biomass-cofiring tests was high, as indicated by baghouse ash analysis that reported carbon values of 0.18–0.33 wt%. The high degree of carbon burnout, >99.6%, observed in the SFS system for these tests is a direct result of adequate furnace temperature and residence time.

During future coal–biomass cofiring tests with the SFS, the biomass fuel should be prepared through a 1.59-mm (0.0625-in.) screen. A smaller screen should result in a more uniform hammer mill product, potentially improving biomass feed stability for the pilot-scale system.

Baghouse Performance

Fly ash generated in the high-temperature SFS is different than observed for a given fuel fired in a conventional pc-fired system. Specific differences include a reduction in mass loading and particle size and a higher concentration of alkaline-earth components. This shift in ash properties was anticipated based on the use of a slag screen at the furnace exit to promote ash collection as slag. Ash passing through the slag screen is expected to represent smaller ash particles as well as ash components volatilized in the furnace and subsequently condensed at lower temperatures. Therefore, the SFS produces a fly ash more representative of a cyclone-fired system.

Baghouse temperatures ranged from 163° to 174°C (325° to 345°F) for Tests XCEL1 and XCEL2 and from 152° to 166°C (305° to 330°F) for Test XCEL3. The filter face velocities for the three coal–biomass-cofiring tests were 0.70–0.85 m/min (2.0–2.9 ft/min). These filter face velocities are low compared to conventional pulse-jet filtration systems typically operating at or near 1.2 m/min (4 ft/min).

The bags used in this project were a 747 g/m^2 (22-oz/yd^2) woven glass–PTFE membrane-fabric combination representing a total filtration area of 52.5 m^2 (565 ft^2). Online pulse cleaning of the PTFE membrane bags was attempted using reservoir pulse-air pressures of nominally 2.8–4.1 bar (40–60 psig). The baghouse differential pressure cleaning set points ranged from 11.2 to 16.8 mmHg (6 to 9 in. W.C.). However, online cleaning was unsuccessful, forcing off-line cleaning for all three biomass cofiring tests. Off-line cleaning frequency was 2–6 hr, depending on the biomass fuel cofired and the off-line cleaning trigger point.

Online baghouse cleaning had not been a problem previously when firing a subbituminous coal. Fly ash chemical composition resulting from biomass cofiring was determined to be the primary contributing factor to online cleaning difficulties. Specifically, concentrations of alkali components increased while silica and alumina concentrations decreased. The primary difference in composition data was an order-of-magnitude or near-order-of-magnitude increase in the potassium content for the baghouse ash resulting from biomass cofiring.

SEM morphology data support the hypothesis that potassium sulfate formation and condensation were responsible for altering the cohesive properties of the baghouse ash, resulting in an inability to control baghouse differential pressure using online cleaning when cofiring coal and biomass. Some sodium enrichment was also observed in the case of hog fuel cofiring. The highest degree of potassium enrichment was observed for corn-stover cofiring, consistent with the bulk fuel data showing the corn stover to have the highest ash content and the highest potassium content in the ash. Calculated mole ratios based on the elemental analysis data indicate that the potassium and sodium were present as sulfates. These sulfates form through condensation from the gas phase so that the particles are relatively small, leading to high van der Waals forces between the particles. In addition, some condensation may have occurred on the particles as they resided in the filter cake, which may have helped to glue the particles together, making them more difficult to remove by

backpulsing. The slagging system magnifies the problem because of the reduced total mass loading to the baghouse and subsequent enrichment of alkali sulfates in the baghouse ash. In order to successfully control baghouse differential pressure with online cleaning, substantially more energy would have to be employed during online cleaning (pulse pressures of >5.9 bar [>85 psig]) or biomass cofiring would have to be reduced from the 20% cofiring rate used during these tests. Further testing would be required to determine if online cleaning would be effective at higher pulse pressures or 15%, 10%, or 5% biomass-cofiring rates.

Coal–biomass cofiring in a conventional pc-fired system, resulting in a dry-ash condition, may not present online baghouse-cleaning difficulties for 20% biomass cofiring. The greater overall mass loading would result in a much lower degree of ash enrichment in alkali sulfates, and the larger average particle size would likely reduce particle cohesion impacts. However, specific tests would be required to verify this observation.

Baghouse inlet mass loading values for the three biomass-cofiring tests ranged from 0.2920 to 0.3923 g/m^3 (0.1275 to 0.1713 gr/scf). These values are at least 1 order of magnitude lower than would be expected in a conventional pc-fired system. This is primarily because of the ash removal as slag in the slag screen. The range in mass loading values was the result of differences in flue gas volumetric flow rate and biomass fuel ash content. Mass loading ranges were found to overlap when comparing the biomass-cofiring tests with previous tests firing subbituminous coal.

Baghouse outlet mass loading values for the three biomass-cofiring tests ranged from 0.0000 to 0.0025 g/m^3 (0.0000 to 0.0011 gr/scf). No measurable particulate emissions were observed for corn stover and switchgrass cofiring. Based on postrun maintenance, the particulate emission rate measured for hog fuel cofiring may have been affected by one bag that was found to be improperly mounted in the tube sheet, potentially creating a minor flue gas leak through the tube sheet. The sampling results showing no mass emissions at the outlet of the baghouse were not expected.

Although low mass emissions have been previously observed, zero values have not. Possible contributing factors to the zero mass loading values include the presence of a permanent ash cake composed of small particles creating a cake with a small pore size which causes a high differential pressures, low filter face velocities, and off-line cleaning requirements. Sampling periods do not reflect spikes in mass emissions as a function of cleaning cycles. The lowest mass loading and emission rates previously observed were 0.0002 g/m^3 (0.0001 gr/scf) and 0.17 $g/10^6$ kJ (0.0004 lb/MMBtu) when firing a Rochelle subbituminous coal. Therefore, if the online cleaning difficulties observed during the biomass-cofiring tests are solved, online cleaning will likely result in mass loadings of <0.002 g/m^3 (<0.001 gr/scf) and mass emissions of <1.3 $g/10^6$ kJ (<0.003 lb/MMBtu).

Assuming baghouse differential pressure can be controlled using online pulse cleaning as a result of operating parameter changes or a reduced biomass cofiring rate in the SFS, the cohesive character of the ash may be beneficial. Specifically, it may reduce emission spikes as a function of cleaning cycle. This benefit would also be likely in a conventional dry-ash pc-fired system.

CAH Performance

CAH tube bank performance has met all objectives relative to heat transfer and its support of the HTHX–RAH panel during this, as well as previous, projects. Performance differences relative to fuel ash properties were expected. The potential effectiveness of sootblowing was not addressed during this project because the EERC elected to permit the formation of ash deposits on CAH tube bank surfaces in order to develop deposits for subsequent recovery and characterization.

As ash deposits developed on the tube surfaces, heat recovery from the CAH tube bank decreased from maximum values of 43,466–47,897 kJ/hr (41,200–45,400 Btu/hr), for inlet and outlet process air temperatures of 499°–544°C (930°–1010°F) and 660°–688°C (1220°–1270°F), to a minimum of 19,306–24,476 kJ/hr (18,300–23,200 Btu/hr), for inlet and outlet process air temperatures of 369°–458°C (695°–855°F) and 444°–538°C (830°–1000°F), respectively. Based on previous experience firing subbituminous coal, if sootblowing had been employed during these coal–biomass-cofiring tests, CAH heat recovery would likely have been maintained in the range of 34,290–42,200 kJ/hr (32,500–40,000 Btu/hr).

The CAH deposits that formed during the coal–biomass-cofiring tests were limited to the leading and trailing edges of the tubes. However, these deposits were found to be friable. CAH tube bank plugging was not a problem when cofiring the North Antelope coal and any of the three biomass fuels. No deposits were observed bridging the flue gas path between the tubes.

On a mass-per-unit-time basis, the ash deposition rates were 36.3–52.8 g/hr (0.082–0.116 lb/hr). Incorporating the surface area of the tube bank (0.58 m^2 [6.28 ft^2]) results in values of 62.6–91.0 g/hr-m^2 (0.013–0.018 lb/hr-ft^2). These calculated values are essentially the same as results for other subbituminous coal-fired SFS test periods, 78.3 g/hr-m^2 (0.017 lb/hr-ft^2). On a coal–biomass-cofiring-rate basis, the CAH ash deposition rates were 15.8–23.0 g/10^6 kJ (0.036–0.053 lb/MMBtu). CAH ash deposition rates followed biomass fuel ash content. However, coal–hog fuel cofiring resulted in a slightly lower ash deposition rate because of the slag screen plugging observed during the test resulting in a lower ash mass loading reaching the CAH tube bank.

The deposits were typically split into two categories, the inner powder layer, and an outer sintered layer. The inner layer is typically composed of very small ash particles that deposit on the tubes through thermophoresis, a process by which small particles are driven from a hot gas to a cool surface. These particles are often much smaller than typical ash particles, and may contain significant amounts of alkali metal, alkaline earth, sulfur or chlorine because these elements often vaporize to a certain extent at the high temperatures in the main furnace, then condense as or onto small particles in cooler zones such as around the CAH. The outer layer consists primarily of larger particles that deposit on the tubes via inertial impaction. That is, they separate from the gas stream as the gas diverges around the tube. Because of their higher inertia, then continue toward the tube, impacting on other ash particles. Because the incoming particles are insulated from the cooled tube by other ash particles, they remain somewhat soft and can sinter, or stick together, into massive deposits, although strong sintering was not an issue in these cofiring tests.

Overall, the inner and outer layers of the CAH deposit formed when cofiring with hog fuel have similar compositions except that the inner layer is more enriched in alkali metals and more

sulfated than the outer layer. The similarity in compositions indicates that there was little difference in the deposition mechanisms of the ash particles in each layer making them much less distinct than is often seen in CAH deposits. Both layers are somewhat depleted in silica as compared to the fuels, most likely because more of the silica-rich ash had deposited in the main furnace and slag screen. SEM analyses showed that most of the silicate material is complex calcium alumina silicate, which is a common ash particle type for Powder River Basin coals. The deposits are also highly enriched in sulfur, indicating that a large proportion of the alkali metals and alkaline earth elements in the deposits have sulfated, the inner layer more so than the outer by virtue of its lower temperature and longer residence time in the furnace.

The inner layer of the CAH deposit formed while cofiring with corn stover is very enriched in sodium and potassium, and depleted in calcium relative to the outer sintered layer of the deposit or the fuels fired. It is also much more highly sulfated. The higher alkali content of this inner layer would make it more corrosive toward the CAH alloy than that formed while cofiring coal and hog fuel. It is enriched in these elements because they vaporize during combustion, and condense at lower temperatures as or on smaller particles that preferentially deposit on the relatively cool bare CAH tubes. The reason for the lower calcium content is not clear. The outer layer, which is formed more from larger particles, and is at a higher temperature, more reflects the composition of the coal ash, except that it too contains a higher potassium concentration and is relatively highly sulfated.

The inner layer and outer sintered layer of the CAH deposits formed while cofiring with switchgrass are very similar except for some enrichment of sodium and potassium, and especially sulfur in the inner layer. This trend was also seen while cofiring with corn stover and occurs because these alkali metals vaporize during combustion and recondense preferentially on or as smaller particles that tend to form the inner layers of ash on cooled surfaces. As was also true for the deposits formed during the other tests, the high sulfur concentrations indicate strong sulfation of the alkaline metal and alkali earth elements on the cooled tubes. As compared to the fuel ashes, the deposits have similar compositions to the coal ash because it forms a much larger proportion of the ash, except for the enrichment of the potassium which predominantly originates from the switchgrass. As was true for the deposits formed while cofiring the other fuels, SEM analyses show that the sulfated materials are relatively complex mixtures dominated by calcium sulfate, whereas the silicates are also complex and dominated by calcium aluminosilicate material. These results are consistent with deposits formed during other tests firing only Powder River Basin coals.

CAH heat-transfer data when cofiring hog fuel and switchgrass were similar. However, the CAH heat recovery rate when cofiring corn stover did not degrade to <21,100 kJ/hr (<20,000 Btu/hr), as was observed for the hog fuel and switchgrass. One possible explanation may be related to the density of the ash deposits formed.

One of the CAH standards of success identified for this project in the original proposal was the production of clean pressurized air at 705°C (1300°F) while limiting convective pass flue gas temperature to 1010°C (1850°F). Based on temperature measurements, clean pressurized-air temperatures generally stabilized at 510°–538°C (950°–1000°F), indicating that the proposed standard of success was not achieved. However, based on previous HTHX tests and the data generated during the coal–biomass-cofiring tests, reducing the process air flow rate to design volumes or adding sufficient CAH surface and surface to adequately preheat process air upstream

of the CAH, and employing sootblowing would easily result in CAH outlet process air temperatures of 927°C (1300°F).

HTHX Performance

Alloy tube surface temperature was to be limited to <1052°C (<1925°F) when cofiring coal and biomass to minimize the potential for slag corrosion–erosion of the alloy tube surfaces. However, the control thermocouple failed during each test period, and two compressor trips resulted in minor temperature spikes. As a result, indicated maximum HTHX tube surface temperatures were controlled at <1055°C (<1930°F) and typically ranged from 1033° to 1049°C (1890° to 1920°F). These are lower than for previous HTHX tests firing coal by 110°–205°C (230°–400°F) because of the lower alloy surface temperature limit selected for the coal–biomass-cofiring tests due to the lower solidus temperature of the slags produced during cofiring and the requirement that the surface temperature of the tubes be kept below the solidus temperature of the slag.

During the coal–biomass-cofiring tests, the range of process air temperatures at the exit of the HTHX decreased from nominally 721° to 749°C (1330° to 1380°F) to 635° to 666°C (1175° to 1230°F). This decrease is a direct result of decreasing heat transfer caused by ash–slag deposition on HTHX alloy tube surfaces as well as ash deposition on downstream heat-transfer surfaces (CAH and air preheat surfaces) preheating HTHX process air. Differences in HTHX outlet process air temperatures between individual coal–biomass-cofiring tests were consistent with a combination of furnace temperature and process air flow rates.

Deposition on the HTHX alloy tube surfaces began with a low-density sintered layer, followed by a higher-density intermediate layer, and finally a high-density molten slag layer. However, during cooldown, the slag layer consistently fractured on the surface of the alloy tubes. As a result, the slag layers had either partially or completely fallen off of the tubes. Also, there was no evidence of slag flow down the surface of the alloy tubes. Based on these observations, a higher tube surface temperature limit could have been employed without causing an alloy corrosion problem while firing the various coal–biomass fuel combinations.

Measured heat recovery decreased from 146,010 to 164,580 kJ/hr (138,400 to 156,000 Btu/hr) to nominally 120,590 to 145,270 kJ/hr (114,300 to 137,700 Btu/hr) during the coal–biomass-cofiring test periods as a result of ash and slag deposition on the HTHX alloy tube surfaces. Assuming that HTHX thermal stability was achieved during the last 12 hr of each test period, the measured heat recovery observed during the coal–biomass-cofiring tests is comparable to, if not greater than, the average level of heat recovery (126,600 kJ/hr [120,000 Btu/hr]) previously observed when evaluating the HTHX–RAH in a tile-protected configuration.

The corrected HTHX heat recovery rates for coal–biomass-cofiring tests were 66%–84% of that observed for firing an Illinois No. 6 bituminous coal, 292,450–372,630 versus 440,990 kJ/hr (277,200–353,200 versus 418,000 Btu/hr). The primary reason for this difference was the lower furnace temperature, 1433°–1488°C (2610°–2710°F), for the biomass-cofiring tests versus 1571°C (2860°F) when firing just coal. In addition, the lower tube surface temperature allowed for the cofiring tests to prevent corrosion slightly lowered the heat removal rate.

Comparisons of heat recovery data for the coal–biomass-cofiring test periods showed that heat recovery was 27% and 24% greater for the switchgrass and corn stover tests, respectively, when compared to the hog fuel test. The reason for the difference in heat recovery rates was furnace temperature, 1488°C (2710°F), 1477°C (2690°F), and 1433°C (2610°F) for the switchgrass, corn stover, and hog fuel, respectively.

In general, coal–biomass cofiring resulted in HTHX heat recovery rates consistent with previous tests firing NG and bituminous coal at comparable operating temperatures. Therefore, at comparable temperatures, coal–biomass cofiring does not present any unique impediments to HTHX heat recovery. However, biomass ash–slag properties may limit HTHX alloy surface temperatures. In that event, it is not likely that HTHX heat recovery rates observed for bituminous coal can be practically achieved when cofiring biomass.

XRF analyses of the inner layers of the deposits formed on the HTHX during all three tests showed that they have compositions very much like that of the slag except that it is enriched in alkali elements and sulfur. SEM analyses show that most of the alkali and alkaline earth elements are associated with aluminosilicate ash particles, and that a large fraction of these elements, along with the calcium, have sulfated. This sulfation does not occur when the surface temperature of the HTHX is maintained at higher temperatures as it is when firing only on coal. As the deposit builds, and therefore reaches higher temperatures leading to sintering, sulfation no longer occurs, and the deposits become highly enriched in silica which dilutes the concentrations of the other elements. It is likely that the high silica contents reflect preferential deposition of larger mineral grains which are rich in silica in both the coal and the biomass. The outer layers also showed a relatively low alumina content relative to the slag composition indicating that only a relatively small fraction of the aluminosilicate-rich clay particles from the coal deposit in the main combustor. Instead, they appear to be preferentially removed in the slag screen. These differences in deposit composition relative to the slag indicate that using the fuel slag for longer term laboratory corrosion testing is not sufficient to understanding the alloy corrosion mechanisms or rates. Instead, some computer modeling of ash formation and deposition should be performed in order to better understand the properties of the inner deposit layers, so that more realistic laboratory corrosion tests can be designed.

One of the standards of success identified for this project in the original proposal was the production of clean pressurized air at 927°C (1700°F) while the slagging furnace was operated at a temperature of no more than 1566°C (2850°F). Clean pressurized-air temperatures generally stabilized at 635°–666°C (1175°–1230°F) near the end of each test. At face value, these data indicate that the proposed standard of success was not achieved. However, based on previous HTHX tests and the data generated during the coal–biomass-cofiring tests, the EERC is confident that process air temperatures of >927°C (>1700°F) can be achieved and maintained if the entire surface of the HTHX is exposed to furnace conditions, the alloy tube surface temperature limit is raised to <1094°C (<2000°F), and routine sootblowing of CAH and air preheat surfaces is employed to maintain inlet process air temperatures at 705°C (1300°F).

Economic Analysis of IFCC Systems

A brief study was performed to identify the performance and the first-order economics of an IFCC employing an HTHX. The results were compared to a variety of systems including typical pc-fired plants, IGCCs, and NGCCs. Since the pilot-scale testing of coal–biomass cofiring showed no significant influence of biomass cofiring on the operation of the combustor, and since the cost of biomass is only slightly less than that of coal, it was assumed that costs for cofiring would be essentially the same as for just firing coal so no separated calculations were included for cofiring. Two main IFCC firing scenarios were investigated; coal- fired with air and coal-fired with O_2. Because IFCC systems have a high potential for operation as zero-emission power plants, special focus was placed on firing with O_2, and including CO_2 recovery.

Even with the limited number of configurations analyzed, it is apparent that the IFCC with CO_2 recovery offers better performance and lower COE than pc plants with CO_2 recovery. This is also true with the lower-performing all-coal IFCC. The IFCC also has competitive COE's to IGCC plants. At NG prices above $\$4.70/10^6$ kJ ($5.00/MMBtu), the IFCC systems are attractive alternatives NGCC systems with CO_2 recovery while maintaining the standard operations of a pc plant. A near zero-emission IFCC is also cheaper to operate than a modern pc system if a carbon tax of more than $55/metric ton ($50/ton) C is imposed. If 20% biomass cofiring is employed in the IFCC only, the breakeven point would be $44/metric ton ($40/ton) of carbon.

A more detailed analysis allowing wider evaluation of alternative IFCC configurations and lower level cost analysis should be performed. For example, the IFCC is uniquely suitable for use with membrane transfer oxygen units and such a system should have significantly higher performance and lower costs. More detailed design and accompanying cost analysis, especially for alternative firing sequences for the HTHX and also the entire furnace assembly and enclosure, would identify critical issues and supply better cost estimates for this unique enabling technology. The EERC is currently in discussions with the DOE National Energy Technology Laboratory to them perform these calculations in a manner consistent with their previous analyses of other advanced power system concepts.

Task 2 – Laboratory-Scale Testing

Joining

The ODS alloys used to construct the HTHX exhibit extremely high corrosion and creep resistance. These properties are imparted to the alloys because of the dispersion of the yttria particles throughout the alloy structure. However, because they must remain dispersed, the alloys cannot be welded because melting would allow the oxides to segregate in the joint, diminishing the usefulness of the metal. Therefore, the EERC has been working with ORNL to develop a method for joining the MA956 using TLP bonding. This work was begun under an earlier DOE program, but was further advanced under the biomass cofiring program described in this document.

Because of the proprietary nature of the results of the method development, full details cannot be disclosed in this document. However, a method of joining the MA956 has been developed in which the only a few pores remain along the line of the joint, and in which the joining alloy is

approximately 95% dispersed within the ODS alloy. Samples of different joints have been sent to ORNL for evaluation and tensile strength testing under their Fossil Energy Materials program but these initial results indicate that the TLP method is likely to be suitable for joining the alloy for use in construction of a demonstration-sized HTHX.

Slag Viscosity Measurements

In order to determine the melting and rheological properties of the biomass and biomass–coal slags so that the solidus temperatures can be inferred, their viscosities were measured with a high temperature rotational viscometer, and their crystallization behavior upon cooling was measured by heated-stage XRD. In addition, the behavior of synthetic slags made from fuel ash was compared to that of the slags made in the SFS. The comparison was made to determine if testing of synthetic slags, which are much more easily produced than combustor slags, can be a valid way of determining probable slag behavior.

Viscosity measurements indicated that these synthetic mixtures did behave similarly to the slags produced in the SFS, but also were not exactly the same. Due to variations in mineral deposition behavior, the combustor slags contain higher amounts of silica and alumina and lower levels of alkali metals, causing the viscosity to be slightly higher and the solidification of the slags to proceed at slightly higher temperatures. The temperature at which the viscosity of the slag reached 250 poise (T_{250}), and therefore may cause flow problems, for the coal slag is similar to that of the coal–hog fuel slag, slightly lower than the T_{250} for the coal–corn stover slag, but higher than that of the coal–switchgrass slag, although only the synthetic coal–switchgrass ash slag was tested (i.e., not the actual SFS slag). It is somewhat surprising that the synthetic coal–switchgrass slag would have a significantly lower T_{250} than the other cofire test slags because of its similar composition, although it does have somewhat higher alkali metal and lower alumina contents.

Generally, the synthetic coal–biomass ash mixtures behave similarly to the SFS slags, and their behaviors can be used to provide rough approximations of the flow behavior of the slags within the SFS. The similarity of the curves made when using different rotational rates for the viscometer bob indicate that the slags are Newtonian in that they are not prone to shear thinning or thickening. However, the compositions of the synthetic and even actual slags do not approximate the compositions of the ash and slag initially depositing on the HTHX, and therefore can not be used to predict the solidus temperatures of the HX deposits in order to determine the appropriate operating temperature of the HTHX so as to reduce corrosion of the alloy by the slag. This implies that instead of performing simple laboratory experiments to determine the appropriate operating temperature, it will be necessary to either employ computer models of ash formation and deposition, or perform pilot-scale tests of the fuels using air-cooled probes on which to form ash deposits for further analysis.

Flowing Slag Corrosion Testing of HTHX Alloy

The DSAF testing provides a worst-case-scenario type of test for the alloys because the corrosion mechanism is more severe than would be encountered by a HX in a power system. It is more severe because the slag is dripped directly onto the surface of the alloy whereas in a power system the surface would be coated with a thin layer of less reactive fly ash before building to the

thickness at which the slag would become molten. Six 100-hr corrosion tests were performed on MA956 which was air-cooled to surface temperatures of 1050°C (1922°F) for the first three tests and 1150°C (2102°F) for the final three. The lower temperature was chosen because it was substantially below the temperature at which the slag begins to solidify. This means that the slag would essentially freeze to the surface of the alloy, and therefore the rate of reaction between the slag and the alloy or oxide scale on the surface of the alloy would be relatively low. The higher temperature was chosen because it was closer to, but still below, the temperature at which solidification begins, but slightly above the T_{250} for the synthetic switchgrass blend so that the slag would not freeze at the point at which it dropped on to the surface of the alloy for that slag. Because the switchgrass slag is molten at 1150°C (2102°F), we expected that it would be more reactive toward the alloy than the frozen slags.

In all tests the corrosion rates were very low and could not be measured by caliper at temperatures up to 1150°C (2102°F). With the exception of the coal–switchgrass slag test at 1150°C (2102°F), SEM analyses showed that the protective oxide layer was not lost through spallation of the slag during thermal cycling. In fact, an alumina-enriched layer of slag remained attached to the alloy providing further protection during temperature cycling. The analyses also show that aluminum was not significantly depleted from the alloys except for minor depletion above the slag drip point in the 1050°C (1922°F) hog fuel test, and at the drip point of the 1050°C (1922°F) corn stover test. It is not clear at this time if these two exceptions would preclude the use of the alloy under these conditions, especially since there does not appear to be depletion in the 1150°C (2102°F) tests. However, the fact that the switchgrass slag remains molten at 1150°C (2102°F), and that the slag appears to have dissolved the protective alumina scale at that temperature, does indicate that temperature is likely too high for safe operation of the HTHX when firing that coal–biomass blend. In all cases however, longer tests should be performed before commercial demonstrations of the HTHX are performed. In addition, tests should be performed with sintered ash of the correct composition rather than just with flowing slag since the composition of the sintered ash layer on the surface of the HTHX after the pilot-scale combustion tests was significantly different from that of the slag.

ACKNOWLEDGMENTS

The authors would like to thank the DOE National Energy Technology Laboratory for funding this work through Cooperative Agreement DE-FC26-98FT40321, Richard Read, Contracting Officer's Representative (COR), and Cooperative Agreement DE-FC26-01NT41129, Andrew O'Palko, COR.

REFERENCES

1. Klara, J.M. HiPPS: Beyond State-of-the-Art Part I. *Power Eng.* **1993**, *Dec.,* 37–39.

2. Klara, J.M. HiPPS Can Compete with Conventional PC Systems: Part II. *Power Eng.* **1994**, *Jan.,* 33–36.

3. United Technologies Research Center. *Combustion 2000 Phase II Final Technical Report*, DE-AC22-95PC95144, 2001.

4. Wright, I.G.; Stringer, J. Materials Issues for High-Temperature Components in Indirectly-Fired Cycles. In *Proceedings of the International Gas Turbine and Aeroengine Congress and Exhibition*, Orlando, FL, 1997.

5. Weber, G.F.; Hurley, J.P.; Seery, D.J. Testing of a Very High-Temperature Heat Exchanger in a Pilot-Scale Slagging Furnace System. In *Proceedings of the 2000 International Joint Power Generation Conference*, Miami Beach, FL, 2000.

6. Hurley, J.P.; Weber, G.F.; Jones, M.L. Tests of High-Temperature Heat Exchangers for Indirectly Fired Combined Cycles. In *Proceedings of the 20th Annual International Pittsburgh Coal Conference*, Pittsburgh, PA, 2003.

7. Mann, M.K.; Spath, P.L. The Net CO_2 Emissions and Energy Balances of Biomass and Coal-Fired Power Systems. In *Proceedings of the 4th Biomass Conference of the Americas: Biomass: A Growth Opportunity in Green Energy and Value-Added Products, 1999;* Overend, R.P.; Chornet, E., Eds.; 1999; Vol. 1, pp 379–385.

8. Bhattacharya, S.C. State of the Art of Biomass Combustion. *Energy Sources* **1998**, *20*, 113–135.

9. Easterly, J.L.; Burnham, M. Overview of Biomass and Waste Fuel Resources for Power Production. *Biomass Bioenergy* **1996**, *10* (2–3), 79–92.

10. Turnball, J.H. Strategies for Achieving a Sustainable, Clean and Cost-Effective Biomass Resource. *Biomass Bioenergy* **1996**, *10* (2–3), 93–100.

11. McGowin, C.R.; Wiltsee, G.A. Strategic Analysis of Biomass and Waste Fuels for Electric Power Generation. *Biomass Bioenergy* **1996**, *10* (2–3), 167–175.

12. Bauen, A.; Kaltschmitt, M. Contribution of Biomass Toward CO_2 Reduction in Europe. In *Proceedings of the 4th Biomass Conference of the Americas: Biomass: A Growth Opportunity in Green Energy and Value-Added Products, 1999;* Overend, R.P.; Chornet, E., Eds.; 1999; Vol. 1, pp 371–378.

13. Frandsen, F.J.; Nielsen, H.P.; Jensen, P.A.; Hansen, L.A.; Livbjerg, H.; Dam-Johansen, K.; Sorensen, H.S.; Larsen, O.H.; Sander, B.; Henriksen, N.; Simonsen, P. Deposition and

Corrosion in Straw and Coal–Straw Cofired Utility Boilers. In *Proceedings of the Engineering Foundation Conference on the Impact of Mineral Impurities in Solid Fuel Combustion*; Kona, HI, Nov 2–7, 1997; Wall, T.F.; Baxter, L.L., Eds.; 1997; 14 p.

14. Frandsen, F.J.; Nielsen, H.P.; Hansen, L.A.; Hansen, P.F.B., Andersen, K.H., Sorensen, H.S. Ash Chemistry Aspects of Straw and Coal–Straw Cofiring in Utility Boilers. In *Proceedings of the 15th Annual International Pittsburgh Coal Conference*; Sept 14–18, 1998; 14 p.

15. Skrifvar, B.; Lauren, T.; Backman, R.; Hupa, M. The Role of Alkali Sulfates and Chlorides in Post Cyclone Deposits from Circulating Fluidized Bed Boilers Firing Biomass and Coal. In *Proceedings of the Engineering Foundation Conference on the Impact of Mineral Impurities in Solid Fuel Combustion*; Kona, HI, Nov 2–7, 1997; Wall, T.F.; Baxter, L.L., Eds.; 1997; 10 p.

16. Jensen, P.A.; Stenholm, J.; Hald, P. Deposition Investigation in Straw-Fired Boilers. *Energy Fuels* **1997**, *11*, 1048–1055.

17. Olanders, B.; Steenari, B. Characterization of Ashes from Wood and Straw. *Biomass Bioenergy* **1995**, *8* (2), 105–115.

18. Nordin, A. Chemical Elemental Characteristics of Biomass Fuels. *Biomass Bioenergy* **1995**, *8* (2), 339–347.

19. Boylan, D.M. Southern Company Tests of Wood/Coal Cofiring in Pulverized-Coal Units. *Biomass Bioenergy* **1996**, *10* (2–3), 139–147.

20. Brouwer, J.; Owens, W.D.; Harding, S.; Heap, J.P. Cofiring Waste Biofuels and Coal for Emission Reduction. In *Proceedings of the 2nd Biomass Conference of the Americas: Energy, Environment, Agriculture, and Industry*; Portland, OR, Aug 21–24, 1995; NREL/CP-200-8098, DE95009230, 1995; pp 390–399.

21. Rudinger, H.; Kicherer, A.; Greul, U.; Spliethoff, H.; Hein, K.R.G. Investigations in Combined Combustion of Biomass and Coal in Power Plant Technology. *Energy Fuels* **1996**, *10*, 789–796.

22. Hughes, E.; Tillman, D. Biomass Cofiring: Status and Prospects 1996. In *Proceedings for the Engineering Foundation Conference, Biomass Usage for Utility and Industrial Power*; Snowbird, UT, April 28–May 3, 1996; 19 p.

23. Battista, J.; Tillman, D.; Hughes, E. Cofiring Wood Waste with Coal in a Wall-Fired Boiler: Initiating a 3-Year Demonstration Program. In *Proceedings of BioEnergy 98: Expanding BioEnergy Partnerships*; Madison, WI, Oct 4–8, 1998; pp 243–250.

24. Moore, T. Harvesting the Benefits of Biomass. *EPRI Journal* **1996**, *May/June*, 16–25.

25. Prinzing, E.E.; Hunt, E.F. Impacts of Wood Cofiring on Coal Pulverization at the Shawville Generating Station. In *Proceedings for Engineering Foundation Conference: Biomass Usage for Utility and Industrial Power*; Snowbird, UT, April 28–May 3, 1996; 15 p.

26. Gold, B.A.; Tillman, D.A. Wood Cofiring Evaluation at TVA Power Plants. *Biomass Bioenergy* **1996**, *10* (2–3), 71–78.

27. Miles, T.R.; Miles, T.R., Jr.; Baxter, L.L.; Bryers, R.W.; Jenkins, B.M.; Oden L.L. Boiler Deposits from Firing Biomass Fuels. *Biomass Bioenergy* **1996**, *10* (2–3), 125–138.

28. Moe, T.A. *Wastepaper Pellets as a Source of Fuel for Auxiliary Home Heating*; Final Report for Western Area Power Administration; Energy & Environmental Research Center: Grand Forks, ND, June 1995; 21 p.

29. Miles, T.R.; Miles, T.R., Jr.; Baxter L.L.; Bryers, R.W.; Jenkins, B.M.; Oden, L.L. Boiler Deposit from Firing Biomass Fuels. *Biomass Bioenergy* **1996**, *10* (2–3), 125–138.

30. Aerts, D.J.; Ragland, K.W. Cofiring Switchgrass in a 50-MW Pulverized Coal Utility. In *Proceedings of BioEnergy 98: Expanding BioEnergy Partnerships*; Madison, WI, Oct 4–8, 1998; pp 295–305.

31. Segrest, S.A.; Rockwood, D.L.; Stricker, J.A.; Green, A.E.S.; Smith, W.H.; Carter, D.R. Biomass Cofiring with Coal at Lakeland, Florida, Utilities. In *Proceedings of BioEnergy 98: Expanding BioEnergy Partnerships*; Madison, WI, Oct 4–8, 1998; pp 315–325.

32. Kendall, A. Barriers to the Progress of Bioenergy. *Energy World* **1996**, *May*, 10–13.

33. Graham, R.L.; Lichtenberg, E.; Roningen, V.O.; Shapouri, H.; Walsh, M.E. The Economics of Biomass Production in the United States. In *Proceedings of the 2nd Biomass Conference of the Americas: Energy, Environment, Agriculture, and Industry*; Portland, OR, Aug 21–24, 1995; NREL/CP-200-8098, DE95009230, 1995; pp 1314–1323.

34. D.R. Piperno. *Phytolith Analysis*; Academic Press: New York, 1988.

35. Baxter, L.L.; Miles, T.R.; Miles Jr., T.R.; Jenkins, B.M.; Milne, T.; Dayton, D.; Bryers, R.W.; Oden., L.O. The Behavior of Inorganic Material in Biomass-Fired Power Boilers: An Overview of the Alkali Deposits Project. Bridgwater, A.V.; Boocock, D.G.B., Eds.; In *Developments in Thermochemical Biomass Conversion*; Blackie Academic & Professional: London; Vol II, pp 1424–1444; NICH Report No. 24259.

36. Robinson, A.; Baxter, L.; Junker, H.; Shaddix, C.; Freeman, M.; James, R.; Dayton, D. Fireside Issues Associated with Coal-Biomass Cofiring. Presented at BioEnergy ‘98, Madison, WI, Oct 4–8, 1998.

37. Mann, M.D. *Modular Fluid Bed Biocombustor – Phase 1 and 1A Final Report*; Final Report for Sandia National Laboratories Contract No. BC-0002C; EERC Publication 99-EERC-12-03; Energy & Environmental Research Center: Grand Forks, ND, 1999; 67 p.

38. Schmidt, D.D.; Pinapati, V.S. *Opportunities for Small Biomass Power Systems*; Final Technical Report for U.S. Department of Energy Contract No. DE-FG02-99EE35128; EERC Publication 2000-EERC-11-01; Energy & Environmental Research Center: Grand Forks, ND, Nov 2000.

39. Collings, M.; Dockter, B.; Eylands, K.; Hajicek, D.; Henderson, A.; Hurley, J.; Kleven, P.; Lillemoen, C.; Weber, G. *Lignite Testing in a Pilot-Scale High-Temperature Advanced Furnace*; Final Report for U.S. Department of Energy Federal Energy Technology Center Contract DC-FC26-98FT40321; Energy & Environmental Research Center: Grand Forks, ND, April 1999.

40. Hurley, J.P.; Weber, G.F.; Henderson, A.K.; Collings, M.E. *Subtask 3.7 – High-Temperature Heat Exchanger Development and Testing*; Final Report for U.S. Department of Energy National Energy Technology Laboratory Cooperative Agreement No. DE-FC26-98FT40320, August 2004.

41. Serry, D.J. et al. Combustion 2000 Phase II, Final Technical Report; *Volume I*, DE-AC22-95PC95144, March 2001.

42. Parsons Engineering, *Advanced Fossil Power System Comparison Study*, DOE Report, June 2002.

43. Hurley, J. P., et al. *High-Temperature Heat Exchanger Development and Testing*, Final Report; DE-FC26-98FT40320, June 2004.

44. TAG™ Technical Assessment Guide – Electricity Supply – 1993, EPRI TR-102276, June 1993.

45. David, J. and Herzog, H., The Cost of Carbon Capture, MIT, 2002.